University of Nottingham
Department of Manufacturing Engineering
& Operations Management

Reducing the surface deviation of Stereolithography components

By

Philip E. Reeves

Thesis submitted to the University of Nottingham
For the degree of Doctor of Philosophy

November 1998

Table of Contents

Abstract

The Stereolithography (SL) process has developed into an accurate method of replicating 3D CAD images into tactile objects used for functions such as product evaluation, pre-production testing or as patterns around which tool cavities can be formed. One of the main limitations with the SL process is the surface roughness of parts resulting from the layer manufacturing process. To-date surface roughness has only been reduced using techniques such as additive coating or abrasive finishing. Research has shown however, that these techniques are both detrimental to the accuracy of parts and can prove to increase the cost of SL parts to the end user.

The object of this research is to assess the fundamental cause of surface roughness in layer manufacturing and develop techniques that can be used during the build process to produce SL parts with lower surface deviation. To do this a comparison of the most common commercial RP systems was undertaken to identify the attributes causing surface deviation. From these attributes a mathematical model of layer manufactured surface roughness was developed. Parts manufactured using different SL machines were compared to the mathematical model showing a variety of causes in surface deviation not considered in earlier research, such as layer composition, layer profile and the affects of over curing or print-through on surface deviation. The layer edge profile caused by the shape of the scanning laser also has a significant effect on roughness deviation. However, by using a combination of part orientation and optimal shaped meniscus smoothing, the surface deviation of SL parts was found to be reduced by up to 400% on at least 90-

degrees of continuous surfaces. A better understanding of layer manufactured surface roughness has now been achieved and a new smooth build algorithm has been developed.

Acknowledgements

The author is indebted to a great number of people for their help and encouragement during this work. Special thanks are extended to:

Dr Richard Cobb for his invaluable supervision throughout this research program. His guidance and enthusiasm have been a positive influence during this research work.

Special thanks is extended to the vast number of RP&T associated companies who offered both practical assistance and test samples during this research, for no financial gain. In no specific order, thanks are extended to Richard Rogers at Rolls Royce Aerospace, Dr Chris Bocking at GEC-Marconi, Martin Koch at California State Polytechnic, Professor Tom Childs at Leeds University, Dr Jouni Partanan at 3D Systems USA & Andrew Chantrell & Andrew Chadwick at 3D Systems UK, Henri-Jacques Topf at Schneider Prototyping GmbH and Dr Ian Gibson at Hong Kong University,

The staff in the department workshop at the University of Nottingham, with particular mention to John Webster for his invaluable assistance in developing the meniscus smoothing software.

I would also like to acknowledge the guidance of Professor Phill Dickens at De Montfort University for his time and patience in proof reading much of this work and providing an insight into RP&T which would have otherwise been overlooked.

Glossary

ABS	Acrylonitrile-Butadiene-Styrene.
ACES	Accurate Clear Epoxy Solid: Build style used for the creation of solid epoxy models on a Stereolithography machine.
Active recoating	A recoater systems that automatically wets the top surface of a Stereolithography model in between layers, in preparation for the scanning of the following layer.
Actua	3D Printing process developed by 3D Systems.
AFM	Abrasive Flow Machining.
ASCII	American Standard Code for Information Interchange.
Beam Width	The width of the laser beam at the interface with the photo-curable monomer.
Beta test	A second stage of testing prior to release.
Build direction	The direction a Rapid Prototype part is orientated during the build process.
CAD	Computer Aided Design.
CLA	Centre Line Average.
CMM	Co-ordinate Measuring Machine.
CNC	Computer Numerical Control.
Deep-dip	A method of recoating.
Delamination	Separation of individual build layers in a layer manufactured part.
DOE	Diffractive Optical Element.

DOS	Disc Operating Systems.
Down facing surface	A surface on a Stereolithography model that is orientated in the X-Y build direction and facing the bottom of the Vat of photo-polymer during the part build.
DTM	Desk Top Manufacturing.
EDM	Electrical Discharge Machining.
EOS	Electro Optical Systems.
EPSRC	Engineering and Physical Science Research Council.
FDM	Fused Deposition Modelling: A type of Rapid Prototyping process.
Green	A semi-stable state of a material prior to post-processing.
Hard tooling	A tool that is capable of withstanding multiple use.
Hatch spacing	Distance between cured laser lines in the internal hatching of Stereolithography models.
Infiltration	Introduction of a molten material into a porous solid.
Injection moulding	A process of producing multiple plastic components by forcing molten polymer into a cavity.
Ink-jet	Process of selectively depositing a measured amount of liquid from a nozzle or array of nozzles.
INSTANTCAM	Layer manufacturing research project undertaken by a consortium of Benelux based Universities and research establishments.
Investment casting	The process of producing a metal part from a thermally expendable patter by the creation of a mould around the pattern by the 'investment' of layers of ceramic material.

ISO	International Standards Organisation.
Layer composition	The physical makeup of each layer in terms of material composition.
Layer profile	The profile of a section taken in the Z-axis of the edge of each layer used to build a rapid prototype model.
Layer thickness	The thickness of the cross sectional profiles used to build rapid prototype models.
Layerwise	Built in layers.
LMT	Layer Manufacturing Technique.
LOM	Laminated Object Manufacture.
Over-cure	When more energy than is needed to cure a single layer thickness is applied (see Print-through).
PCA	Post Cure Apparatus.
Photo-curable	A resin cured by electromagnetic radiation; referred to as a photo-monomer.
Post-cure	The final curing of a Stereolithography mode after it has been built (Usually in a PCA).
Post-processing	Work undertaken to a part after the layer manufacturing process is complete.
Pre-processing	Work required before a rapid prototype model can be built.
Print-through	The mechanism by which photo-curable layers of material are bonded to form a three-dimensional structure.

Pro-Lux	A coating and abrasive finishing process developed for Stereolithography models.
PVD	Physical Vapour Deposition.
QuickCast	A Stereolithography build style for investment casting.
Ra	Roughness average.
RapidTool	Process of producing metal parts from polymer coated metal powder using the SLS process.
Recoating	The process of preparing the surface of a rapid prototype model for the generation of the following layer.
RMS	Root Mean Squared.
RP	Rapid Prototyping.
Rt	Maximum peak to trough deviation of a topography over a given distance.
RT	Rapid Tooling.
RTV	Room Temperature Vulcanisation.
SEM	Scanning Electron Microscope.
SFF	Solid Freeform Fabrication.
Sinter	To coalesce a powder into a solid by heating.
SL	Stereolithography.
SL5143	A brand of acrylic photo-monomer.
SL5149	A brand of acrylic photo-monomer.
SL5170	A brand of epoxy photo-monomer.

SL5181-1	A brand of epoxy photo-monomer.
SL5180	A brand of epoxy photo-monomer.
SL5190	A brand of epoxy photo-monomer.
SLA	Stereolithography apparatus.
Slice	A layer.
SLS	Selective Laser Sintering.
Soft tooling	A mould used for short run production of high volume prototype manufacture.
Solid model	A form of CAD model suitable for rapid prototyping.
Spray Metal	A metal forming process in which a molten metal is atomised and sprayed onto a model to form a thin shell.
Stair-stepping	The surface topography of angled surfaces produced by building objects in layers.
STAR-Weave	A Stereolithography build style for use with acrylic photo-monomers.
Stereolithography	The method of producing a three dimensional object directly from a CAD model using the laser curing of layers of photosensitive monomer.
STL file	A triangular approximation of a solid model used to transfer geometric data to the RP process.
Support structure	sacrificial material added to the base of a rapid prototype model to act as support for overhanging and unsupported features.
Surface model	A form of CAD model suitable for rapid prototyping.

Taly-surf	contact device for measuring the surface roughness of flat planes.
Thermoplastic	A plastic material that is softened by heat and hardened by cooling in a reversible process.
Thermoset	A plastic material that is hardened by an irreversible chemical change.
TSR	Terminate Stay Resident.
UFP	Ultrasonic Flow Polishing.
Uncured resin	Photo-monomer in its liquid form prior to exposure to electromechanical radiation.
Up facing surface	A surface on a Stereolithography model that is orientated in the X-Y build direction and facing the top of the vat of photo-monomer during the part build process.
UV	Ultra Violet.
Zephyr	An active recoater system used on the 3D Systems Stereolithography apparatus.
3DP	Three Dimensional Printing.
3D Systems	Main Manufacturer of Stereolithography apparatus.

Nomenclature

Uppercase

K	Up facing composition roughness (Calculated)	μm Ra
K_1	Down facing composition roughness (Calculated)	μm Ra
A_n	Area above or below the line of the arithmetic mean	m^2
L_n	Cut off distance	m

Lowercase

a_1	Subdivision of A_n	m^2
a_2	Subdivision of A_n	m^2

Greek

α	Layer thickness	m
δ	Half layer thickness	m
ξ	Distance below undercut	m
ρ	Distance above undercut	m
ϕ	Layer profile	Degrees
θ	Surface angle	Degrees
κ	Up facing roughness (measured)	μm Ra
κ_1	Down facing roughness (measured)	μm Ra

Subscript

$_{Max}$	Maximum
$_{Min}$	Minimum

CHAPTER 1

1.0 Introduction

In the last 15 years a range of manufacturing processes have evolved which produce accurate and repeatable components by adding material in 2-dimensional layers to create a 3-dimensional object. Over 20 of these Layer Manufacturing Techniques (LMT) are now commercially utilised [1]. The process is also known as Solid Freeform Fabrication (SFF) or more commonly, Rapid Prototyping (RP). The acronym LMT is generally used only in Scandinavia [2]. The principle of RP is to use 3-dimensional Computer Aided Design (CAD) data to generate solid objects, layer-upon-layer. The method of layer generation differs between processes, but four distinct groups can be defined [3]. RP processes generate layers either through the deposition of liquid materials and subsequent solidification, or by selective sintering a powder into a solid form. Other systems use the phase change of a liquid to a solid state through radiation curing. The most basic systems simply cut entire layers from sheet material, which are subsequently bonded. With each system, layers are continually deposited, cured or sintered until the object defined by the CAD data is complete.

Although some systems may take a number of days to produce a component using layer manufacturing, the time taken to manufacture complex engineering prototypes can be significantly faster than using conventional model making techniques or CNC machining. More importantly, because the model has been manufactured directly from the CAD data, the part will always be a faithful replication of the initial design intent, irrespective of product complexity. RP has therefore proved a valuable tool in

reducing the product development cycle and increasing the competitiveness of many manufacturing organisations. Given the rapid speed by which parts can be manufactured, RP has found applications in many fast moving consumer markets including automotive manufacture, aerospace, and white goods design in addition to consumer products such as the telephone, CD and Walkman design. The most common applications for RP are in the manufacture of prototype injection mouldings, to prove design and functionality before the manufacture of expensive tooling.

Through continual process improvement, RP parts are now used as patterns for a variety of down stream tooling processes in the emerging field of Time-Compression-Technology (TCT), which is a natural progression from RP [4]. The philosophy of TCT is to reduce the time taken between the design phase of a new product and the ultimate sale of the finished goods to the consumer.

Studies have shown that those who ship a product six months late face losing 33% of their lifetime profit. However, a massive 50% over spend during the product development phase will only result in a 3.5% loss in total lifetime profit of a similar product if the launch is kept on track [5]. The limiting factor in many product development cycles is the time associated with tool manufacture, without which parts cannot be produced. Hence, by reducing the tooling lead times a significant decrease in the product development cycle can be achieved.

TCT uses a combination of RP in the product design phase and Rapid Tooling (RT) in the tool development phase. RT is a generic term used to describe a number of tool-cavity manufacturing processes, all based on additive manufacturing. RT tool cavities

are produced in one of two ways, by either moulding or forming a cavity around an RP master pattern, or by generating the tool cavity directly on the RP machine. By eliminating the need for subtractive tool manufacture, both product development lead-times and associated costs can be dramatically reduced [4][6].

A study by General Motors in the US has shown that by using Rapid Tooling in a typical 12-18 week product development programme, lead time can be reduced by up to 4 weeks [7]. In such cases, the increased revenue generated from getting a product to market in 30% less time has been found to exceed the cost of the initial Rapid Tooling cavities. Given the limited life expectance of the RT cavities, General Motors manufactured concurrent hard tooling in preparation for the failure of the rapid tools. The increased revenue was then used to justify the additional RT cost.

It is important to note the limitations of layer manufacturing technology, in terms of accuracy and repeatability, as inaccuracy in the master pattern will be inherent in any down stream tooling and subsequent parts produced. Rapid Tooling is in direct competition with high speed CNC machining, hence the accuracy of the RP master must be at least equivalent to that of CNC machining, if the process it to gain a broader acceptance in the manufacturing sector.

As yet RP has not been able to match CNC machining in terms of accuracy [8], although a great deal of research has centred on improving both RP machine control and RP build materials, to produce more robust, accurate prototypes and patterns [9]. However, the process has been accepted by a number of companies, as the need for lengthy post-processing and tool cutter path planning is eliminated, producing

valuable savings in product lead times. One of the major limitations to RP now facing downstream tool manufacture though, is the poor surface deviation of parts, which is inherent when patterns are manufactured using additive layers [10]. Parts need to be finished and to-date this is mainly undertaken manually. This is acceptable if the part is only an aesthetic model or verification prototype [11], but if the part is intended as a pattern for down stream tooling, the surface roughness is transferred to the tooling system. Finishing is therefore essential but is detrimental, as the process removes both accuracy and traceability within the manufacturing process [12]. Manual finishing is also a costly and laborious process. It requires a high degree of skilled labour and is a bottleneck in the production of parts and tools. In 1994 it was estimated that manual finishing would account for over 48,000 man-hours of skilled labour within the RP sector [13].

1.1 Aims of the work

The overall aims of this PhD are (i) to identify and understand the fundamental causes of surface roughness in RP and (ii) to develop a strategy for reducing surface deviation during part manufacture. This might help to reduce or possibly eliminate the need for post-process surface finishing following part manufacture.

The main objective of this work is to demonstrate that significant improvements in surface roughness can be achieved using existing 3D Systems SL hardware. There are a wide variety of commercially available RP systems but the research is focused on the Stereolithography (SL) process, specifically the SLA-250 system. Stereolithography represents over 50% of the world RP market and is the preferred process for the manufacture of patterns for RT [14].

1.2 Organisation of the thesis

This thesis begins with a literature review, which outlines the history of layer manufacturing processes and the evolution of commercial RP. It covers the applications of layer manufacturing and the different mechanisms by which part are made. The limitations of surface roughness associated with layer manufacturing are then discussed and a review of previous research to reduce surface roughness on RP parts is made. From the literature review, the need to improve surface deviation during the layer manufacturing process is discussed. An experimental methodology is then outlined in chapter 3 to assess the fundamental cause of surface deviation in generic layer manufacturing. From a comparative analysis of LMT processes the attributes affecting surface deviation are identified and verified using a mathematical model of surface deviation derived in chapter 4. The mathematical model is then used to assess attributes within the Stereolithography process, which may prove beneficial to surface smoothing. A new build algorithm is discussed which can be used to produce inherently smoother surfaces over a limited range of angled planes. The thesis goes on to discuss methods of extending this smooth build envelope, to encompass at least 90-degrees of angled surfaces. Using a technique of stretching meniscus between layers during the build process, the thesis demonstrates that the surface roughness of different angled planes can be reduced using different shaped meniscus during the Stereolithography build process.

CHAPTER 2

Literature review

2.0 Introduction

This literature review has two distinct sections. The review starts with a background to the evolution of layer manufacturing from the turn of the century. Current commercial RP processes are then discussed in terms of market share, application and cost. The layer manufacturing process cycle is outlined showing the progression from 3D CAD, through file transfer and part orientation into RP machine selection, build mechanisms and support structures. The review then focuses on the market leading Stereolithography process and the application of SL in down-stream Rapid Tooling.

The second section of the review highlights the limitations of layer manufacturing, in terms of surface deviation. A review of previous research into finishing has then been undertaken, showing how processes such as abrasive and additive finishing have been used at a cost of geometric integrity. The section concludes that the most suitable method of reducing surface deviation is to modify attributes within the layer manufacturing process.

2.1 The history of layer manufacturing

The concept of manufacturing 3-Dimensional components using layers is not new. The layer manufacturing of functional objects can be traced back to the turn of the present

century, when in 1902 Peacock filed a US patent for the laminate manufacture of horse shoes [15]. In the same year Carlo Baese of Berlin, filed a U.S. patent, *'photographic process for the reproduction of plastic objects'* [16].

Hopkins patent in 1921 showed that if a pattern were scanned or traced in a series of layers, using a mechanical link, these layers could be replicated by means of a cutting head. The initial concept was to scan facial features, and create a direct stone copy. Hence the process name *'photo-sculpture'* [17]. The process was developed and electrically automated in 1930 by Howey [18], becoming what we now know as pantographic scanning. Pantographs were commonly used prior to the development of CNC, for the replication of designs from a master pattern onto a variety of materials.

The development of 'functional' laminated components continued with a patent by Seiichi Kojima in 1956. Kojima demonstrated that very complex geometries such as conceptual furniture could be continually reproduced in layer form, to a greater degree of repeatability than by conventional machining techniques, provided that each laminate could be accurately aligned [19].

In 1967 Swainson filed a revolutionary patent for a system using two perpendicular scanning light beams, with the ability to read and store data from 3-dimensional objects. The shape of the object could then be replicated in a special photopolymer [20]. No physical model was presented to collaborate the patent application, and research remained dormant until the mid-1970's.

During 1974 it was reported by Port [21] that a Californian based company, Formigraphic Engineering, headed by Swainson, had resurrected the 1967 patent using a dual light source to initiate cross polymerisation of a photosensitive fluid. The Formigraphic system used a mercury vapour UV lamp focussed through a *'slit'* mask to energise a light-sensitive fluid. A Xenon-Hydrogen laser was then set perpendicular to the mercury vapour source, causing cross polymerisation of the liquid where the two light sources intersected [22]. When a sufficient intensity of photons, at the correct wavelength was focused onto the photo-reactive liquid, the *'light energy'* would cause a cross-linking reaction, in effect changing a liquid monomer into a cross-linked polymer chain [23]. By moving both the 'slit' mask and the laser beam, solid objects or prototype components could be generated within a transparent chamber [24].

The process termed *'solid holography'* was considered as a method of producing patterns around which cavities could be created using processes such as spray metal tooling or resin casting [21]. The main limitation to Swainson's research was computing power, which in the mid 1970's was unable to calculate the complex sequence of real-time optics motions required to locate the two light sources.

Following an application by Dimatteo in 1974, a patent was granted in 1975 for the process commercially known as Laminated Object Manufacture (LOM). Dimatteo's system used an electronic pantograph linked to a computer [25]. The pantograph generated a series of tool paths by taking *'sectional scans'* on an object's surface. The data was either stored or directly down loaded to an X-Y motion plotter located above a static table. By means of either a rotating head or laser cutting device, individual layers could

be cut into sheet material loaded onto the static table below [26]. These layers could then be manually stacked to reproduce the original pattern. Dimatteo saw this process as a method of producing both component parts and tool cavities using a wide range of sheet materials including steel [27].

2.2 Single light source photo-curable systems

A seminal development in LMT design occurred in 1981, with the construction of a photocurable system using a single light source. Following a Japanese patent application in 1980 Hideo Kodama published three new methods of solid holography [28]. Kodama stated that only a single light source was required to initialise photo-polymerisation, and that this could be focused onto the photosensitive resin in a number of ways. Kodama proposed that layers could be built within a vat of liquid, on a movable stage, capable of indexing by a single layer thickness. Layers were either generated as a whole, by '*mass*' light exposure through a mask, or by moving an optical fibre over the liquid surface. Although crude, the range of models generated by Kodama's research did show significant promise for layer manufacturing using photosensitive resin.

A variation to Kodama's single light source was proposed in 1982 by Herbert [29]. By replacing the optical fibre with a series of directional mirrors a significant increase in scan speed was proposed. However, no quantitative results were produced to corroborate this claim.

Takashi Morihara of Fujitsu Ltd [30] identified one major limitation to the photocurable

resin process, being the settling time required between the polymerisation of each layer. Based on current machine design, parts were immersed into the vat to allow resin to pass over the polymerised layer. The part was then withdrawn less the thickness of the next layer. The process was then halted to allow for settling of the resin and damping of any currents induced by the platform motion. Takashi proposed that additional resin be added to the system by means of a slotted blade moving over the vat surface between the scanning of each layer. In effect, the process would eliminate the need for part dipping and prevent any unwanted motion during the build process.

The development of photo-curable RP systems has continued in both Asia and the USA, with seven system manufacturers located within the pacific ring [1]

2.2.1 The development of Stereolithography

The first commercially available RP system was patented in the USA by Charles Hull during 1986 [31]. It was similar in design to Kodama's earlier photo-curable resin process. Photo-polymerisation was initiated by light, directed down onto an open vat of resin by a series of static and dynamic mirrors. In the original system known as the SLA-1, no blade was used to settle the resin between layers. The system relied on a long 'z-wait' time, resulting in both lengthy build times and inaccuracies in the Z-axis. Based on this early machine configuration, Hull and research partner Ray Freed formed their company 3D Systems Incorporated, naming their new process '*Stereolithography*' (SL) [32].

The SL process in its commercial form has been at the forefront of LMT, beginning with

the early SLA-1 system. This was modified to produce the market leading SLA-250 system commercialised in 1988 [33]. The SLA 250 uses a helium-cadmium laser and is fitted with a levelling blade to improve part accuracy and reduce build time. In 1989 the SLA 500 using a higher-powered argon-ion laser was introduced to the market shortly followed in 1990 by the entry-level SLA 190 using identical optics to the SLA 250.

By 1992, 3D Systems sales figures exceeded 300 units world wide, with the introduction of the SLA-400 in 1993 thus giving 3D Systems a product range suited to a large percentage of the prototype development market [34]. 1996 saw the most radical machine re-design to-date, with the launch of the SL-350. The gas laser used on previous machines was replaced with a higher power, more stable, long life solid-state laser [33]. The re-coater blade was also replaced with a more accurate slotted wiper blade similar to that proposed by Morihara of Fujitsu Ltd [30]. The slotted 'Zephyr' blade allows for thinner layers and reduces the risk of delamination caused by trapped volumes of resin [35].

The most recent development in SL technology is the SLA-5000. The machine uses the body of the SLA-500 but replaces both the levelling blade with a 'Zephyr' blade and the Argon-Ion laser with a solid state model. The manufacturers claim the machine is highly reliable due to the solid state laser, accuracies of +/- 75 μm in the X and Y-axis, +/- 50 μm in the Z-axis and a build envelope suitable for part manufacture up to ½ m^3 [36].

Although considered market leaders, 3D Systems are not without competition. In addition to seven Pacific-rim manufacturers all producing SL clone machines [1], photo-curable RP systems have also been manufactured in Belgium, France, Germany and the US. The

Belgium system manufactured by Materialise although not sold commercially is used for commercial bureau work. In addition to a French research machine developed by Claude Modal, two commercial systems have been developed in Germany. A photo-curable system manufactured and sold by Fockele and Schwarze is currently available through Europe [37]. A similar system manufactured by Electro-Optical Systems (EOS) was made commercially available in the early 1990's [38]. Following patent litigation dating back to 1994 [39], 3D Systems have now successfully stopped the manufacture of photo-curable RP systems by EOS. To-date no such report of action on Fockele and Schwarze has been announced. 3D Systems are now in patent litigation with US manufacturer Aaroflex, who have attempted to sell their SLA clone within the USA [40].

2.3 LMT market evaluation

Despite competition, 3D Systems remain the LMT market leader, with cumulative sales of all SLA system variants at the end of 1996 of 617 machines, this being 43% of the world market [41]. A personal communication with 3D Systems UK sales director now puts worldwide sales of SLA units in excess of 1000 machines [42]. The machine market for 1997 was estimated to exceed £185 million with additional services such as material supply, training and support, estimated at a further £207 million [43].

The LMT market is now split into two distinct groups, these being RP machines used to produce accurate prototypes and master patterns and concept modellers used in the design environment for the rapid 3-dimensional printing of CAD images. The most common RP processes used in Europe and North America are listed in Table 2.1, which details both

the manufacturer and layer manufacturing mechanism in addition to machine cost, part materials and maximum build volume [44][41].

System	Manufacturer	Build mechanism	Cost	Build envelope (Cubic Inches)	Material
Stereolithography (SL)	3D Systems EOS	Photo-curable liquid monomer	£99,000 - £450,000	1000 – 9200	Epoxy Acrylic
Selective Laser Sintering (SLS)	DTM EOS	Laser sintering of powder	£300,000 - £400,00	1696 – 3257	Wax Nylon Polycarbonate Sand Polystyrene Metallic powder
Fused Deposition Modelling (FDM)	Stratasys	Deposition and solidification of liquid	£90,000 - £210,000	1000 – 7776	Wax Nylon ABS
Laminated Object Manufacturing (LOM)	Helysis	Lamination of pre-cut layers	£110,000 - £220,000	2100 – 14080	Paper Polyester Glass-ceramic
Actua	3D Systems	Deposition and solidification of liquid	£57,000	640	Paraffin wax
Drop on Demand Inkjet printing (DODI)	Sanders	Deposition and solidification of liquid	£64,000	648	Investment casting wax
Solid Ground Curing (SGC)	Cubital	Photo-curable monomer	£270,000 £470,000	2744 – 5600	Acrylic photo-polymer

Table 2-1 Commercially available RP processes

The world-wide sales distribution of systems by each of the leading manufactures is shown in Figure 2.1.

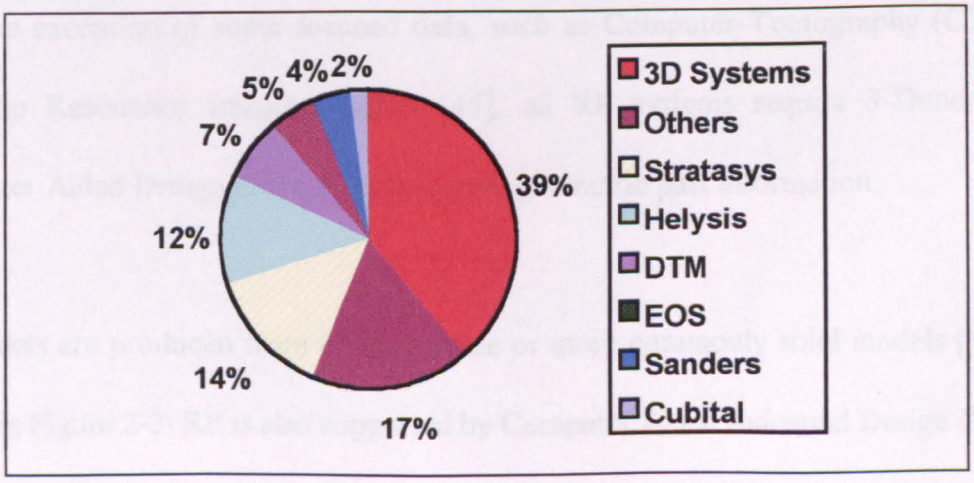

Figure 2-1 - Distribution of worldwide RP sales by company (1996)

As seen in Figure 2-1, 3D Systems maintains a large percentage of the world RP market with the sales of all Stereolithography machines including the Pacific rim manufacturers accounting for over 50% of the world market. From this is can be concluded that the SL system is without doubt the leading RP process in terms of commercial acceptance and market share.

2.4 The layer manufacturing process cycle

To fully understand the potential benefits of RP and the limitations of the process to down stream tooling, we must first understand both the enabling computer technology of CAD and the layer manufacturing mechanisms used by the commercial systems. As this research is targeted towards improving the Stereolithography process, the process is explained in detail. An overview of the other three most common RP processes and two concept modelling systems is included in Appendix A.

2.4.1 CAD and solid modelling

With the exception of some scanned data, such as Computer Tomography (CT) and Magnetic Resonance Imaging (MRI) [45], all RP systems require 3-Dimensional Computer Aided Design (3D CAD) to supply geometric part information.

RP models are produced from either surface or more commonly solid models [46], as shown in Figure 2-2. RP is also supported by Computer Aided Industrial Design (CAID) packages producing RP compatible files of high quality [47].

2.4.2 File transfer

At present it is not possible to directly link a CAD system to an RP machine and print a 3-dimensional model in the same way as obtaining a print or plot. Before a CAD image can be translated into a layer manufactured part, the file must be converted into a suitable format for 'driving' the wide variety of RP machines.

The STereoLithography or Surface Tessellation Language (STL), has become the defacto standard for all RP systems and is supported by all the major CAD vendors. The principle of the STL format is to represent the geometry defined within the CAD system, Figure 2-2 using a mesh of triangles over the part surface, as shown in Figure 2-3. This simple approximation can be quickly generated within CAD and produces relatively small binary files [48]. The smaller the triangular tolerance the nearer the approximation to the intended geometry. However, smaller triangles increase the number of facets and hence increase the STL file size [49]. Hence, a compromise must be made between quality and file management.

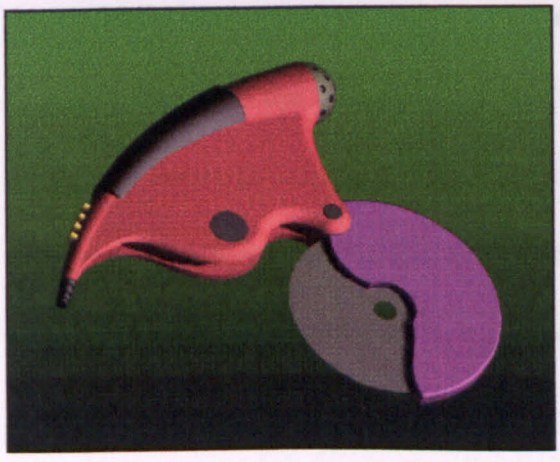

Figure 2-2 3D solid Model

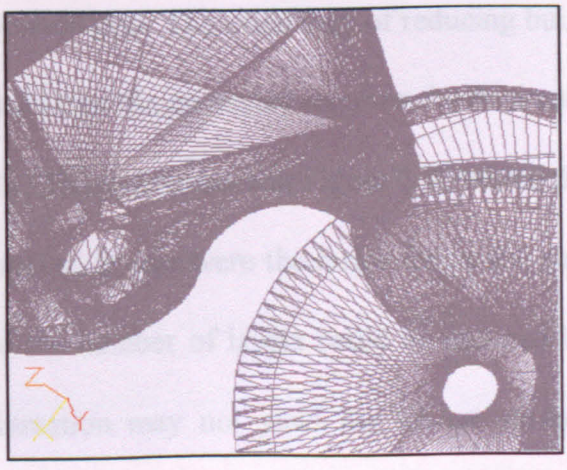

Figure 2-3 STL file of Fig 2-2

2.4.3 Part Build Orientation

Once generated, the geometry defined within the STL file is fixed. Although software is available for scaling, translating and sectioning STL files, with the exception of specialist software such as Delcam DUCT, it is not possible to read such files back into a CAD system and modify the design intent. Hence, the CAD data must be correct before the STL file is generated.

Before the STL file can be transferred to the RP system, a number of modifications may be needed to produce satisfactory data. For instance, if the final LMT part is to be used as a pattern for down stream rapid tooling, a scaling tolerance may need to be added to the RP master pattern to allow for polymer shrinkage in the tool [50]. In other cases, if the CAD model is larger than the LMT build envelope, the STL file must be sectioned and the data treated as separate models. It is also at this stage that the orientation of the build within the machine is defined, as this affects both part quality and cost.

The cost of an RP part is a direct reflection of its build time. Hence, if the build time can be decreased, the cost of the part can be reduced also. The usual way of reducing build time is to orientate the STL file in such a way that the geometry requires the minimum number of layers to complete the build [51]. This can be seen in Figure 2-4, where the same part is shown in two different orientations. If cost were the major factor the part would be built horizontally, as in this case the number of layers could be reduced by almost one third. However, such an orientation may not yield the lowest surface roughness.

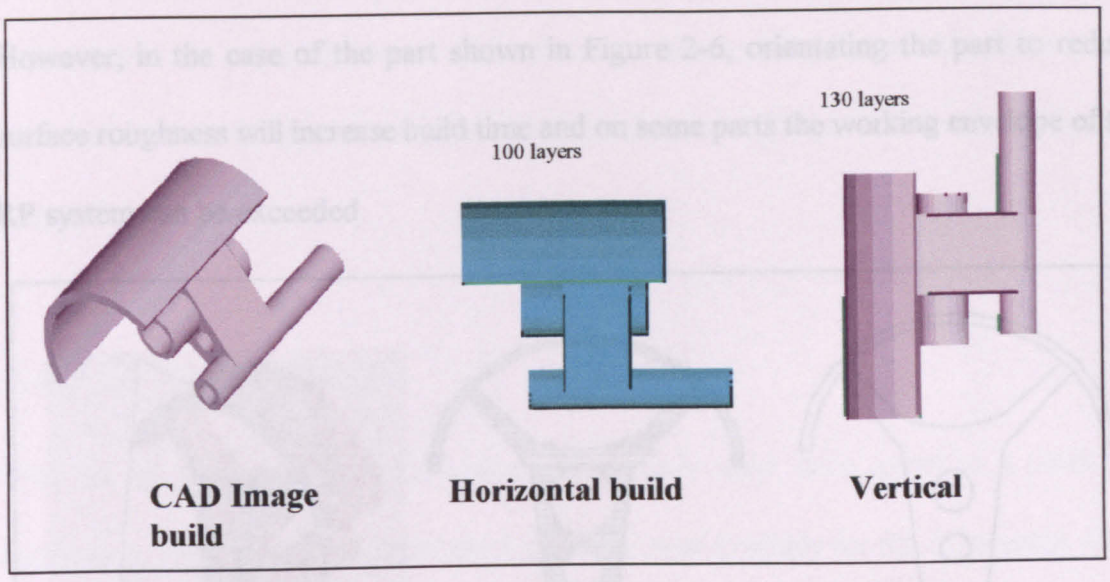

Figure 2-4 The effects of part orientation on build time

Given that each layer has a finite thickness, it is not always possible to achieve a smooth finish if an angled or curved surface is built at an angle to the Z-axis. Where a layer does not intercept the desired geometry as shown in Figure 2-5, a phenomenon known as 'stair stepping' occurs [52][53].

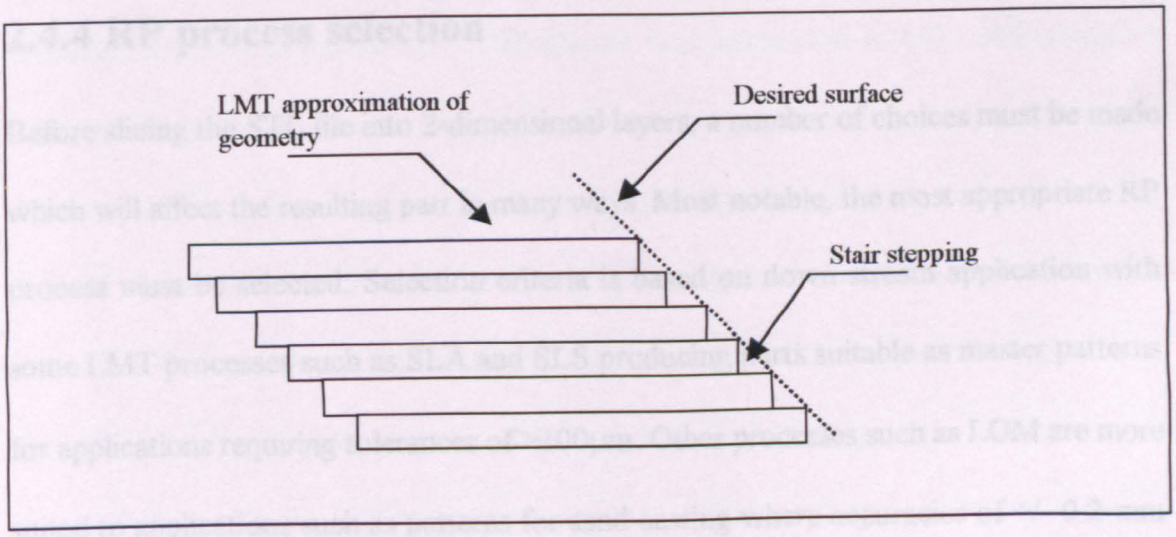

Figure 2-5 The effects of 'Stair-Stepping' on surface roughness

Irrespective of layer thickness or the LMT mechanism, stair stepping will always occur if the profile of each layer edge is not parallel to the desired geometry. By selecting an orientation to reduce 'stair stepping' it is possible to alter the eventual surface roughness

of the RP part [54] and commercially many parts are built favouring particular surfaces. However, in the case of the part shown in Figure 2-6, orientating the part to reduce surface roughness will increase build time and on some parts the working envelope of the RP system can be exceeded.

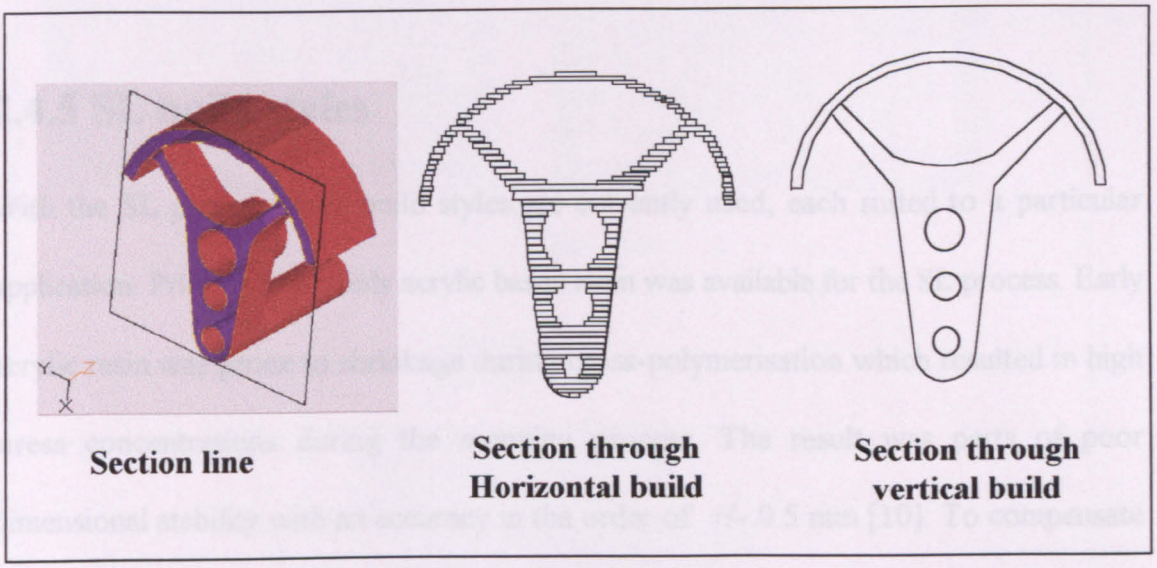

Figure 2-6 The effects of build orientation on surface roughness

2.4.4 RP process selection

Before slicing the STL file into 2-dimensional layers, a number of choices must be made which will affect the resulting part in many ways. Most notable, the most appropriate RP process must be selected. Selection criteria is based on down stream application with some LMT processes such as SLA and SLS producing parts suitable as master patterns for applications requiring tolerances of >100μm. Other processes such as LOM are more suited to applications such as patterns for sand casting where accuracies of +/- 0.2-mm are considered acceptable. Processes such as FDM are particularly suited to the manufacture of prototype enclosures and housings as parts are manufactured in materials made to simulated injection moulded polymers such as ABS and nylon [44]. Once the

correct RP process has been selected, both the build material and build style must be defined. It is not within the remit of the thesis to discuss RP process selection criteria, however further information on build styles for alternative RP processes can be found in Appendix A.

2.4.5 SL build styles

With the SL process three build styles are currently used, each suited to a particular application. Prior to 1993, only acrylic based resin was available for the SL process. Early acrylic resin was prone to shrinkage during cross-polymerisation which resulted in high stress concentrations during the scanning process. The result was parts of poor dimensional stability with an accuracy in the order of +/- 0.5 mm [10]. To compensate for shrinkage during scanning, a build style was developed that used a complex scanning path designed to compensate for material contraction. The Staggered and Alternated Retraction build style known as STAR-Weave, was introduced in 1991 and works by scanning the boundary of each layer before cross-hatching the interior using alternative direction hatching. The hatch is only attached to the boundary in one position, hence the material is allowed to contract freely without deforming the boundary as shown in Figure 2-7. After scanning in one direction, the scan path is rotated through 90-degrees and retracted scanning is repeated. Each subsequent layer is then staggered to prevent further stresses between layers and increase the structural rigidity of the part as shown in Figure 2-7. The resulting part resembles a waffle or lattice, with many voids of uncured resin within. This must then be cured as a post-process operation in a UV oven. Although a vast improvement on earlier build styles, STAR-weave is only accurate to +/- 0.2 mm and

remains prone to distortion during the post-process curing of parts [10].

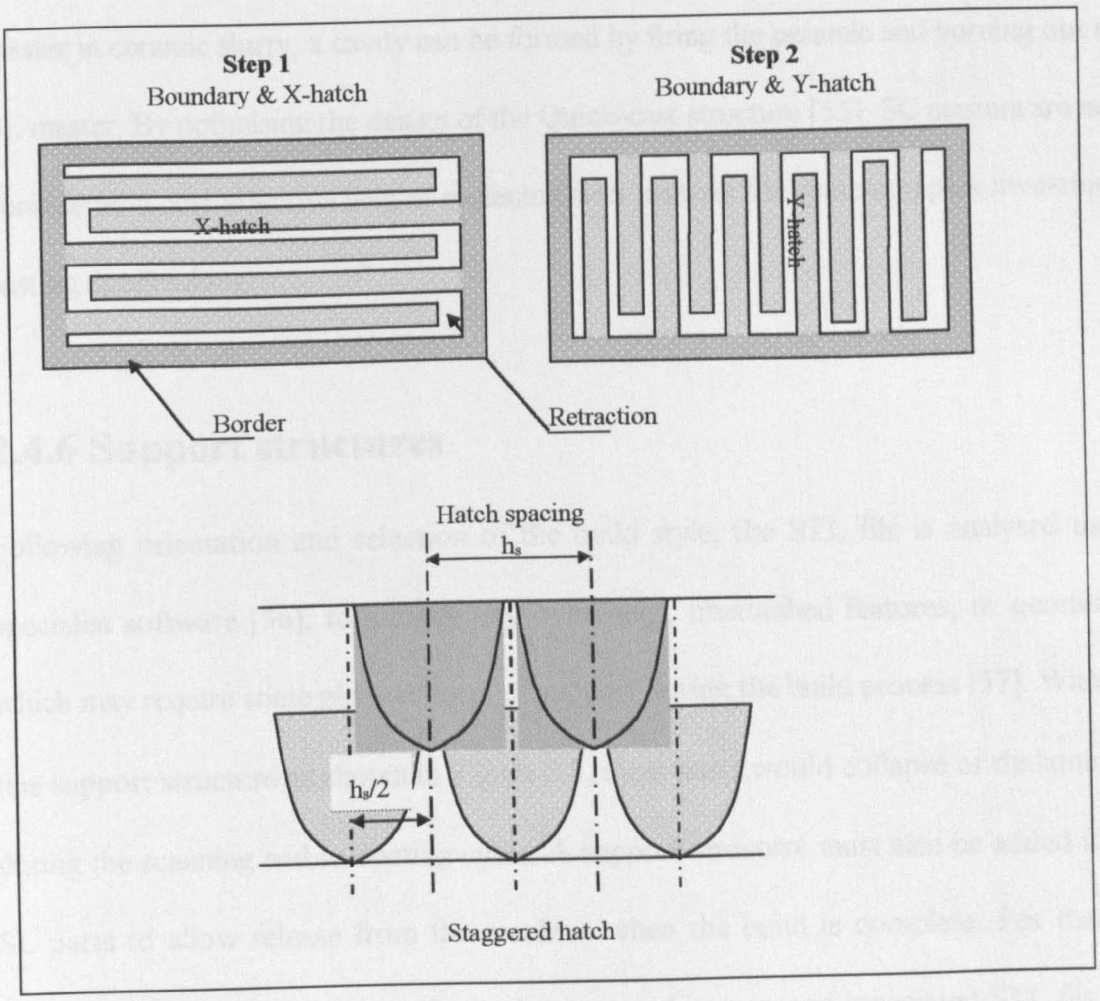

Figure 2-7 3D Systems Acrylic – STAR-Weave build style

In 1993 a new formulation of resin was made commercially available based on an Epoxy-ester photo-monomer. Epoxy SL resin differs from the earlier acrylics in that the material does not undergo excessive shrinkage during cross-polymerisation. The result is that parts can be built with a fully dense crosshatch without inducing stresses. Using the Accurate Clear Epoxy Structure (ACES), parts can be manufactured to +/- 0.075 mm with only minimal distortion over time [36].

Using the Epoxy-ester photo-monomer parts can also be built using a hollow honeycomb

structure called Quick-Cast. Quick-Cast has been developed to enable SL parts to be used in place of wax patterns in the investment casting process. By coating a Quick-cast SL master in ceramic slurry, a cavity can be formed by firing the ceramic and burning out the SL master. By optimising the design of the Quick-cast structure [55], SL masters are now considered a cost effective way of replacing wax masters for some complex investment casting applications.

2.4.6 Support structures

Following orientation and selection of the build style, the STL file is analysed using specialist software [56], to identify any overhangs, unattached features, or geometry, which may require some physical form of support during the build process [57]. Without this support structure as shown in Figure 2.8, most parts would collapse or de-laminate during the scanning and re-coating cycle. A support structure must also be added to all SL parts to allow release from the machine when the build is complete. For the SL process, the support structure information is stored as a second associated STL file.

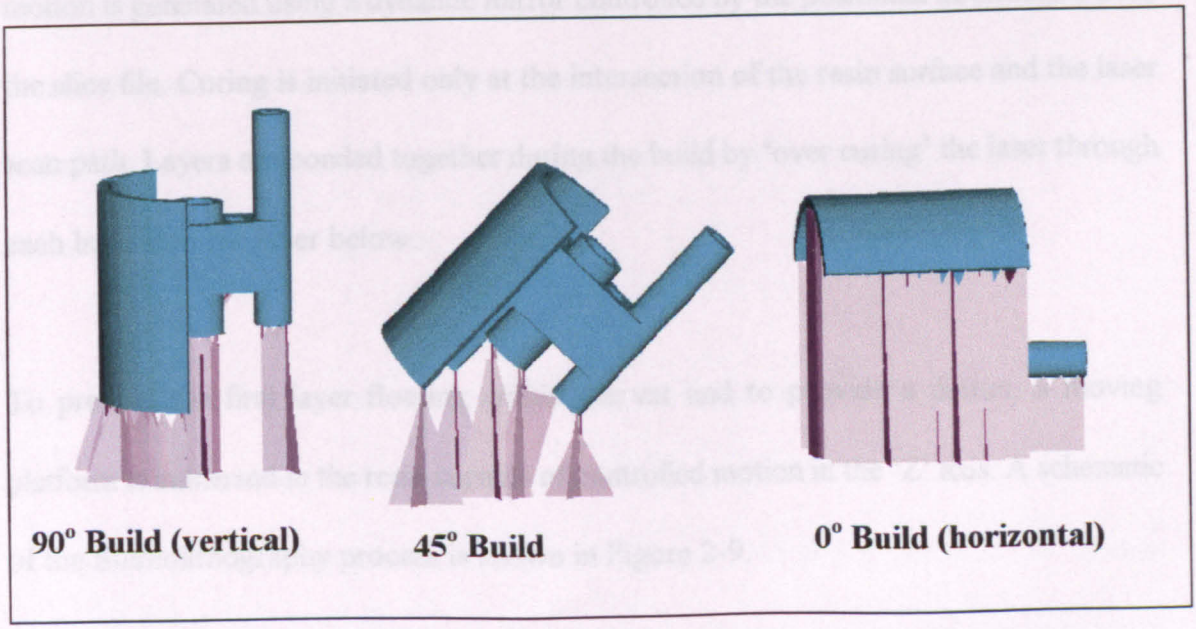

Figure 2-8 The effects of orientation on support structure

Following the generation of the support structure and the choice of build style both the part STL file and support STL files are sliced by the computer into a series of discrete layers, each representing a section through the solid model. The slice file contains positional information for the scanning of each layer, the retraction distance of the build platform and subsequent layer thickness, parameters for the re-coater blade, scan speed and laser power.

2.5 The Stereolithography Process

In simple terms, the Stereolithography process (SL) works by 'printing' with an ultraviolet laser, layers of polymer which are stacked to form a solid [58]. The 'Photo-polymerisation' process is initiated using an Ultra-violet (UV) source of radiation, positioned over a vat of light sensitive monomer. The UV laser source is focussed by a beam expander, and directed through an optical window onto the resin surface. Scanning motion is generated using a dynamic mirror controlled by the positional information from the slice file. Curing is initiated only at the intersection of the resin surface and the laser scan path. Layers are bonded together during the build by 'over curing' the laser through each layer into the layer below.

To prevent the first layer floating within the vat and to provide a datum, a moving platform is immersed in the resin capable of controlled motion in the 'Z' axis. A schematic of the Stereolithography process is shown in Figure 2-9.

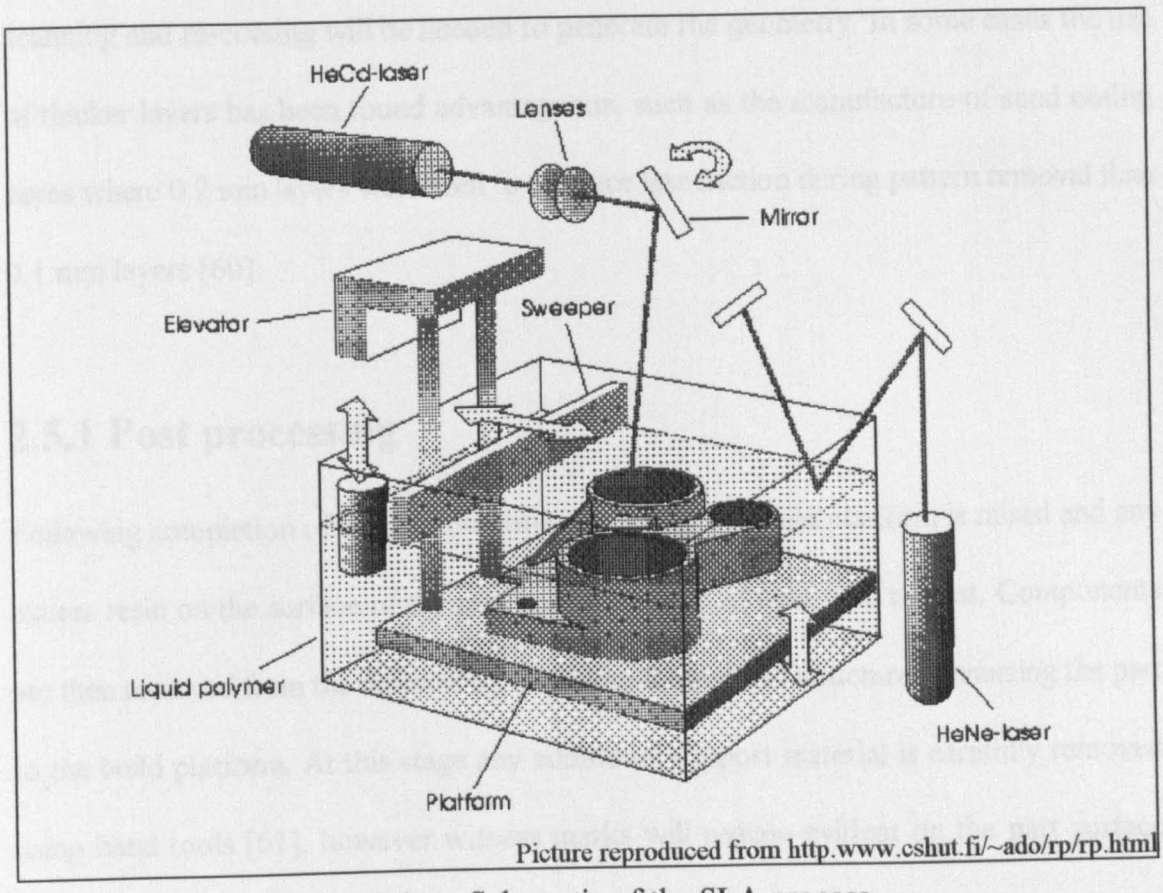

Figure 2-9 Schematic of the SLA process

Following the curing phase of the first layer, the platform is lowered into the vat to allow resin to flow over the surface of the solidified polymer. The platform is then raised up, resulting in the previous layer sitting proud of the resin surface. A wiper blade is then drawn across the surface of the resin to remove any air bubbles and smooth deviations caused by surface tension. The part is then retracted to one layer thickness below the resin surface and the process repeated.

A number of studies have shown that optimum SL layer thickness ranges between 0.05 mm and 0.15 mm depending on the application [59]. Thinner layers are generally considered to produce higher accuracy in the Z-axis [58] and result in lower surface roughness deviation [36]. However, thinner layers will also increase build time as more

scanning and re-coating will be needed to generate the geometry. In some cases the use of thicker layers has been found advantageous, such as the manufacture of sand casing cores where 0.2 mm layers were seen to produce less friction during pattern removal than 0.1 mm layers [60].

2.5.1 Post processing

Following completion of the photo-curing processes, the build platform is raised and any excess resin on the surface of the part is allowed to flow back into the vat. Components are then removed from the machine by fracturing the support structure connecting the part to the build platform. At this stage any additional support material is carefully removed using hand tools [61], however witness marks will remain evident on the part surface unless removed using abrasive paper. Following support removal, the part is immersed in a spray wash tank and rinsed in a solvent solution. The 'green part' is then exposed to intensified UV light, to initiate full photo-polymerisation of any uncured resin. Post curing increases the mechanical strength of the SL resin [62], making the parts suitable for a wide range of applications.

2.5.2 Applications of the Stereolithography process

Through continual process improvement, SL has developed into a highly accurate and repeatable method of component manufacture, with accuracies up to +/- 0.075 mm being quoted by the machine manufacturer [36]. Applications for SL parts include fluid flow models such as valve housings for proving the design of complex pipe-work and ducting [63], models for the aerodynamic analysis of aircraft components [64], patterns for the

photo-elastic stress evaluation of automotive components [65], and complex internal components for the motor industry such as locking assemblies, gearbox designs and dash board layouts [66].

2.6 Rapid Tooling

For many prototype applications more than one 'model' may be required, or the prototype must be manufactured in a production material. Using conventional product development tools, such a scenario would necessitate the manufacture of production tooling, which would be both costly and time consuming during the product development phase. However, a range of Rapid Tooling (RT) solutions have been developed which use layer manufacturing as a method of producing a tool cavity. RT is a generic term used to describe a range of manufacturing technologies associated with reducing time-to-market and providing tooling at a fraction the cost of conventional manufacturing techniques. Rapid tooling is also referred to as soft tooling, low volume tooling, low cost tooling or rapid response tooling.

The principle behind rapid tooling is to utilize both Computer Aided Design (CAD) data and Rapid Prototyping (RP), to produce patterns around which tooling cavities can be manufactured. RT techniques do not rely on lengthy material removal processes such as milling, die sinking or wire erosion [67]. Rather than removing material from a solid block, RT uses a variety of techniques to add material into the form of a cavity.

Two types of RT process have evolved, these being direct tool manufacture and indirect

tool manufacture. Direct RT uses layer-manufacturing machines to produce tool cavities layer on layer in the same way as RP parts are manufactured. A flow chart detailing the manufacturing route for a direct RT cavity is shown in Figure 2-10. Currently, direct cavities are produced from resin using SL [68] or in metallic powder [69], using Selective Laser Sintering (SLS). A considerable amount of research is being directed towards these techniques as tool life and running conditions must be optimized before the process is commercially accepted. By using direct CAD data of the tool cavity, Rapid Tools can be produced in a matter of days in comparison to the weeks needed to produce conventional machined tooling [70]. Although direct RT cavities are not as robust as machined aluminum or steel and may need to be replaced, the increased profit associated with reducing time-to-market can in many cases exceed the additional cost incurred using the technology [71].

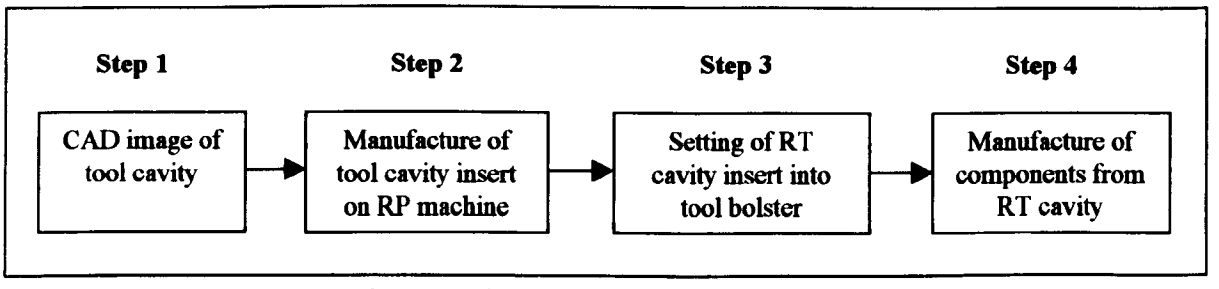

Figure 2-10 The manufacturing route for Direct Rapid Tooling

More commonly, RT cavities are produced by replicating an RP master pattern, using secondary or indirect Rapid Tooling processes, the most common commercially used RT process being silicon tooling. The manufacturing principle for silicon tooling is similar to many other indirect RT processes all of which require an accurate and smooth master pattern produced from CAD data using processes such as SL. The manufacturing route for indirect RT is shown in Figure 2-11. The first step to indirect tool manufacture is to

contain the master pattern in a bolster and coat with a release agent. The master pattern is then encased in liquid silicon [72] or a suitable casting medium such as ceramic [50]. With silicon based tooling, following Room Temperature Vulcanization (RTV) the cavity is cut open and the master pattern is removed. Alternatively, in the case of ceramic tooling the cavity is separated along a pre-defined split line. The resulting tool cavity is then filled either under vacuum or a pastoral pressure with a range of polyurethane based thermo-plastics, formulated to simulate engineering polymers such as ABS, Nylon and Polypropylene [73].

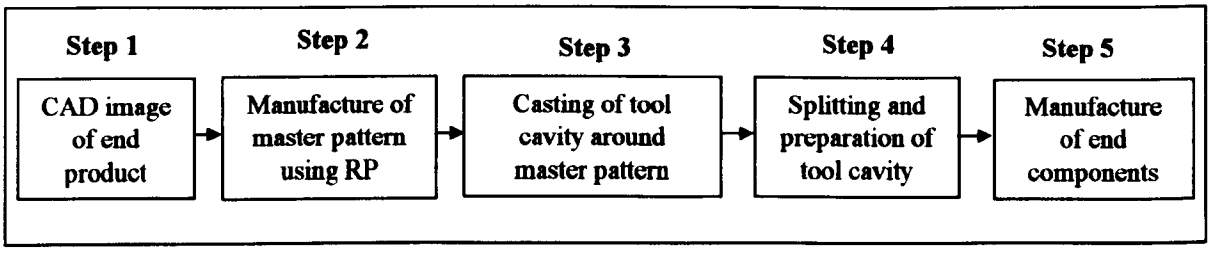

Figure 2-11 The Manufacturing route for In-direct Rapid Tooling

Other indirect tooling processes such as sprayed metal tooling and the powder metallurgy Keltool process can also be used for thermoplastic injection molding and have been used to produce many thousands of 'real' engineering components [74]. Table 2.2. details the current commercially available RT processes, manufacturing lead-times, tool costs and expected tool life [75].

Tooling route	Application	Lead-times	Tool Cost	Tool life
Vacuum casting (Indirect Silicon Tools)	Suitable for the production of low volume thermoset parts	2 days – 2 weeks	Tools £200 - £1000	2 – 20 off
Thin-RIM (Indirect silicon tools)	Suitable for the production of low volume thermoset parts	2 days – 2 weeks	Tools £100 - £900	2 – 50 off
RIM (Indirect silicon tools & sprayed metal tools)	Suitable for the production of low volume / low cost thermoset parts	2 days – 3 weeks	Tools £400 - £2000	2 – 100 off
Spin casting (Indirect Silicon)	Suitable for the production of low melt zinc alloy parts and precious metals	5 days – 2 weeks	Tools £500 - £3000	2 – 500 off
Cast ceramic tooling (Indirect)	Suitable for thermoset and thermoplastic moulding of low temp polymers	2 days – 5 days	Tools £200 - £400	2 – 1000 off
Cast epoxy tooling (Indirect)	Suitable for thermoset and thermoplastic moulding of low temp polymers	2 days – 5 days	Tools £200 - £400	2 – 10,000 off
Spray metal Zinc (Indirect)	Suitable for thermoset and thermoplastic moulding of low temp polymers	2 – 4 weeks	Tools £500 - £4000	2 – 200 off
Spray metal Steel (Indirect)	Suitable for injection moulding of most polymers	3 – 6 weeks	Tools £1000 - £5000	2 – 10,000 off
SL tooling (Direct)	Suitable for thermoplastic injection moulding of PP & ABS	1 – 2 weeks	Tools £300 - £2000	2 – 500 off
Laser sintered tooling (Direct)	Suitable for injection moulding of most polymers	1 - 3 weeks	Tools £500 - £4000	2 – 20 off
Laminated tooling (Direct)	Suitable for injection moulding of most polymers and die casting of aluminium	4 – 6 weeks	Tools £1000 - £5000	2 – 10,000 off
Cast Zinc tooling (Indirect)	Suitable for injection moulding of most polymers	1 – 2 weeks	Tools £1000 - £5000	2 – 1,000 off
Cast steel tooling (Indirect)	Suitable for injection moulding of most polymers and die casting of aluminium	2 – 4 weeks	Tools £3000 - £10,000	2 – 10,000 off
Investment cast tooling (Indirect)	Suitable for injection moulding of most polymers and die casting of aluminium	2 – 4 weeks	Tools £1000 - £5000	2 – 10,000+ off
Keltool (Indirect)	Suitable for injection moulding of most polymers and die casting of aluminium	2 – 4 weeks	Tools £1000 - £5000	2 – 10,000+ off
Electro-formed tooling (Indirect)	Suitable for injection moulding of polymers	4 - 8 weeks	Tools £1000 - £5000	2 – 10,000+ off

Table 2-2 – Rapid Tooling processes, applications, costs and lead-times

2.6.1 TCT

By combining techniques such as RP and RT with 3D CAD, Reverse engineering and Product Data Management (PDM), an emerging group of Time-Compression-Technologies (TCT) have evolved which have had a profound effect on many businesses, in terms of both reduced lead times and product quality [76]. The world-wide revenue generated from TCT now exceeds £360-million and is estimated to exceed £660-million by the year 1999. It should be noted that much of this revenue comes from within the injection moulding industry, which dominates the TCT sector [43]. Although this growth appears impressive, it should be noted TCT represents only a small percentage of manufacturing as a whole, with the European plastics injection molding industry currently valued at £10-billion [77]. If RT is to gain a larger proportion of this market share, the technology must be used to replace existing tool manufacturing techniques such as CNC milling, die sinking and wire erosion. The continued growth of the TCT is therefore dependent on new applications being identified and the transfer of the technology to manufacturing sectors who remain sceptical of tool quality. Such acceptance will only arise with increased process knowledge and quantitative data.

In addition to the limited process knowledge available to the users of RT cavities, one of the main limitations now facing users of Rapid Prototyping and Rapid Tooling is the inherent surface roughness associated with building cavities using master patterns manufactured in additive layers [78]. With subtractive tool manufacturing processes such as CNC milling and die-sinking, much of the lead-time is associated with the finishing of the machined cavity using polishing techniques such as chemical etching, electrode

polishing and Ultra-Sonic Flow Polishing (UFP) [79]. The result is that using conventional techniques, cavities can be produced with a sub-micron surface finish [80]. However, lead-times in excess of 16 weeks are not uncommon within the industry.

The surface roughness of either direct or in-direct RT cavities will always be a function of the initial LMT process roughness, which is inherently greater than conventional tool manufacture. However, the lead-time associated with RT manufacture can be significantly reduced over conventional techniques. Masters used for RT must therefore exhibit surface deviation equal or below that of machined cavities if RT is to compete on a level playing field. At present such surface deviation can only be achieved by applying post-process finishing techniques which will inevitably increase part and tool manufacturing lead times. Analyses have shown the typical surface roughness of Stereolithography components to range between 2 and 50 μm Roughness average [81]. The typical roughness of a production injection-molding tool will not exceed 0.1μm Ra and can be as low as 0.01μm Ra if required [80]. For this reason a significant improvement in RP surface finish is required if RT is to compete with conventional tool manufacture.

2.7 The limitations of SL surface finish

As with all machining or fabricating processes, RP results in distinctive markings on the component surface [82]. This is mainly attributed to the effects of *'stair stepping'* as noted in section 2.4.3 and occurs for all RP components and will be transferred to the rapid tooling system if not reduced or eliminated.

2.7.1 Comparison of RP surface roughness

To-date, the only available data for comparing the surface roughness of the different commercial RP processes has been the result of wider studies. For instance Iuliano's comparative research compared the accuracy of different RP processes and also included some analysis of surface topography [83]. The system manufacturers also publish data, however this is mainly limited to vertical and horizontal surfaces, which tend to be the optimum values with minimal stair stepping. Furthermore those manufacturers quoting roughness have not used a common unit of roughness measurement and so a direct comparison is not possible. Of the system manufacturers, Sanders Prototyping quote roughness figures on sales literature for the ModelMaker II system, producing parts between 32 – 63 micro-inches RMS [84]. However, the relationship between these roughness figures and the surface angle of planes on which they occur is not given, this is essential in order to interpret the results. In 3D Systems publication The Edge, values for the SL process have been quoted between 1.5-8 μm Ra [85]. It should be noted the surface quoted at 1.5 μm Ra is an up-facing plane manufactured using the ACES build style, where no stair stepping is present. Similarly, the 8μm Ra surface is vertical, also on a plane where no stair stepping is present. The 1.5 μm Ra surface roughness may be suitable for some tooling applications, if an RP master pattern could be produced with a uniform roughness at this level. In reality however, few surfaces will exhibit this low level of roughness and many exceed that acceptable for tool cavity manufacture. For example 30-degree surfaces may typically possess a surface roughness value of 40μm Ra.

In order to gain an objective understanding of surface roughness, a number of research

initiatives were undertaken dating back to the early 1990's. As SL has been the most established and largest market sector most of these studies have been directed towards this process.

2.8 Manual post-process improvements

The majority of SL finishing is undertaken manually, using the recommended method of hand finishing with progressively finer grades of abrasive papers and compounds [58]. The process of manual finishing is however highly selective and considered detrimental to model geometry as many of the sharp corners and fine detail are lost [63]. The procedure is both labour intensive and contrary to the philosophy of rapid manufacturing, as all traceability within the automated system is lost. Although some companies supplying RP parts will measure critical planes using Co-ordinate Measuring Machines (CMM), this service is both limited and costly. Statistical data on hand finishing estimates the process to account for over 48,000 hours of skilled labour during 1993 alone [12]. In 1993 the revenue from RP services was valued at £30 million [41], and hence putting the cost of skilled labour and overheads at £40 per hour, it is not unreasonable to assume that hand finishing accounts for approximately 7% of the total cost of RP to the end user. In addition to the costs incurred by manual finishing, the increase in manufacturing lead time must be considered. With small complex geometries it may only take a matter of hours to produce the RP part, however the post-process finishing can take a matter of days [12]

Research into the effects of post-process finishing techniques applied to RP parts was not undertaken until the late 1980's and early 1990's. Up to this point, improvements in

surface finish were the result of changes in the fundamental workings of the RP machines, such as the new build styles, materials and reduced layer thickness [86] and manufacturers simply recommended hand finishing procedures.

The effects of surface finish on RP parts were first discussed in 1991 by Chua and Lee [87]. They demonstrated that stair stepping on an SL model would be replicated into a silicon tool and the subsequent resin castings, if the part was not finished. Initial attempts to reduce surface deviation were undertaken by the research group using a fine grinding head fitted to a pneumatic dentists drill [88]. The process although considered successful was found to be selective and only applicable to a small number of parts where dimensional tolerance of +/- 10% was considered acceptable.

2.8.1 Abrasive 'mass' finishing of SL components

Research into SL part finishing using a range of post-process techniques was reported in the 1992 INSTANTCAM project by both the Instituto-Superior-Technico, [89] and the Danish Technological Institute [90]. It should be noted this research was initiated in 1989 and pre-empted work by Chua and Lee. The research assessed a variety of different finishing systems including spray painting, sand blasting, tumble peening and manual sanding. The processes were applied to a standard geometry with a range of angled surfaces manufactured from acrylic XB 5143 SL resin on the SLA-250. The surface roughness of each of the standard geometries was then measured using a surface profile measurement instrument to assess changes in surface topography. Techniques such as tumble peening and sand blasting were seen to reduce surface deviation by over 50% from

over 30 μm Ra to below 15 μm Ra. However, many detailed features of the standard geometry such as edges and sharp corners were seriously damaged by these techniques. CMM analysis of the parts showed a significant change in part geometry of up to 2% across critical planes. The conclusion of this research area was that manual sanding is the preferential method of surface finishing if geometric integrity is to be maintained within the part as surfaces can be reduced to 5μm Ra with this technique. However, no data on post-process lead times was presented.

A number of 'mass' finishing processes were also investigated in 1993 by Spencer et al [91]. SL parts manufactured in both XB 5081-1 a general purpose resin and XB 5143 a durable acrylic resin were post-processed using barrel and centrifugal tumbling systems in addition to abrasive blasting. The geometry used for this research was limited, as the part contained only vertical and horizontal surfaces. The main research findings established that centrifugal barrel tumbling was capable of reducing surface deviation by 500% to a minimum of 1.25 μm Ra. On inspection using a Scanning Electron Microscope (SEM) extensive damage to parts was seen following both centrifugal and barrel tumbling. Damage occurred in two forms, either by the rounding of edges and corners on the durable XB 5180-1 or the shearing of material at edges and corners of the general purpose XB 5143. The research concluded that barrel tumbling resulted in less part damage than blasting or centrifugal tumbling, however the process can take a number of days to reduce surface deviation to 1.28 μm Ra.

Further work by Spencer et al during 1993 [92] applied XB 5180-1 and XB 5143 SL

parts to a vibratory finishing system using both fused ceramic and resin bonded ceramic abrasive media types. Process duration was limited to 1 1/4 hours, which although suitable for the final polishing of hardened tool steel [93], did not yield any significant changes in the surface roughness of the polymer parts. Further work by Spencer at al, also attempted to reduce SL surface deviation using ultrasonics abrasive polishing [94]. A system was developed whereby an SL part was retained in a closed vessel containing a carborundum abrasive powder. The sealed vessel was then agitated using an ultrasonic horn. Experimentation was limited to only a seven-second period and applied only to the durable XB 5143 resin parts. On visual inspection, significant damage to the part was observed with little change in surface deviation. No detail of process frequency or media variation was given and research did not continue.

During 1993 Lee [95] continued earlier work by Chua into the application of SL jewellery master patterns for down stream tooling. Research evaluated both vibratory bowl and barrel finishing using a range of ceramic media in addition to abrasive jet deburring using 30 μm glass beads. The test sample used was a simple ring design of approximately 25-mm diameter with three tapered spikes. As with Spencer's earlier work, a short experimental processing time of 1 hour and 45 minutes applied to both vibratory and barrel finishing respectively did not yield significant reductions in surface roughness. The work simply reports that *a 'smooth surface was obtained but marks not well removed'*. Abrasive jet blasting was visually seen to give the best reduction in surface roughness after only one-minute of processing. However, due to the limited geometry of the samples no quantitative surface data was derived from the investigation.

In retrospect, the failure of this early research work into post-process SL finishing was both the limited abrasive media types and limited process duration applied to the SL models. With the exception of the INSTANTCAM research, none of the test samples were specifically designed for roughness analysis. Hence, much of this early research does not quantify the changes in surface topography in terms of roughness average.

Mass finishing processes are well documented [96] and a number of studies into the mass finishing of conventional polymers have been undertaken. However in the case of polymers, such research is noted as being, *'one of the most undocumented areas of mass finishing'* [97]. The most common form of polymer surface finishing to-date is barrel tumbling, using modified equipment and specialist pre-form media [98].

During the 1980's a system was developed for the *'dry process mass finishing'* of thermoplastic mouldings [99]. The system was adapted from a conventional tumbling machine, incorporating a hardwood barrel liner. Through a reaction between the abrasive media and the hardwood lining, friction induced heat within the system is seen to cause micro-deformation of a thin layer at the periphery of the components. This peripheral layer then becomes 'plasticised' due to the localised heat, causing 'peaks' to flow into adjacent 'valleys' [100]. For dry process mass finishing, a range of 'composite' abrasives has been developed, using pre-formed hardwood pellets impregnated with a resin binder and silicon powder [101].

Based on this system, an EPSRC research project was undertaken by the author at the University of Nottingham to investigate the effects of dry process mass finishing on SL

parts [102]. Using a bespoke hardwood barrel, a series of experiments were undertaken to establish optimum process parameters for the finishing of both epoxy XB 5170 resin and acrylic XB 5149 resin parts produced on an SLA-250. Using a range of specially designed geometries with a range of surface angles including vertical, horizontal, 45 degrees and 30 degrees the most effective media types and abrasive additives were established, in addition to the optimum process duration. The research found that significant reductions in surface deviation were attainable on all planes and 5 μm Ra could be achieved on surfaces initially possessing 40 μm Ra. However, this improvement is at the expense of a loss to part edges and corners. Figure 2-12 shows a part before and after 4hours barrel tumbling in ceramic media and it can be seen that although surface deviation has been reduced geometric integrity has been severely affected.

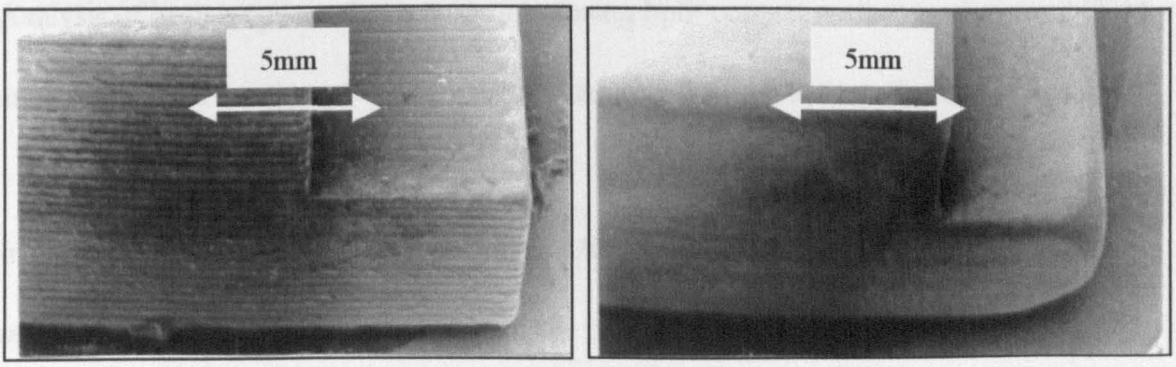

Figure 2-12 – Topography and geometry of acrylic part before and after tumbling

As the SL resin is thermosetting, the effects of plastic deformation would be limited; hence any smoothing was the result of abrasion alone.

Similar, optimisation experiments were undertaken by the author using vibratory finishing, ultrasonic finishing and abrasive flow machining [102].

Using a conventional vibratory finishing system, a range of specialist hardwood finishing media were processed with both epoxy and acrylic SL parts to assess the reduction in surface deviation possible using such a system. The research concluded that the specialist hardwood media was of insufficient mass to function correctly in the vibratory finishing process. Hence, irrespective of process duration, no change in surface roughness was noted.

A system was also developed using a liquid filled tank fitted with 2K watts of ultrasonic transducers. The liquid in the tank was then impregnated with a range of abrasive media and held in suspension with surfactant. The principle of the system was to use ultrasonic cavitation to initiate motion of abrasive particles over an SL part immersed within. Analysis of both acrylic and epoxy samples using both contact surface analysis and SEM analysis showed no change to parts using this system, irrespective of process duration.

In addition to the mass finishing systems such as barrel tumbling and vibratory finishing, research by the author also assessed the use of abrasive flow machining on SL components [102]. Abrasive flow machining or the Extrude-Hone process, reciprocates an abrasive loaded 'putty' over the surface of a work piece clamped between two chambers. As the abrasive media flows over the part, material is then progressively removed from high-points. The process is conventionally used for the finishing of gas flow pipes, automotive engine bores and turbine blades. Ultrasonic Flow Polishing (UFP) is a similar system developed by the company for the polishing of tool cavities and dies, but uses an additional ultrasonic motion applied to the abrasive through a horn attached to the machine nozzle. With UFP the work piece is retained in a bed and a nozzle is used to

direct the abrasive media over the part. Through consultation with Extrude-Hone, research by the author has applied specially designed epoxy SL parts to both abrasive flow machining and ultrasonic flow polishing. On advice, experimentation was only undertaken on epoxy resin, as acrylic resin was considered too brittle for either process. Using abrasive flow machining an SL component with a number of through cavities was processed using different abrasive media, flow rates and system pressures. The research concluded that for parts with >5mm wall thickness abrasive flow machining was capable of reducing surface deviation to below 2 μm Ra on SL parts possessing an initial 40μm Ra roughness. Due to the pressures involved in the Extrude-Hone process parts with walls below 5-mm were seen to fail during processing.

A test sample with a range of angled planes in 10-degree increments from 0 to 90 degrees was also finished using the UFP process. Although limited to only 3 types of abrasive media this research did show that SL surfaces can be polished to below 1 μm Ra, however control of the process is difficult as different parameters were required for different surface angles. The research concluded that both processes show promise for the post-process finishing of SL parts if further process optimisation is undertaken. It should be noted that both processes are now under investigation by the Rapid Prototyping and Tooling research group within the UK automotive manufacturer Rover Group. The company see abrasive flow machining as a method of reducing the surface deviation on the internal surfaces of SL parts such as engine manifolds and exhaust pipes. They are also assessing the application of UFP in the finishing of direct rapid tool cavities produced using both the SL and SLS processes.

To summarise previous research, it can be concluded that abrasive finishing is not suited to RP parts, as the high degree of dimensional change cannot be tolerated if parts are to be used for applications such as master patterns and tool cavities. At present no abrasive finishing system is wholly suited to the finishing of SL parts as those which reduce surface deviation also change part geometry. Processes such as abrasive flow machining and ultrasonic flow polishing may be suitable for finishing without causing excessive change to part geometry. However, both processes require specialist machine tools and require process lead times in the order of 1 to 5 working days.

2.8.2 Additive finishing of SL parts

One alternative to the removal of material from RP parts is the addition of material to fill the stair stepping caused by layer manufacturing. During the preparation of rapid tooling patterns, a number of additive coatings are often used to impart specific properties to the RP part surface. Coatings include release agents for techniques such as sprayed metal tooling [103], surface fillers such as wax for investment casting [104] and as conductive coatings in the manufacture of electroplated tooling [105].

Additive coatings research was also undertaken during the INSTANTCAM project in 1992 [89][90]. Electrical Discharge Machining (EDM) electrodes were produced through the metallizing of SL part surfaces using both copper and chromium plating. Analysis showed the surface roughness of vertical, horizontal and 45-degree surfaces to have reduced from 10μm Ra to below 7 μm Ra, 4μm Ra to 3.5μm Ra and 30μm Ra to below 20 μm Ra respectively. Given the limited geometry of the test sample no data was given

for other surfaces.

Research into SL electrode manufacture by Arthur in 1996 [106] also demonstrated the partial filling of steps by the metal coating of RP parts. He found that the system replicated the surface detail of the part and transferred it to the EDM electrode surface on the tool. Although no quantifiable data was produced, he concluded that a significant degree of post-process polishing would be required following the use of SL die-sinking electrodes, if the cavity was to be of similar quality to one manufactured using machined copper electrodes.

Research into photo-elastic stress analysis by Farrell and Roth [107] applied specialist reflective coatings to acrylic SL test samples manufactured from XB 5143 resin. Using between 4 and 8 layers of photosensitive stress-coat, they showed that 'stair-stepping' could be masked on models used for both static and dynamic stress analyses, however no mention of the effects of coating on part accuracy and geometry were reported.

Research at the University of Nottingham has investigated the effects of a number of coatings applied to SL parts used as sacrificial patterns for investment casting. A test sample with vertical, horizontal, 45-degree and 30-degree surfaces was coated by spraying, dipping and hand painting using both investment casting wax and epoxy primer. Although many of the coatings were seen to yield exceptional reductions in surface deviation the change in geometric integrity was excessive. For instance, the surface roughness of a typical sample dipped in 2 layers of epoxy primer was found to reduce from 40μm Ra to below 2 μm Ra. However, the process did not produce a uniform layer

thickness and the critical dimensions of the part were seen to change from 25mm to over 28mm. [108]. Figure 2-13 shows a sample coated in both 2 and 10-layers of epoxy filler material applied by dipping. It can be seen that the coating produces an inherently smoother surface, but the geometry of the part is significantly changed.

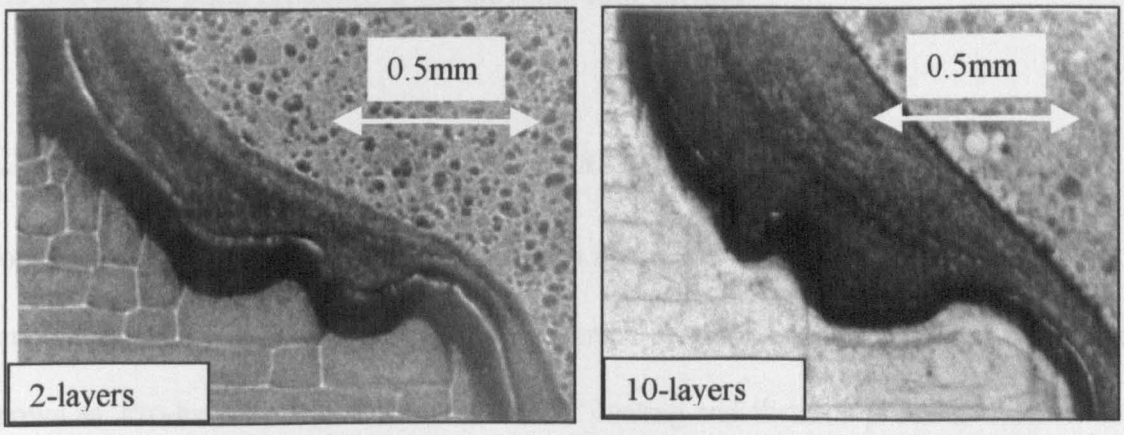

Figure 2-13 The effects of variable thickness coatings on SL geometry

For many applications, research did identify a number of useful coating techniques and materials were identified. These included epoxy and acrylic-based primers and top coats, in addition to PVD and ion-implantation coatings used to impart conductive surfaces onto acrylic and epoxy SL parts. [109].

A comparative study on the finishing of SL master patterns used for indirect Rapid Tooling was undertaken in 1995 by Chadwick [13]. His research identified the most common functional coatings used in the preparation of SL master patterns for silicon tooling, epoxy cast tooling and sprayed metal tooling. Through surface analysis of the SL test samples, the tool cavity and a series of production mouldings, Chadwick showed functional coatings can be used to reduce surface roughness by up to 88 %. The research

showed that by adding a number of coats of high build primer, roughness on the master pattern could be reduced from 36μm Ra to 4μm Ra. As with earlier research however, the application of such coatings increased critical dimensions by up to 10%. The research summarised that although significant reductions in roughness were possible, part geometry was rendered unacceptable on master patterns and would be replicated through tooling into inaccurate parts produced from the rapid tool cavities.

2.8.3 Combining additive & abrasive finishing

To-date, only one patent application has been filed for the post-process finishing of SL parts. U.S. based Pro-Tech Engineering, claimed in 1993 to have patented a process known as 'Pro-lux finishing'. Pro-lux is a *'dual'* coating and abrasion process, which when applied to SL components is claimed to achieve almost mirror like surfaces [110]. However, no quantifiable results of this process have been published. Consultation by the author with Pro-Tech Engineering in May 1997 suggests that the patent has not been successful and only the name is protected by copyright. The process uses an epoxy based high build primer coating, which is manually abraded following curing.

A similar process to Pro-Lux finishing was investigated by the University of Nottingham, for Rolls-Royce aerospace and used to improve the surface of SL master patterns used in investment casting [111]. The process termed 'Dual Finishing' is a combination of epoxy primer coating and dry process mass finishing in a modified barrel tumbling system. Following process optimisation with a range of standard test sample and abrasive media types, the process was applied to a number of Rolls Royce SL turbine blades master

patterns. Using contact roughness analysis, the average reduction in surface deviation over four critical surfaces was 12.26μm Ra before processing to 1.29μm Ra after processing. Although this roughness value was lower and the process achieved the 2.2 μm Ra bench-mark set by Rolls-Royce, CMM analysis showed the parts to be outside the geometric tolerance allowed for SL turbine master patterns used for investment casting.

In summary, it has been shown that attempts to reduce roughness by adding material or removing material from SL part have all resulted in an unacceptable loss to geometric integrity. This is particularly important if the parts are to be used as either patterns for indirect RT manufacture or as direct RT cavities.

2.9 In-process factors affecting surface deviation

One alternative to the post-process finishing of RP parts is through changes to the fundamental workings of the layer manufacturing process. This can be achieved through modifying either the layer thickness or the profile of each layer edge, to form a closer approximation to the original CAD model.

2.9.1 Effects of layer thickness

For a given layer thickness stair stepping will always produce surface roughness. This can be quantified in terms of the surface roughness average (Ra) which is shown as a function of the layer thickness (α) and the surface angle (θ) in Figure 2-14.

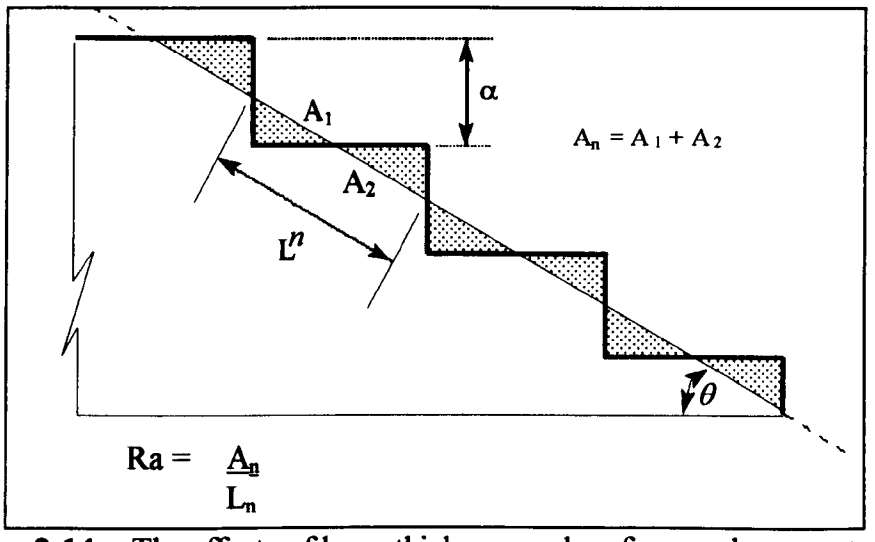

Figure 2-14 The effects of layer thickness and surface angle on part roughness

Reducing layer thickness has been investigated by Ikuta, using a scaled down photo-curable system similar to the SL process [112]. Photo-polymerisation takes place through a quartz screen onto the base of a movable stage, rather than from above. This system configuration benefits from there being no surface tension in the 'cure zone'; hence very thin layers can be produced. The system uses 1μm layers and claims an X-Y accuracy of 0.25 μm as compared to the +/- 75μm tolerance quoted by 3D Systems [36]. The main limitation of the process is build time, which can run into many days for objects any larger than 10 mm^3. Micro-layer manufacture has also been investigated by Loechel and Maciossek [113] using a micro UV curing system capable of producing 6 μm layers. Components have then been galvano-plated with Fe/Ni alloy and used in the microelectronics industry.

On a Nano-technology scale, research by Pegna et al has used a gas-vapour deposition technique to build cylindrical structures in nickel and graphite using 0.1μm layers [114].

However, excessive build time prevents manufacturing parts of significant size and limits the process application to very specific manufacturing sectors.

2.9.2 Layer Profile

Research has also addressed how modifying the profile of layers using variable cutting, curing or deposition angles can affect the roughness of laminated components. By producing layer edges tangential to the desired surface a *'near net'* representation of the CAD geometry can be achieved. An adaptation to the LOM process by Cawley et al [115] uses a six-axis robot to manipulate a laser cutter over sheet material. Given the almost limitless motion of the system it is possible to cut each layer with a varying profile at the desired angle. Layers are then stacked and aligned as a post process operation. One significant advantage of the system is the ability to use variable thickness laminates of any material, hence reducing manufacturing time on large parallel sections [116].

A variation to the SL process, using modified layer profiles was proposed in 1993 by Mashinsky [117]. Through the use of an optical fibre, Mashinsky demonstrated that it is possible to construct a five-axis photocurable system capable of *'stepless SL manufacture'*. The resin is cured tangentially to the CAD file and not perpendicular to the Z-axis, as with current technology. However, due to both process accuracy and patent infringements these modifications have remained within the research domain.

One of the limitations to these types of modification is that existing LMT hardware must be replaced with new tools and so commercial acceptance and take-up is slow. Some

improvements in surface finish by research groups in Japan and the USA have been made and these are now explained.

Work by Narahara at the Kyushu institute of technology, has investigated the use of meniscuses of liquid resin trapped between layers during the build process [118][119]. The meniscus is generated by retracting the SL platform above the level of the vat producing a meniscus effect on the surface of the resin. It is then locked in place by the laser using scan data from the previous layer. Narahara's research which was undertaken on a SONY JSC 2000 SL machine, with Japanese Synthetic Rubber company resin JSR 200 was successful, but only for surfaces between 10 and 30 degrees. In retrospect, the limited success of Narahara's research appears to be due to the limited number of process parameters investigated during the study. Narahara only assessed the effects of meniscus smoothing on parts with different layer thickness. He did not assess what affects meniscus shape and the influence this has on the surface roughness of different angled planes.

A similar solution to Narahara was patented in 1992 by Smalley of SL manufacturers 3D Systems [120]. The patent covers a range of theoretical solutions to surface roughness reduction using the existing SL machine configuration. Smalley suggested the use of either single or multiple meniscuses in addition to the use of thinner layers and combinations of thin and thick layers throughout a single part. Although extensive, no practical evidence was presented with the patent to corroborate any of Smalley's theories.

To date no practical results have been shown by any party on the use of in-process smoothing using the market leading 3D Systems SLA technology.

2.9.3 Reducing the deviation of other RP processes

A number of research initiatives have been undertaken to improve the surface roughness of other commercial RP systems. However, they have met with limited success. Research by DTM Corporation to reduce the surface deviation of the SLS process was reported by McAlea in 1996 [121]. Their approach was to develop new build materials formulated as finer powders, and new build styles enabling the manufacture of thinner layers. McAlea demonstrated that parts produced using the new 'Trueform PM polymer' have a surface deviation of 5.5μm Ra on up-facing planes. This is some 20% of that of parts manufactured using the earlier SLS polycarbonate material, which produces up-facing surfaces with a 28μm Ra roughness. Of the test samples produced, McAlea also demonstrated that parts can be hand finished to achieve low surface roughness values. A polycarbonate part was hand abraded to 6.8μm Ra and the Trueform PM part was abraded to 0.6μm Ra. The final surface roughness of the SLS parts was seen to be a function of the powder particle size and so appeared to be a limiting factor.

Other research by Tumer et al has made a study of the mechanisms affecting surface deviation in the SLS process [122]. Using a series of standard test samples positioned in a variety of build orientations, they studied the effects of process attributes on part roughness and mechanical strength. The study investigated parameters including particle size and distribution, the shifting of layers during the re-coating process, layer thickness, laser power and part orientation. The research showed that laser power, layer thickness and build orientation all have a significant effect on surface deviation. However, no

comparison of different parameter settings was reported.

The research concluded that with the SLS process a 'trade-off' must be made between surface roughness and part strength. If a good surface finish is required, a low scanning power must be used. However, low scanning power will result in inherently weak parts. As a result, when trying to improve surface quality, other measures of quality, such as part strength, must be considered.

Research by Sachs et al, has improved the surface deviation of parts made using the 3D printing process by optimising the position of drop placements [123]. In many ways 3D printing is similar to conventional 2-dimensional ink jet printing but the main difference is that the paper is replaced with a powder bed capable of motion in the Z-axis. As the print head scans in the X and Y-axis, a molten binder is ejected from nozzles in the head through rapid heating and subsequent expansion. As the molten binder falls onto the build platform, rapid cooling takes place, binding the powder on the platform around the droplet. As the print head moves each layer is formed by selectively switching the binder nozzle on and off. After each layer is scanned the build platform is retracted and a fresh layer of powder is distributed across the previous layer. The binding process is then repeated and the process cycle continued until the part is complete.

Using high speed optical sensing Sachs et al noted that much of the surface roughness in 3D printing is a function of small changes in the position and velocity of the print head during the binder deposition phase. Using real-time measurements a control strategy was developed to accurately position drops of binder onto individual particles of powder.

Using the system the positioning of droplets was improved from +/- 100μm, to within 10μm in a fast scan mode and 3μm in a slow scan mode, the result being much smoother surfaces. However, no quantifiable data has been published to corroborate this claim.

Other research activities into the finishing of RP parts include work in the USA at both the California State polytechnic and Ann Arbour University, into reducing the surface deviation of the FDM process using new build styles and materials. Work is also being undertaken in the UK, at Nottingham University, on the finishing of 3D Systems Actua parts using solvent and chemical based techniques to dissolve surface imperfections. At present all this work remains at undergraduate level and has not reached publication.

CHAPTER 3

3.0 Experimental Methodology

Although the research activities for reducing surface deviation of Rapid Prototyping parts have intensified, no solution has been presented that will improve SL components to a level whereby manual finishing can be eliminated.

From the review of previous work, it is the author's opinion that if SL parts are to be used as either direct RT cavities or master patterns for indirect tooling, post-process finishing should be avoided. Research should therefore be directed towards improving the existing SL build process to achieve an acceptable roughness for down stream applications.

Given the limited and often misleading data available on RP part roughness, it is the intention of this research to develop a greater understanding of the fundamental characteristics of generic LMT surface topography and to determine the process attributes responsible for producing high surface deviation in the SL process.

3.1 Comparative analysis of LMT surface roughness

In order to develop an understanding of LMT surface topography, an experimental methodology has been derived. This is shown in Figure 3-1 and begins with a comparative analysis of different layer manufacturing process, which forms the basis for an evaluation of process attributes effecting surface roughness. The program of research starts with the design of a test sample from which accurate roughness measurements can be obtained. The methodology goes on to identify suitable LMT process by which the test geometry can be manufactured. Using both roughness measurement and microscope analysis, the process attributes affecting surface deviation will be identified. From the surface analysis

of the test samples, a mathematical model will then be developed to assess the degree each attribute within the build process has on surface deviation. By comparing the mathematical model against measured data it will then be possible to verify the accuracy of the model and the roughness attributes against different SL parts. Having identified the cause of surface deviation within the SL process, research will then be directed towards modifying those attributes seen to produce rough surface topography.

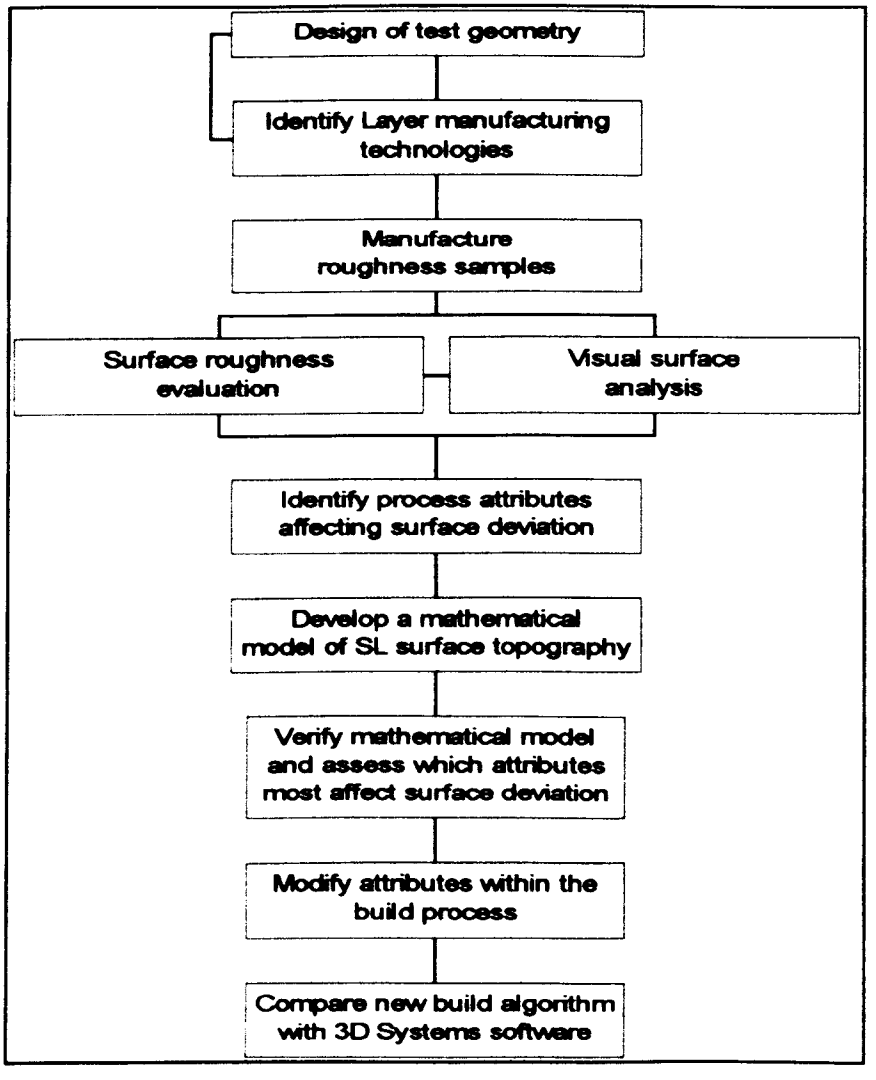

Figure 3-1 Methodology for comparative roughness study and improvement of SL process

3.1.1 Design of roughness benchmark

In order to make an accurate comparison of different layer manufacturing mechanisms an appropriate test geometry was required from which accurate topographic data could be measured. Given the very limited data available on commercial LMT surface deviation, a suitable test geometry must exhibit a varied range of angled planes, in addition to both the horizontal and vertical surfaces such that it represents typical RP parts. The geometry shown in Figure 3-2 was designed by the author for this reason. It possesses both up-facing and down-facing planes and provides 0-90 degrees surfaces in 10-degree increments, with sufficient surface area to derive accurate statistical roughness measurements, yet maintain an overall build volume that can be easily manufactured using a range of different layer manufacturing technologies.

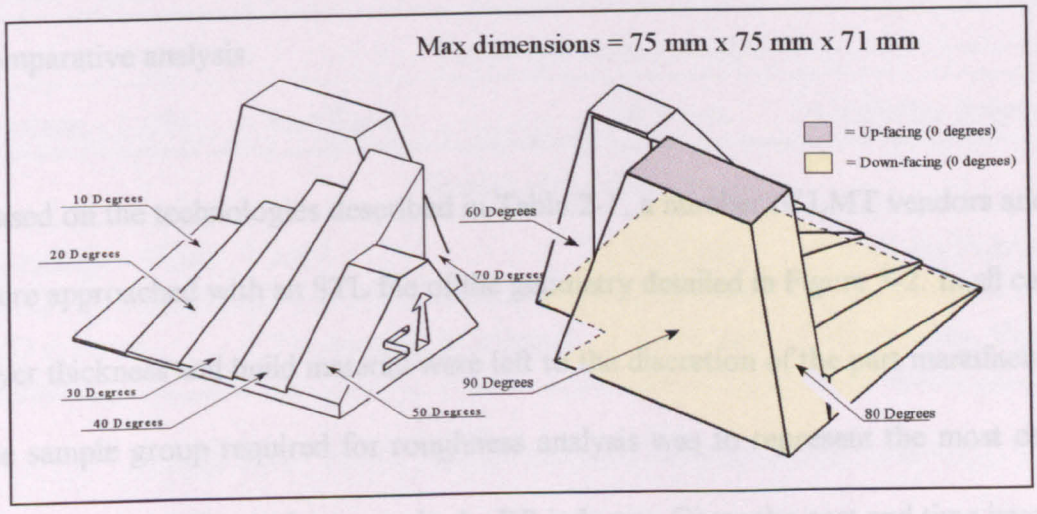

Figure 3-2 Surface roughness benchmark geometry

3.1.2 LMT process selection

Although all RP systems use layers to produce components, the thickness, material and make-up of layers differ greatly for each process. When considering a comparative

analysis of machine types, it is important to include as many different layer manufacturing mechanisms as possible. For this work only North American and European technologies have been considered, which encompasses all the main commercial LMT mechanisms and represents over 80% of the worldwide RP market.

Of the commercial processes described in section 2.2, only the drop-on-demand inkjet process was excluded from this study, as the manufacturer Sanders declined to benchmark their product against their competitors. With the exception of this technology, the 14% of the remaining RP market, is represented by eight Japanese manufacturers. Seven of these have simply replicated the Stereolithography process, the eighth having replicated the LOM process. It can therefore be stated that with the exception of the Sanders 'model-maker', almost 95% of the world's RP techniques have been included in the comparative analysis.

Based on the technologies described in Table 2-1, a number of LMT vendors and users were approached with an STL file of the geometry detailed in Figure 3-2. In all cases the layer thickness and build material were left to the discretion of the part manufacturer, as the sample group required for roughness analysis was to represent the most common parameters used for each process in the RP industry. Given the cost and time involved in sample manufacture, only one part per manufacturer was requested from each source. More components would have been accepted but given the high level of process repeatability quoted by the RP machine manufacturers, it is the author's opinion that one sample is representative of each process. Table 3.1 lists the LMT processes used in this study in addition to the build material, layer thickness and part source.

LMT Vendor & Process	Material / Build Style	Layer Thickness	Source
	Photocurable systems		
3D Systems – SLA	Epoxy 5170 ACES	0.15 mm	University of Nottingham
3D Systems – SLA	Acrylic 5149 STAR Weave	0.125 mm	University of Nottingham
Solider – Cubital	Solimer – G/506001 Acrylic	0.15 mm	Schneider Prototyping, Germany
	Sintered powder systems		
EOS – EOSINT P	Polystyrene	0.2 mm	EOS GmbH, Germany
EOS – EOSINT P	Polystyrene / Wax Impregnated	0.2 mm	EOS GmbH, Germany
DTM – SLS	Fine Nylon	0.1 mm	University of Leeds, UK
	Laser cut sheet systems		
Helysis – LOM	Fast Paper	0.1 mm	California Polytechnic, USA
	Molten deposition systems		
Stratasys – FDM	ABS	0.25 mm	California Polytechnic, USA
3D systems – Actua	Thermosetting polymer	0.099 mm	3D systems, Valencia, California

Table 3-1 LMT process included in the comparative study

3.1.3 Manufacture of roughness benchmark

All models were built full size from the supplied STL file, and returned to the University of Nottingham for analysis. The collection of supplied samples is shown in Figure 3-4.

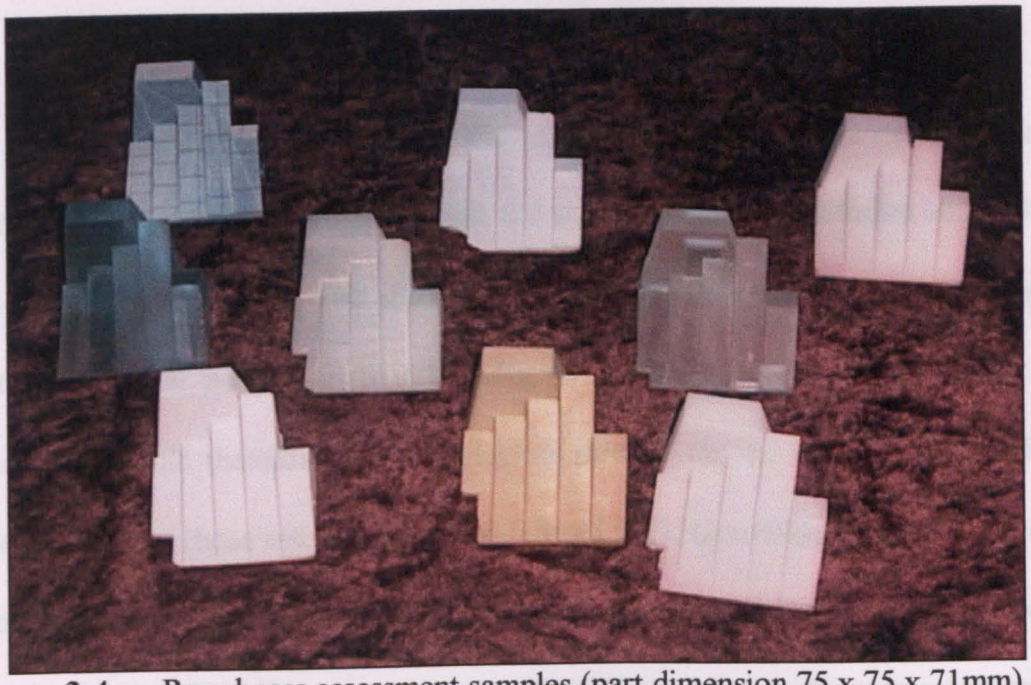

Figure 3-4 Roughness assessment samples (part dimension 75 x 75 x 71mm)

Although it was stressed by the author that no post process finishing to the models was to be undertaken, some light surface abrasion was clearly evident on the Cubital model supplied by Schneider prototyping. For this reason, no direct roughness comparison was made between this part and other test samples.

3.1.4 Roughness measurement units

From the literature review, it was found that of the small amount of roughness data published on LMT surface topography, no direct comparison could be made between parts quoted by either the manufacturers or researchers as different units of roughness measurement had been used. Therefore in order to assess part topography and quantify roughness, a standard unit of measurement must be defined. However, over twenty recognised standards of unit exist for topographic measurement, each developed for a specific application [124].

When considering a topographic assessment of LMT components, we must take into account the deviation between the roughest and smoothest surfaces. Studies undertaken during the INSTANTCAM project showed roughness deviation can vary between 1.5μm Ra for a horizontal surface up to 60μm Ra for an angled surface [90]. A unit of measurement should therefore be used which is suitable for the analysis of glass like surfaces through to those resembling 3-axis milling [125]. Given this level of deviation, the most suitable units have been identified as either peak to trough deviation (Rt.), Root Mean Squared (RMS) or Roughness average (Ra) [124]. A schematic representation of each measurement unit is detailed in Figure 3-5.

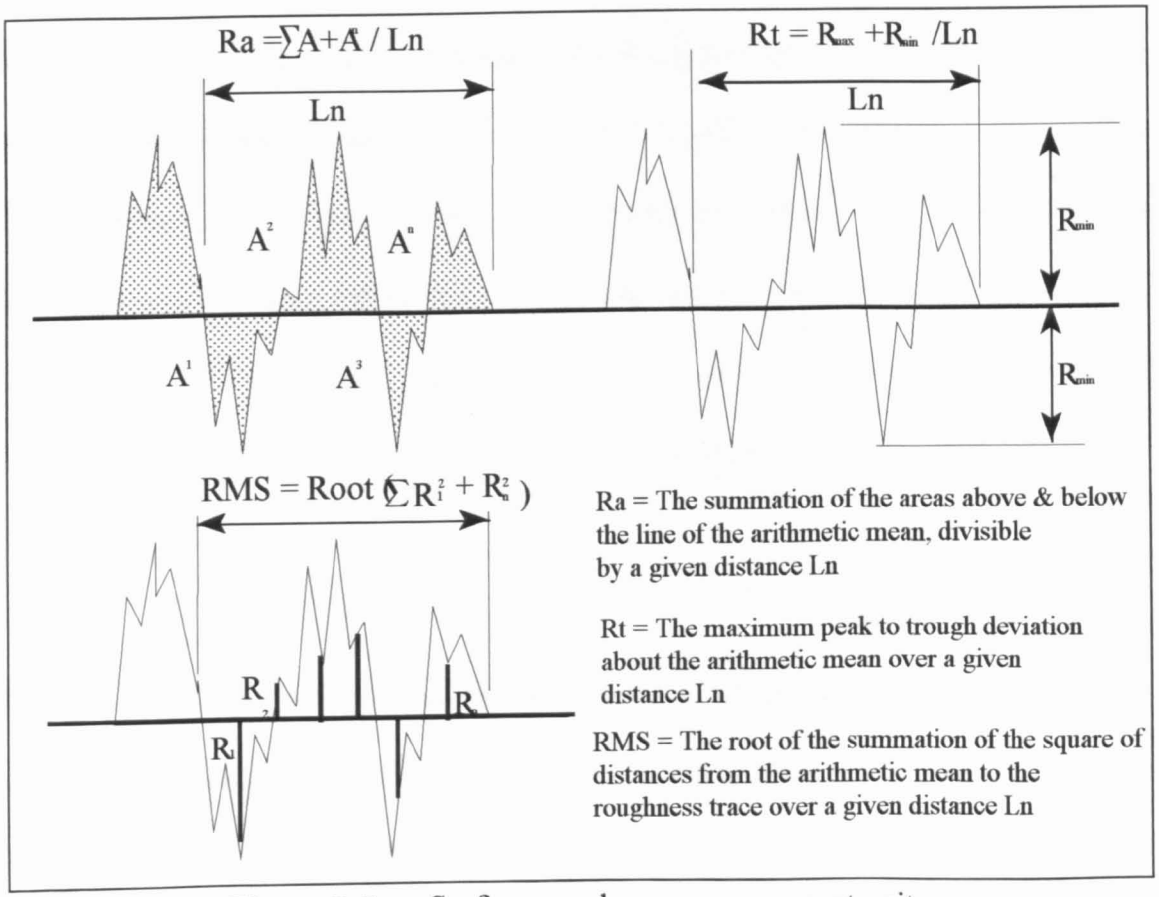

Figure 3-5 Surface roughness measurement units

Rt. is simplistic and only gives a limited picture of surface deviation. The measurement

only considers the highest and lowest points of surface topography over a given sample length. Hence less pronounced features are neglected, irrespective of their frequency. Similarly, RMS measurement is only a limited approximation of true surface roughness, as the system uses a low sampling frequency of 10 measurements per cut-off, missing much of the surface texture. Roughness average (Ra) is therefore considered to be the most suitable measurement unit for analysing layer manufactured parts. Ra is defined as, the summation of all the areas above and below the line of the arithmetic mean (A_n), over a given distance (L_n) as described earlier in section 2.8.1.

3.2 Measurement of surface roughness on LMT samples

Roughness average represents the most common form of topographic measurement, and is supported by a wide variety of contact and non-contact measurement devices. For this research the surface topography of each LMT sample was analysed using a Rank Taylor-Hobson, 'Surftronic 3' contact measurement instrument. The contact probe was interfaced to a PC based surface analysis package and calibrated to +/- 0.1 μm Ra using a Rubert gauge. Topographic data was then converted into Ra units using a computer analysis package, capable of analysing surfaces between 0.01 μm Ra and 100 μm Ra [126].

Roughness data was derived using the maximum ISO sampling distance of 2.5 mm (L_n). However, the surface area of the part used for scanning must be somewhat larger. The Surftronic collates data over 7 consecutive sample 'cut-offs', using a total probe movement of 17.5 mm. The resulting Ra value was then calculated as the average of the

5 middle cut-offs. The first and last cut-off values were discarded to allow for disturbance and damping caused by acceleration and deceleration of the contact probe [127].

One major limitation to scanning LMT surfaces using a contact Taly-surf is the relationship between topographic frequency and the 'cut off' distance (L_n). When the distance between layers nears or exceeds the maximum cut-off distance of the probe, surface roughness measurements become distorted. Hence, for low angled surfaces with a high degree of stepping, roughness measurements may deviate greatly between scans. This can be seen graphically in Figure 3-6, where six random samples of roughness data were derived from each of the angled surfaces on the 3D Systems Epoxy SL model. As surface angle increases, so the number of peaks and troughs per cut-off also increases. The positioning of the probe becomes less critical and the roughness data becomes more reliable and indeed the measurements appear to deviate less. For this reason, all roughness values used in this research were the average of six measurements taken at random positions across the sample surface.

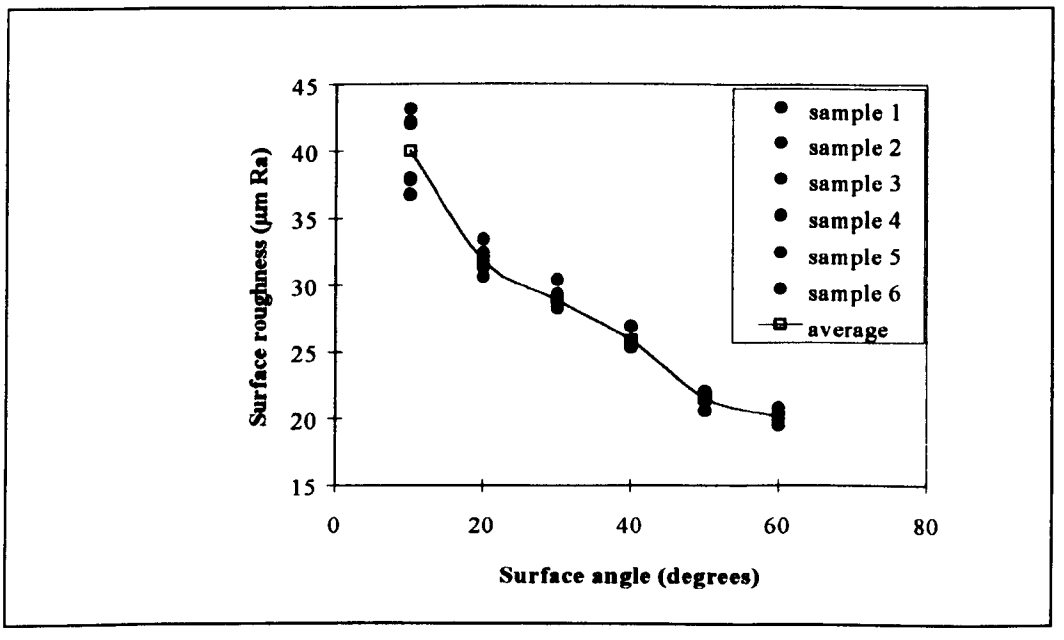

Figure 3-6 Roughness sampling error due to insufficient cut-off length

3.3 Comparison of roughness on LMT samples

To measure the samples accurately, a variable angle measurement jig was constructed to position the surface of interest parallel to the Taly-surf probe. Each sample was then scanned at six random positions, with the average roughness being recorded for statistical analysis. The results of the Ra measurements can be found in Appendix B.

By plotting the relationship between surface angle and roughness deviation using the data from Appendix B, a comparison between different LMT surfaces has been made. This is shown in Figure 3-7.

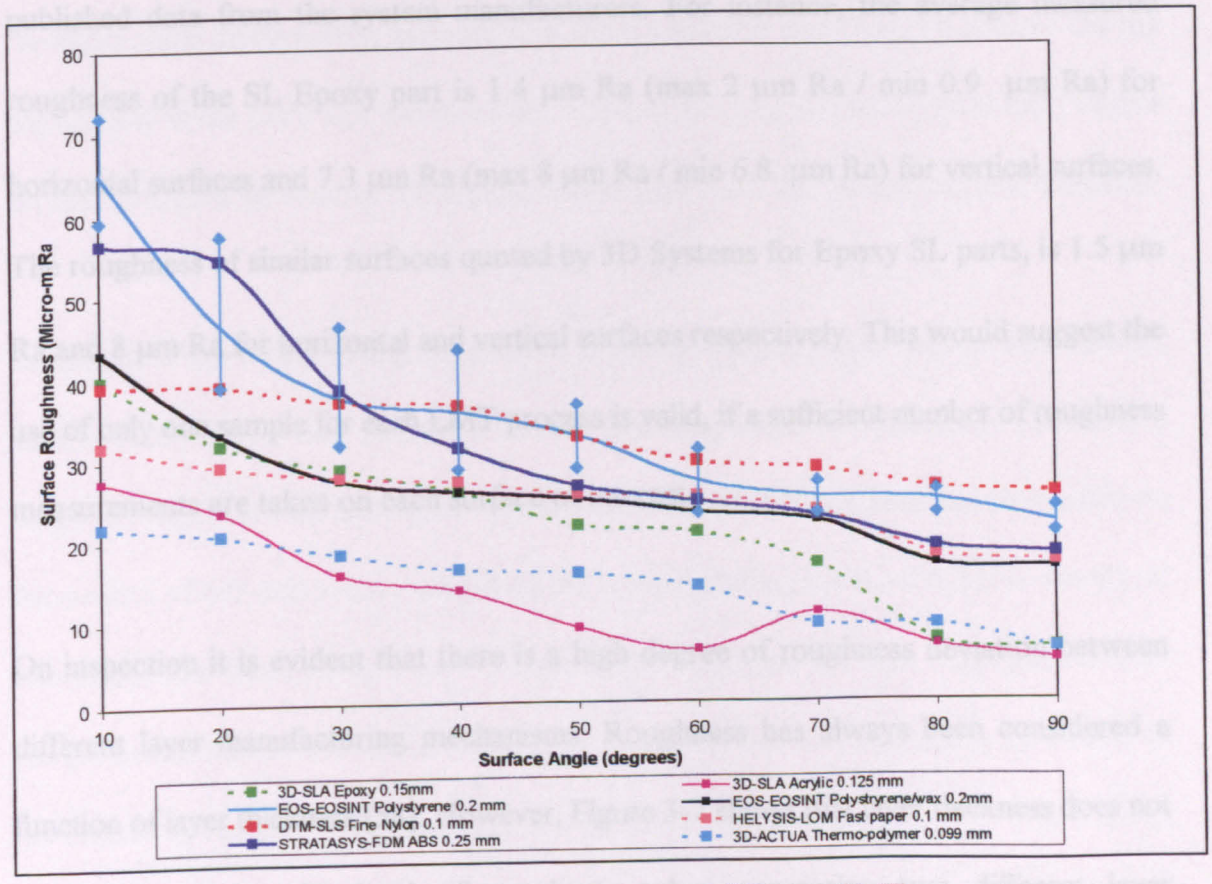

Figure 3-7 Measured surface roughness of different LMT processes

The figure shows the surface deviation for each of the LMT process between 0 and 90-degrees. It can be seen that each sample exhibits a similar roughness trend, with the lower

angled surfaces exhibiting higher surface roughness than the steeper planes. This is attributed to the area of surface deviation above and below the line of the arithmetic mean being greater on low angled planes, but the horizontal zero degree surface shows much lower roughness values. The standard deviation for surface roughness measurement has only been shown on the 0.2-mm EOS laser sintered polystyrene part. As seen in Figure 3-6, the standard deviation is greater for low angled planes with high angles surfaces having a smaller deviation.

Where available the measured data in Figure 3-7 also compares closely to the previous published data from the system manufacturers. For instance, the average measured roughness of the SL Epoxy part is 1.4 μm Ra (max 2 μm Ra / min 0.9 μm Ra) for horizontal surfaces and 7.3 μm Ra (max 8 μm Ra / min 6.8 μm Ra) for vertical surfaces. The roughness of similar surfaces quoted by 3D Systems for Epoxy SL parts, is 1.5 μm Ra and 8 μm Ra for horizontal and vertical surfaces respectively. This would suggest the use of only one sample for each LMT process is valid, if a sufficient number of roughness measurements are taken on each surface of interest.

On inspection it is evident that there is a high degree of roughness deviation between different layer manufacturing mechanisms. Roughness has always been considered a function of layer thickness [58]. However, Figure 3-7 shows that layer thickness does not necessarily dictate the level of roughness when comparing two different layer manufacturing mechanisms. If we consider both the LOM fast paper and SLS fine nylon samples produced with the same layer thickness, the roughness on many of the surfaces

exceeds that of the SLA epoxy sample. However, the SL sample is manufactured using a layer thickness 50% thicker than that of either the LOM or DTM SLS parts. Similarly, the EOS laser sintered polystyrene is manufactured in layers 100% thicker than the DTM laser sintered nylon, however both samples have similar roughness values on planes between 30 and 90-degrees. This would suggest that attributes within the LMT process other than layer thickness have a significant effect on surface roughness.

3.4 Surface topographical analysis

In order to gain a better understanding of the cause and subsequent effect of surface deviation these additional or 'secondary' attributes must be identified. To achieve this the topography of the parts was examined and a section of material was cut from each sample on the 10-degree surface, as this represents the plane with the greatest surface deviation.

Each sample was cleaned using compressed air and gold sputtered to provide a conductive surface [128]. It was then inspected under a Scanning Electron Microscope (SEM) at a range of magnifications. During the normal operation of an SEM, heat can be induced on the surface of non-conductive samples if the sputter coating is not sufficient in density or continuity. For this reason it was not possible to examine the wax impregnated EOS sample as the wax was found to undergo localised melting during analysis. However, all the remaining samples were viewed as shown in micrograph images 3-8-1 – 3-8-8. Even though it had not been measured, the Cubital sample was also inspected to assess the effect of the light surface abrasion applied by the company Schneider Prototyping after manufacture.

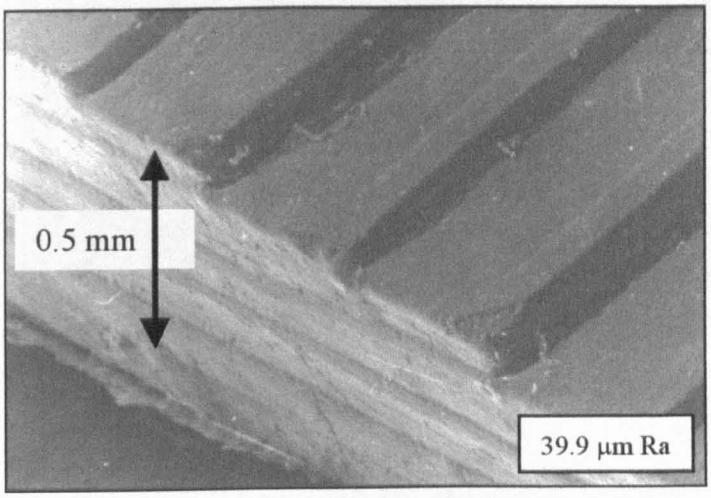

Figure 3-8-1 Micrograph of SLA epoxy10° surface- 0.15 mm layer thickness

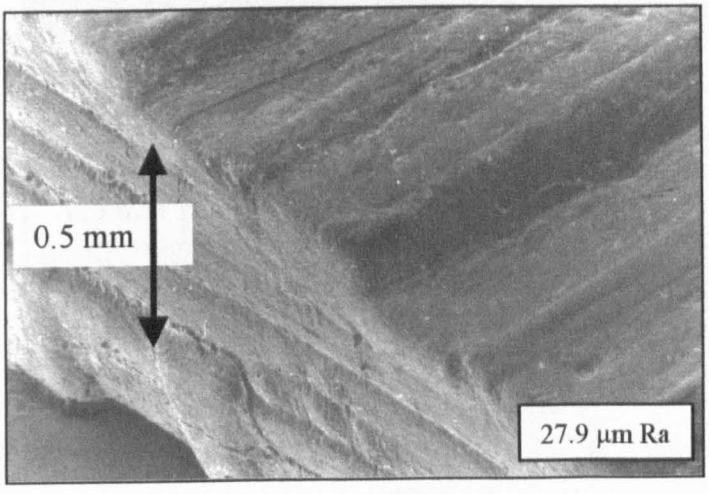

Figure 3-8-2 Micrograph of SLA acrylic10° surface- 0.125 mm layer thickness

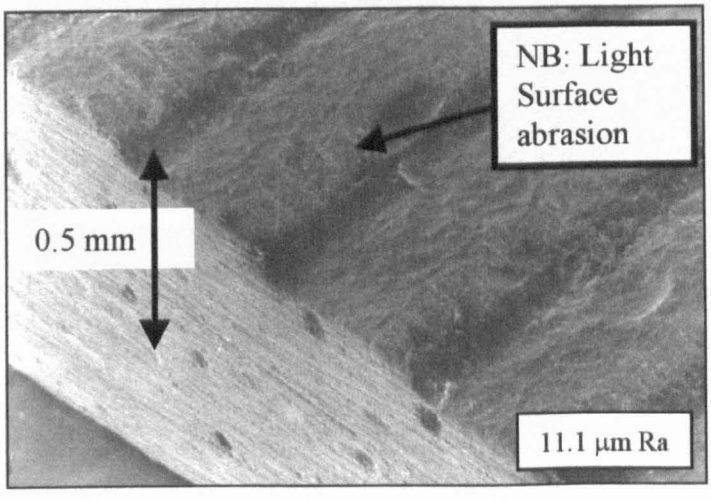

Figure 3-8-3 Micrograph of Solider acrylic 10° surface - 0.15 mm layer thickness

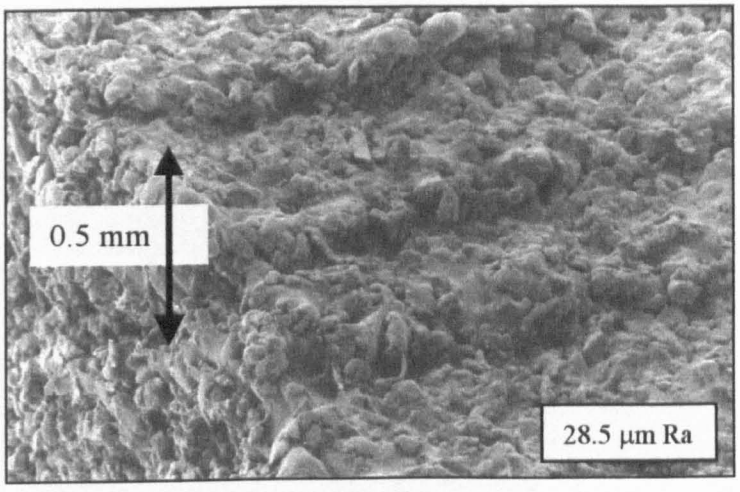

Figure 3-8-4 Micrograph of SLS fine nylon 10° surface - 0.1 mm layer thickness

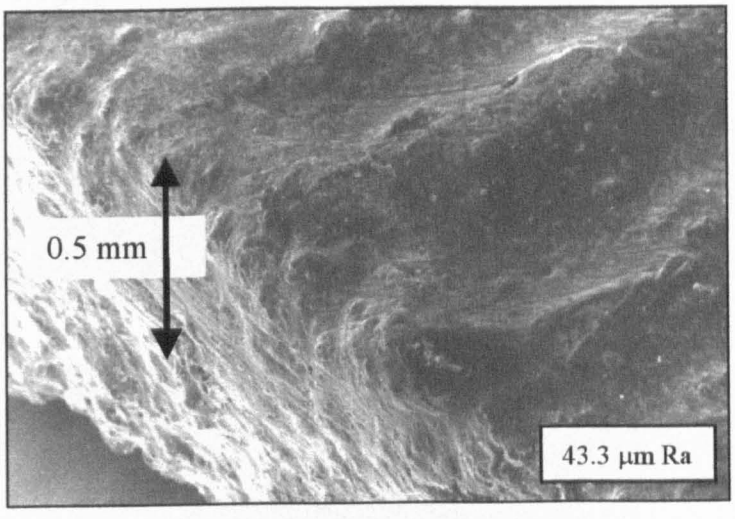

Figure 3-8-5 Micrograph of SLS polystyrene 10° surface - 0.2 mm layer thickness

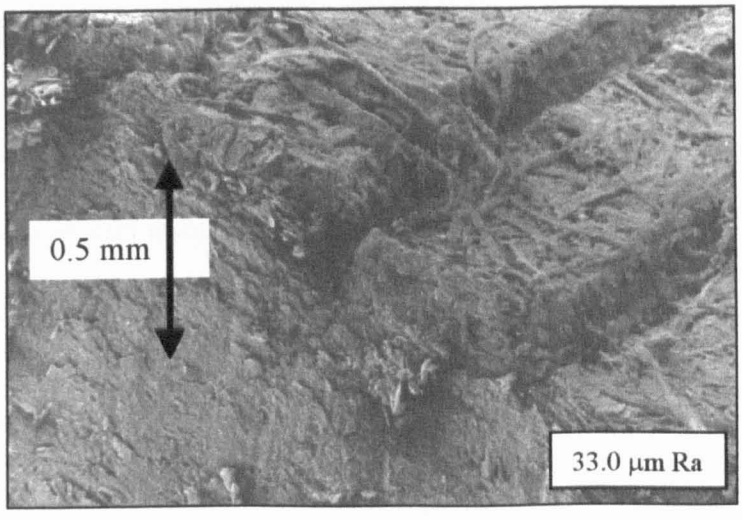

Figure 3-8-6 Micrograph of LOM fast paper 10° surface - 0.1 mm layer thickness

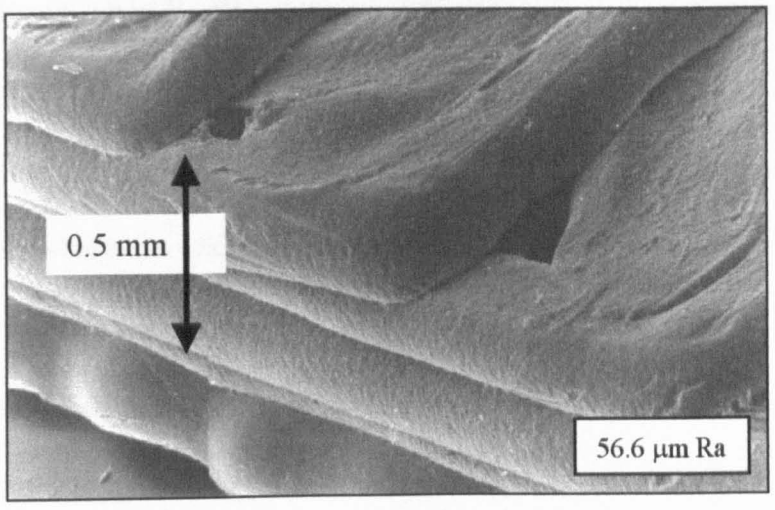

Figure 3-8-7 Micrograph of FDM ABS 10° surface - 0.25 mm layer thickness

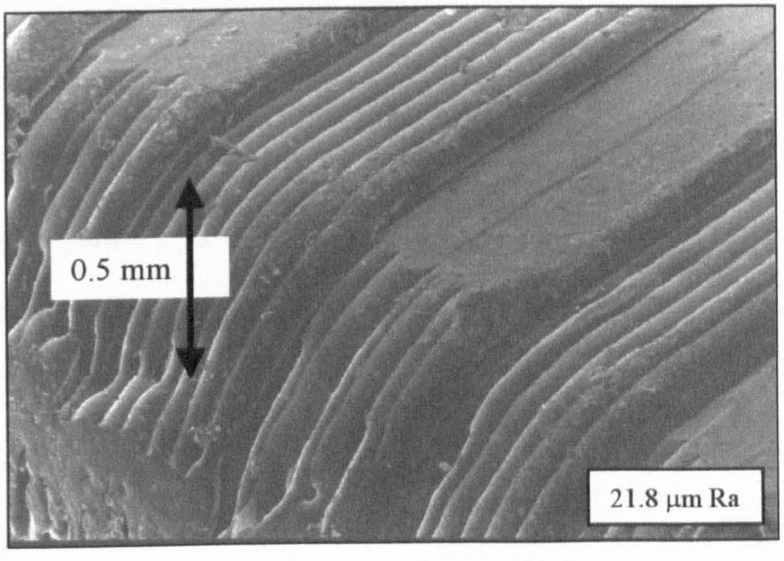

Figure 3-8-8 Micrograph of Actua Thermopoly 10° surface - 0.09 mm layer thickness

On inspection it can be seen that each sample has a defined layer thickness but it also has a distinct layer edge profile, and layer composition as a function of the LMT mechanism. The result is that each LMT process appears to have a distinct ' micro-topography' characteristic of the mode of manufacture. It is suggested that this 'micro-topography' could be responsible for the deviation in surface roughness rather than be attributed solely to layer thickness.

Layer profile is characterised by the edges of each exposed layer, and differs for each LMT process. Some LMT processes, which use deposition through a nozzle such as the FDM process shown in Figure 3-8-7 and Actua process shown in Figure 3-8-8, produce layer edge profiles which are radiused as a function of the nozzle geometry. Other processes such as SLA produce undercut layers as a function of the laser profile used to initiate photo-polymerisation. With processes such as SLS and LOM as shown in Figures 3-8-4 and 3-8-6 respectively, the layer edge profile is random and a function of the initial material used to generate the layer.

Layer composition is a function of the method by which a layer is generated from its raw material, such as sintered powder, cured resin or fibrous woven paper. Layer composition can be seen to cause significant variations in surface topography as a function of the build material such as the SLS part in Figure 3-8-4 and LOM part in Figure 3-8-6. The EOS polystyrene part in Figure 3-8-5 clearly shows the melted surface topography generated using this process. The characteristic fibrous nature of the LOM part in Figure 3-8-6 is also clearly evident.

It is the combination of layer profile and layer composition with layer thickness, which is now considered to have an effect on the roughness distribution of the different LMT processes. Returning to Figure 3-7 it can be seen that between 0 and 90 degree surfaces, the SLS fine nylon part produced in 0.1mm layers has a surface roughness some 50% greater than that of the epoxy SLA part manufactured using thicker 0.15mm layers. If we consider the topography of the two parts in Figures 3-8-1 and 3-8-4 respectively, it can be seen that the composition of the laser-sintered material will increase surface deviation

above that of other layer composition mechanisms. On the SLA part however, roughness is only a function of stair-stepping and the undercut caused by the laser profile. The SLA part has a relatively smooth composition roughness as a function of the ACES build style. It is therefore the composition roughness of SLS, which produces an increase in overall surface deviation above that of SLA parts manufactured using thinner layers.

3.4.1 Surface decomposition

Using the PC based analysis package interfaced to the contact Taly-surf, it is possible to breakdown and visualise the effects of layer profile, composition and layer thickness on surface roughness. Figures 3-9-1 to 3-9-4 show a topographic analysis of both 10-degree and 40-degree surfaces on both FDM and SLS parts.

Figure 3-9-1 exhibits the topography plot of a 10-degree FDM surface manufactured in 0.25-mm layers. At this layer thickness, only 3 'stair-steps' will be evident over the 4-mm sample distance. These are shown as the high-peaks and troughs of the topographic scan. In addition the scan also shows a secondary 'minor' peak occurring prior to the 'stair-step' peak. If we consider the micrograph image in Figure 3.8.7, this can be explained by the composition roughness resulting from the deposition of the molten ABS from the machine nozzle, which will be evident on low angled planes. In addition to layer thickness and composition, as the Taly-surf moves over the surface, the profile of each layer has also been seen. The rounded peaks shown prior to the gradual dip in the waveform are the result of the contact stylus moving around the extruded layer edge before dropping sharply onto the layer below. Hence the layer produced by the FDM process has a

smoothing effect on part roughness. However, the overall part roughness is high as a function of the composition and the layer thickness. In Figure 3.9.2 a 40-degree surface from the FDM model has been analysed using the same test equipment. In this case a greater number of stair-steps are present within the sample distance, with 5 peaks now occurring every 2-mm. At this angle, layer composition is not seen to effect the overall surface deviation, as the boundary of each layer now covers much of the composition roughness of the layer below. However, the rounded layer edge profile is still present at the peak of each scan. It can be noted from the 'Y-axis, that as surface angle increases so the maximum peak-to-trough deviation decreases.

Figure 3-9-1 Surface topography plot of 10-degree FDM sample (0.25-mm layers)

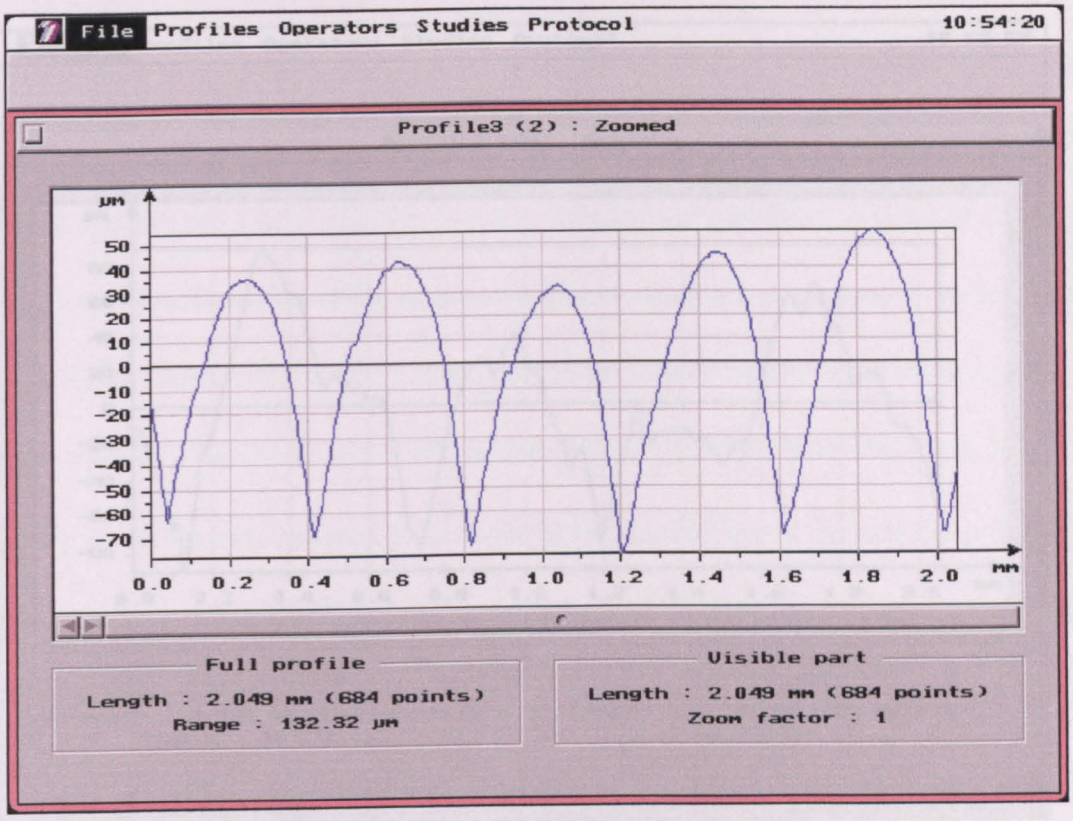

Figure 3-9-2 Surface topography plot of 40-degree FDM sample (0.25-mm layers)

In the case of the laser sintered polystyrene samples manufactured in 0.2-mm layers shown in Figures 3-9-3 and 3-9-4, the scan topography is notably different from the FDM parts. Figure 3-9-3 clearly shows the peaks of each layer caused by stair-stepping however, the layer profile at the peak of each wave does not exhibit a uniform topography in the same way as the FDM samples. This would support the observation in Figure 3-8-4 that the layer profile of the SLS process is random. Although layer profile is nondescript, the layer composition between the peaks appears more pronounced than the FDM, with continuous topographic change occurring between the peaks caused by stair stepping. This can be attributed to the roughness caused by the powder composition of each individual layer.

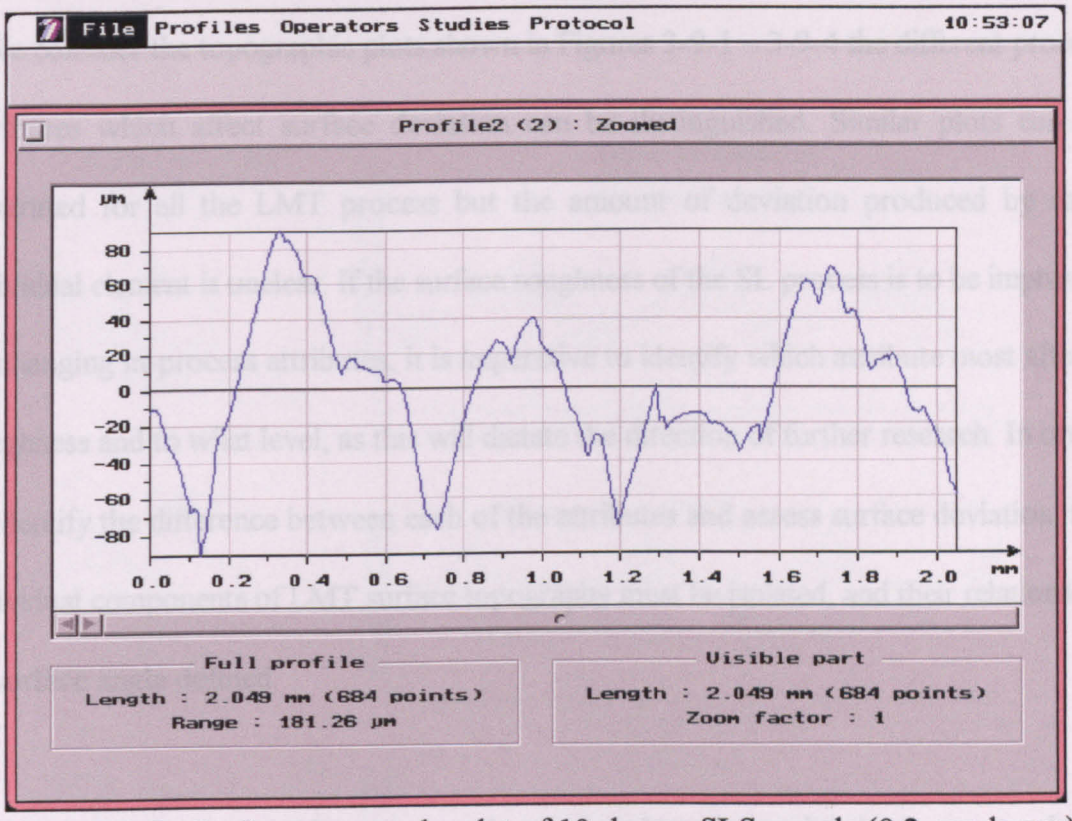

Figure 3-9-3 Surface topography plot of 10-degree SLS sample (0.2-mm layers)

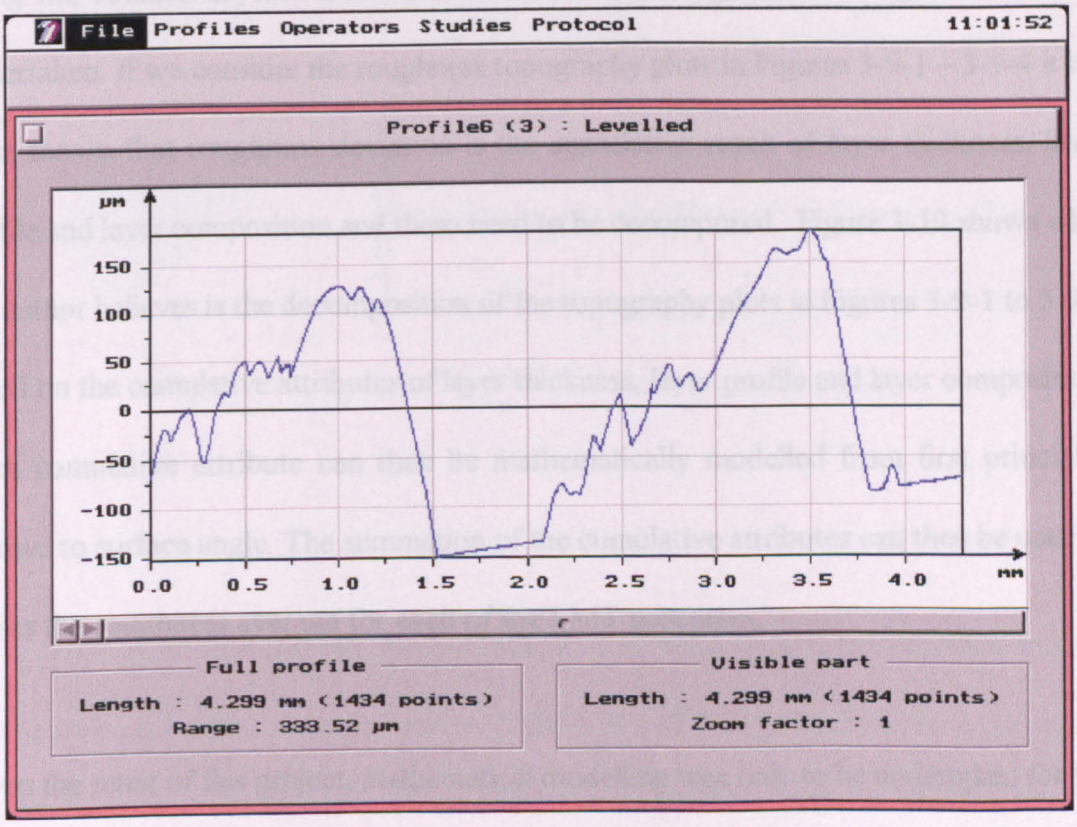

Figure 3-9-4 Surface topography plot of 40-degree SLS sample (0.2-mm layers)

If we consider the topographic plots shown in Figures 3-9-1 – 3-9-4 the different process attributes which affect surface deviation can be distinguished. Similar plots can be generated for all the LMT process but the amount of deviation produced by each individual element is unclear. If the surface roughness of the SL process is to be improved by changing in-process attributes, it is imperative to identify which attribute most affects roughness and to what level, as this will dictate the direction of further research. In order to identify the difference between each of the attributes and assess surface deviation, the individual components of LMT surface topography must be isolated, and their relationship to surface angle defined.

Unfortunately, is not possible to analyze the measured roughness data in any greater depth using the contact talysurf. Hence, an alternative investigation of roughness must be undertaken. If we consider the roughness topography plots in Figures 3-9-1 – 3-9-4 it has been shown that roughness deviation is the cumulative result of layer thickness, layer profile and layer composition and these need to be decomposed. Figure 3-10 shows what the author believes is the decomposition of the topography plots in Figures 3-9-1 to 3-9-4 based on the cumulative attributes of layer thickness, layer profile and layer composition. Each cumulative attribute can then be mathematically modelled from first principles relative to surface angle. The summation of the cumulative attributes can then be used to assess the roughness average for each of the LMT processes.

Given the remit of this project, mathematical modelling was only to be undertaken for the Stereolithography process. However, it is envisaged that a mathematical model of LMT surface roughness could take a generic form and may be suitable for assessing the surface

deviation of other LMT processes.

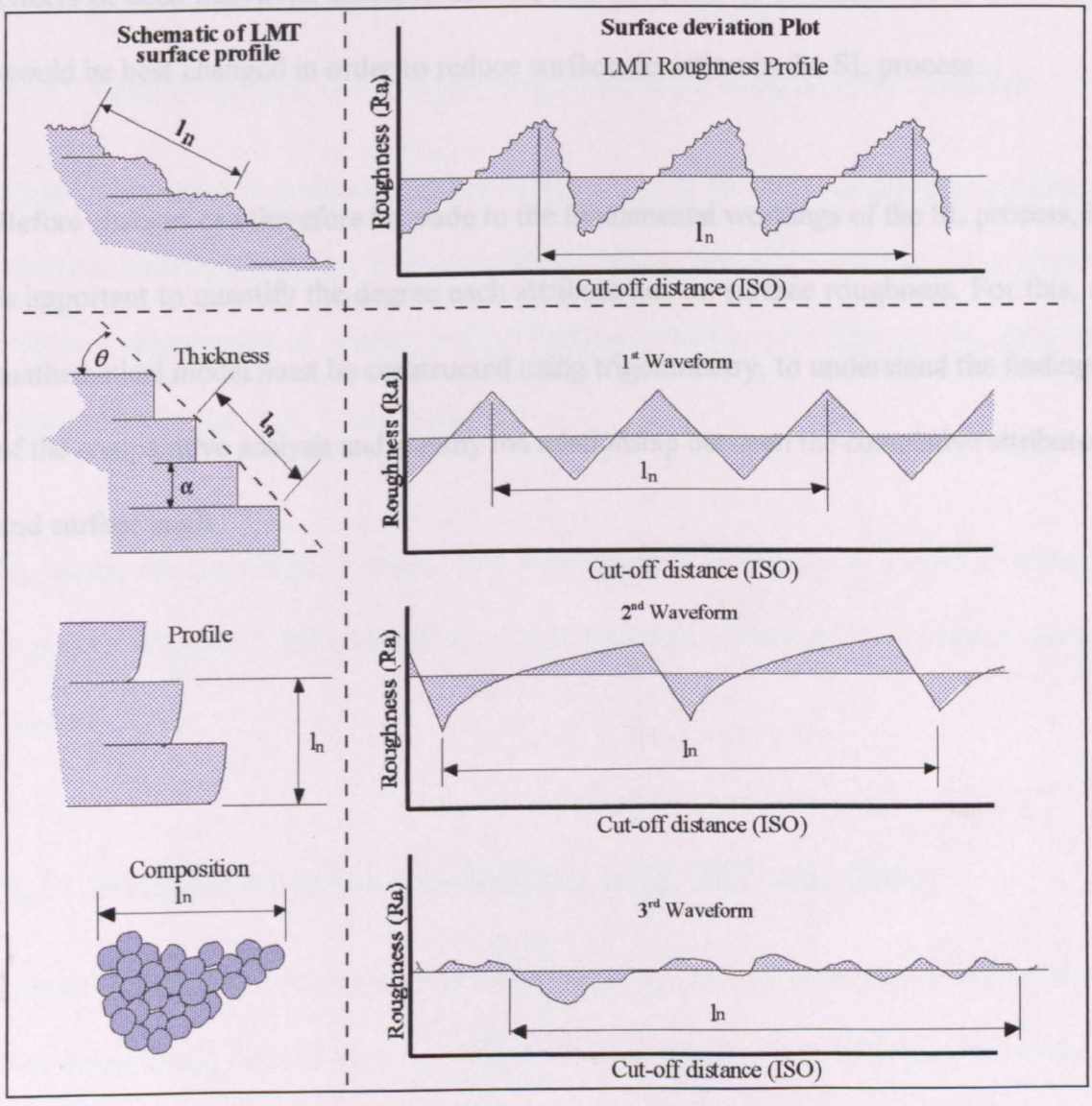

Figure 3-10 Decomposition of surface roughness plot

3.5 Summary

It has been shown that layer thickness is not the sole cause of surface roughness as layer profile and composition both affect the surface of LMT parts in different ways. If the surface roughness of the SL process is to be reduced the attributes affecting surface deviation must be prioritised, as some influence the surface more than others. However,

using contact surface analysis or micrograph analysis, it is not possible to quantify the effects of each individual attribute. Hence, it is not possible to assess which attributes would be best changed in order to reduce surface deviation in the SL process.

Before changes can therefore be made to the fundamental workings of the SL process, it is important to quantify the degree each attribute has on surface roughness. For this, a mathematical model must be constructed using trigonometry, to understand the findings of the comparative analysis and identify the relationship between the cumulative attributes and surface angle.

CHAPTER 4

4.0 Derivation of a mathematical roughness model

If any improvement in surface deviation is to made during the build process, the attributes affecting surface topography must be modified. Given that layer thickness, layer profile and layer composition all appear to affect surface deviation, a modification to any or all these attributes may prove beneficial.

By taking the individual attributes and building up a mathematical model of surface roughness in Ra units, different values of layer thickness, profile and composition can be assessed.

4.1 Mathematical modelling of LMT surfaces

A basic description of 'layer generated' roughness has already been seen in Figure 2-14. This description is derived from layer thickness alone and neglects both layer profile and composition. The model makes the assumption that layer thickness and surface angle are the only causes of deviation, an assumption which has been proven as unfounded by the comparative roughness analysis detailed in Chapter 3, section 3.3.

4.1.1 Modelling of layer thickness and layer profile

A more accurate description of deviation can be developed if we consider both layer thickness, and the layer profile described in Figure 3-10. A mathematical representation

can then be developed using layer thickness (α), surface angle (θ) and layer profile (ϕ). By considering the area of the layer both above and below the line of the arithmetic mean as detailed in Figure 4-1, trigonometry can be used to calculate the relationship between α, θ, ϕ, and surface roughness (Ra).

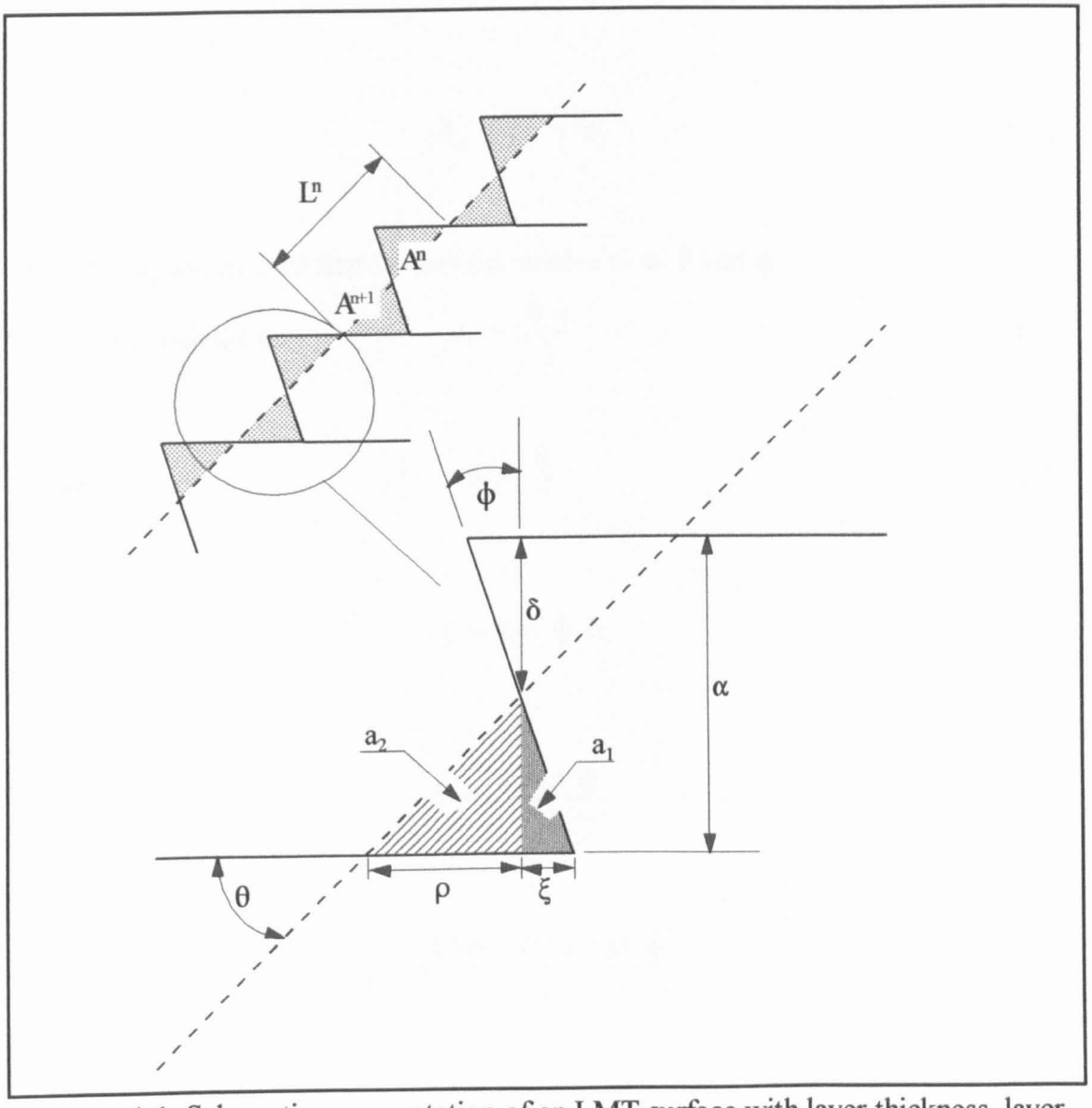

Figure 4-1 Schematic representation of an LMT surface with layer thickness, layer profile and surface angle

If we first consider the basic roughness equation:-

$$Ra = \frac{\sum A_n}{L_n} \qquad 4\text{-}1$$

Roughness is a direct function of A_n and L_n. However, A_n is now affected by the angle of layer profile (ϕ). To determine the relationship with ϕ for the area above and below the arithmetic mean, the area must first be subdivided into a_1 and a_2, as shown in Figure 4-1. Each sub-area can then be calculated as a function of ϕ, and subdivided into equation 4-2.

$$A_n = a_1 + a_2 \qquad 4\text{-}2$$

The areas a_1 and a_2 must first be derived relative to α, θ and ϕ.

a_1 can be calculated as $$a_1 = \frac{\delta\ \xi}{2} \qquad 4\text{-}3$$

Where:- $$\delta = \frac{\alpha}{2} \qquad 4\text{-}4$$

and $$\xi = \tan \phi\ \delta \qquad 4\text{-}5$$

From 4-4 $$\xi = \frac{\alpha \tan \phi}{2} \qquad 4\text{-}6$$

Therefore:- $$a_1 = \frac{0.5\alpha\ .\ 0.5\alpha \tan \phi}{2} \qquad 4\text{-}7$$

Hence:- $$a_1 = \frac{\alpha^2 \tan \phi}{8} \qquad 4\text{-}8$$

Similarly the area a_2 be calculated as :-

$$a_2 = \frac{\delta\ \rho}{2} \qquad 4\text{-}9$$

Where:-

$$\rho = \frac{\delta}{\tan \theta} \qquad 4\text{-}10$$

But from 4-4

$$\rho = \frac{\alpha}{2 \tan \theta} \qquad 4\text{-}11$$

Therefore:-

$$a_2 = \frac{0.5 \,.\, 0.5\ \alpha \,.\, 0.5\ \alpha}{\tan \theta} \qquad 4\text{-}12$$

Hence:-

$$a_2 = \frac{\alpha^2}{8 \tan \theta} \qquad 4\text{-}13$$

From 4.2 the total area of a single peak or trough about the arithmetic mean can now be described by the equation:-

$$A = \frac{\alpha^2 \tan \phi}{8} + \frac{\alpha^2}{8 \tan \theta} \qquad 4\text{-}14$$

Over the required ISO scan length (L_n), two areas above and below the mean line must be considered. Therefore $A_n = 2A$

Hence area:-

$$A_n = 2\left[\frac{\alpha^2 \tan \phi}{8} + \frac{\alpha^2}{8 \tan \theta}\right] \qquad 4\text{-}15$$

Therefore:-

$$A_n = \frac{\alpha^2 \tan \phi}{4} + \frac{\alpha^2}{4 \tan \theta} \qquad 4\text{-}16$$

In order to derive a roughness average unit, the scan length of the arithmetic mean (L_n) must also be calculated relative to α, θ, and ϕ.

From Figure 4-1:-

$$L_n = \frac{\alpha}{\sin \theta} \qquad 4\text{-}17$$

Surface roughness is defined as:-

$$Ra = \frac{\sum A_n}{L_n} \qquad 4\text{-}18$$

Hence :-

$$Ra = \frac{\frac{\alpha^2 \tan \phi}{4} + \frac{\alpha^2}{4 \tan \theta}}{\frac{\alpha}{\sin \theta}} \qquad 4\text{-}19$$

Therefore:-

$$Ra = \frac{\alpha^2 \tan \phi \sin \theta}{4 \alpha} + \frac{\alpha^2 \sin \theta}{4 \alpha \tan \theta} \qquad 4\text{-}20$$

$$Ra = \frac{\alpha \tan \phi \sin \theta}{4} + \frac{\alpha \sin \theta}{4 \tan \theta} \qquad 4\text{-}21$$

$$Ra = \frac{\alpha \tan \phi \sin \theta}{4} + \frac{\alpha \cos \theta}{4} \qquad 4\text{-}22$$

$$Ra = \frac{(\alpha \tan \phi \sin \theta) + (\alpha \cos \theta)}{4} \qquad 4\text{-}23$$

Therefore :-

$$Ra = \frac{\alpha \, (\tan \phi \sin \theta + \cos \theta)}{4} \qquad 4\text{-}24$$

It is now possible to plot the relationship between surface angle and surface roughness for a layer manufactured component with both variable layer thickness and variable layer profile. Before values can be derived from equation 4-24, the constants of layer thickness α, and layer profile ϕ must all be defined. For model verification purposes a layer thickness (α) of 0.15-mm will be used, as this represents the default layer thickness for epoxy parts manufactured on the SLA-250 system. Using micro-graph images of sections taken through parts manufactured in epoxy SL resin, it is possible to measure the average layer profile on the undercut produced between each layer. An average layer profile value (ϕ) of 13-degrees has been derived from micrograph images previously produced by Rahmati [129]. Using the process constants of 0.15 mm layer thickness (α) and 13-degrees layer profile (ϕ), surface roughness has been plotted in Figure 4-1, for all surface angles between 0 and 180-degrees (θ).

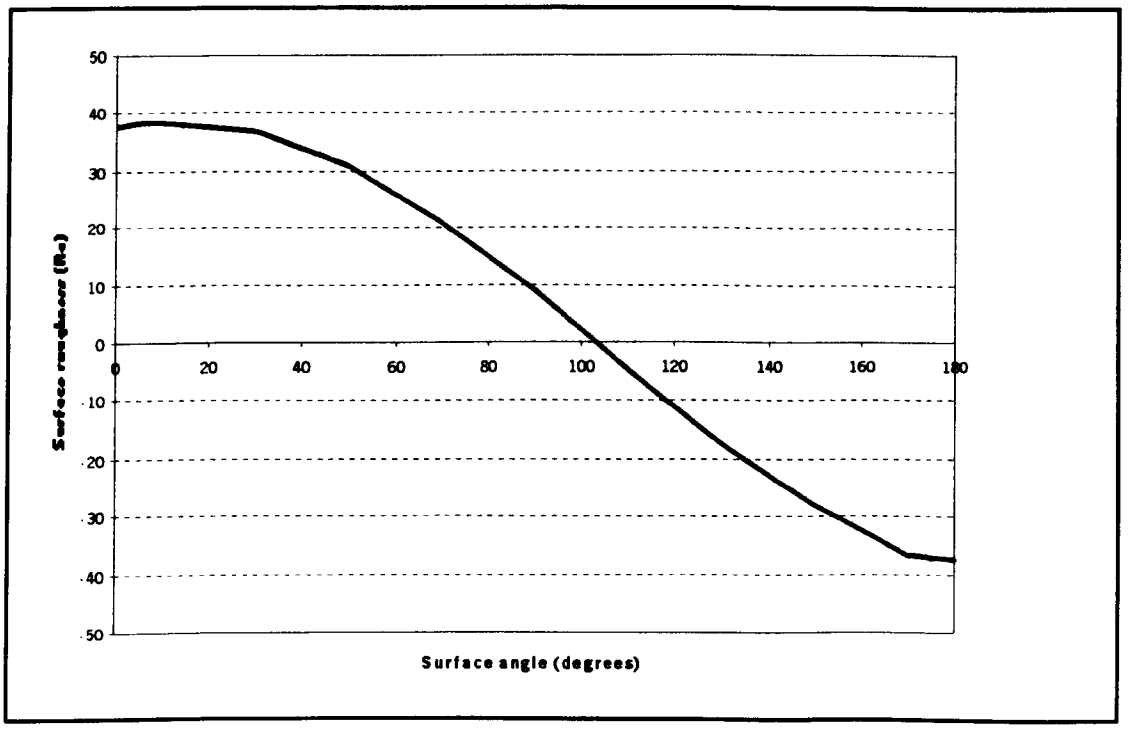

Figure 4-2 Roughness values derived using equation 4-24

By plotting the values of roughness relative to surface angle using equation 4-24, the model is seen to give only realistic values for some surfaces. This is shown in Figure 4-2 where the mathematical model is seen to break down above 103-degrees and produce negative values of roughness up to 180-degrees. It is however, not possible to have a negative value of surface roughness, as an Ra value of 0 represents a topography with no surface deviation about the arithmetic mean. This being the smoothest possible surface.

By analysing the mathematical model, the error is found to be the result of the mathematical term: $\tan \phi \sin \theta + \cos \theta$, which in some instances can produce a negative value. However, this will only occur when the cosine of the surface angle θ, is a negative value, which is larger than the tangent of the layer profile ϕ multiplied by the sin of the surface angle θ.

For the model verification in Figure 4-2, a value of 13-degrees has been used for the profile angle (ϕ). However, the model will only return a negative value when $\cos \theta$ is greater than $\tan \phi \sin \theta$. This will always occur when $\theta - \phi \geq 90$. Hence, as shown in Figure 4-2, the equation breaks down at 103-degrees, as this is the point where $\theta - \phi \geq 90$. Similarly, if a layer profile value (ϕ) of 17-degrees had been used, the model would have returned a negative roughness at 107 degrees.

4.1.2 Modelling down facing surfaces

Like all 3-Dimensional objects SL parts possess down facing surfaces. Some act as faces of geometric interest others are simply supports for geometries higher in the part. If an

accurate mathematical description of surface roughness is to be produced, down facing surfaces must be included in the model. However, the current mathematical model cannot be used to calculate values where $\theta - \phi \geq 90$.

When considering the modelling of surfaces where $\theta - \phi \geq 90$, one solution is to invert the angle of the layer profile and consider the surface to be at a positive angle between 0 and 90-degrees, therefore creating a ' mirror function' as detailed in Figure 4-3.

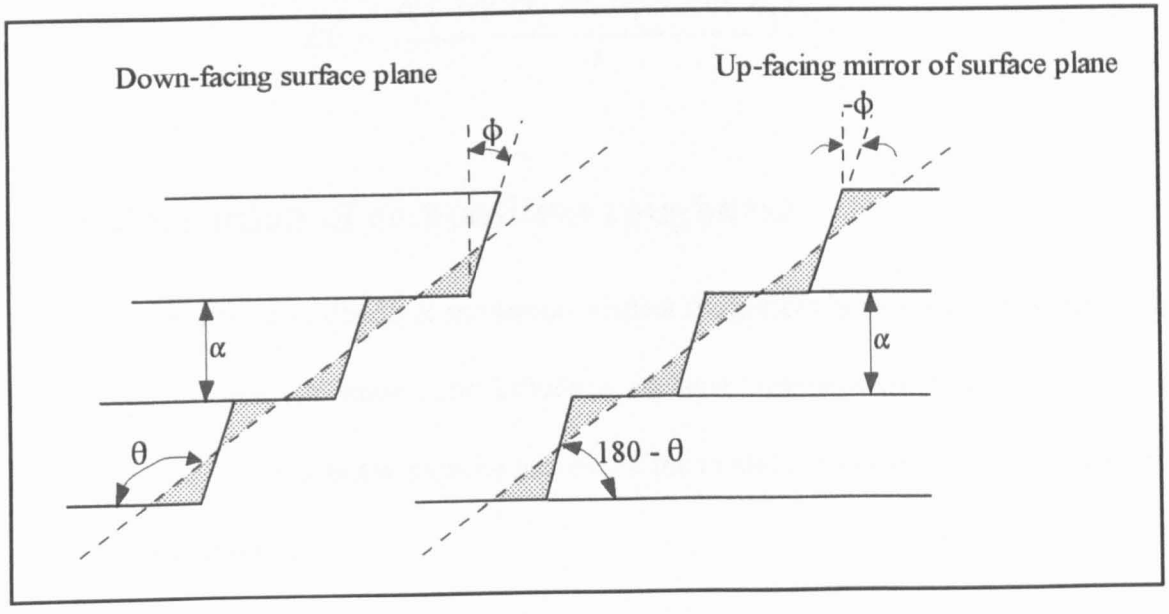

Figure 4-3 The down-facing 'mirror function' of an up-facing surface plane

From the 'mirror function' we can now consider two separate equations representing surface roughness, on both up-facing and down-facing surface planes. The boundary limit can be defined by equations 4-25 and 4-26:-

$$Up\text{-}facing\ equation = \theta - \phi \leq 90° \qquad 4\text{-}25$$

$$Down\text{-}facing\ equation = \theta - \phi \geq 90° \qquad 4\text{-}26$$

When the down-facing equation 4-26 is applicable, the 'mirror values' for θ and ϕ must be used.

When $\theta - \phi \geq 90$: $\theta_1 = 180 - \theta$ 4-27

And when $\theta - \phi \geq 90$ $\phi_1 = -\phi$ 4-28

The equation for down-facing surface roughness can now be defined as:-

$$Ra = \frac{\alpha \left(\tan \phi_1 \sin \theta_1 + \cos \theta_1 \right)}{4} \qquad 4\text{-}29$$

4.1.3 Derivation of composition roughness

Although the effects of the layer profile on surface roughness have now been combined with those of layer thickness, the influence of layer composition has not yet been considered. Layer composition must be included if the model is to be a true representation of surface topography.

Layer composition has been seen to vary greatly between different LMT processes, as shown in Section 3.3. With some systems such as SLS, layer composition is a function of the initial particle size and the degree of distortion caused by phase changes. Other systems such as LOM, have a unique composition roughness as a function of the raw material being made from random fibres. As the objective of this research is to focus up on the Stereolithography process, only the composition roughness caused by the curing of photopolymers has been investigated further.

From previous research by Rahmati, composition roughness for Stereolithography appears to be the result of a number of laser associated parameters in the process [129].For example the initial hatch or weave patterns, secondary solid phase material shrinkage caused by cross hatching, and the cross sectional geometry of the laser scan profile. These will be investigated in more detail.

4.1.4 Up facing composition roughness on SL surfaces

Two scanning techniques are currently used in SL. Staggered, Alternative, Retracted (STAR) build used with the acrylic resin and the Accurate Clear Epoxy Structure (ACES) used with the epoxy material. Each build relies on layers being cured through a series of perpendicular scans. However, the spacing of the scan differs considerably for each build style. With the STAR-Weave build, following the scanning of the layer boundary, the laser 'infills' the bounded area using an offset hatch in one direction before repeating the 'in-fill' at 90 degree to the original scan path, as detailed in Figure 2-7. The result is a 'waffle' or 'grid' like structure with pockets of uncured resin, as shown in Figure 4-4.

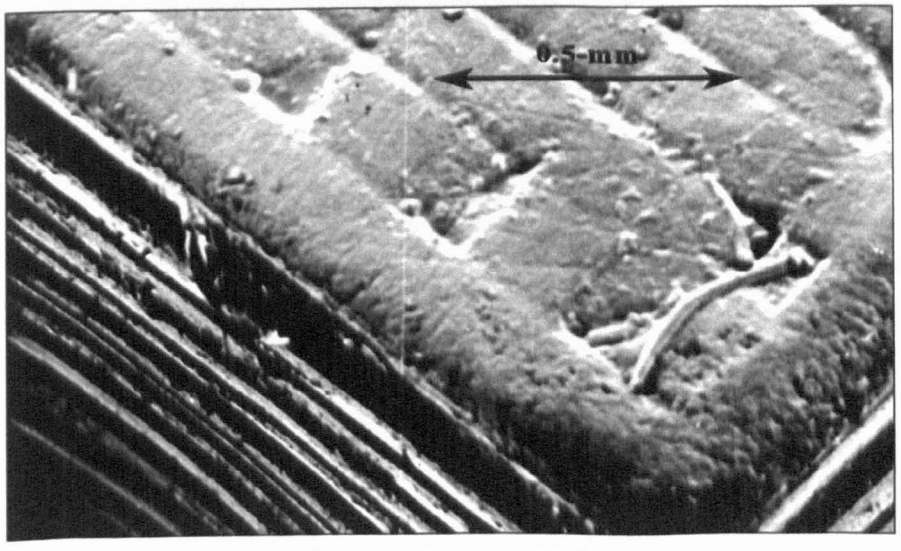

Figure 4-4 Micro-graph of Up-facing STAR-Weave surface

This scanning algorithm is designed to minimise stresses in the build structure and prevent both warpage and subsequent creep. However, the resulting parts exhibit high roughness as a result of both the laser beam width and the distance between each laser scan of the hatch pattern. Up facing roughness as a function of laser scanning can be seen detailed in Figure 4.5.

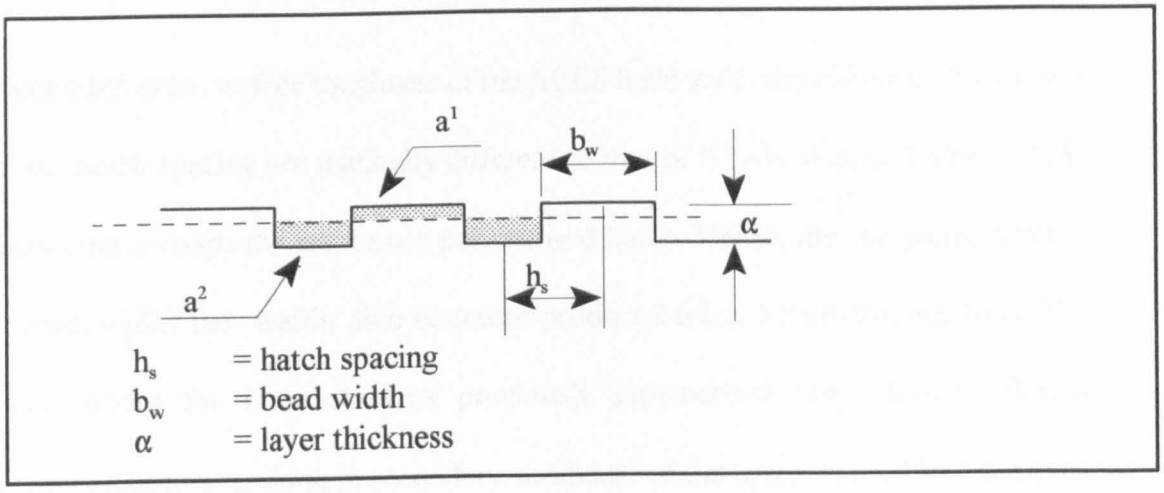

Figure 4-5 The effect of laser scan path on surface roughness

The effect of scan path on surface roughness can therefore be defined in terms of the hatch spacing and the area above and below the centre line a_1, a_2.

$$Ra = \frac{[[a_1 + a_2] / 2]}{h_s} \qquad 4\text{-}30$$

From Figure 4-6 it can be seen that both a_1 and a_2 are functions of the laser beam width and layer thickness. The beam width (b_w) is a function of the laser power initiating photo polymerisation and laser power can be variable during the build process, as changes in operating temperature and duration can affect laser performance. This can in turn result

in a variable width hatching during the build process and an unpredictable part surface. In addition many of the voids between the scan path are filled with liquid resin during the build process. Resin is then retained in the model during post-curing and acts as a filler on the surface of the cured model. Given the number of process variables involved it is therefore impractical to attempt to model up-facing surface deviation from first principles.

When considering the surface roughness of the ACES build style, the effects of laser beam width and hatch spacing are markedly different to that of STAR-Weave. Using ACES, each laser scan overlaps the previously polymerised hatch. Hence, the completed layer is fully dense, unlike the 'waffle' like structure produced using STAR-Weave. In ACES however, where the laser overlaps previously polymerised resin, further photo-polymerisation occurs resulting in secondary shrinkage of the epoxy resin. Hence, ACES surfaces although significantly smoother than STAR-Weave, do exhibit an uneven 'micro-rutted' topography as a function of secondary resin shrinkage on each layer, as shown in Figure 4-6.

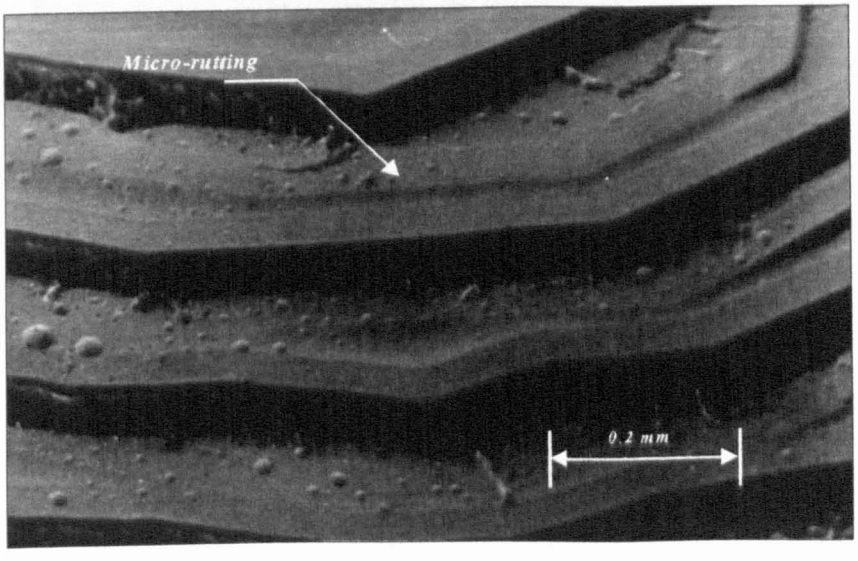

Figure 4-6 Micro-graph of Up-facing ACES surfaces

When we consider the image of 'micro-rutting' in Figure 4-6, the attribute appears to have less influence on surface deviation than other attributes such as layer thickness or layer edge profile. The maximum peak-to-trough deviation caused by secondary photo-polymerisation or 'micro-rutting' is no more than 10-μm, in comparison to the 150 μm peak-to-trough deviation caused by stair-stepping. The need to include the composition roughness of up-facing ACES in the mathematical model may therefore be questioned, as the attribute appears to have only a minimal effect in comparison to other factors.

In addition it should be noted that only epoxy SL parts manufactured using the ACES build style are used as cavities for RT, as the acrylic material is too brittle. Hence, if research is to be directed towards improving the surface deviation of RT cavities the surface roughness of STAR-Weave need not be considered.

4.1.5 Down facing surface deviation

With the acrylic star-weave build, down-facing surfaces are similar in appearance to up-facing, with the characteristic waffle like structure clearly evident. With ACES, the down facing planes exhibit a distinctive pattern of peaks and troughs, as a function of the laser beam profile. The ideal laser-resin combination used in SL should result in a uniform distribution producing parallel sided layers, as described in Figure 4-7.

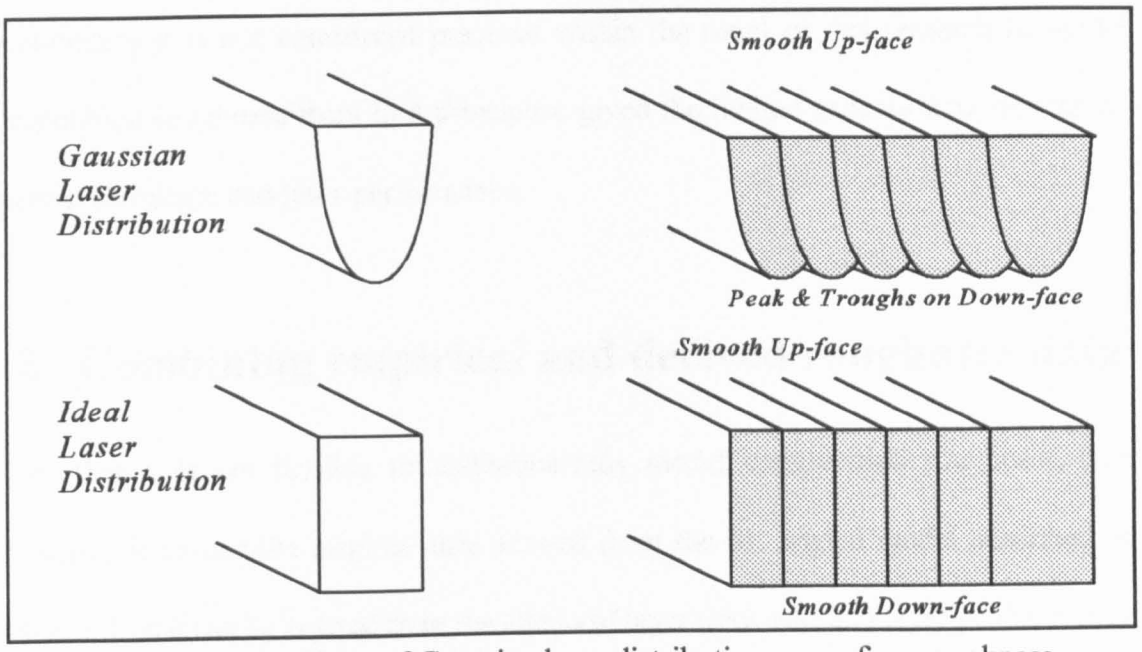

Figure 4-7 The effects of Gaussian laser distribution on surface roughness

However, the true profile of SL lasers is parabolic, resulting in the down-facing surface being composed of a series of peaks and troughs as detailed in Figure 4-8. The topography of a down facing ACES surface is the complex result of a number of process functions, including laser power, laser draw speed, resin temperature and the spacing of any support structure. As with up-facing planes, additional resin on the part surface may also cause some surface smoothing during post-processing.

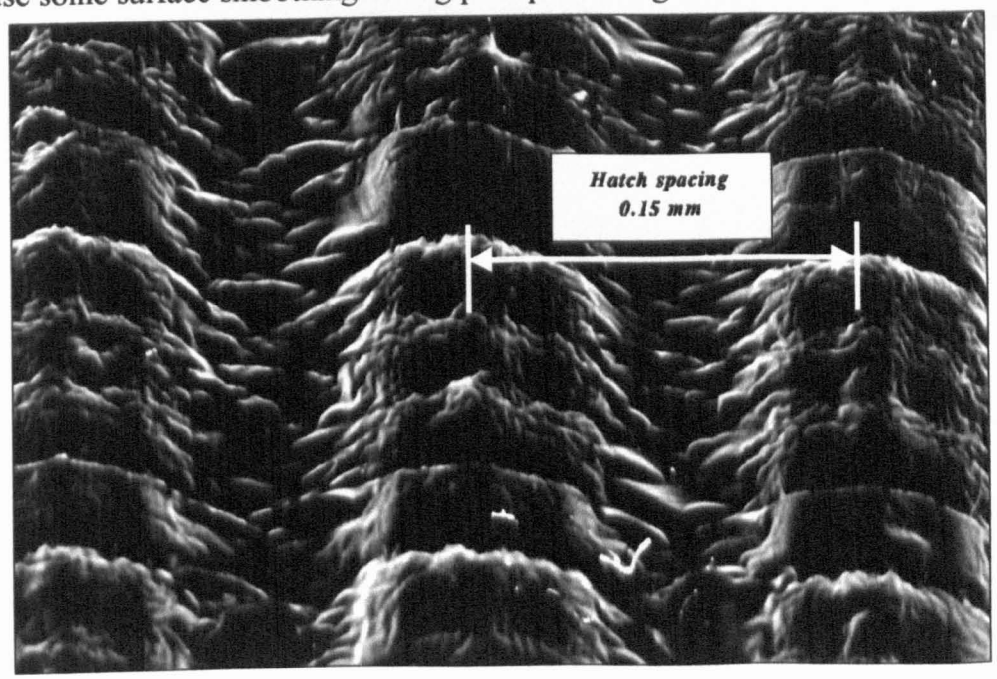

Figure 4-8 Down facing surface produced by ACES

In summary it is not considered practical within the remit of this research to model composition roughness from first principles, given the limited process data relating to material shrinkage and laser performance.

4.2 Combining empirical and derived roughness data

Given that it is not feasible to mathematically model composition roughness, one alternative is to use the original data derived from the SL angled model described in section 3.2. If it can be isolated from the effects of layer thickness and layer profile it may be possible to assess composition roughness alone, using measured data. In the case of horizontal surfaces, composition alone will affect the measured roughness, as the surfaces contain no layers or stair-stepping. Composition roughness on SL surfaces has already been measured in section 3.2 and is represented in Appendix B as the 0-degree and 180-degree roughness. If a 0-degree surface exhibits 100% composition roughness it could be assumed that a 45-degree surface will only exhibit 50% composition roughness. Hence the level of composition roughness could be considered a function of surface angle as shown in Figure 4-9.

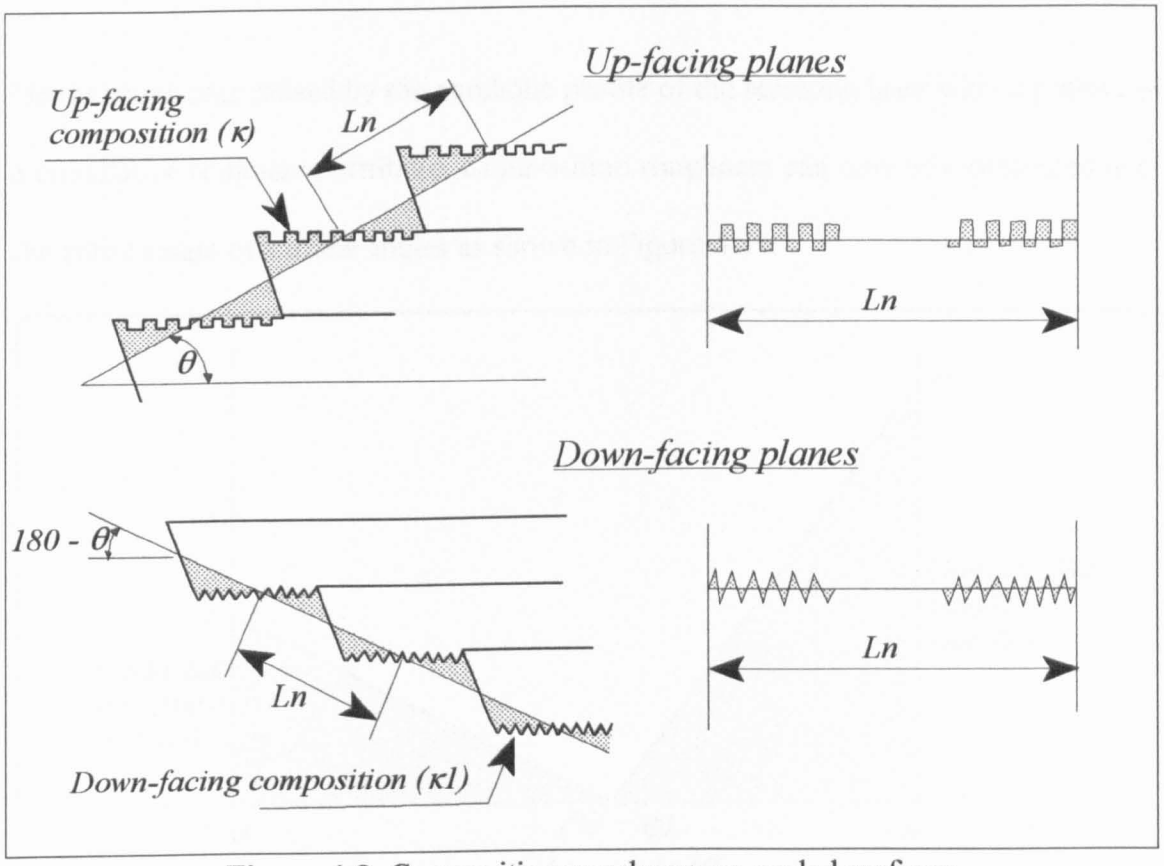

Figure 4-9 Composition roughness on angled surfaces

In Figure 4-9, the surface topography of a single scan distance L_n is shown across a stair-step. For the angled surfaces shown, a percentage of the surface topography is solely a function of composition roughness, depending on surface angle. As surface angle increases so the percentage of surface exhibiting composition roughness will decrease. Inversely, on low angled planes the surface exhibiting composition roughness will increase.

Due to the undercut of the laser profile, as described in Figure 4-1, the only surface which exhibits no composition roughness will be $90+\phi$ degrees. Any surface angle less than $90+\phi$ degrees will exhibit some up-facing surface roughness as each layer of the component will not fully cover the composition of the previously layer. Similarly for surface angles greater than $90+\phi$ degrees, each new layer will override the previous layer.

Hence roughness caused by the parabolic profile of the scanning laser will be present as a cumulative roughness attribute. Composition roughness can now be represented over the entire range of surface angles as shown in Figure 4-10.

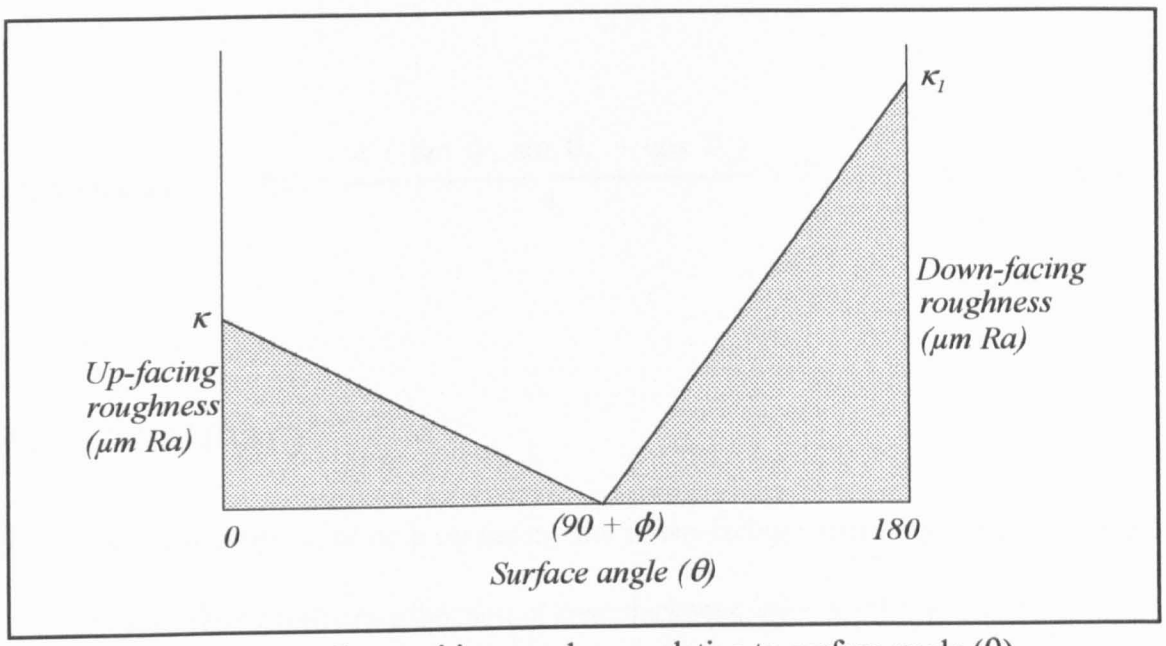

Figure 4-10 Composition roughness relative to surface angle (θ)

The composition roughness for any surface plane can be calculated as a percentage of either up-facing or down-facing 'measured' roughness, using equations 4-31 and 4-32.

Up-facing roughness

$$K = \frac{(90 + \phi) - \theta}{(90 + \phi)} * \kappa \qquad 4\text{-}31$$

Down-facing roughness

$$K_1 = \frac{(180 - (90 + \phi)) - (180 - \theta)}{180 - (90 + \phi)} * \kappa_1 \qquad 4\text{-}32$$

The overall surface roughness of Stereolithography models based on the cumulative attributes of layer thickness (α), layer profile (ϕ) and layer composition (K & K_1) can now be derived mathematically for both up-facing and down-facing planes using equations 4-33

and 4-34 respectively and the boundary equations 4-25 and 4-26.

Up facing $$Ra = \frac{\alpha\ (\ \tan\ \phi\ \sin\ \theta\ +\ \cos\ \theta)}{4} + K \qquad 4\text{-}33$$

Down facing $$Ra = \frac{\alpha\ (\ \tan\ \phi_1\ \sin\ \theta_1\ +\ \cos\ \theta_1)}{4} + K_1 \qquad 4\text{-}34$$

4.3 Summary

In summary a description of both up-facing and down-facing surface roughness has been derived using trigonometry as a function of layer thickness, layer profile and surface angle. Given the limited process data available, the composition roughness has been obtained using empirical data.

From the model derived in this Chapter the variables of layer thickness, layer profile and surface angle can all be changed to assess which attribute most effects surface roughness. Such senarios can either be undertaken manually or using a spreadsheet package. Alternatively, by using the equations in a CAD software package the user could select a specific surface of the Stereolithography component and define a maximum permissible roughness value. The model could then be used to derive the optimum build angle for the selected surface. A similar system could be used to identify the level of roughness a part will possess prior to the part being built. Post process finishing could then be planned and budgeted for in advance.

If the model were expanded to cover other RP processes it may be possible to develop an LMT selection tool, where maximum and minimum roughness values are placed on specific planes of a geometry, the software would then select the most appropriate LMT system to produce the part.

The mathematical model could also be used to establish RP pattern suitability for down stream tooling and the level of post process finishing required prior to tool manufacture as shown in Figure 4-11.

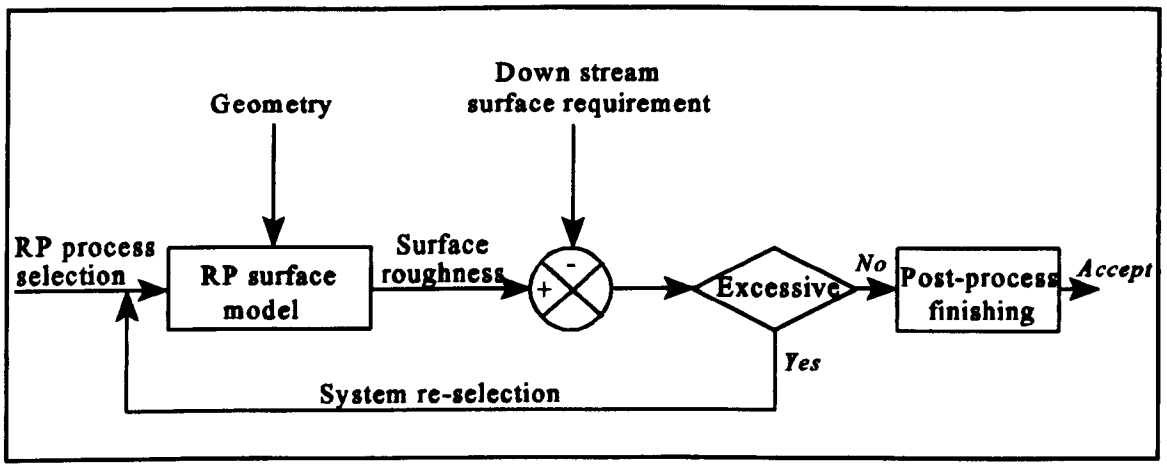

Figure 4-11 Down stream applications for the roughness model

However, before the model could be used for any of these applications, it must be verified against a number of real SL parts to identify the degree of accuracy. Only after verification can the attributes in the model be accepted.

CHAPTER 5

5.0 Verification of the roughness model

Before the mathematical model described in Chapter 4 can be used to any degree of certainty, it must be verified against an accurate sample of measured roughness data. The test sample used for the comparative analysis in Chapter 3, section 3.1.1, provides only a limited range of up-facing data derived from parts produced on an SLA-250. The model must therefore be verified using a number of sample parts manufactured on a range of different SLA machine variants, which exhibit a broader range of both up-facing and down-facing surfaces.

5.1 Verification methodology

In order to verify the model for different SLA technologies a range of different SL machines with a variety of resin types need to be considered. Comparative surface roughness data is required and the test samples must also be used to derive the roughness constants for profile angle (ϕ), up-facing surface roughness (K) and down-facing surface roughness (K_1), as these are used to evaluate the mathematical model.

5.1.1 Design of a validation test sample

A suitable test sample to verify the mathematical model must exhibit a variation of surface planes, of sufficient length to measure roughness accurately. The down facing planes must also be designed so no support structure is generated on the surfaces to be measured, as this will produce inaccurate roughness measurements. A part was designed by the author known as the 'truncheon', which shown in Figure 5-1.

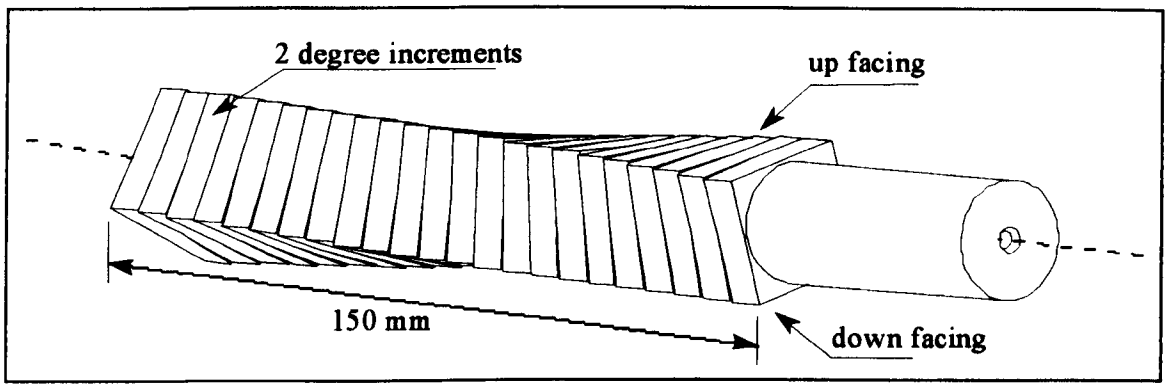

Figure 5-1 Roughness measurement 'Truncheon'

The geometry of the part has 90 different surface planes in two-degree increments from 0 to 180-degrees. The design allows sufficient area on each angled surface to accumulate accurate roughness data. With the symmetry of the design, the part can be positioned in a dividing head and rotated through 2-degree increments and hence each surface can be scanned. Using this design, the support structures can also be positioned at the edge of each face to prevent witness marks on the surfaces of interest.

5.1.2 SL machine selection

The SL machine market is continually changing, with new lasers, optics and resin systems emerging on an almost yearly basis. In the original comparative analysis, only the market dominating SLA-250 machine was used to define the cumulative roughness attributes. Process up-dates such as the solid state laser and the 'Zephyr' active wiper must also be considered in addition to the higher powered Argon-Ion laser used on the SLA-500. Table 5-1 lists the SL machine types, resins, build styles, layer thickness and source of Truncheon test samples used to validate the mathematical model.

Machine type	Laser	Resin type	Build style & layer thickness	Source
SLA-250	Helium-Cadmium	Epoxy SL5170	ACES 0.15 mm	University of Nottingham
SLA-250	Helium-Cadmium	Acrylic SL5149	STAR-Weave 0.125 mm	University of Nottingham
SLA-350	Solid State	Epoxy SL 5190	ACES 0.10 mm	3D Systems UK
SLA-500	Argon-Ion	Epoxy SL5180	ACES 0.15 mm	Rolls-Royce Aerospace Bristol

Table 5-1 SL samples used for model validation exercise

Measured roughness data derived from each of the test samples listed in the table can be found in Appendix C. To compensate for sampling errors caused by cut-off distance, which was explained in Section 3.2, the average of six roughness measurements has been used for comparative analysis with the mathematical model.

5.1.3 Derivation of SL process constants

Before a comparison can be made between the mathematical roughness model and the surface data from the 'Truncheon', a number of process constants must be defined. If we consider Equations 4-33 and 4-34, the mathematical model will only work given values for layer profile (ϕ), up facing composition roughness κ, and down facing composition roughness κ_1. Composition roughness can be derived from the measured 0 and 180-degree surfaces of the 'Truncheon' models listed in Appendix C.

Profile angle ϕ must however be derived from the SL test parts. This was achieved by sectioning the 'Truncheon' model and using a Shadowgraph to establish the profile of each laser-resin combination. Figure 5-2 shows both the solid state and gas laser distributions in epoxy resin.

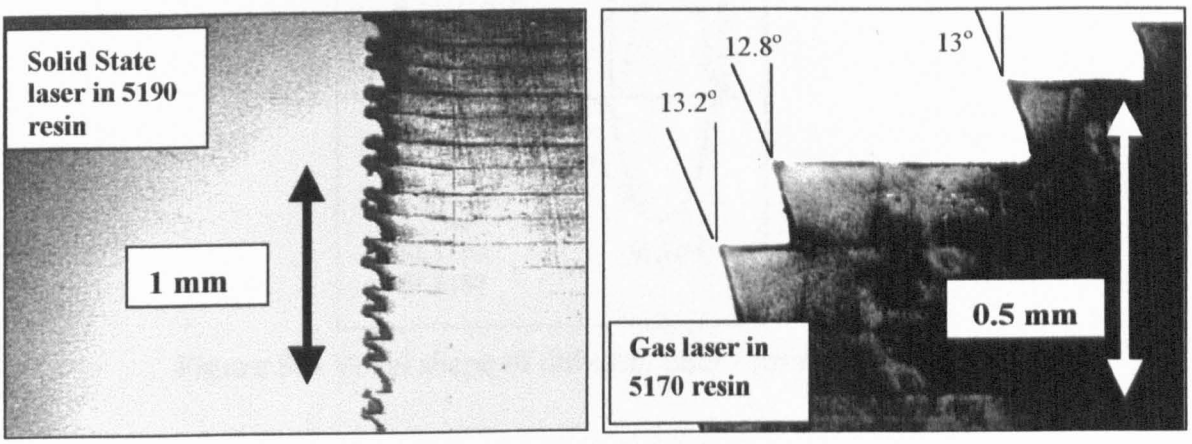

Figure 5-2 Layer profiles of solid state and gas laser in epoxy resin

If we consider the section taken through the SLA-350 shown in Figure 5-2, it can be seen that the combination of solid state laser and epoxy resin results in a radically different layer profile to the other SLA configurations. The 'sharks tooth' profile is a function of the solid state laser distribution through the SL 5190 resin. The laser used in the SLA-350 is a Solid State-Diode Pumped laser (SS-DPL). The SS-DPL is not used in a constant mode as with gas laser, but is pulsed to form a chain of over-lapped 3D pixels or 'Voxals' [130].

The energy distribution of the SS-DPL produces less of a 'Gaussean' distribution seen with gas lasers, and more of a 'T' shape distribution; hence the layer profile appears more acute, with a defined 'bell' or ' sharks tooth' as shown in Figure 5-3. This gives as average profile angle of 25 degrees following 6 measurements of the sectional profile derived from the Shadowgraph.

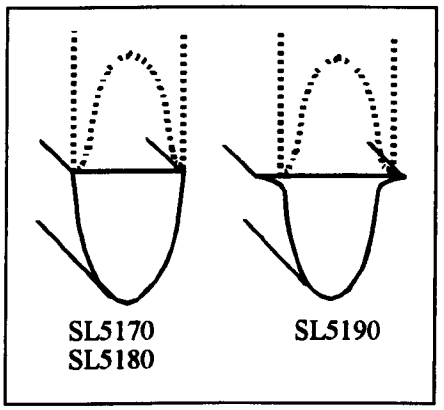

Figure 5-3 Voxel shape of different laser / resin combinations

For each of the SL samples the values of layer profile (ϕ), up facing composition roughness κ and down facing composition roughness κ_1 can now be described and these are listed in Table 5-2.

SL machine type	SL resin type	Average Up-facing roughness k	Average Down-facing roughness k1	Average Layer profile (ϕ)	Profile deviation (ϕ) (+/- degree)
SLA-250	Epoxy	2.2 μm	10.6 μm	13 degrees	-1 / +2
SLA-250	Acrylic	3.8 μm	14.1 μm	12 degrees	-2 / +2
SLA-350	Epoxy	1.8 μm	13.4 μm	25 degrees	-3 / +2
SLA-500	Epoxy	1.7 μm	11.6 μm	13 degrees	-2 / +2

Table 5-2 Constants required for mathematical model (Derived from 6 samples)

5.2 Results of the comparative analysis

Before a comparison can be made between measured and calculated surface roughness using the average values of layer edge profile and composition roughness, as detailed in Table 5-2, the effects of maximum and minimum deviation must be considered. It was shown in Figure 3-6 that the measured value of surface roughness on LMT parts can deviate considerably depending on the position of the contact probe relative to the surface topography. Using the 'truncheon' test sample each part is held in a static and repeatable position between centres when scanning. Hence,

measurement deviation is minimised. Figure 5-4 shows the measured and calculated values of surface roughness for the SLA-250 epoxy samples. The measured high and measured low values are taken from maximum and minimum surface roughness measurements in Appendix C. The calculated high values of roughness are derived using a layer edge profile (ϕ) of 15-degrees an up-facing surface roughness value (k) of 2.42 μm Ra and a down facing surface roughness value (K_1) of 11.7 μm Ra. The calculated low values of roughness are derived using a layer edge profile (ϕ) of 12-degrees an up-facing surface roughness value (k) of 2.1 μm Ra and a down facing surface roughness value (K_1) of 9.4 μm Ra.

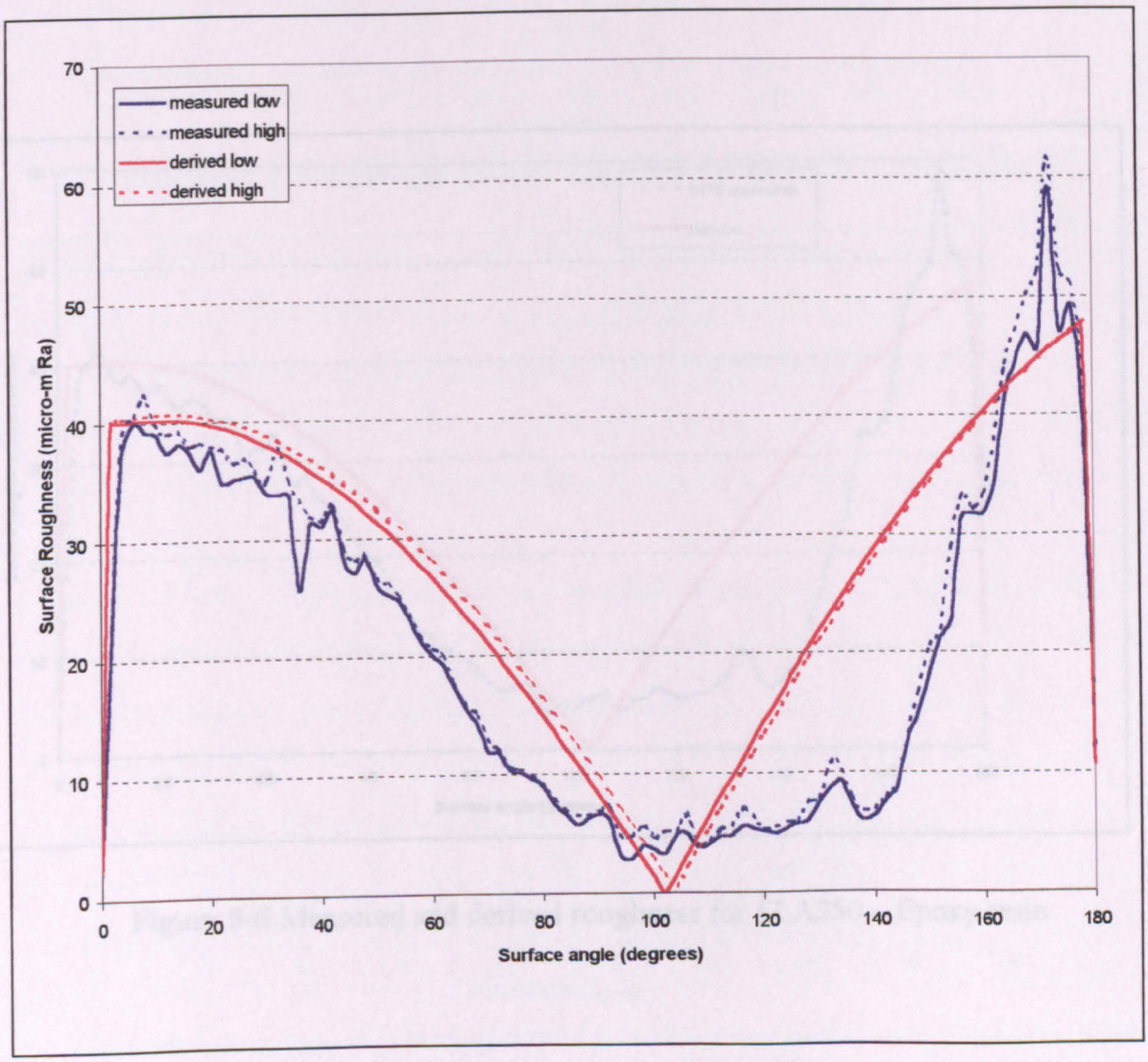

Figure 5-4 Measured and derived roughness of SLA-250 epoxy with deviation

As it can be seen in Figure 4-5, irrespective of measurement deviation both measured and calculated surface roughness plots show distinctive trends which are not radically effected by the deviation in the measurement data. Given the minimal deviation between the maximum and minimum plots shown in Figure 5-4, further comparisons will be under taken using the average values of layer profile and composition roughness detailed in Table 5-2.

Figures 5-5 to 5-8 show the comparison between measured and derived surface roughness using the data shown in Table 5-2.

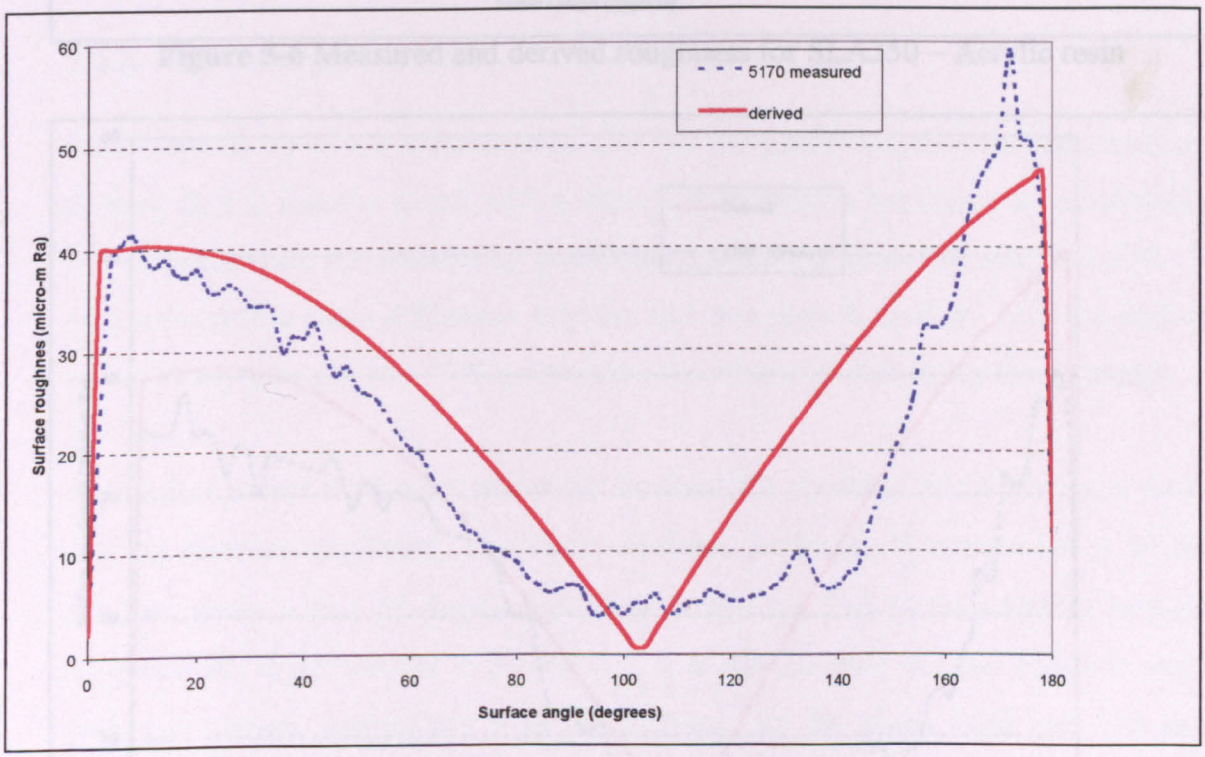

Figure 5-5 Measured and derived roughness for SLA250 – Epoxy resin

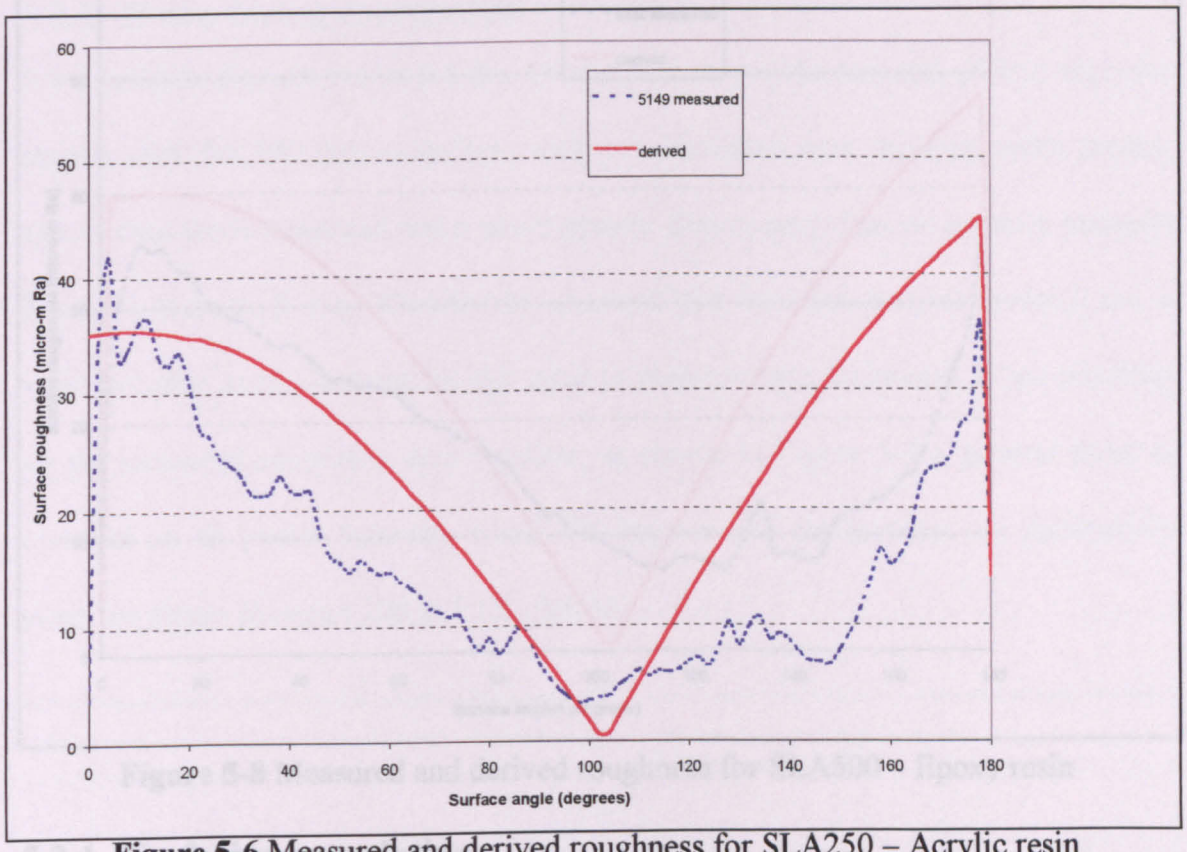

Figure 5-6 Measured and derived roughness for SLA250 – Acrylic resin

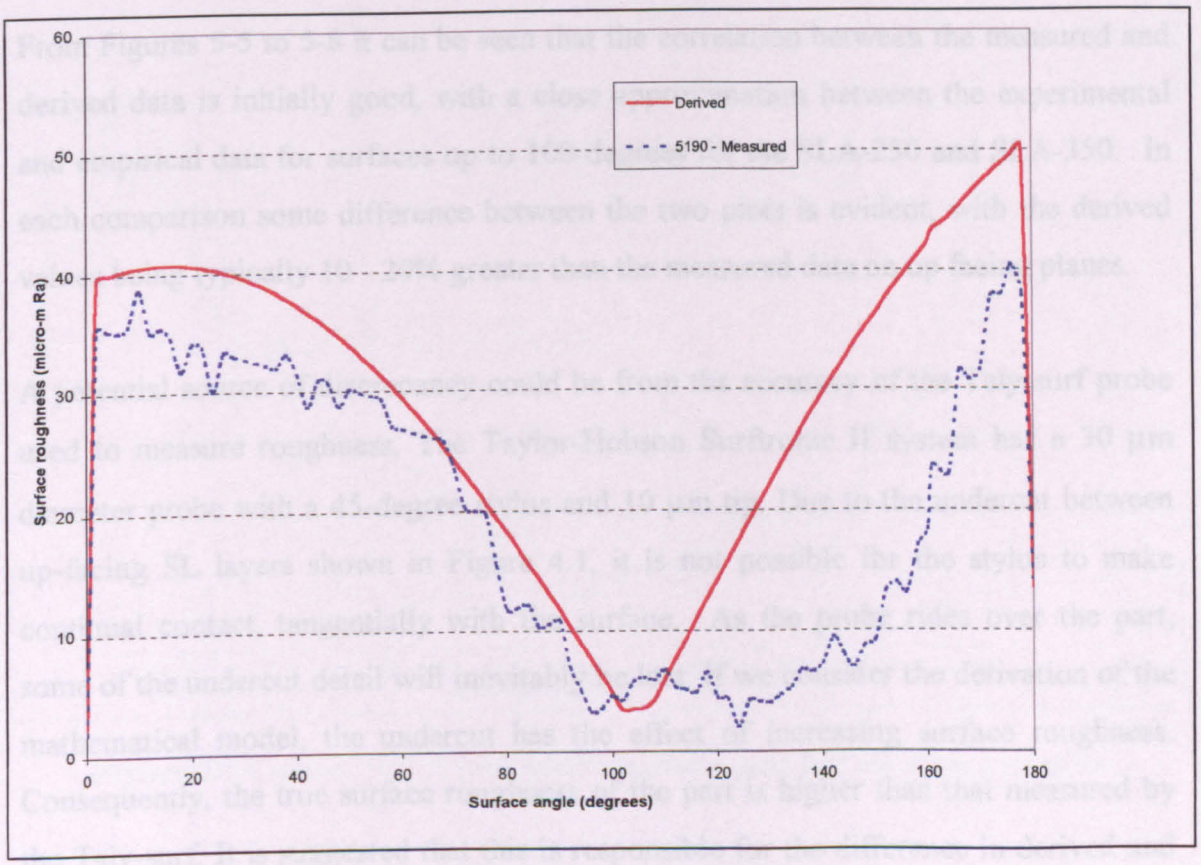

Figure 5-7 Measured and derived roughness for SLA350 – Epoxy resin

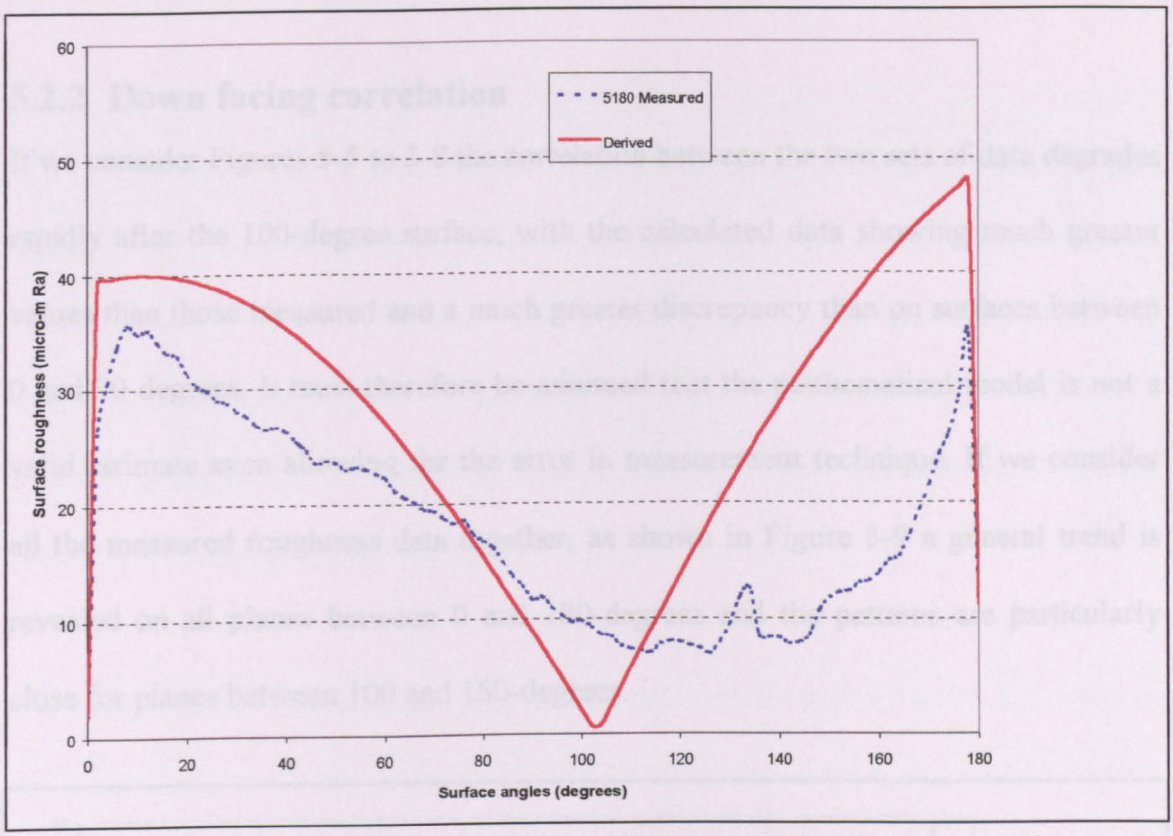

Figure 5-8 Measured and derived roughness for SLA500 – Epoxy resin

5.2.1 Up facing correlation

From Figures 5-5 to 5-8 it can be seen that the correlation between the measured and derived data is initially good, with a close approximation between the experimental and empirical data for surfaces up to 100-degrees for the SLA-250 and SLA-350. In each comparison some difference between the two plots is evident, with the derived values being typically 10 - 20% greater than the measured data on up facing planes.

A potential source of discrepancy could be from the accuracy of the Taly-surf probe used to measure roughness. The Taylor-Hobson Surftronic II system has a 30 μm diameter probe with a 45-degree stylus and 10 μm tip. Due to the undercut between up-facing SL layers shown in Figure 4.1, it is not possible for the stylus to make continual contact, tangentially with the surface. As the probe rides over the part, some of the undercut detail will inevitably be lost. If we consider the derivation of the mathematical model, the undercut has the effect of increasing surface roughness. Consequently, the true surface roughness of the part is higher than that measured by the Taly-surf. It is suggested that this is responsible for the difference in derived and measured data for the SLA-250 and SLA-350 parts up to the 100-degree angle.

5.2.2 Down facing correlation

If we consider Figures 5-5 to 5-8 the correlation between the two sets of data degrades rapidly after the 100-degree surface, with the calculated data showing much greater values than those measured and a much greater discrepancy than on surfaces between 0 and 90 degrees. It must therefore be assumed that the mathematical model is not a valid estimate even allowing for the error in measurement technique. If we consider all the measured roughness data together, as shown in Figure 5-9 a general trend is revealed on all planes between 0 and 180-degrees and the patterns are particularly close for planes between 100 and 150-degrees.

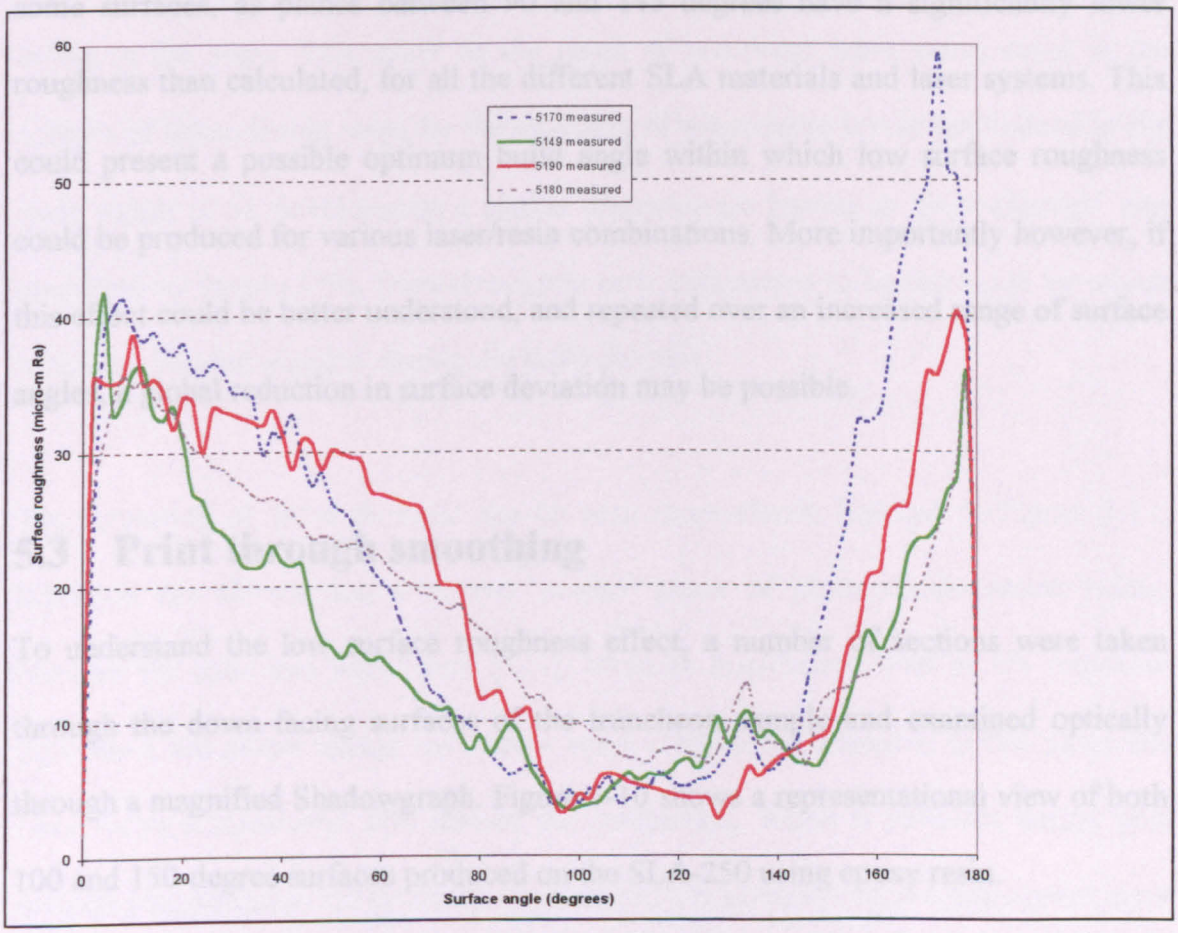

Figure 5-9 Comparison of measured roughness data for Truncheon samples

It would be surprising if measurement inaccuracy alone would cause such a high degree of difference between the overall measured and derived data, as the measured data in Figure 5-9 derived from 4 different samples all show the same roughness trends. It is therefore suggested that some as yet, unidentified attribute affects the surface roughness of down-facing planes and this must be considered in the mathematical model, Equation 4-34.

If we consider the measured data, this additional attribute appears to be beneficial to some surfaces, as planes between 90 and 145 degrees have a significantly lower roughness than calculated, for all the different SLA materials and laser systems. This could present a possible optimum build angle within which low surface roughness could be produced for various laser/resin combinations. More importantly however, if this effect could be better understood, and repeated over an increased range of surface angles, a global reduction in surface deviation may be possible.

5.3 Print through smoothing

To understand the low surface roughness effect, a number of sections were taken through the down facing surfaces of the truncheon sample and examined optically through a magnified Shadowgraph. Figure 5-10 shows a representational view of both 100 and 150-degree surfaces produced on the SLA-250 using epoxy resin.

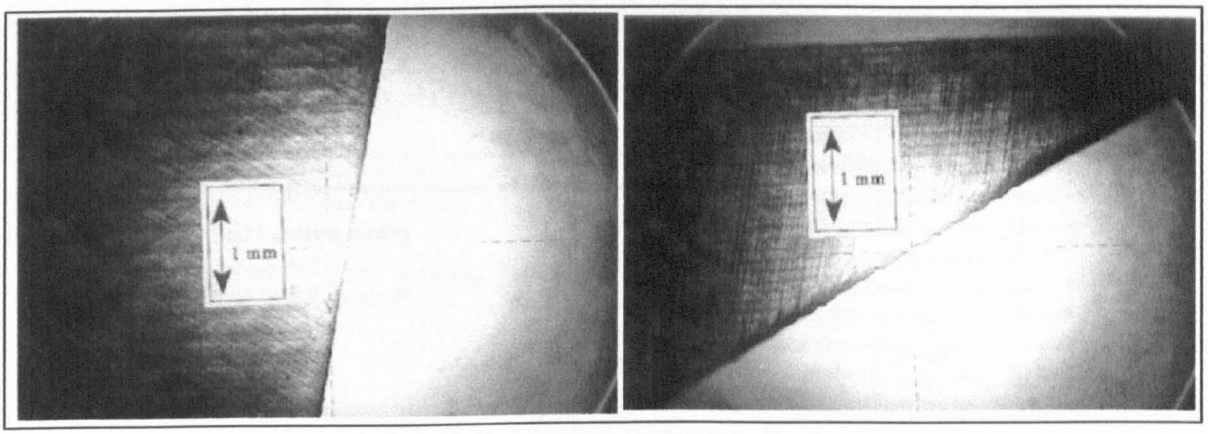

Figure 5-10 100 & 150-degree down facing SL surface

Whereas the up-facing planes have revealed a clearly defined profile, this is not the case in Figure 5-10. Material appears to be present covering the layer profile and filling in the steps. This could be the result of additional resin being cured in the corners of down-facing steps by the scanning of subsequent layers and indeed in the early stages of SL development a similar phenomenon known as 'print-through' was identified by Jacobs [58]. Print-through is now understood to be the mode by which layers are bonded together during the build process.

The formation of 'print through' can be seen more clearly detailed in Figure 5-11. Research has shown that a second 'partial' phase of photopolymerisation exists, between the solid and liquid state [131], when an insufficient level of UV exposure prevents a full phase change yet causes some cross-polymerisation. In this phase the resin forms a semi-solid skin around the component, which is removed during post process part cleaning. On down-facing planes if the boundary of the subsequent layer exceeds that of the previous layer, this semi-solid skin will be cured at the interface of two layers. It is the additional energy from the 'print-through' which causes this

cross-polymerisation. The resulting 'cure zone' forms a 'fillet' between the two layers, causing a modification to the layer profile and reducing surface deviation.

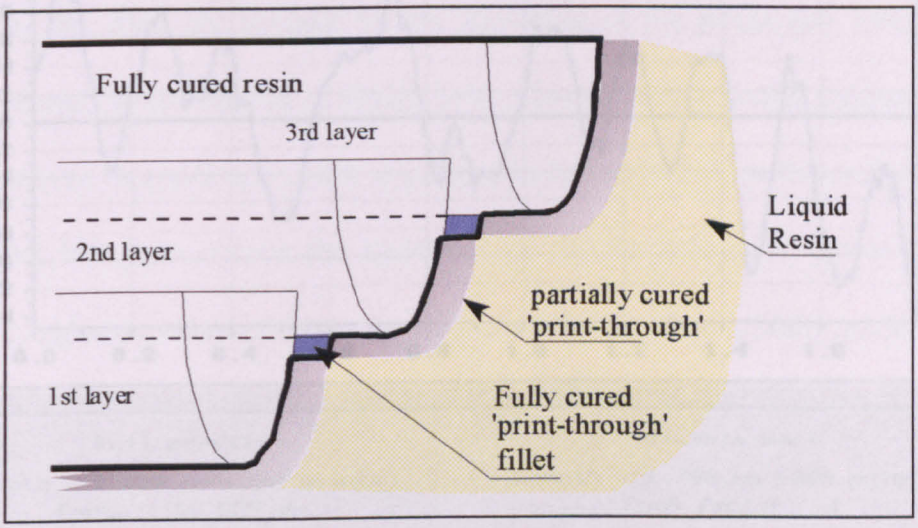

Figure 5-11 The formation of print-through on down facing planes

The existence of print-through can be seen further is we consider the surface deviation plots detailed in Figures 5-12 and 5-13.

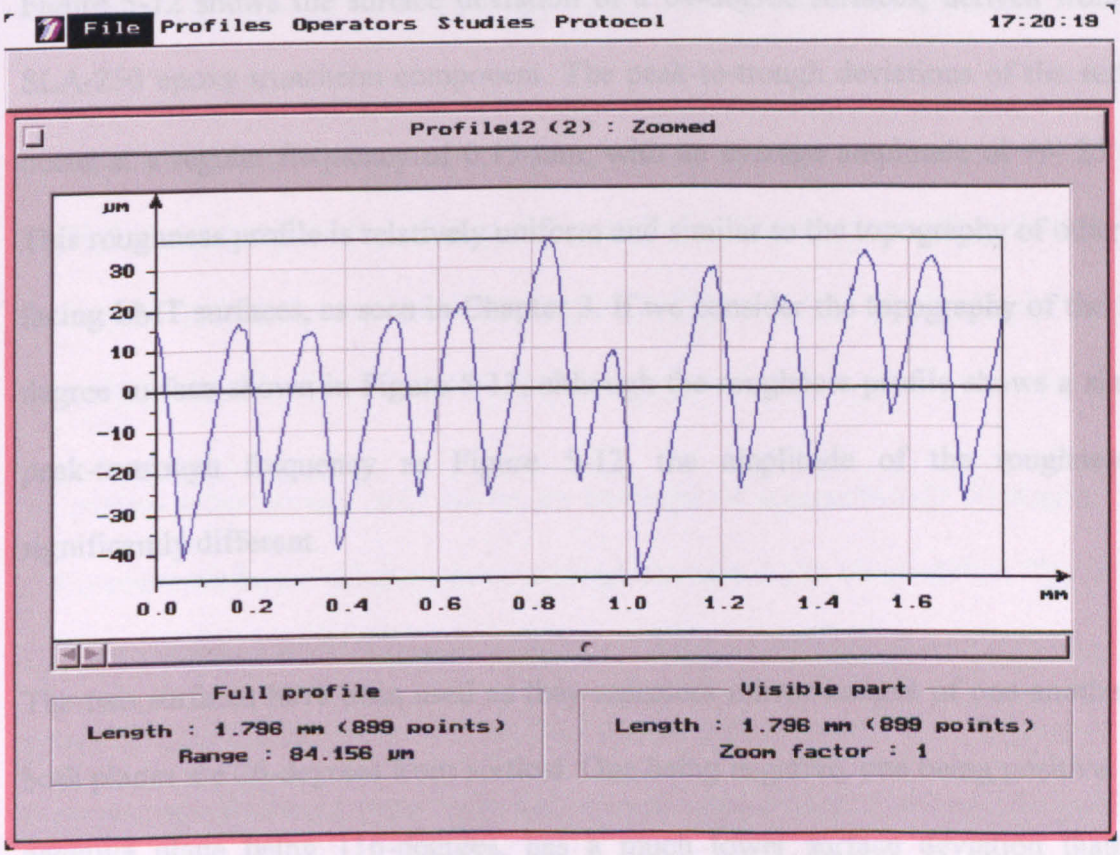

Figure 5-12 Surface plot of 64-degree SLA-250 epoxy surface 0.15 mm layers

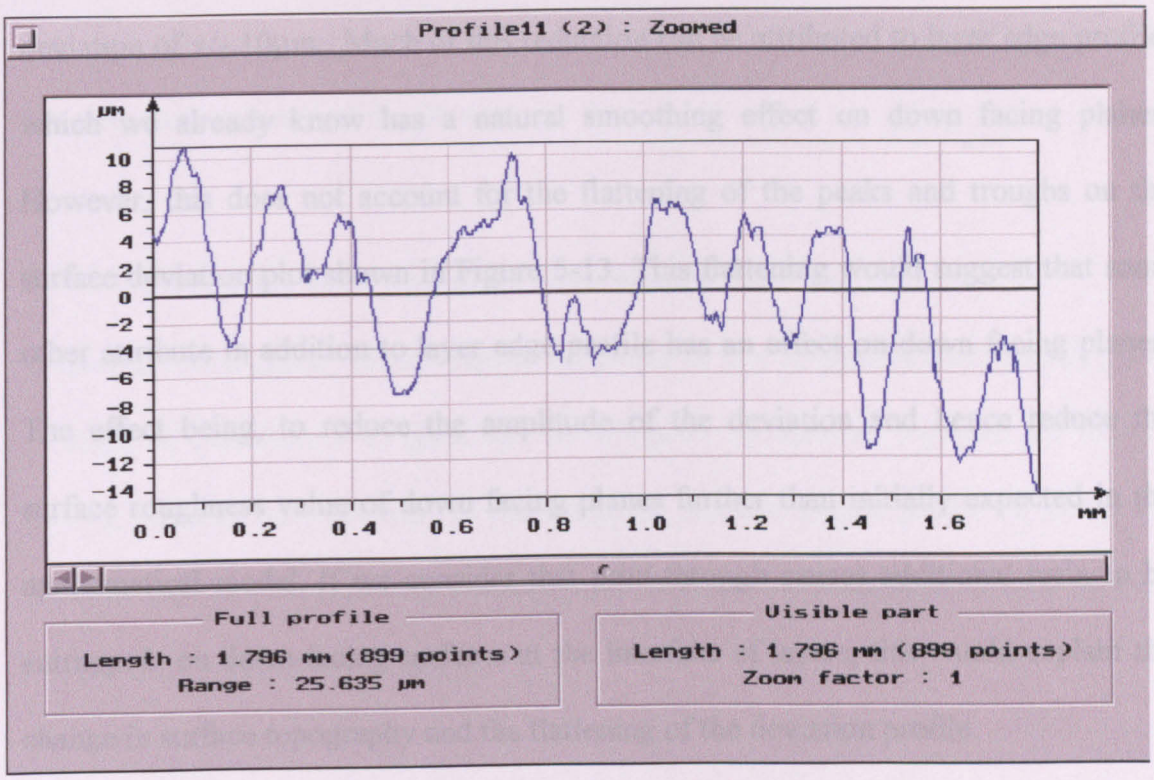

Figure 5-13 Surface plot of 116-degree SLA-250 epoxy surface 0.15 mm layers

Figure 5-12 shows the surface deviation of a 64-degree surfaces, derived from the SLA-250 epoxy truncheon component. The peak-to-trough deviations of the surface occur at a regular frequency of 0.15-mm, with an average amplitude of +/- 25 µm. This roughness profile is relatively uniform and similar to the topography of other up-facing LMT surfaces, as seen in Chapter 3. If we consider the topography of the 116-degree surface shown in Figure 5-13, although the roughness profile shows a similar peak-to-trough frequency as Figure 5-12, the amplitude of the roughness is significantly different.

The two surfaces have been used as they represent mirror images of one-another, as both planes are 26-degrees from vertical. One being negative, one being positive. The negative plane being 116-degrees, has a much lower surface deviation than the positive plane as the amplitude of the deviation shows a average peak-to-trough

deviation of +/- 10μm. Much of this reduction can be attributed to layer edge profile, which we already know has a natural smoothing effect on down facing planes. However, this does not account for the flattening of the peaks and troughs on the surface deviation plot shown in Figure 5-13. This flattening would suggest that some other attribute in addition to layer edge profile has an effect on down facing planes. The effect being, to reduce the amplitude of the deviation and hence reduce the surface roughness value of down facing planes further than initially expected in the mathematical model. If we consider that print-through causes additional resin to be entrapped on down-facing surfaces at the interface of layers, this would explain the change in surface topography and the flattening of the deviation profile.

The size of the smoothing fillet will always be uniform, irrespective of the surface angle, as print-through is a function of energy distribution within the liquid resin and can only be changed through variations in laser power. As the angle of the down-facing plane increases, the effects of print-through on surface roughness will become negligible compared to the other process attributes. The presence of print-through is shown by the roughness measurement plot in Figure 5-12, which clearly shows a secondary area of material between each layer edge of peak.

At present print-through only covers an envelope of approximately 50 degrees, and the process attributes affecting print-through can not easily be modified. The size of the 'print through' fillet is related to the laser energy initiating photo polymerisation, which is in turn, affected by both the laser power and the scan speed. If either or both these process attributes could be varied, then the size of the 'fillet' could be modified and matched to surface angle. So producing a smoother down-facing surface plane. In

reality, both scan speed and laser power, are complex attributes of the SL process and are outside the control of the SL user.

5.3.1 The limitations of 'Print-through smoothing'

Although encouraging, this 50-degree 'envelope' of low roughness produced by print-through, is insufficient to generate the complex geometries required for today's tooling patterns and cavities. If the range of smooth angles produced by 'print-through' could be increased to encompass 90 degrees, then a significant step forward in part finishing could be obtained.

Print-through smoothing may also provide a possible solution to the finishing of parts for some down stream tooling processes. With the increasing use of both direct SL tooling and cast tooling produced from SL masters, a need now exists for parts with only 90 degrees of smooth surfaces. In both cases, any overhanging or undercut features would prevent part ejection from the tool and would be replaced by sliding cores. Hence, for the manufacture of RT cavities the critical tool face only requires a maximum 'smooth build' envelope of 90-degrees, much of which can be achieved using print-through. If print-through smoothing is to be beneficial to the SL user, it must therefore be combined with other modifications to the current build strategy.

5.4 Summary

In summary it can be said that the initial mathematical model in equations 4.35 and 4.36 is only an approximation for the true surface roughness of an SLA part. The

difference between derived and measured roughness occurs because of print-though on down-facing planes.

In theory it is possible to modify equation 4-36 to include print-through as a process constant, in the same way as composition roughness k and k_1 were included in the original model. This refined model could then be used for many of the down stream applications described in section 4.3.

If we look at the process constants used to produce the derived roughness data in Figures 5-5 to 5-8, it can be seen that composition roughness has little effect on the overall surface topography of part when compared to either layer thickness or layer edge profile. For this reason, any changes made to the build strategy using either new scanning algorithms or build styles will have little effect on the overall surface of the final part.

In terms of layer thickness, this is predetermined by resin viscosity and so would be difficult to modify using existing SL technology. More importantly however, the thinner the layer, the more layers are needed to manufacture a given geometry. Unless we can significantly increase the scanning speed, such a change will inevitably increase build time and the associated part cost.

One alternative approach currently under investigation by the 3D Systems company [14] is to use thinner layer exteriors and thick layer interiors for parts. Using this build strategy, a thin layer is scanned at the perimeter of a part, prior to the retraction of the 'Z' platform. Following re-coating, a 'thin' second perimeter is scanned following

which the area within the 'two wall enclosure' is cross-hatched with a higher power scan. This results in curing of a layer twice as thick as the bounding walls. Using the 'thin-fill' layer strategy it is claimed by manufacturer 3D Systems, that build time is significantly faster than using solely thinner layers, yet is marginally slower than the current ACES build cycle. One major limitation is that the 'thin-fill' strategy is only available on SL machines fitted with the 'Zephyr' re-coater system and the solid state laser such as the SLA-350 and SLA-5000 machines. It was shown however in Figure 5.2 that it is the layer edge profile of the solid state laser that has a major influence on surface roughness, and not necessarily the layer thickness. For example the measured roughness of the SLA-350 with the 25-degree layer profile shown in Figure 5.2, shows a much higher roughness than parts produced using thicker layers with a gas-laser. It can therefore be said that 3D Systems thin-fill smoothing strategy has centered around changing the wrong process attribute as layer profile has a greater effect on surface roughness than layer thickness when building parts using solid state lasers.

If a fast effective strategy for surface finishing during the build process is to be developed, it is the author's opinion this should be focused towards the layer profile. By modifying the layer profile it may be possible to build in thicker layers and reduce build time yet improve surface roughness. Conversely it may be possible to use the current layer thickness and for a small increase in build time yield a significant improvement in surface roughness.

It is now the focus of this research, to develop a build strategy based on modifying the layer profile of up-facing surfaces for the gas laser systems. By using a combination

of some smooth up-facing surfaces and the effects on print through between 90 degrees and 150 degrees, it may be possible to develop a smooth build envelope and claim a significant step towards improving SL surface deviation and part quality.

CHAPTER 6

6.0 Modification of layer profile

According to the theoretical model developed in Chapter 4, roughness is directly related to layer thickness (α), composition (κ) layer profile (ϕ), and surface angle (θ). In addition we now know 'print through' also affects the roughness of down-facing planes. We have seen in Chapter 5 that changes to either layer composition or layer thickness cannot practically be used to produce any significant change in surface deviation without influencing the build time as the two attributes are limited by scanning parameters and resin viscosity. However, the effects of print-through were seen to be beneficial for specific angles of down-facing planes. It is the aim of this chapter to propose methods of modifying layer profile on up-facing planes, as this may produce more radical changes in surface deviation on SL models.

6.1 In-process modification to layer profile

In order to change the layer profile during the build process either the laser distribution must be changed, the phase change characteristics of the resin must be modified, or some additional axis of motion must be added to the SL process. As the research aim is to improve existing SL technology, fundamental changes to the SL hardware such as additional axis of motion have not been considered feasible.

6.2 Diffractive optical elements

One method of changing layer profile is to change the beam distribution of the laser used to initiate photo-polymerisation. At present the laser profile is either a Gaussian distribution for the gas lasers or, a 'T' shaped distribution for the solid state lasers. The distribution patterns of both lasers are illustrated in Figure 5-3. It is possible to change the profile of a near Gaussian laser beam into a more uniform cross section using a 'beam shaper' or 'Diffractive Optical Element' (DOE). A DOE is an optical 'grating' device placed between the laser source and the focal point. The DOE restricts the beam path and realigns the energy distribution of the laser into a defined pattern [132]. Using a DOE, it is possible to dictate both the laser profile and the spot shape. DOE's can be used to produce an infinite number of beam profiles from Gaussian lasers including 'top hat', 'split intensity' or angles beam profiles suitable for a range of applications. A range of typical shape patterns formed using DOE's can be seen in Figure 6-1.

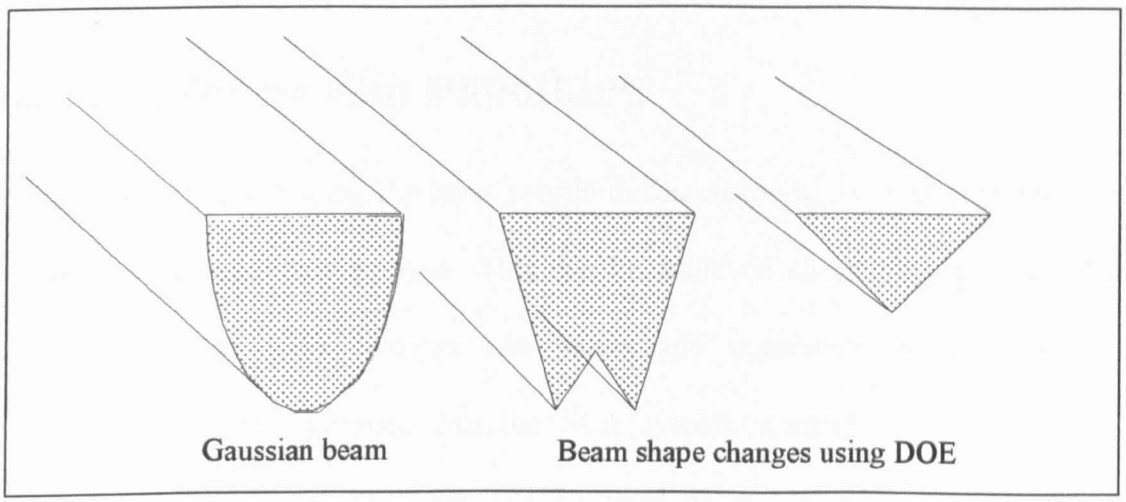

Figure 6-1 The effects of Diffractive Optical Elements on layer profile

In addition to beam profile, a DOE can also be used to transform circular profile beams into regular polygons at the focal point. It is possible to use a DOE to change the SL laser spot from circular to square. Hence sharp corners can be produced on SL models rather than the 0.2mm radiused corners produced by the Gaussian distribution lasers.

In theory a DOE could be used to match beam distribution with surface angle, and produce tangentially sided layers, hence reducing surface deviation. However, the reality is somewhat different. The DOE is a fixed device, designed to accept only a given input and produce a given output. At present, it is not possible to modify the operational characteristics of a DOE once it has been manufactured. If it were possible to manufacture a fully variable DOE, then it may be possible to synchronise the laser output to the SL part geometry, and produce continually tangential sided components.

6.3 In-process skin smoothing

One alternative to changing the layer profile during scanning is to change the layer profile using a secondary process. This can be achieved simply by applying filler materials such as resin coatings and paints and numerous systems are used commercially for this purpose. For the SLA system research by the author has demonstrated that liquid SL resin can be used as an effective coating applied following the build process [108]. Although effective, the major limitation with all

these systems is the difficulty in maintaining the accuracy and repeatability of the coating process.

One alternative to coating parts after layer manufacturing is to use in-process techniques such as 'skin' smoothing or 'passive meniscus smoothing'. The process developed by the author and Davey, is an SL build strategy where parts are manufactured in sections using groups of layers and skins of liquid resin. The principle of 'skin smoothing' is an extension from earlier research by the author that applied SL resin to parts following manufacture. Using skin smoothing the coating is applied during manufacture.

The process is described as follows;

Following the scanning of between 10 and 20-layers, dependent on geometry, the build cycle is stopped. The part is then retracted from the resin to a position where the first layer is level with the surface of the vat. After retraction a smooth 'skin' of liquid resin held by surface tension covers the part. The majority of the liquid resin is then allowed to drain from the part surface, leaving a smoothing meniscus covering much of the surface deviation. After a predetermined time period, depending on geometry, the laser is scanned over the surface of the liquid meniscus using hatching information for the first layer. By repeating the scanning a number of times, the meniscus is locked in place producing a smoothing skin over the stepped surface. After curing, the part and skin are dipped back into the vat and the build process is continued from the last layer.

Although limited in application, skin smoothing has shown reductions in roughness on some surfaces of over 80% from 35 μm Ra to below 4 μm Ra, with only minimal change in overall part geometry. Figure 6-2 shows a wineglass geometry manufactured using skin smoothing. The base of the glass was built as normal, using the ACES build style up to the start of the stem. Prior to the scanning of the stem the part was retracted from the resin vat pulling a skin of liquid resin. The scanning data from the first layer of the part was then used to lock the surface meniscus in place. After repeated scanning to initiate full photopolymerisation, the part was dipped back into the vat and the build cycle restarted on the first layer of the stem. Given the geometry of the glass no further smoothing was needed on either the stem or the upper bowl as all surfaces fall within the smooth 100 to 145-degree build envelope.

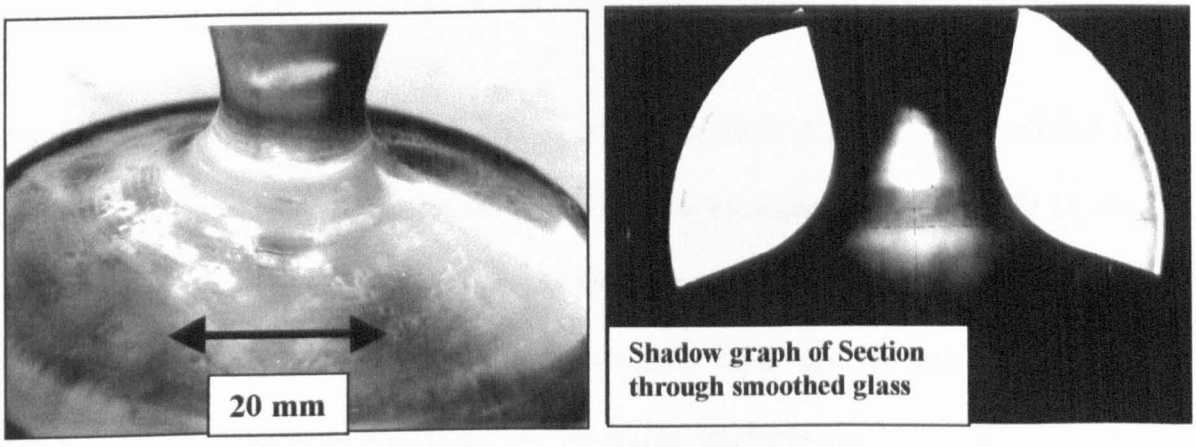

Figure 6-2 The application of skin smoothing on a 'wine glass' geometry.

The main limitation of skin smoothing is one of complexity. The technique will not work on complex geometries with multiple angled faces or solid objects with internal

features and trapped volumes. Consequently for most components skin smoothing is not a viable solution to in-process surface finishing and has therefore not been investigated further.

6.4 Meniscus smoothing

As identified in Chapter 2, two other research groups have discussed the use of meniscuses generated during the build process, as a means of reducing surface deviation. Research by Narahara at the Kyushu institute of technology, has investigated the use of meniscuses generated on parts manufactured using a Japanese SONY JSC 2000 SL machine, with the Japanese Synthetic Rubber company resin JSR 200 [91, 92]. Narahara's 'lift-up irradiation method' uses a similar process to 'skin smoothing' but is undertaken between each layer as shown in Figure 6-3, rather than following a group of layers.

The purpose of Narahara's research was to prove a mathematical model developed to derive an optimum layer thickness in Stereolithography using variable profile layers. Narahara's 'Stock-removal model' derives the change in peak-to-trough deviation of a layer-manufactured surface, using both variable layer profile and layer angle. However, the model only functions on up-facing surfaces and neglects all other attributes affecting surface deviation.

Using the SONY machine with a 600 μm beam, Narahara performed a number of trials to verify his mathematical model. Experimental layer thickness ranged between

100 μm and 300 μm. Although proving the principle of the 'stock-removal model', Narahara's experiments showed little control over the meniscus shape and the subsequent change in layer profile. No investigation into optimum meniscus shape was performed, as Narahara was only successful in reducing the surface deviation of planes between 10 and 30 degrees from the horizontal. Nevertheless, Narahara's research did show a reduction in peak-to-trough deviation of 75%.

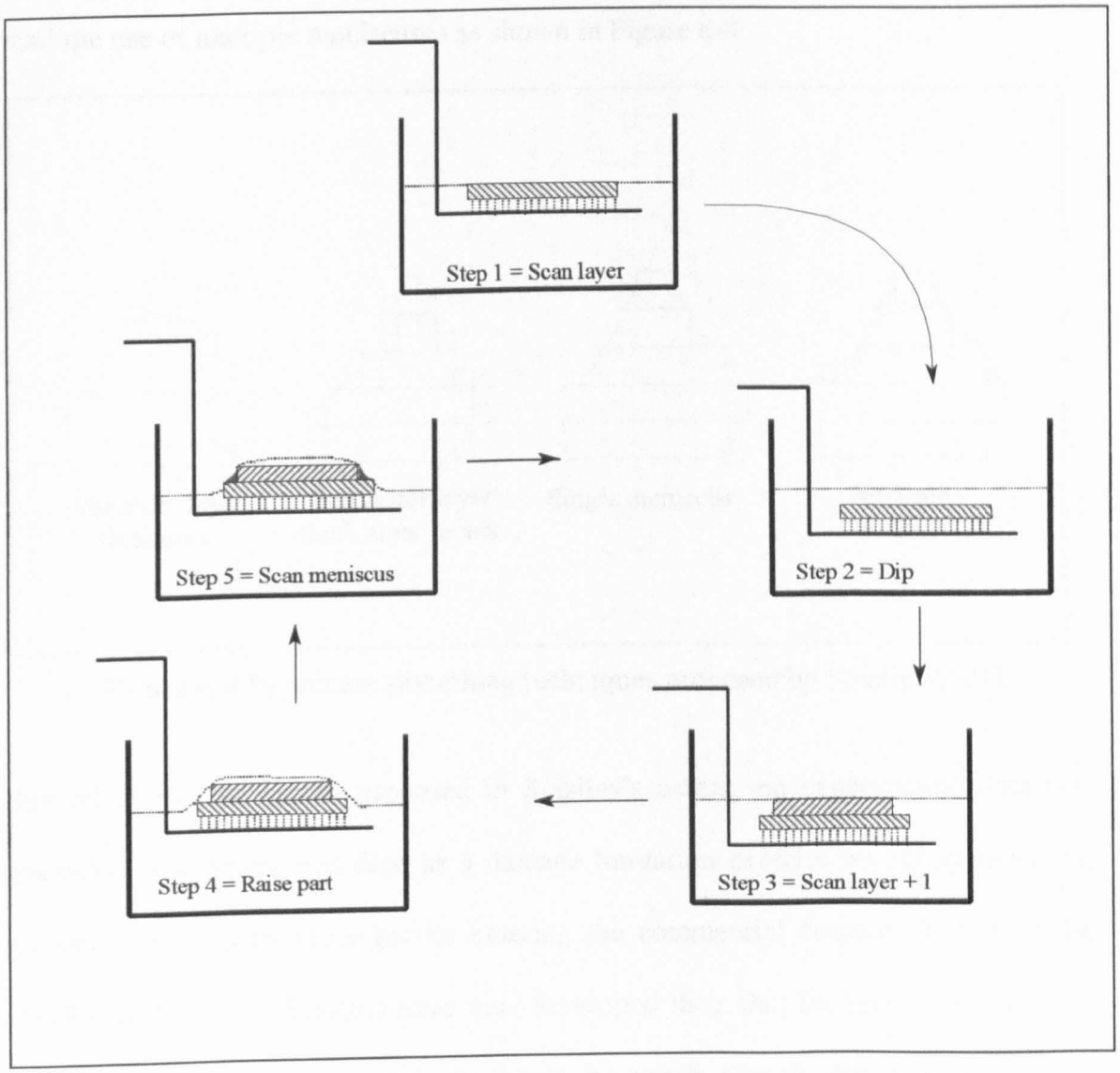

Figure 6-3 Surface smoothing using the 'Lift up irradiation method'

6.4.1 3D systems and meniscus smoothing

In addition to the work undertaken by Narahara, Smalley has also discussed the concept of 'meniscus smoothing', in US patent 5,209,878 [121]. The patent registered to 3D Systems covers a variety of in-process techniques suitable for smoothing SL surfaces. The patent includes the use of variable thickness layers, thin outer layers and thick inner layers, the use of single meniscuses such as in Narahara's research and the use of multiple meniscuses as shown in Figure 6-4.

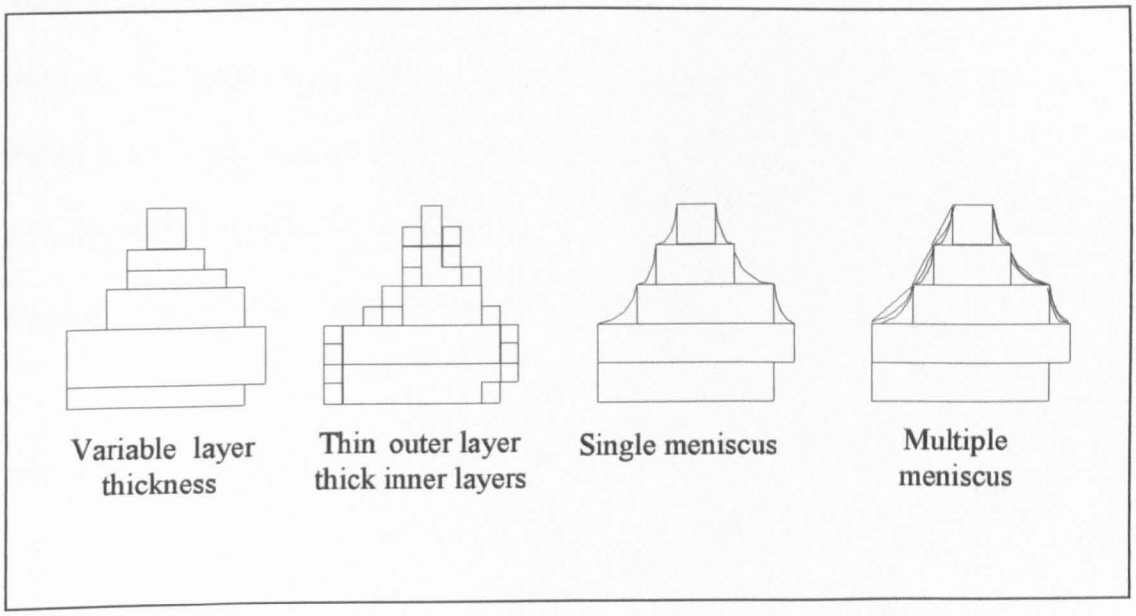

Figure 6-4 In-process smoothing techniques proposed by Smalley [121]

For all of the techniques proposed in Smalley's patent, no experimental data was provided. The patent was filed as a damage limitation exercise by 3D systems and prevents research by other parties entering the commercial domain. It is from the 1993 patent that 3D Systems have now developed their thin fill layer 'tooling build style' described in section 5.4. It should be noted though that this build style identified in the patent is only possible using the Zephyr re-coating system, which was not developed until 1996.

Meniscus smoothing appears to be a positive approach towards reducing surface deviation as an in-process technique. To-date however, no experimental results have been published on the benefits of meniscus smoothing using 3D systems SLA technology. More importantly, no research has been undertaken to apply meniscus smoothing to patterns and cavities used for down stream rapid tooling.

Before beginning any practical research into meniscus smoothing using the SLA-250 system, the author approached 3D Systems to establish the current state-of-the-art based on previous work. Through a personal communication with chief executive Chuck Hull, a number of limitations to meniscus smoothing were discussed which have prevented further research by the company [133].

3D systems concentrated their meniscus smoothing research on parts with only up-facing surfaces. For simple parts like the wineglass in Figure 6-2, meniscus smoothing can be successful.

If we consider more complex geometries such as the cavity in Figure 6-5, it is not possible to form a meniscus during the build process. As the part is retracted from the vat, the liquid resin within the scanned area is trapped and cannot flow over the surface forming a meniscus. The current solution proposed by 3D systems is to use the Zephyr active re-coating blade to vacuum the excess resin out of the trapped

volume, leaving a meniscus on the part surface. The meniscus could then be cured before the part is lowered back into the vat. To-date this solution is only theoretical.

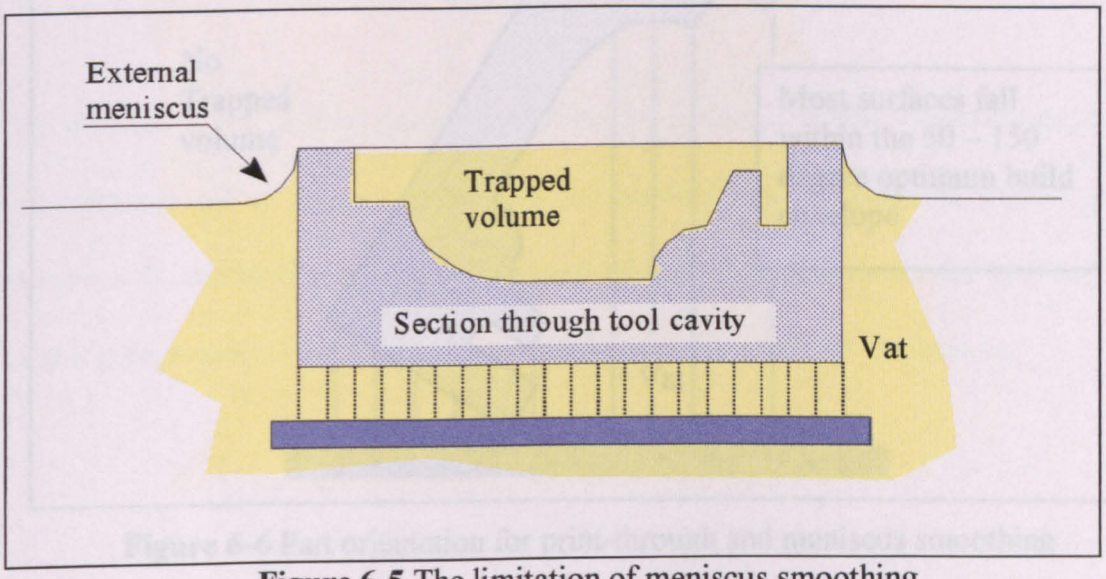

Figure 6-5 The limitation of meniscus smoothing

6.5 Meniscus smoothing research aims

If we consider the findings of the roughness model verification in Chapter 5, the effects of print through were identified on down-facing surfaces between 90 and 145 degrees.

If meniscus smoothing is to be combined with the benefits of print-through, it must be developed for angles between 50 and 90 degrees, resulting in an overall smooth build envelope of at least 90 degrees. If the cavity from Figure 6-5 is positioned in an orientation to benefit from both process attributes it may be possible to prevent the inclusion of trapped volumes and also significantly reduce surface deviation, as shown in Figure 6-6.

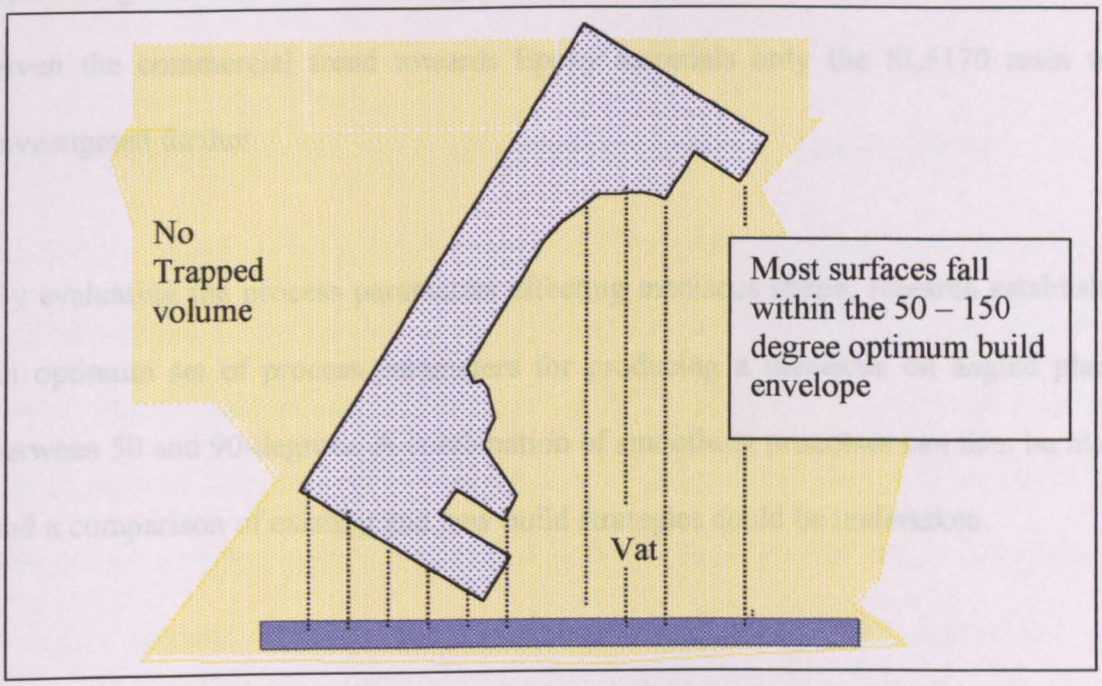

Figure 6-6 Part orientation for print-through and meniscus smoothing

By orientating the part as shown on Figure 6-6, it is possible to build most of the critical surfaces within the optimum build envelope. However both the build time of the part and the number of support structures required can increase. In addition, it should be noted that support structures now connect to the critical surfaces of the component. This should be minimized if possible, although experienced model makers who work with SL parts consider the removal of support structure and witness marks considerably easier than the removal of heavy stair stepping.

6.6 Summary

The review of previous work has established meniscus smoothing as a positive direction for further research. Based on both the limited results of Narahara's work and the process limitations identified by 3D systems, research was directed towards

optimizing the meniscus smoothing process using an SLA-250 system. Furthermore, given the commercial trend towards Epoxy materials only the SL5170 resin was investigated further.

By evaluating the process parameters affecting meniscus shape, research established an optimum set of process parameters for producing a meniscus on angled planes between 50 and 90-degrees. A combination of smoothing processes can then be made and a comparison of existing and new build strategies could be undertaken.

CHAPTER 7

7.0 Development of a meniscus smoothing cycle

From the research by both 3D Systems and the Kyushu institute, it has been shown that meniscuses generated during the build process may provide a suitable alternative to post-process part finishing of SL models, if the meniscus shape can be predicted and controlled. Meniscus shape is a function of process variables such as the surface area of the retaining step, the temperature of the resin and the dwell time between meniscus scanning. In addition the wetting characteristics of the liquid resin on the polymerised monomer must also be considered, as this affects the surface tension of the meniscus and the resulting shape of the smoothing fillet.

The current SL control software has been written to give the machine operator only the basic commands required to manufacture parts. It is not possible therefore to build parts with meniscuses between layers, as this control function does not exist within the current software. This is because a build 'algorithm' must be developed which can be initiated using the existing software, yet retaining control over the variables affecting meniscus shape. The build algorithm must also be repeatable through the build cycle and able to run in an automated sequence. Before fully automated smoothing software can be written, a build algorithm must be developed for the generation of a single layer.

7.1 Controlling 3D systems software build algorithm

The 3D systems 'Build station' software is a DOS driven series of menus designed to control the mechanics of the SLA 'machine tool'.

Using the 'build station' software it is possible to control hardware attributes such as the platform position, the re-coater blade, and the position of the scanning mirrors. In addition the 'build station' software can also be used to build specified layers of a part from the slice file. It is possible to initiate all the sequences shown in Figure 7-1 using the existing 3D systems SLA-250 operating system albeit as a series of manual commands.

STEPS 1-3 Support structure generation and the first layer

Steps 1-3 involve the manufacture of the part support structure and the first layer of the part. When building 0.15-mm layers, there are 12 CAD layers to every build layer. In addition every part has 7.5 mm of support structure. Hence, the end of the first build layer comprising support layers n_s and part layers n_p, can be calculated as (7.5/0.15*12)+12 = 612. Each subsequent build layer is then defined by the addition of 12 CAD layers.

To prevent the loss of the machine datum following the scanning of the last build layer, commands must be used to prevent the build platform from returning to the home position and prevent the automated levelling sequence between each new layer. Automatic levelling can be prevented using the command Z off. Similarly, the build

platform can be prevented from returning to the home position using the command No Drain. The build sequence for the Steps 1-3 is described in Figure 7-1.

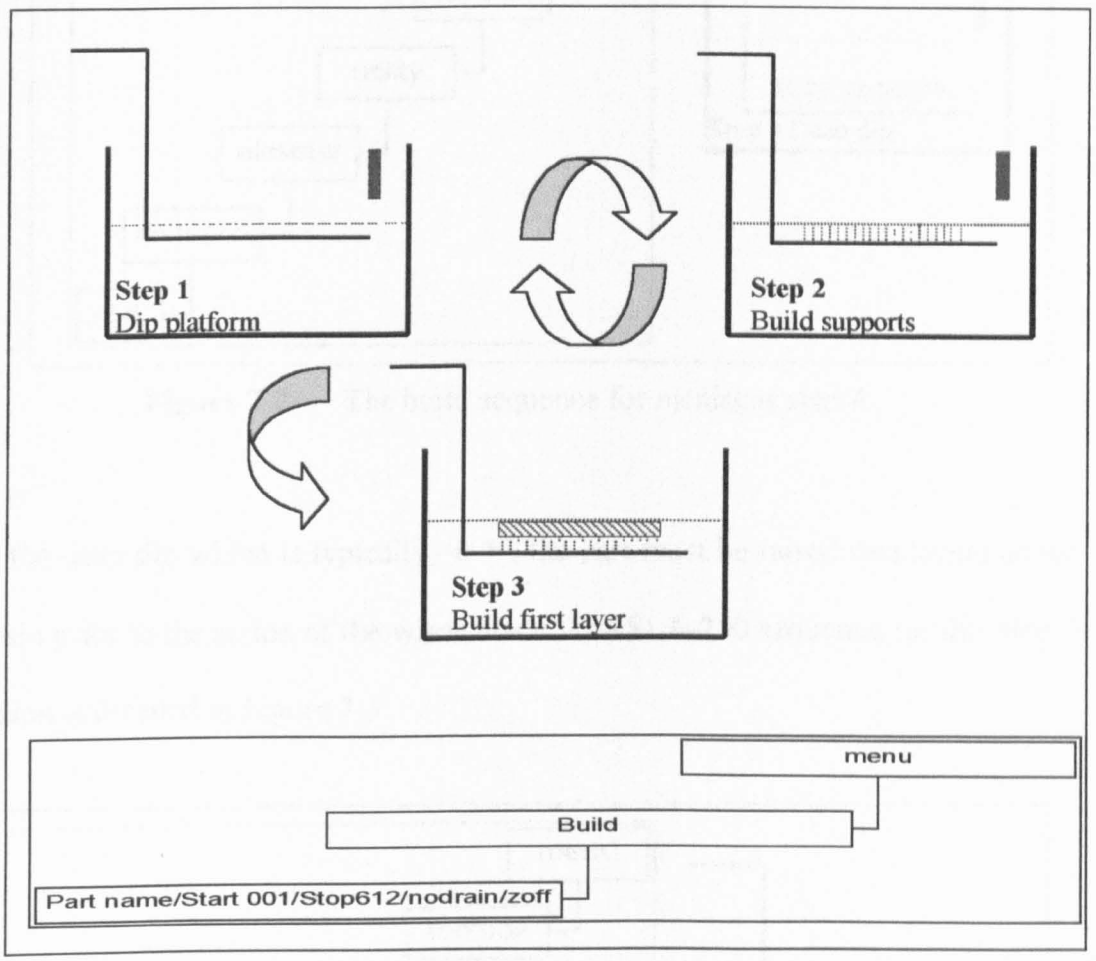

Figure 7-1 The build sequence for meniscus steps 1-3

STEP 4 -7 Deep dip, Re-coating & Retraction

To prevent inaccuracies in the Z-axis and improve the flatness of up-facing surfaces, the wiper blade must be used to level each layer between scanning. Before the wiper blade can be used, a layer of liquid resin must be formed over the previously polymerised layer. The SLA-250 sequence for this operation is shown in Figure 7-2.

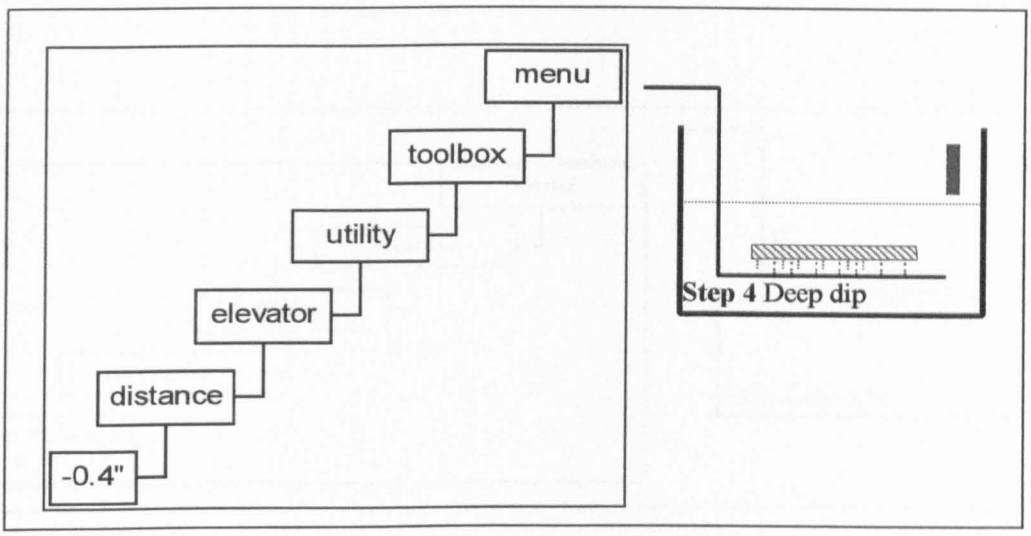

Figure 7-2 The build sequence for meniscus step 4

After the deep dip which is typically –0.4", the part must be raised two layers above the resin prior to the action of the wiper blade. The SLA-250 sequence for this step 5 operation is detailed in Figure 7-3.

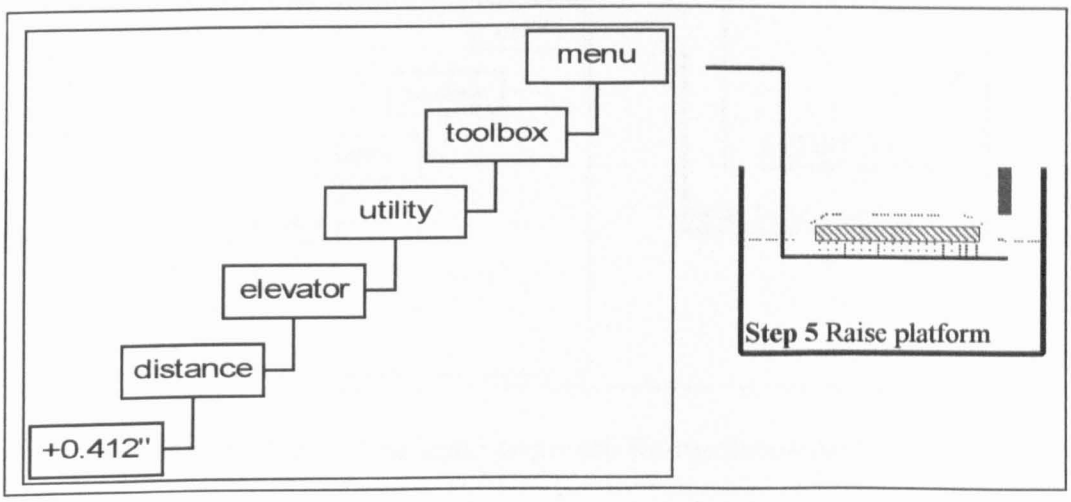

Figure 7-3 The build sequence for meniscus step 5

Following the retraction of the part and the resin layer from the vat, the wiper blade is pushed over the surface to level the resin used to generate the next layer. The SLA-250 sequence for this step 6 operation is detailed in Figure 7-4.

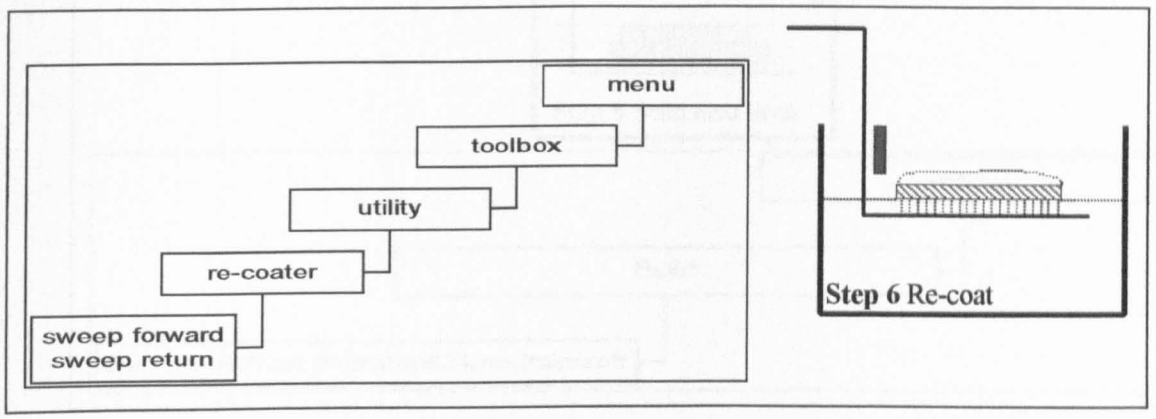

Figure 7-4 The build sequence for meniscus step 6

After the re-coater blade has been returned to the home position, the part must be retracted so the polymerised material is a single layer thickness below the top of the liquid vat, this is achieved by dipping two-layer thicknessess. The SLA-250 sequence for this step 7 operation is detailed in Figure 7-5.

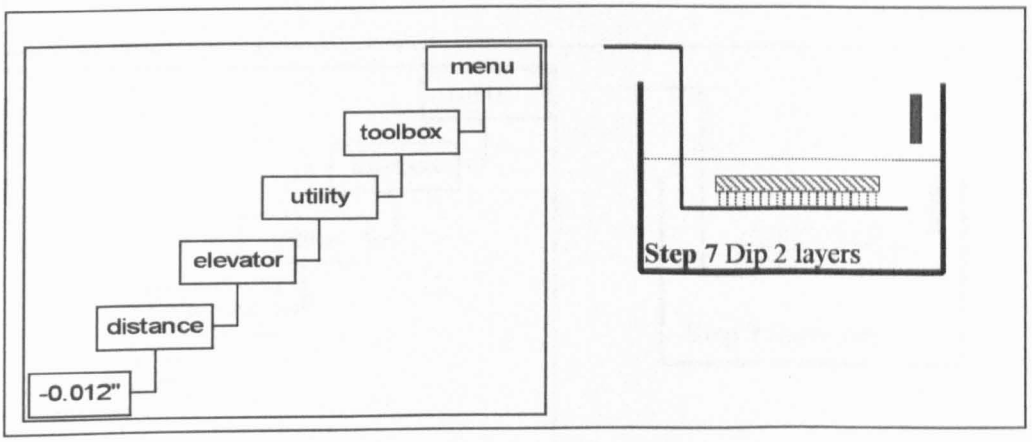

Figure 7-5 The build sequence for meniscus step 7

STEP 8 - 11 Scanning of the next layer & meniscus fillet

Following the retraction of the first layer and resin, the second build layer can be scanned onto the surface of the vat. The SLA-250 sequence for this step 8 operation is detailed in Figure 7-6.

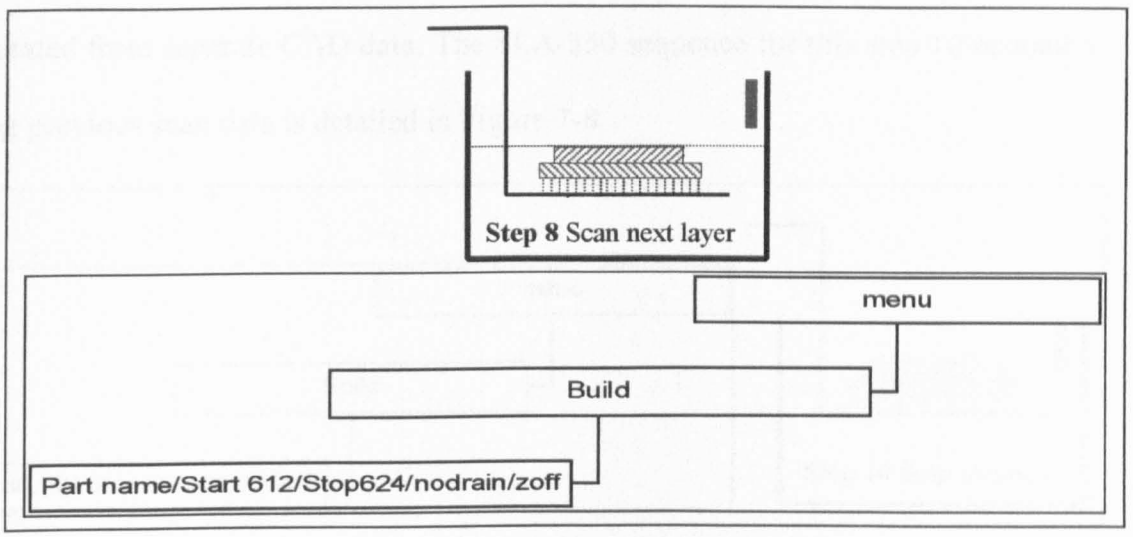

Figure 7-6 The build sequence for meniscus step 8

After the scanning process the platform is raised from the vat forming a meniscus between the two layers. The shape and subsequent smoothing characteristics of the meniscus are a function of this retraction distance. The SLA-250 sequence for this step 9 operation is detailed in Figure 7-7.

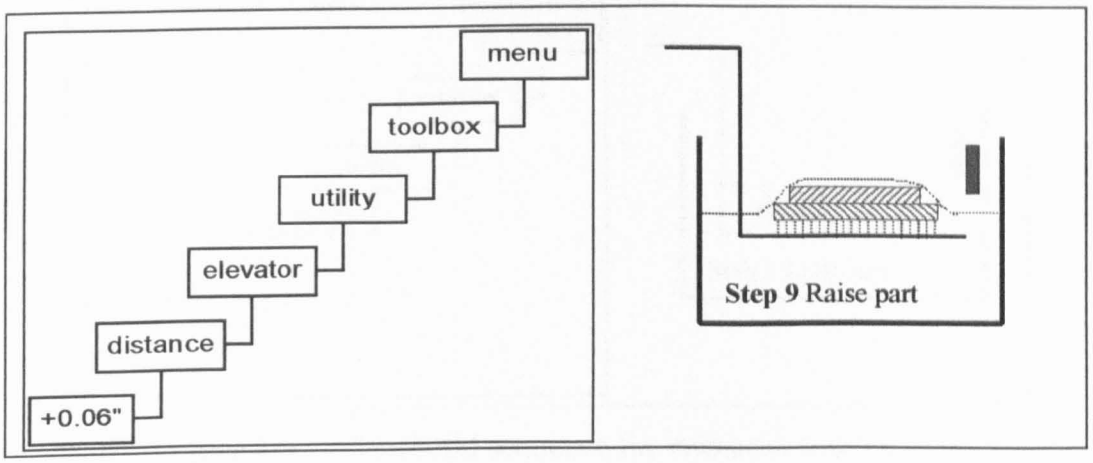

Figure 7-7 The build sequence for meniscus step 9

Following retraction of the second layer above the resin, a single scan pass of the laser can be used to 'lock' the smoothing meniscus in place. The scan data can be information from a previous layer or information from a separate smoothing file

generated from separate CAD data. The SLA-250 sequence for this step 10 operation using previous scan data is detailed in Figure 7-8.

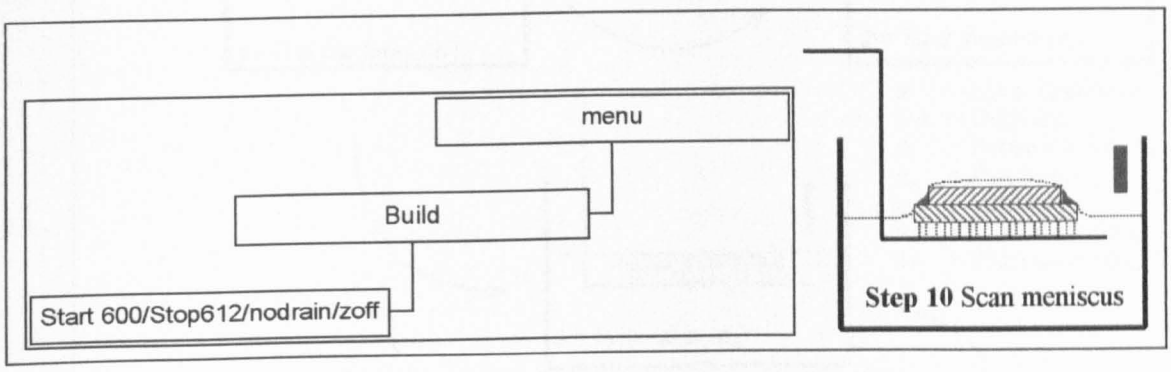

Figure 7-8 The build sequence for meniscus step 10

After the smoothing meniscus has been locked in place, the part must be returned back to the home position by lowering the platform by the distance added in Step 9. The SLA-250 sequence for this step 11 operation is detailed in Figure 7-9.

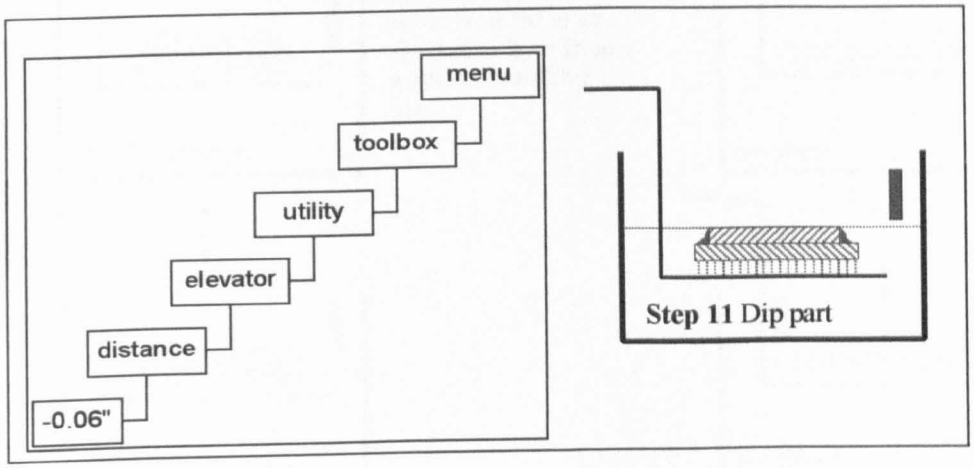

Figure 7-9 The build sequence for meniscus step 11

Following the return of the 2-layer build and meniscus to the home position the smoothing cycle can be repeated from Step 4. The complete meniscus smoothing cycle for the SLA-250 system can be seen illustrated in Figure 7-10.

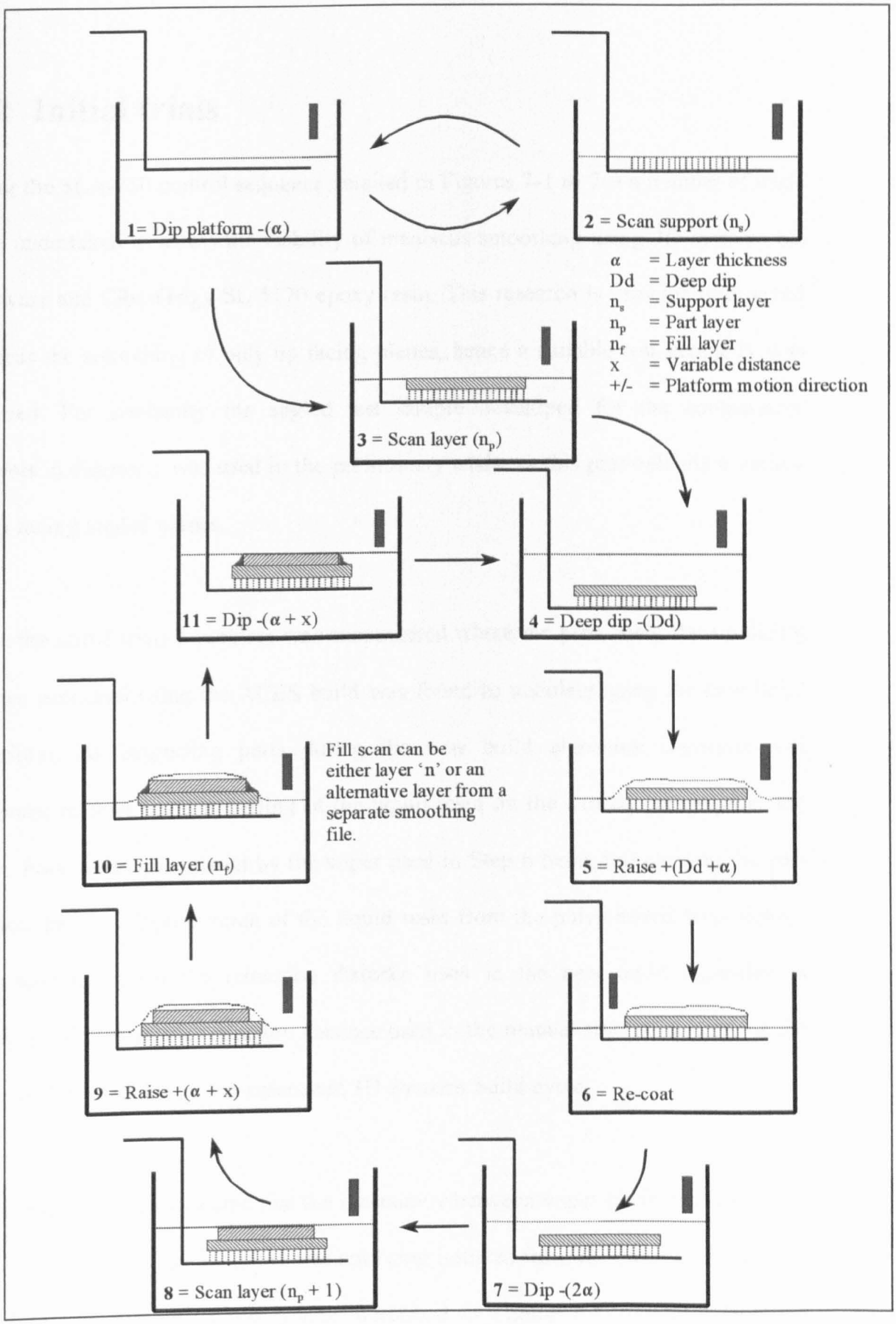

Figure 7-10 The Meniscus smoothing algorithm for an SLA-250

7.2 Initial trials

Using the SLA-250 control sequence detailed in Figures 7-1 to 7-9 a number of trials were undertaken to assess the viability of meniscus smoothing using 3D systems SL hardware and Ciba-Geigy SL 5170 epoxy resin. This research is principally directed towards the smoothing of only up facing planes, hence a suitable test geometry was required. For continuity the angled test sample developed for the comparative analysis in chapter 3 was used in the preliminary trials, as this part exhibits a variety of up-facing angled planes.

From the initial trials a problem was encountered where the previously flat up-facing surface produced using the ACES build was found to undulate using the new build algorithm. By inspecting parts during the new build algorithm waviness was attributed to poor surface wetting of the liquid resin on the subsequent polymerised layer. Poor wetting is caused by the wiper used in Step 6 being too close to the part surface, hence stripping much of the liquid resin from the polymerised layer below. This would suggest the retraction distance used in the new build algorithm is incorrect. However, the retraction distance used in the manual smoothing trials is the same as that used during the automated 3D Systems build cycle.

On investigation it was found that the inaccuracy between wiper blade and part is the cumulative result of the build process not being initiated from the machine datum. By initiating the build using the process described in Figure 7-1, the resin levelling function is disabled using the command zoff. Hence the platform is not in the correct

position at the start of the first layer and accuracy is lost over each subsequent layers. Using the 3D systems software it is possible to datum the build platform, and prevent the inaccuracy caused by waviness. By initiating and stopping a normal build cycle at CAD layer 1 it is possible to position the platform in the datum location.

7.3 Automating the systems using TSR software

Using the new build algorithm it should be possible to build any geometry irrespective of complexity. However Steps 4 to 11 of the smoothing cycle are labour intensive and require a dedicated machine operator to produce a single part. Such a solution although potentially more accurate than post-process finishing is not a viable option for rapidly finishing components. Hence, an automated program must be developed to loop Steps 4 – 11 of the smoothing cycle. In addition, a 'counter' must be added to the program to index both the building and smoothing scan data by 12 CAD layers for each loop of the cycle. The program must also run in parallel with the 3D systems operating system, as this controls the build attributes detailed in Figures 7-1 to 7-9.

A program was developed in 1991 by J Mathisen [134], which may be suited to the meniscus smoothing cycle. The Terminate Stay Resident (TSR) program is designed to occupy a small percentage of a computers high level memory, and perform a series of tasks using data in a pre-written script file. The program can then be run alongside other software. The script file contains a sequence of time delays and keystrokes, which would be initiated manually if an operator were present at the computer. Hence

a manual series of computer tasks can be performed without the need for an operator. Figure 7-12 shows how a TSR program can be run concurrently with the 3D systems build station software as a method of generating automated meniscuses between layers.

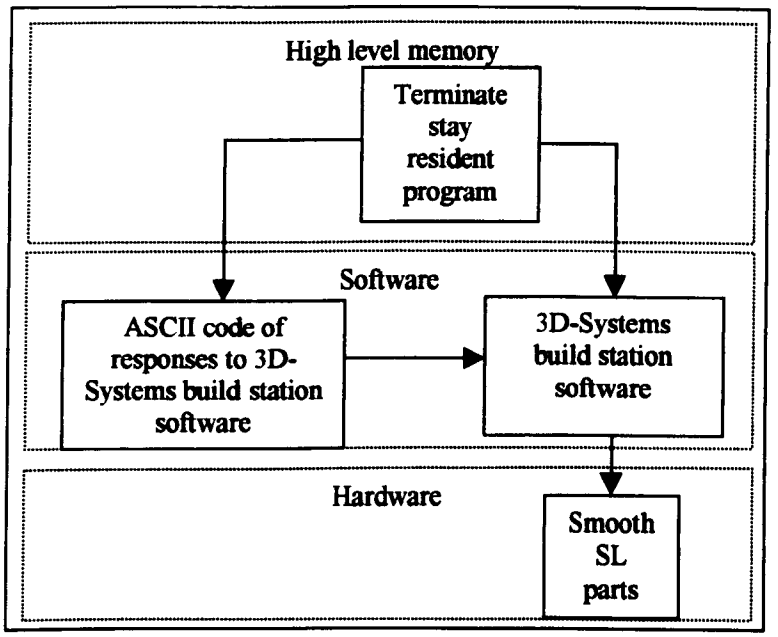

Figure 7-12 Automation of the smoothing cycle using TSR software

If we consider Step 4 of the meniscus smoothing cycle shown in Figure 7-2, a script can be written to control the machine using Matheson's software provided that the corresponding ASCII codes can be defined for each of the 3D systems build station menus.

Table 7-1 shows the 3D systems software sequence for Step 4 and the associated ASCII codes, which would be input by a manual operator as keyboard responses.

PAGE
MISSING
IN
ORIGINAL

program. After the correct ASCII commands and delays have been initiated the ASCII script must return the 3D-systems build station menu back to the DOS prompt before the next operation. In most cases this is undertaken by using the Exit command 'X' which equates to ASCII number 120. The resulting ASCII script for smoothing cycle Step 4 is detailed in Figure 7-13. The code includes both suitable time delays and commands to start from the DOS prompt and return to the DOS prompt after dipping the platform by a pre-determined distance.

```
REM Smoothing cycle Step 4

+0 109 101 110 117 13
+2 54
+4 49
+7 51
+10 100
+5 45 46 52 48 48 13
+10 120
+10 120
+10 120
+10 120
+10 121
```

Figure 7-13 ASCII Script for Step 4 of the meniscus smoothing cycle

By generating code for each step of the smoothing algorithm, an ASCII command script has been developed for the total automation of a single cycle. The ASCII script for a single cycle is detailed in Figure 7-14.

ASCII code	Software action & response
+10 98 117 105 108 100 13 +10	Del 10 sec's, Build, rtn
+15 'men1/start001/stop614/nodrain' 13 +45:	Del 15 sec's, start 001, stop 613, nodrain, rtn
+0 109 101 110 117 13	Del 0 sec's, menu, rtn
f37,4,5,'C:\WORK'	Wait for screen text work at location 4,5
+2 54	Del 2 sec's, option 6 (tool box)
+4 49	Del 4 sec's, option 1 (utility)
+7 51	Del 7 sec's, option 3 (elevator)
+10 100	Del 5 sec's, option d (distance)
+5 45 46 52 48 48 13	Del 5 sec's, -0.400, rtn
+10 100	Del 10 sec's, option d (distance)
+10 43 46 52 48 54 13	Del 10 sec's, +0.406, rtn
+10 120	Del 10 sec's, option x (exit)
+10 120	Del 10 sec's, option x (exit)
+10 120	Del 10 sec's, option x (exit)
+10 120	Del 10 sec's, option x (exit)
+10 121	Del 10 sec's, option y (yes)
+10 99 100 92 51 100 115 121 115 13	Del 10 sec's, cd/3dsys, rtn
+10 114 101 99 111 97 116 101 114 47 122 111 102 102 13	Del 10 sec's, recoater / zoff
+8 50	Del 8 sec's, option 2 (sweep)
+8 50	Del 8 sec's, option 2 (sweep)
+6 120	Del 6 sec's, option x (exit)
+6 99 100 92 119 111 114 107 13	Del 6 sec's, cd/work, rtn
+4 109 101 110 117 13	Del 4 sec's, menu, rtn
+5 54	Del 5 sec's, option 6 (tool box)
+4 49	Del 4 sec's, option 1 (utility)
+4 51	Del 7 sec's, option 3 (elevator)
+10 100	Del 5 sec's, option d (distance)
+6 45 46 48 49 50 13	Del 6 sec's, -0.012, rtn
+15 120	Del 10 sec's, option x (exit)
+15 120	Del 10 sec's, option x (exit)
+15 120	Del 10 sec's, option x (exit)
+15 120	Del 10 sec's, option x (exit) Del 20 sec's
+15 121 +20	Del 10 sec's, option y (yes)
+10 98 117 105 108 100 13 +10	Del 10 sec's, build, rtn
+15 'men1/start614/stop628/nodrain/zoff/nosweep' 13 +2:	Del 15 sec's, start 614, stop 628, nodrain, zoff, rtn, Del 2 min's
+5 'menu' 13	Del 5 sec's, menu, rtn
+2 54	Del 2 sec's, option 6 (tool box)
+4 49	Del 4 sec's, option 1 (utility)
+7 51	Del 7 sec's, option 3 (elevator)
+10 100	Del 10 sec's, option d (distance)
+5 43 46 48 48 54 13	Del 5 sec's, +.006, rtn
+15 120	Del 10 sec's, option x (exit)
+15 120	Del 10 sec's, option x (exit)
+15 120	Del 10 sec's, option x (exit)
+15 120	Del 10 sec's, option x (exit) Del 20 sec's
+15 121 +20	Del 10 sec's, option y (yes)
+10 98 117 105 108 100 13 +10	Del 10 sec's, build, rtn, Del 10 sec's
+15 'men1/start602/stop614/nodrain/zoff/nosweep' 13 +2:	Del 15 sec's, start 614, stop 628, nodrain, zoff, no sweep, rtn, Del 2 min's

Figure 7-14 Software commands and ASCII code for a single smoothing cycle

7.4 Developing a smoothing cycle loop

Using the program code in Figure 7-14 it is possible to build any two layers of a part and a meniscus fillet, with an operator required only to load the TSR program.

Although this eliminates the need for a dedicated machine operator the process of re-loading the TSR file for each layer remains labour intensive if parts with many layers are required.

In order to optimise the parameters affecting meniscus smoothing, sufficient numbers of the part detailed in Figure 3-2 were to be built to obtain statistical quality roughness measurements. Hence, at least 50 layers of the part must be generated using each of the variable process parameters. Software must therefore be developed to automate the smoothing cycle further.

Using the script file detailed in Figure 7-14 a program has been written using the simple loop algorithm, which produces copies of the new build algorithm as shown in Figure 7-15. The algorithm incorporates a counter, to produce a 'string' of incremental smoothing cycles each incremented by 12 CAD layers. The resulting ASCII script contains all the commands required to manufacture a multiple layered part using the meniscus-smoothing algorithm.

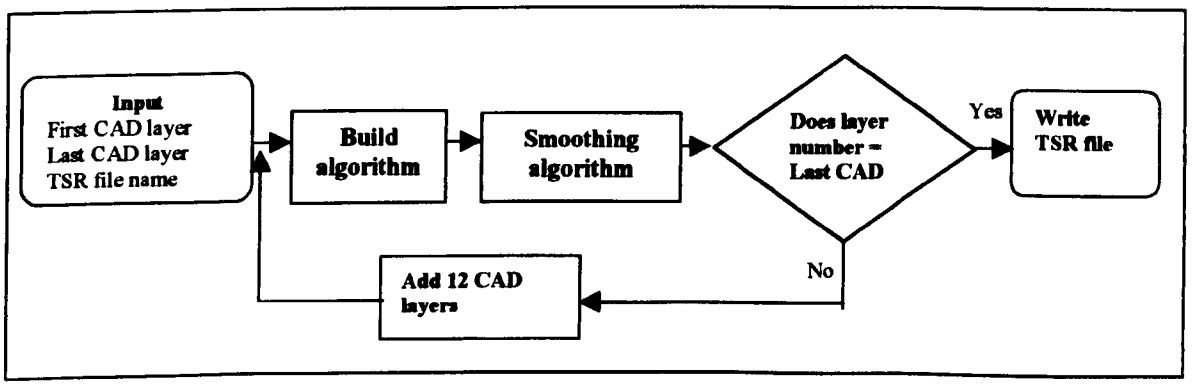

Figure 7-15 The loop program for the smoothing cycle

Using the new software a number of 'looped' files were produced to assess the suitability of the program. The main limitation found when running the TSR programs was file size. As the TSR file is designed to occupy the computers high level memory the code is limited to only 64 Kbytes. Given that each loop of the meniscus smoothing cycle accounts for 1.2 Kbytes, the automated program is limited to only 53 layers. Using 0.15-mm layers it is therefore possible to build 8 mm of a part without needing to re-load a new TSR file.

If we consider the evaluation of roughness units from section 3.1.4 we require at least 17.5 mm of surface to accumulate statistically accurate roughness data. Hence three TSR files must be generated for each set of meniscus parameters, these being 0 – 8 mm, 8 – 16 mm and 16 – 24 mm.

7.5 Summary

In summary it can be said that both a suitable algorithm for accurate meniscus smoothing has been developed for the SLA-250, in addition to a computer program suitable for automating the process. Although only parts in 8-mm sections can be built without manual intervention, the program is suitable for further experimental trials.

Using the smoothing cycle software, the next stage was to undertake a series of experiments to define the optimum parameters required to generate the most appropriate shape meniscus for the smoothing of up-facing planes. Only then could

the combination of print-through and meniscus smoothing be evaluated and applied to SL parts used for down stream applications such as rapid tooling.

CHAPTER 8

8.0 Meniscus shape optimisation

From the experimental work detailed in Chapter 7, a software tool has been developed which can be used to produce a meniscus between layers during the SL build process. The presence of a meniscus has been shown, in the research by Narahara to result in a significant reduction in roughness deviation on some SL surfaces [119, 120].

However, no research to-date has looked at the variables affecting meniscus shape, or used these to create optimal smoothing effects on different angled planes. If meniscus smoothing is to be beneficial over more than the 20-degree envelope of surfaces seen in Narahara's research, a number of process attributes must be identified and optimised to produce different shaped meniscus on different angled surfaces. An experimental programme was set up to investigate the various process attributes responsible for producing the different shaped meniscus.

By optimising meniscus shape on surfaces between 40 and 90-degrees and combining this with the effects of print-through, a 90-degree envelope of smooth surfaces could be produced. Such a build strategy could then be applied for smoothing models and to the increasing range of down stream rapid tool cavities and patterns manufactured using the SL process.

8.1 Attributes affecting meniscus shape

The shape of the resin meniscus between each layer has been shown to be a function of a number of process attributes [135]. These include attributes such as resin viscosity, the wetting characteristics of the solid and liquid resin and the shape and size of the contact surfaces.

8.1.1 Surface wetting and viscosity

The wetting characteristics of the liquid and solid resin are a function of material rheology and cannot be changed without the formulation of a new resin material. Similarly, resin viscosity can only be changed through an increase in build envelope temperature, however such changes will also influence the accuracy and repeatability of the SL process. For this reason the experimental work has been directed towards changing the surface contact angle of the liquid and solid or the retraction distance of the polymerised layer above the resin vat before the meniscus scanning step.

8.1.2 Surface contact angle

The shape of a liquid meniscus held by surface tension is known to be a function of the contact angle and area of the surfaces holding the meniscus in place [135]. The meniscus contact surface is in itself a function of the part geometry, with low angled surfaces having a larger contact area than high-angled planes. Figure 8.1 shows a schematic of a section taken through different contact angle surfaces. It can be seen

that meniscus shape is highly dependent on the geometry of the contact surface in addition to the surface tension of the liquid.

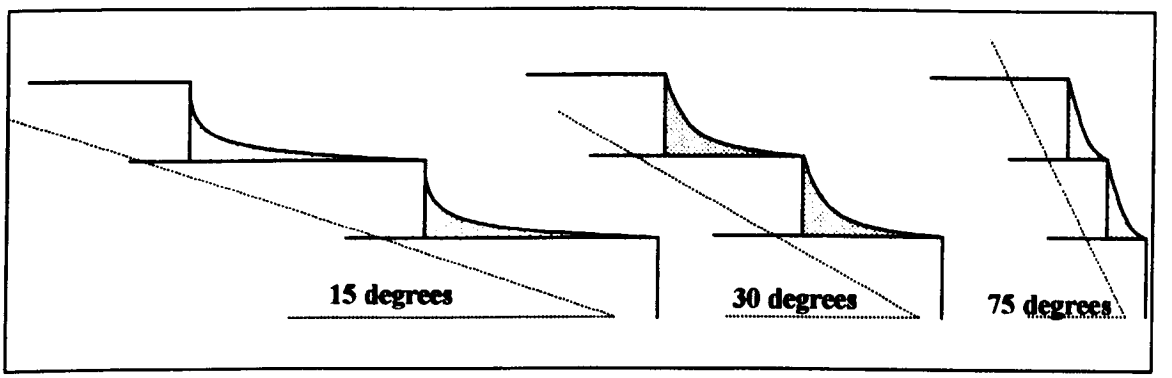

Figure 8-1 The effect of surface contact area on meniscus shape

In order to investigate the effects of contact area on meniscus shape, a range of angled SL planes were investigated in the experimental programme with the aim of determining which benefit from particular shaped meniscus fillets.

8.1.3 Process dwell time

In addition to the contact surface angle, meniscus shape will also be affected by the retraction distance of the solid layer above the vat of liquid monomer and the dwell time between liquid meniscus generation and laser scanning.

Dwell time between the pulling of the meniscus and the scanning sequence is dictated by the delays included in the TSR program. The delay is however critical to the function of the program and compensates for the lag of the computer hard drive. From the TSR code detailed in Figure 7-14, we can see the minimum time period

between meniscus generation and laser scanning is 85 seconds. Visual analysis of the smoothing cycle using the SL-5170 resin would suggest the meniscus maintains equilibrium after approximately 7 – 10 seconds. Any increase over the existing 85-second delay will therefore have little, if no effect on meniscus shape. Given the constraints of the SLA-250/40 hardware, the 85-second delay cannot be reduced further. Hence time delay cannot be considered in the experimental analysis of meniscus shape. The experiments were therefore directed towards assessing the effects of different retraction distances over a range of angled surfaces.

8.1.4 Meniscus retraction distance

As the number of process variables that can be changed during the build process is limited, the experimental program undertaken was to identify the relationship between surface angle and meniscus retraction distance.

Meniscus retraction distance is defined as the movement of the platform following the scanning of the top layer, prior to the scanning of the meniscus in-fill. By changing the meniscus retraction distance, it is possible to use surface tension to change the shape of a meniscus between intersecting layers.

The effects of different retraction distances on a stepped surface are well documented and described in Figure 8-2. However, it should be noted that the experimental meniscuses shown in Figure 8-2 are based on work with oil [136], rather than polymer resin. As yet the effects of retraction distance on meniscuses generated from

SL resin are not known. It may be possible using techniques such as a shadow-graph, to visualise the shape of SL resin meniscus in profile. However, such investigation is outside the remit of this research and not practical using the measurement apparatus available to the author. Hence, to-date no research in this area has been undertaken.

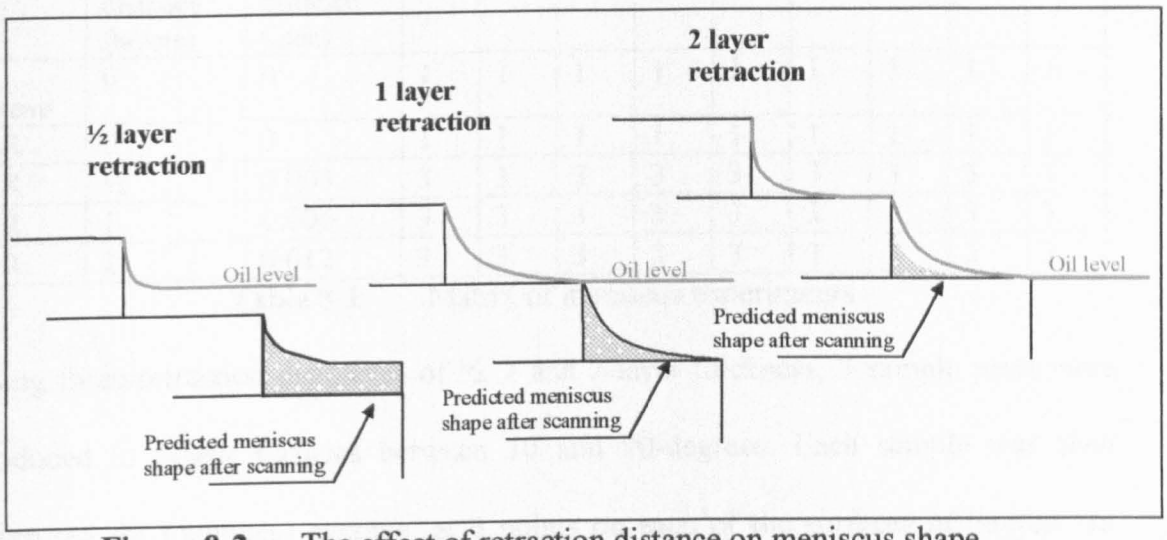

Figure 8-2 The effect of retraction distance on meniscus shape

8.2 Experimental trials

Given that meniscus shape is the result of more than one attribute, an experimental array must be used to assess roughness as a function of surface angle relative to retraction distance. Using the angled test geometry developed in Chapter 3, Figure 3.2, the experimental program was undertaken using a number of surface angles and retraction distances ranging from half a layer thickness, through to two layer thicknesses.

The experimental array used for meniscus smoothing experiments can be seen detailed in Table 8-1. Table 8-1 shows both the surface geometry angle and the

retraction distance for each experiment. In addition, the software used for each experiment and the number of samples produced are also shown.

			Surface angle								
Software	Retraction distance (layers)	Retraction distance (inch)	10	20	30	40	50	60	70	80	90
3D Systems	0	0	1	1	1	1	1	1	1	1	1
TSR	0	0	1	1	1	1	1	1	1	1	1
TSR	½	0.003	3	3	3	3	3	3	3	3	3
TSR	1	0.006	3	3	3	3	3	3	3	3	3
TSR	2	0.012	3	3	3	3	3	3	3	3	3

Table 8-1 Matrix of meniscus experiments

Using three-retraction distances, of ½, 1 and 2-layer thickness, 3 sample parts were produced to assess surfaces between 10 and 90-degrees. Each sample was then measured for roughness average, at 3 points on each of the surfaces of interest. In addition samples manufactured using the standard 3D Systems operating software and the TSR software with no meniscus were also evaluated. The measured roughness data for all the samples listed in Table 8-1 can be found in Appendix D.

8.2.1 Verification of meniscus smoothing software accuracy

Before meniscus shape can be optimised and used to reduce surface roughness, the new build algorithm must be compared against the existing 3D systems software, to ensure that part accuracy and surface roughness are not degraded using the TSR software. The new build algorithm does not rely on the resin levelling system designed to control the accuracy of the Z-axis. Hence, parts manufactured using the new software may result in an uneven layer thickness. Given that surface roughness is

a function of layer thickness as described in section 4.1.1, it is possible to compare the new build algorithm with the 3D Systems software by measuring the roughness average of parts manufactured using the TSR software with the meniscus step of the smoothing cycle bypassed.

Figure 8-3 shows the surface roughness comparison between two parts manufactured using both the TSR software with no meniscus and the 3D Systems build software. In both cases the part has been manufactured in 0.15-mm layers and surface roughness was measured from the average of six measurements at random points on the surfaces of interest.

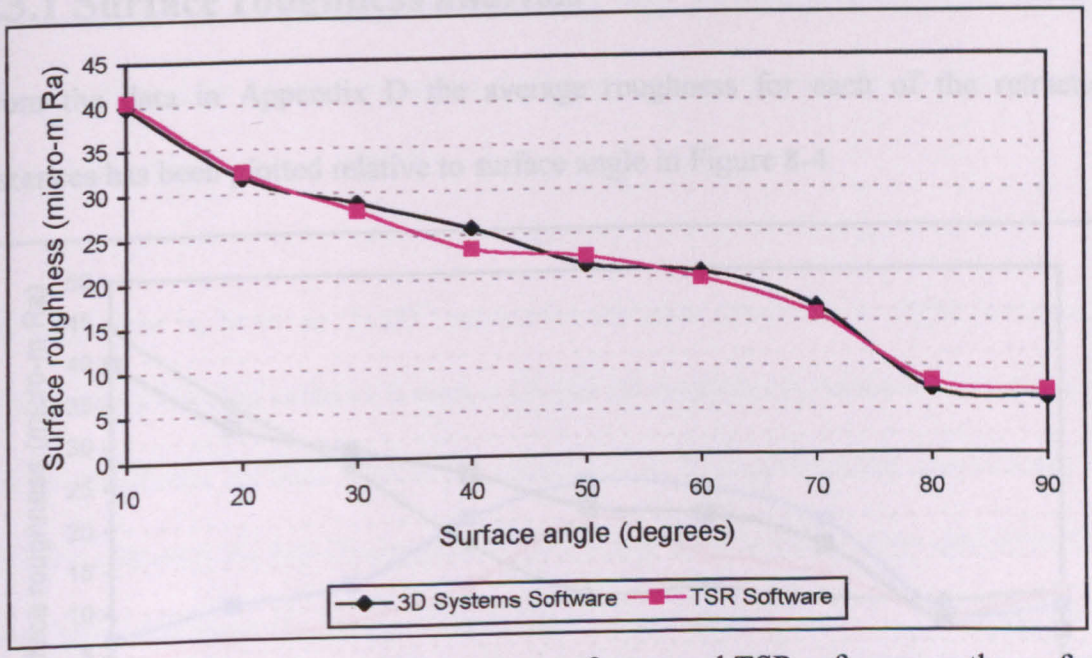

Figure 8-3 Comparison of 3D systems software and TSR software on the surface roughness of a 0.15-mm layer part

It can be seen from the comparison in Figure 8-3 that the new software produced similar parts to the existing 3D systems operating system, with the meniscus-smoothing step of the cycle bypassed. It can therefore be said that the build algorithm

does not degrade the quality of parts manufactured on the SLA-250/40 system. A direct comparison can now be made between the new build algorithm and the existing 3D systems build station software, to assess what improvement, if any, meniscus smoothing makes.

8.3 Experimental results

Based on the experimental matrix detailed in Table 8-1, roughness data has been measured over a range of surface angles using a number of different meniscus retraction distances. The results of this analysis can be found in Appendix D.

8.3.1 Surface roughness analysis

From the data in Appendix D the average roughness for each of the retraction distances has been plotted relative to surface angle in Figure 8-4.

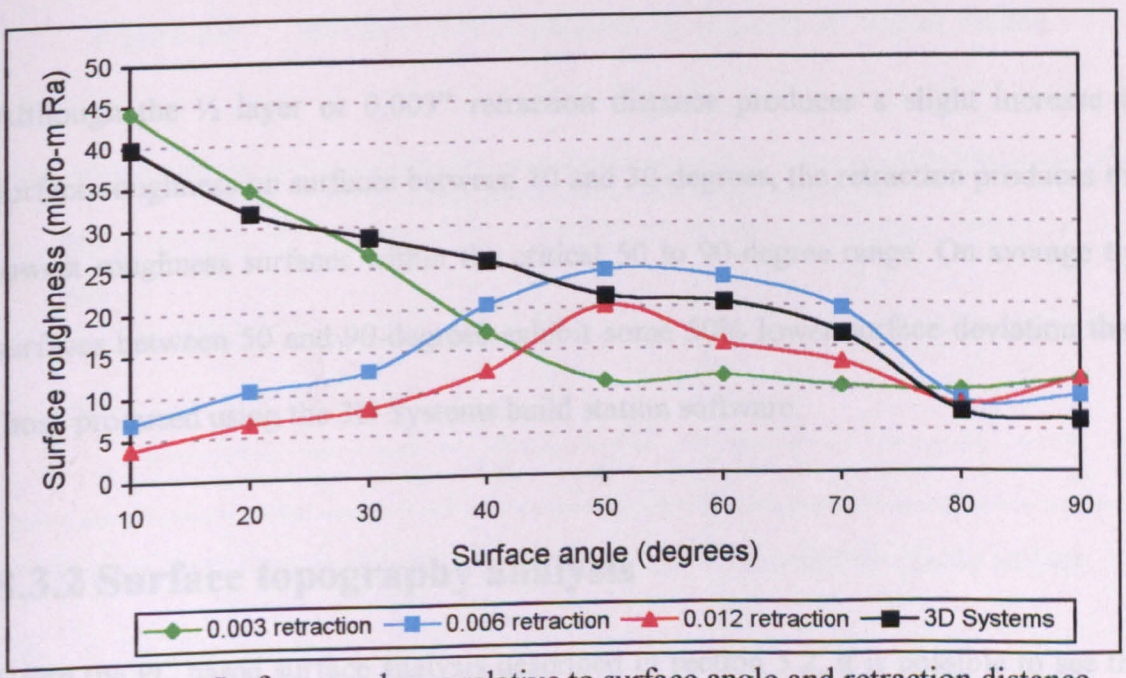

Figure 8-4 Surface roughness relative to surface angle and retraction distance

It can be seen in Figure 8-4 that different retraction distances affect the surface roughness of angled planes in different ways. Certain retraction distance are clearly beneficial to only a limited number of angled surfaces, such as a ½ layer retraction which only reduces the surface deviation of angles between 30 and 70-degree below that of the standard 3D Systems part. However for 0.006" or one layer thickness retraction only reduces the surfaces deviation on planes between 10 and 40-degrees below that of the 3D Systems build. The 0.012" retraction although not giving the lowest reduction in roughness for all planes, does yield an overall reduction in surface deviation below that of the 3D Systems build.

In Narahara's research, meniscus smoothing was only seen to improve surfaces between 10 and 30 degrees. However, Narahara only used a retraction distance equal to one layer thickness, i.e. 0.006".

Although the ½ layer or 0.003" retraction distance produces a slight increase in surface roughness on surfaces between 10 and 30-degrees, the retraction produces the lowest roughness surfaces within the critical 50 to 90-degree range. On average the surfaces between 50 and 90-degrees exhibit some 50% lower surface deviation than those produced using the 3D Systems build station software.

8.3.2 Surface topography analysis

Using the PC based surface analysis described in section 3.2, it is possible to see the changes to the SL surface topography by plotting out the topography profile of a

section through each angled surface. Unlike earlier analysis using the Ra unit of roughness measurement, waviness has been used as an assessment of surface topography. Unlike Ra, waviness is a direct representation of the actual surface, rather than a summation of areas about the arithmetic mean.

Figures 8-5 to 8-8 shows the waviness of the 10-degree surfaces produced using both the variable retraction distances and the standard 3D Systems build station software.

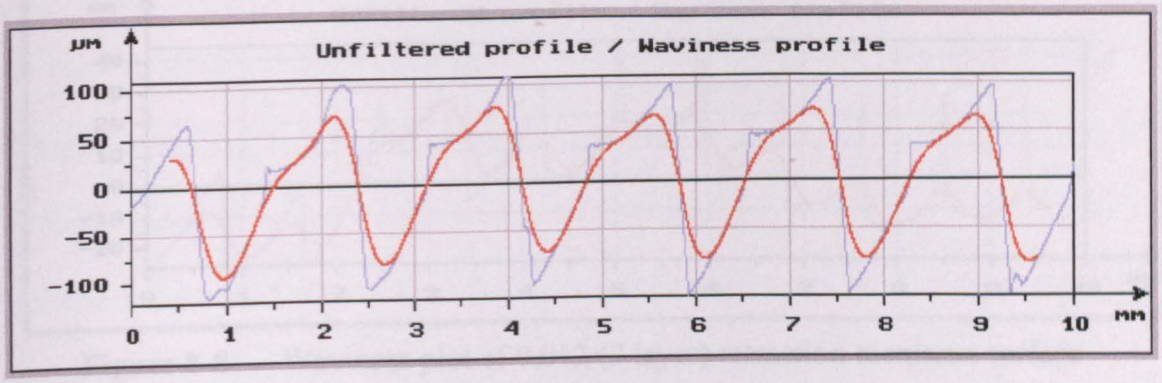

Figure 8-5 Waviness plot of standard 3D Systems 10-degree surface

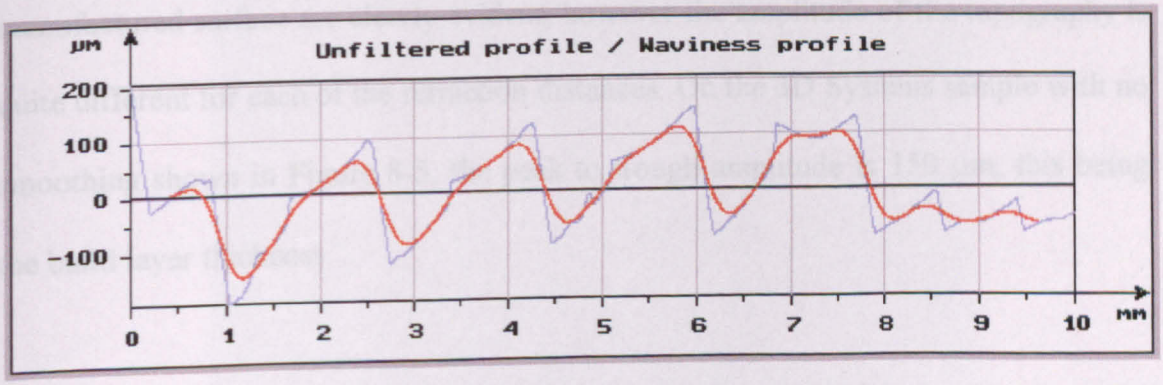

Figure 8-6 Waviness plot of 0.003 (1/2 layer) retraction meniscus surface

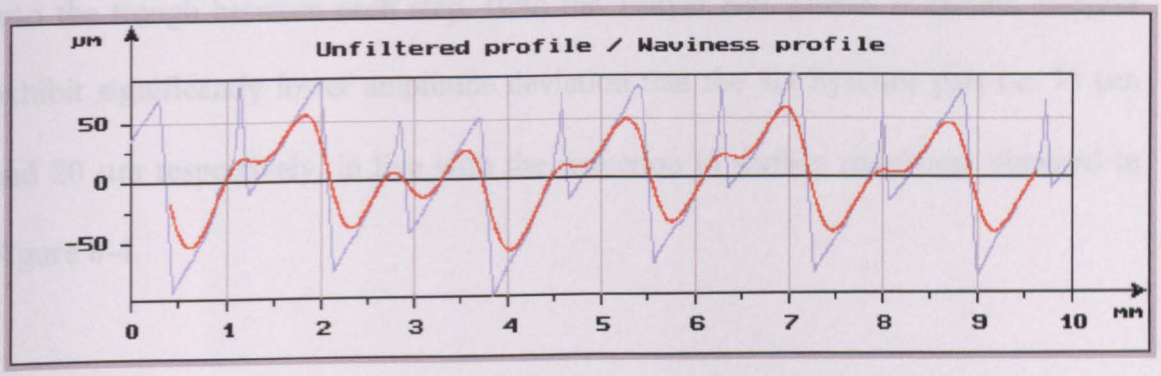

Figure 8-7 Waviness plot of 0.006 (1 layer) retraction meniscus surface

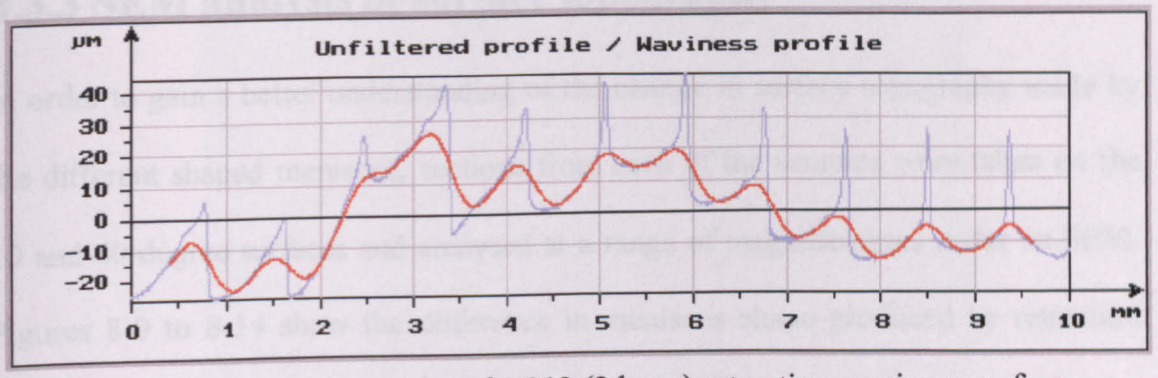

Figure 8-8 Waviness plot of 0.012 (2 layer) retraction meniscus surface

Over the 10-mm scan shown in Figures 8-5 to 8-8, the peaks and troughs of the layer manufactured surface are clearly evident, however the amplitude of the topography is quite different for each of the retraction distances. On the 3D Systems sample with no smoothing shown in Figure 8-5, the peak to trough amplitude is 150 µm, this being the build layer thickness.

On the 0.003" retraction meniscus the deviation in peak-to-trough value is nearer 150 µm. If we consider the roughness values in the Figure 8-4, a retraction distance of 0.003" or ½ layer thickness also causes an increase in surface roughness on the 10-degree SL surface above that of the 3D Systems software. This would suggest the

process causes additional material to be cured onto the peaks of the steps rather than into the trough between each step. Both the 1-layer and 2-layer retraction samples exhibit significantly lower amplitude deviation that the 3D Systems part i.e. 75 μm and 20 μm respectively, in line with the reduction in surface roughness obtained in Figure 8-4.

8.3.3 SEM analysis of surface topography

In order to gain a better understanding of the change in surface topography made by the different shaped meniscus, sections from each of the samples were taken on the 10 and 40-degree surfaces and analysed at a range of magnifications under an SEM. Figures 8-9 to 8-14 show the difference in meniscus shape produced by retraction distance of ½, 1 and 2-layer thickness on both 10 and 40-degree surfaces.

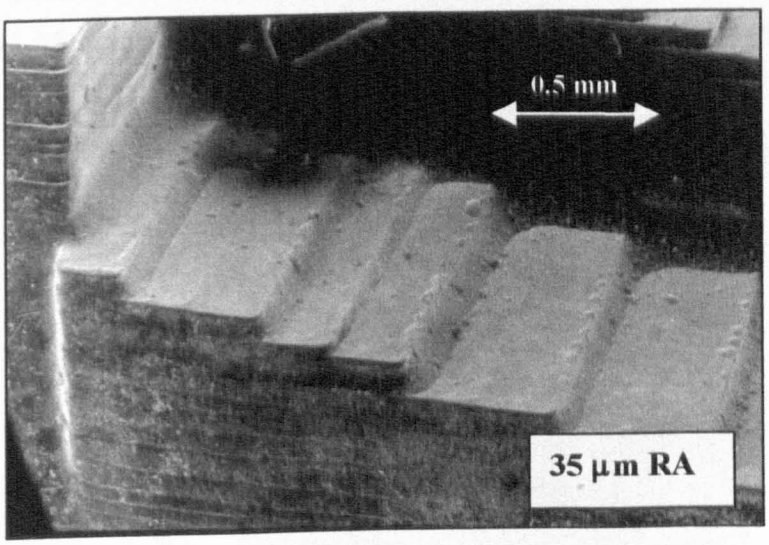

Figure 8-9 Meniscus smoothing with ½-layer retraction on 10-degree slope

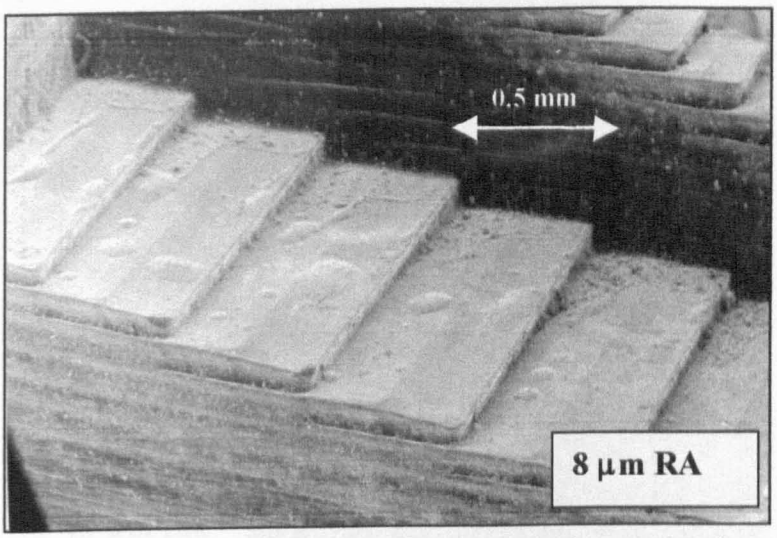

Figure 8-10 Meniscus smoothing with 1-layer retraction on 10-degree slope

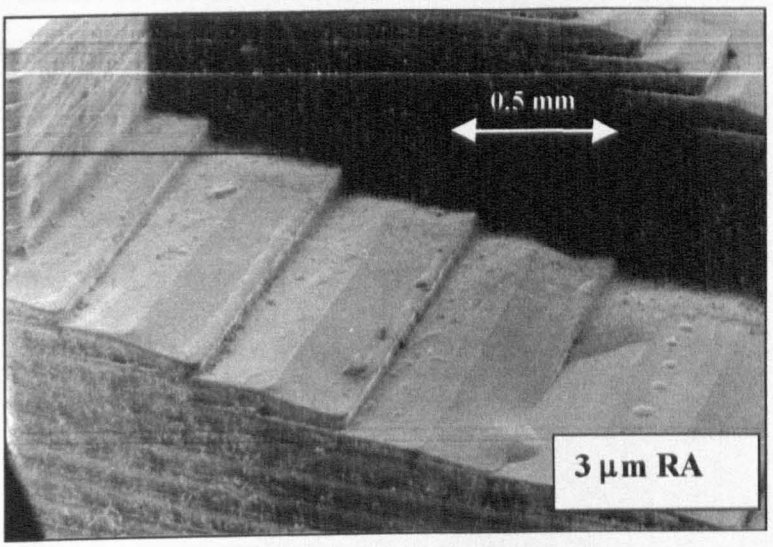

Figure 8-11 Meniscus smoothing with 2-layer retraction on 10-degree slope

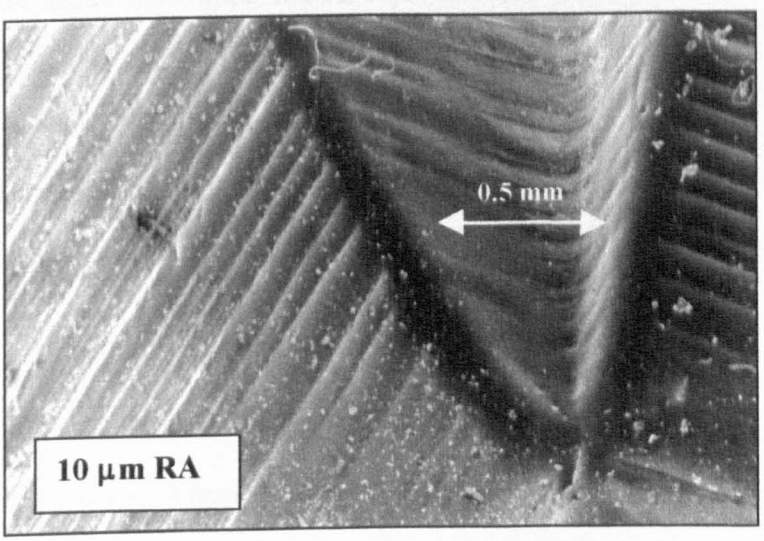

Figure 8-12 Meniscus smoothing with ½-layer retraction on 70 and 90 degree slope

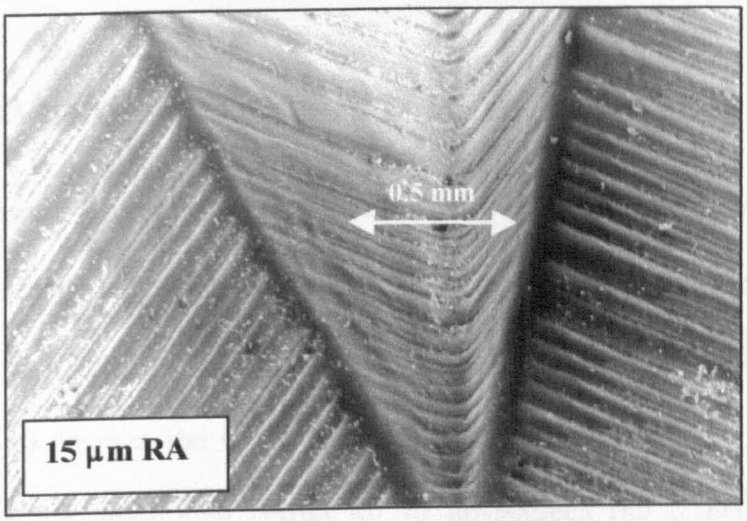

Figure 8-13 Meniscus smoothing with 1-layer retraction on 70 and 90 degree slope

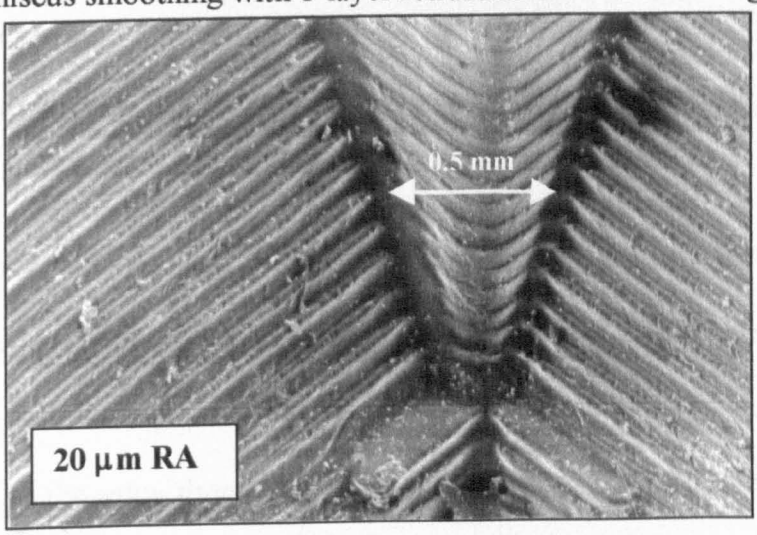

Figure 8-14 Meniscus smoothing with 2-layer retraction on 70-and 90 degree slope

As Figures 8-9 to 8-14 show, one retraction distance is not suited to all up-facing surfaces. The ½-layer retraction in Figure 8-9 clearly has less meniscus smoothing between layers than the 2-layer retraction shown in Figure 8-11. Similarly the ½-layer retraction shown in Figure 8-12 produces notably more filling of the steps than the 2-layer retraction shown in Figure 8-14. This supports the general trend shown in Figure 8-4.

8.4 Observations

As shown in Figure 8-4 and the micro-graph images 8-9 to 8-14, the 0.012" or 2-layer thickness retraction gives the best overall reduction in surface deviation between 10 and 90-degrees, with improvements of up to 90% on some surfaces angles. For angles between 0 and 40-degrees the 0.012" or 2-later retraction produces the optimum shaped meniscus for smoothing. From 40 to 80-degrees the 0.003" or ½-layer retraction produces the optimum shaped meniscus for smoothing. Similarly, the 0.006" or 1-layer retraction benefiting only angles between 80 and 90-degrees.

In theory, meniscus shape could be modified for each layer throughout the build process. However such application would be restricted to very basic geometries. Most SL models have variable angled surfaces on different sides; hence a 10-degree surface may be scanned at the same time as a 50-degree surface. From Figure 8-4 it can be seen that each surface would benefit from a different retraction distance, however the build platform cannot be moved during the scanning process. Hence the best all round retraction distance must be used if a broad range of angles require smoothing over one geometry.

8.5 Summary

One of the original aims aim of this research was to develop an in-process technique that can be used to reduce or eliminate post-process surface finishing on SL master

patterns and tool cavities, possessing 90 degrees of variable surface geometry. Given that print-through smoothing is already suitable for improving planes between 90 and 145 degrees, a complimentary smoothing technique need only be applied to surfaces between 45 and 90 degrees. Hence, producing the 90-degree smooth build envelope suitable for the manufacture of rapid tooling cavities and accurate master patterns. If we consider the effects of different shaped meniscus on surface angle, it can be seen that a retraction distance of 0.003" or ½-layer thickness yields the greatest reduction in surface deviation between 45 and 90-degree surfaces.

In summary it can be said that an optimum meniscus retraction distance has been established for a range of angled surfaces produced in 0.15-mm layers using the SLA-250/40 system. From the research it has been shown that different retraction distances benefit different angled planes.

CHAPTER 9

9.0 Print-through and meniscus smoothing

If smooth models or Rapid Tooling cavities are to be produced, then all critical surfaces must be orientated to take advantage of either the smoothing effects of print-through or the effects of meniscus generated between layers, or a combination of both. In chapter 5 it was shown that a combination of layer edge profile and print-through has a smoothing effect on surfaces between 90 and 140-degrees. In chapter 8 has also been demonstrated that with optimal retraction distances, meniscus can be generated between layers resulting in lower surface deviation. Hence is both techniques are combined by part orientation and the inclusion of meniscuses it should be possible to produce parts with a significantly lower surface deviation than by using the standard 3D Systems build algorithm.

9.1 Comparison of existing and new build strategies

Figure 9-1 shows the surface roughness values now possible using both the optimum shaped meniscus smoothing and print-through together. For surfaces angles between 10 and 40 degrees, roughness values measured on the sample produced using the optimum retraction distance of 0.012" have been included. Between 40 and 90 degrees values from the 0.003" sample have been used. The roughness of SL surfaces between 0 and 180 degrees produced using the existing software in section 5.2 are also shown in the graph as a reference. This also covers the surface angles between 90 and 140 degrees which benefit from print-through following part orientation.

It can be seen that the combination of meniscus smoothing and print-through results in a build envelope on ranging between 10 and 800% smoother than the existing 3D systems software, suggesting in-process part finishing may be a viable solution for accurate models, Rapid Tooling cavities or master patterns.

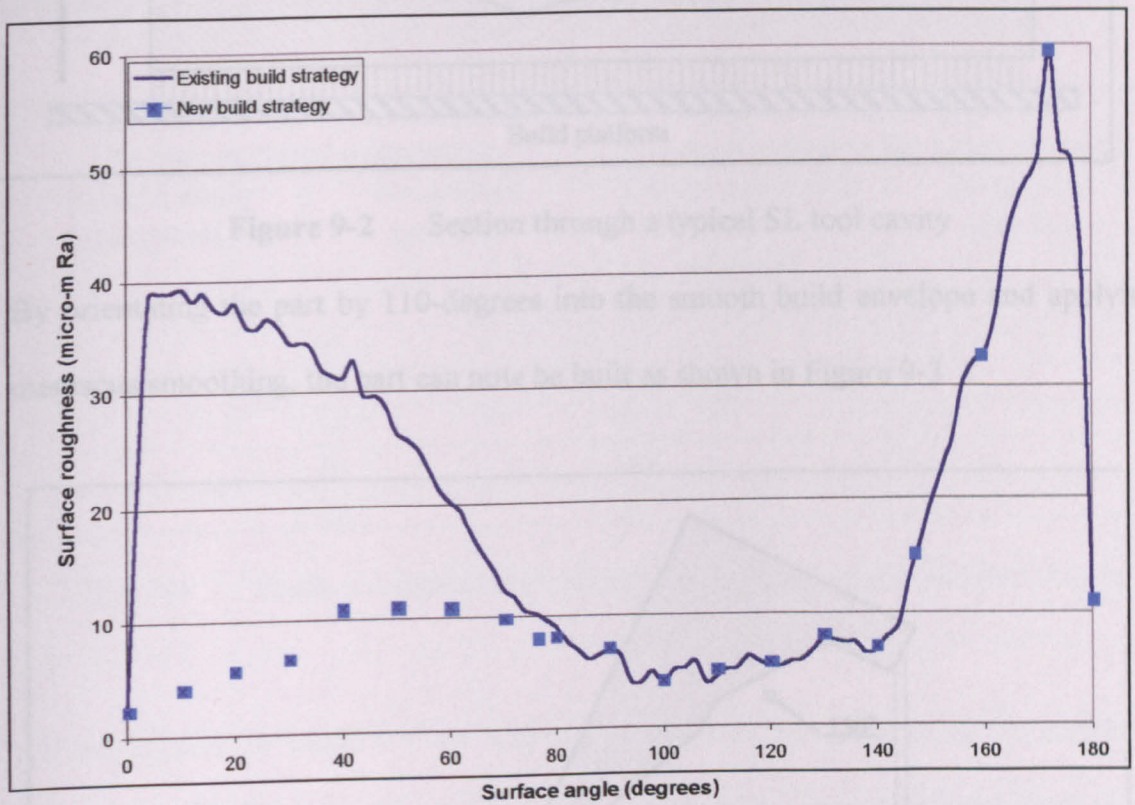

Figure 9-1 Roughness comparison of existing and new build strategies

9.1.1 Application of the new build strategy to a tool cavity

If we consider the schematic of a section taken through a typical tool cavity, it is possible to make an assessment of surface roughness, based on both the conventional build strategy and the new meniscus/print through strategy. By measuring the angle of the surfaces shown in Figure 9-2, the values for surface roughness can be derived from the graph in Figure 9-1.

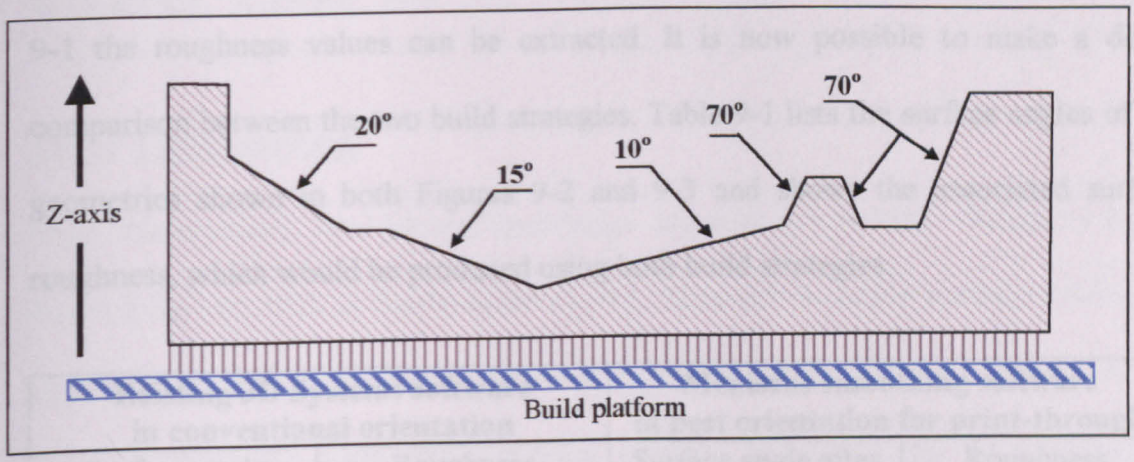

Figure 9-2 Section through a typical SL tool cavity

By orientating the part by 110-degrees into the smooth build envelope and applying meniscus smoothing, the part can now be built as shown in Figure 9-3

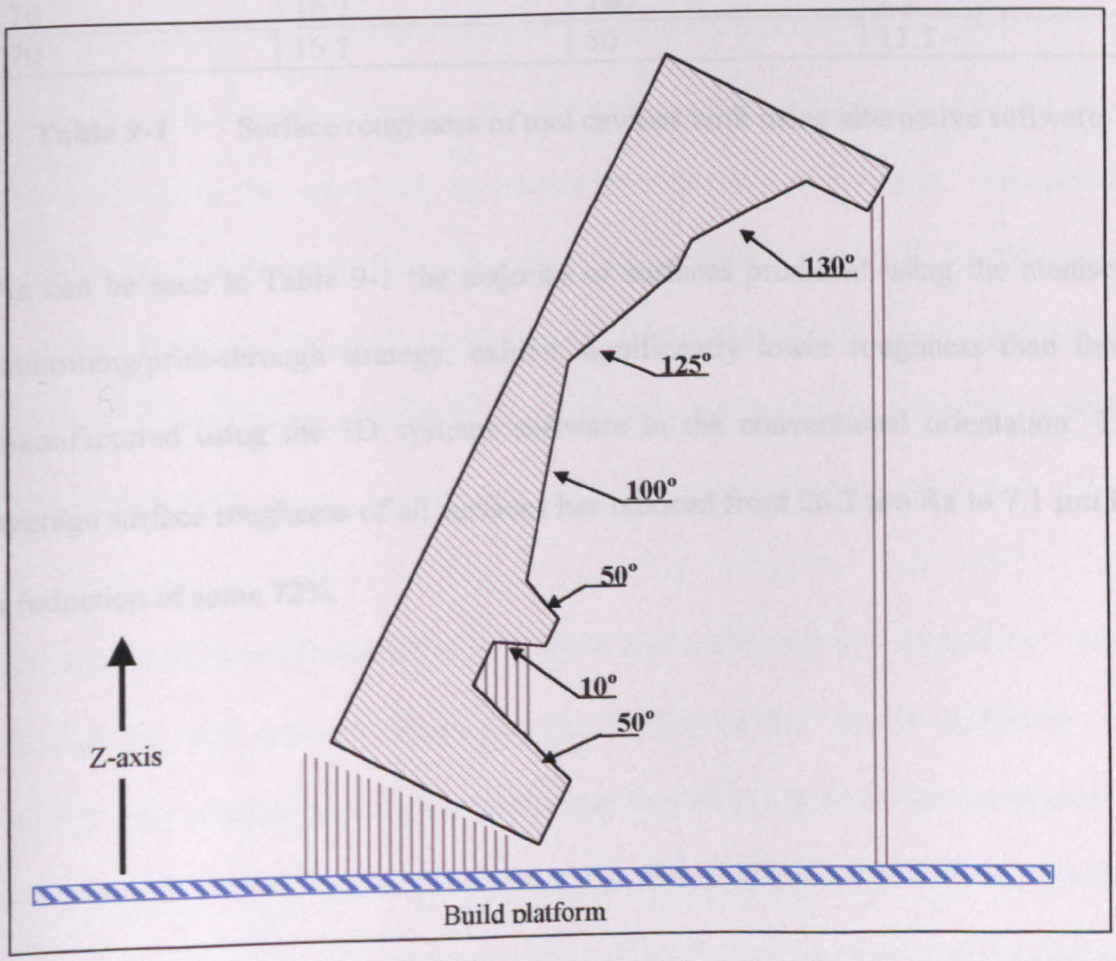

Figure 9-3 Section through an orientated SL tool cavity

The surface angles on the tool are now different and again using the graph in Figure 9-1 the roughness values can be extracted. It is now possible to make a direct comparison between the two build strategies. Table 9-1 lists the surface angles of the geometries shown in both Figures 9-2 and 9-3 and shows the associated surface roughness, which would be produced using both build strategies.

Existing 3D Systems software in conventional orientation		**Meniscus smoothing software in best orientation for print-through**	
Surface angle (degrees)	Roughness (μm Ra)	Surface angle after 110° orientation (degrees)	Roughness (μm Ra)
20	31.8	130	7.5
15	35.5	125	6.2
10	39.9	100	4.7
70	16.7	50	11.1
70	16.7	180	2.2
70	16.7	50	11.1

Table 9-1 Surface roughness of tool cavities built using alternative software

As can be seen in Table 9-1 the majority of surfaces produced using the meniscus smoothing/print-through strategy, exhibit significantly lower roughness than those manufactured using the 3D systems software in the conventional orientation. The average surface roughness of all surfaces has reduced from 26.2 μm Ra to 7.1 μm Ra a reduction of some 72%.

CHAPTER 10

10.0 Discussion

From this research, new process knowledge and user information relating to Rapid Prototyping and Tooling has been developed. Although no single technique has been identified which can be used to reduce deviation during the SL build process, to the levels required for down stream tooling patterns, a strategy has been developed suitable for reducing deviation from as much as 40 μm Ra to below 5 μm Ra on some surfaces, using a combination of techniques. Using the new build strategy, surface roughness can be reduced to similar level produced by both additive coating and abrasive finishing, as discussed in chapter 2. However, as the additional material from the meniscus is located within the step of the layer edge, the process will not effect part accuracy in the same way as post-process finishing techniques. Although no dimensional measurements were taken from the samples in chapter 8, the micrograph images in section 8.3.3 clearly show any additional material within the boundary of the existing part, hence geometric tolerance will not be effected by the meniscus smoothing process.

Unfortunately the new build strategy does not produce the sub-μm Ra polished finish, required for tool surfaces. However, the topography has greater uniformity and requires only minimal post-process finishing. By producing a uniform roughness on all surfaces, it is significantly easier to apply post-process finishing treatments such as abrasive blasting [136, 137] or abrasive flow polishing processes such as the Extrude-hone system [138, 139]. Systems like the Extrude-hone process rely on the tool surface possessing a uniform roughness prior to polishing, as the process exhibits an

equal amount of abrasion over the part irrespective of geometry. This can also maintain the dimensional accuracy of the part and hence production of higher quality parts and make tools cavities faster to produce. Although the new build strategy will inevitably produce more support structures on the critical surfaces, this can easily be removed during the part cleaning and fettling process, prior to post-curing in the UV oven.

From a commercial SL user perspective, two fundamental changes to the existing software must be developed. Firstly, the part geometry defined in the STL file must be orientated automatically into the optimum position to benefit from print-though. This must be undertaken prior to the generation of any support structure and before slicing into 2-dimensional layers. The 2-dimensional slices must then be scanned on the SL machine with meniscus smoothing applied between all up-facing layers, preferably using an optimal retraction distance.

10.1 New process knowledge

During this research project a number of areas of new process knowledge have been identified and investigated relating to surface topography modelling, Rapid Prototyping (RP) and Rapid Tooling (RT).

10.1.1 Fundamental cause of surface deviation in RP

During the early stages of this research new process knowledge was gained relating to the fundamental cause of surface deviation in layer manufacturing. Prior to this thesis the generally accepted cause of surface deviation in layer manufacturing was layer

thickness [52][53]. However, the cumulative effects of both layer edge profile and layer composition have been identified and analysed using SEM analysis and surface topographic scanning.

10.1.2 Generic model of LMT surface deviation

From the new process knowledge relating to the cause of surface deviation on LMT part, a mathematical model was developed from first principles using the variables of layer thickness, layer edge profile and surface angle. In addition, the effects of both up-facing and down-facing composition roughness were investigated and incorporated into the mathematical model using empirically derived data. Although the model was seen to give a realistic prediction for the roughness of up-facing surfaces, the correlation between measured and derived data for the SLA250/350 and 500 machines was disappointing between 90 and 180 degrees. A number of possible causes for this discrepancy were investigated, including sampling errors and measurement inaccuracy through incorrect Taly-surf geometry. Although the contact Taly-surf is not the ideal method for measuring the surface topography of undercut layer edges the difference between measured and derived surface roughness could not be attributed to measurement error alone.

Although applying the mathematical model to other RP processes is outside the remit of this research, Gautham Kattethota at the Arizona State University is currently modifying the generic roughness equations in 4.35 and 4.36 for use with the Fused Deposition Modelling (FDM) process. Kattethota aims to use the roughness equation in a software orientation tool, capable of finding the best build direction for parts built using the FDM system.

10.1.3 Print-through on down facing surfaces

Although print-through has for some time been attributed as the mechanism by which SL layers are bonded [58], its effect on surface deviation has not been discussed until now. By analysing the down-facing surfaces of SL parts the effects of print-through on roughness have been identified as the cause in reduced surface deviation between 90 and 140-degrees. Although encouraging, research has shown that print-through cannot be extended to other surface angles without a significant change in SL machine hardware.

Following the identification of print-through as a roughness attribute it has been possible to modify the mathematical roughness model incorporating print-through in the same way as composition roughness. However, the purpose of the modelling exercise was to identify and understand the process attributes affecting surface deviation, not necessarily to develop a definitive mathematical model of LMT surface topography. Hence, print-through was not included in the final roughness equation for SL surfaces.

10.1.4 Meniscus smoothing

From the new process knowledge relating to print-through, it was shown that only a complementary process is needed to extend the smooth surfaces already produced between 90 and 140-degrees. Two suitable processes were identified as skin smoothing and meniscus smoothing. However, skin smoothing was dismissed due to poor accuracy and the inability to selectively apply smoothing to small areas and features. Meniscus smoothing although undertaken in Japan using a Sony Machine

[119][120] and discussed in US patents [121], had not been practically demonstrated using existing 3D Systems SLA machines.

Using a new build algorithm and software developed by the author new process knowledge on meniscus shape manipulation has been demonstrated. Unlike earlier research by Narahara [119][120], the author's research shows that by optimising meniscus retraction distance smoothing meniscus can be generated on all up facing surfaces between 0 and 90-degrees. Hence, extending the process knowledge shown by Narahara's research, which was only able to show the benefits of meniscus smoothing between 10 to 30-degrees.

10.2 Limitations of print-through meniscus smoothing

The main limitation of using print-through and meniscus smoothing is build time. The limitations of time delays in the TSR file have already been discussed in section 7.3 and cannot be changed without new computer hardware in the SLA-250/40 system. Only by writing a new dedicated machine code within the 3D Systems build station software can the TSR code be replaced, and the processing time delay be reduced. Such research is beyond the remit of this project but should be considered as a further work task in future research projects in the area.

10.2.1 Reducing build time

When using the meniscus-smoothing algorithm, every layer must be subjected to double scanning, including down-facing surfaces, which are intrinsically smooth because of print-through. In addition, large parallel sections of parts that do not

require smoothing will also be subjected to double scanning, although these surface are inherently smooth as they exhibit no stair-stepping. Most of the meniscus scan path covers previously polymerised resin, with only a small percentage being the actual liquid resin meniscus. One alternative would be to use just the boundary scan data from the previous layer, hence eliminating the time taken to scan the hatch fill. Unfortunately, this is not possible, as the boundary data is an integral part of each layer scan file.

10.2.2 The generation of a secondary or shadow file

Another solution to excessive scanning would be the use of a secondary meniscus scan file, or 'shadow' file. The shadow file is a separate slice file containing scan data only on areas where there is a difference between layer profiles. The shadow file is generated at the CAD stage and is based on the difference between first and zero order approximations [140].

Figure 10-1 shows a section through a geometry depicted within the CAD environment. Layer manufacturing process such as SL takes this geometry and produces a first order approximation, as the layer boundary does not fully intersect the CAD definition [141, 142]. By using surface tension it is possible, as shown in Chapter 8, to generate a meniscus on the zero order approximation, in effect transforming it into a first order approximation. To cure only this meniscus, scan data is then needed for the area resulting from the difference between the first and zero order approximation, as shown in Figure 10-1.

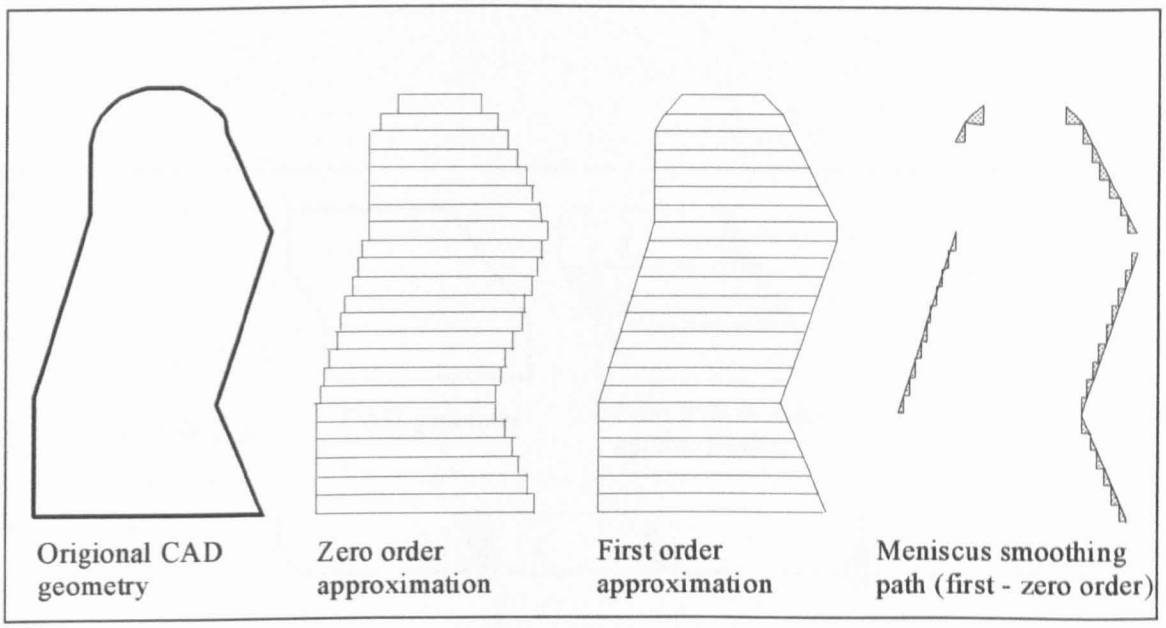

Figure 10-1 Generation of a meniscus scan path

Using a simple macro file, the generation of the shadow file could be undertaken using either native CAD data or more likely, using the part STL file. The shadow file could then be saved in an STL format and treated as a separate component. It should be noted that the shadow file must not be post processed with the support structure, as the part geometry will act as the support structure for each meniscus.

10.2.3 Eliminating down facing meniscus

One limitation when using a secondary meniscus smoothing scan path on a complex geometry is that the current build algorithm cannot distinguish between up-facing and a down-facing surface. If meniscus smoothing is applied to a down-facing surface, the process will have a detrimental effect on surface roughness, much in the same way the incorrect retraction distance was seen to increase surface roughness in Chapter 8.

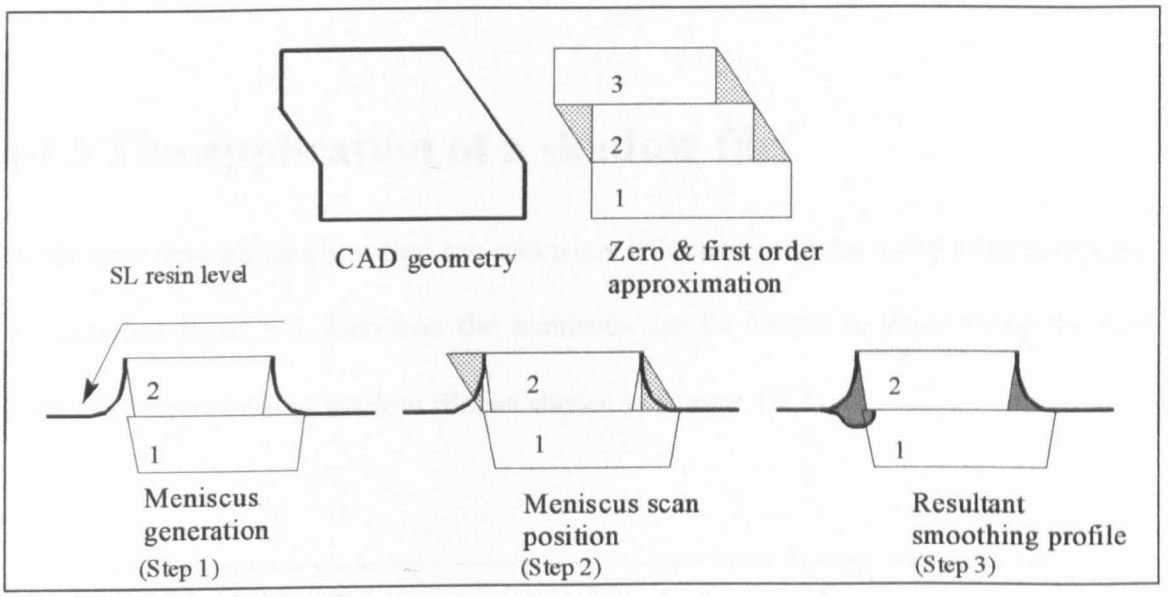

Figure 10-2 Down-facing problems associated with the shadow file

If we consider Figure 10-2, the generation of meniscus between down facing surfaces will result in material within the vat of resin being cured in 'free-space', as the shadow file will have been generated cure information in an area between layers that do not exist. The result will be unwanted material within the vat causing an increase in surface roughness should this material be cured to the part.

The solution to unwanted scanning on down-facing surfaces, is to eliminate all facets within the shadow STL file, which have a down-facing surface normals. Hence, when the shadow file is sliced it will only contain useful scan data, which will correspond with meniscuses generated between up-facing surfaces.

The manipulation of STL files has seen considerable research since the software was developed in the early 1980's [48, 49, 143]. One current solution is to separate the up-facing surface normals using software such as RP toolkit from Imageware or Magic's

by Materialise. Alternatively, a simple C++ program can be written to interrogate the ASCII STL file and remove facets with a negative surface normal.

10.3 The application of a shadow file

In the new smoothing algorithm the meniscus is locked in place using scan data from the previous layer, n-1. However the meniscus can be locked in place using the data from the corresponding shadow file, as shown in Figure 10-3.

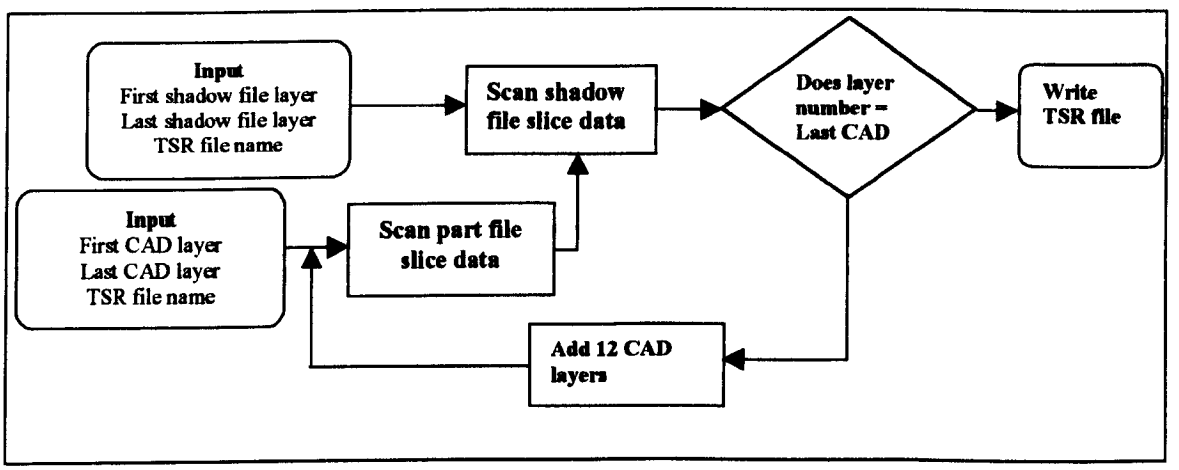

Figure 10-3 Meniscus smoothing cycle using a shadow file

The shadow file will only contain information on surfaces that need meniscus smoothing. Hence, although the meniscus generation step will take place on every cycle of the build, scanning will only take place when a surface with a meniscus is present. In addition, only the area of the layer containing the meniscus will be scanned. Hence, further reducing build time and the possible implications of part distortion caused by excessive exposure to intensive UV.

Using the proposed build cycle meniscus smoothing can be fully integrated with print-through to produce parts with significantly lower surface roughness than the existing 3D Systems software.

If dedicated machine code can be written to control the smoothing cycle without the need for a TSR file, accurate parts can be produced with no adverse damage to down-facing surfaces and with only a minimal increase in build time over the existing 3D Systems build software. Albeit, parts must be orientated into a position which will inevitable increase the Z-axis height. Therefore, requiring a greater number of build layers and resulting in an overall increase in build time and associated part cost.

10.4 Summary

In summary this research has achieved the goals set out in Chapter 1. A comprehensive understanding of LMT surface roughness has been developed, in addition to the development of a mathematical model to represent layer manufactured surface topography and roughness.

Using a combination of naturally occurring smoothing on down-facing planes and by changing up-facing layer profile using meniscuses cured between intersecting layers, a strategy has been developed which can be applied to a range of SL parts including Rapid Tooling cavities and accurate master patterns.

Although no single definitive solution to SL part finishing has been identified, the findings of this research show that significant improvements can be made to LMT

parts during the build process if the system users and vendors can be convinced to adopt a new and unorthodox build strategy.

By combining the new process knowledge of print-through and meniscus smoothing using the SLA-250/40 machine, it is now possible to produce layer-manufactured parts with up to 70% lowers surface roughness than those produced using the existing 3D Systems build software. In addition SL parts built using the new algorithm will exhibit a more uniform surface topography ranging between 5 and 8μm Ra, rather than 0.2 to 40μm Ra deviation seen with the 3D Systems build algorithm.

CHAPTER 11

11.0 Conclusions

In conclusion a number of areas of new process knowledge have been identified and proven using experimentation based on structured methodology. The key points to conclude from this research are:

11.1 A fundamental understanding of the cause of surface deviation in layer manufacturing has been acquired.

11.2 Layer thickness is not the sole cause of surface deviation in layer manufacturing and represents only one of a number of cumulative process attributes. By reducing layer thickness by 50% does not produce 50% lower roughness.

11.3 Layer thickness, layer profile and layer composition all affect different LMT processes in different ways. For powder based LMT processes, particle size effects surface deviation more than layer thickness. Similarly, as seen with the section through the SLA-350 surface, layer profile is of equal importance to layer thickness in the SL process.

11.4 Roughness average (Ra) should be considered the most suitable unit of measurement when analysing LMT surfaces if all the process attributes including composition roughness are to be analysed.

11.5 The surface roughness of any angled SL parts, can now be predicted using the mathematical model in equations 3-35 and 3-36, if the process constants of layer profile ϕ, up-facing composition roughness K and down-facing composition roughness K_1 are derived.

11.6 A mathematical model has been developed which can be used to predict optimum orientation, RP part suitability for down stream applications or as a comparative benchmarking tool for comparing RP processes.

11.7 Solid state lasers produce parts with a higher surface roughness than gas laser when building in a similar layer thickness due to the energy distribution of the laser within the liquid monomer. Hence, if the surface roughness of the SLA-350 process is to be improved, layer profile should be investigated rather than either layer thickness or scan path.

11.8 Both gas and solid state laser systems produce print-through on down-facing SL surfaces between 90 and 145-degrees. Print-through is now known to have a smoothing effect on these surfaces. However, the benefits of print-through cannot be extended without significant changes being made to the SLA hardware.

11.9 Diffractive optical elements cannot be used to produce variable angled layer profiles without significant developmental work in the optical element field. Should variable diffractive elements become available then there use in SL may revolutionise the way liquid monomers are cured using UV radiation.

11.10 Skin smoothing can be used to reduce the surface deviation of SL parts over a limited range of angled surfaces. However, the process is not suited to complex geometries with small featured or cavities with continually changing angled sides.

11.11 Meniscus smoothing cannot be used for parts with trapped volume unless then are either orientated first or a drain hole is made within the geometry to prevent resin inclusion within the part.

11.12 By orientation of parts containing trapped volumes, cavities will inevitably benefit from print-through smoothing if the majority of surfaces are built down-facing. Similarly, any part that requiring 50-degrees of uniform and smooth topography, will benefit from orientation between 90 and 140-degrees.

11.13 If meniscuses are to be used for smoothing SL surfaces, the correct retraction distance must be used when pulling the meniscus between layer, prior to scanning. Incorrect meniscus retraction distance can result in an increase in surface roughness. However, all up-facing surfaces will benefit from the correct shaped meniscus and will be lower then those produced using the 3D Systems build algorithm. By using a combination of orientation, print-through and meniscus smoothing surface deviation can be reduced on complex SL parts, such as tool cavities, by up to 400%.

CHAPTER 12

12.0 Recommendations for further work

The following are recommendations for further work as influenced by the findings contained within this thesis. Three areas of further work have been identified from this thesis, these being the future development of the mathematical model, the development of dedicated smoothing software and the application of meniscus smoothing to other SL technologies.

12.1 Mathematical modelling

Based on the mathematical model developed in Chapter 3, a number of areas of further work are now possible. Given increasing process knowledge on laser/resin interaction and resin material properties, future research may be able to develop a mathematical description of SL composition roughness. In addition, from either first principles or empirical data it may also be possible to develop a mathematical representation of print-through smoothing on down-facing SL surfaces. Other areas of mathematical research are the validation of the mathematical model on other LMT process. At present, Virginia University are undertaking research to establish the composition roughness and layer profile of FDM components [144] These results will then be used to validate the model for FDM surface roughness. Similar work is also being undertaken at the University of Texas in Austin, to apply the model to parts manufactured using the SLS process.

12.2 Software development

Having identified the process parameters required to produce suitable shaped meniscus between layers, further research is now needed to write dedicated software

to control the process within the 3D Systems operating system. The limitations of using the TSR software have been shown, in both process build time and the restrictions of part size, dictated by the level of high-level memory in the SLA-250/40 machine. Other areas of valuable research for the future are in the generation of the shadow file for scanning solely the meniscus generated between each layer. A method using first and zero order CAD approximation has already been discussed in Chapter 10 and could form the starting point for additional research. Other software must also be developed to separate up-facing and down-facing facets of the STL file. The up-facing facets would then be used as the basis of the shadow file.

12.3 Applications to other SL processes

This research program has only looked at the application of meniscus smoothing on the SLA-250/40 machine, with the passive re-coating system. More recent SL technology includes the active Zephyr blade, which adds resin onto the part prior to the scanning of each new layer. It may be possible therefore, to use the Zephyr to lay a skin of resin over a retracted part, producing a meniscus from above, rather than pulling the meniscus using the previously polymerised layers. This approach may produce larger meniscus between the peaks and troughs of the surface, resulting in mush smoother surface topography. Given the increased power of solid state laser systems, it may also be possible to manufacture parts in significantly thickness layers, with the inclusion of meniscus. Hence, parts could be manufactured more rapidly, yet retain an equal if not better surface resolution than using the current build strategy.

References

[1] DICKENS, P.M. Rapid Prototyping in Japan, Report on the Overseas Science and Technology Expert Mission Scheme (OSTEMS), University of Nottingham, 1995.

[2] BJØRKE, Ø. Layer Manufacturing – A Challenge of the Future -, Tapir Publishers, Trondheim, Norway, 1992, ISBN 82-519-1125-7

[3] BURNS, M. Rapid Prototyping: System selection & implementation guide, Published by the Management Roundtable, Inc, Boston, Massachusetts, USA, 1991, ISBN 0-932007-23-6.

[4] SFERRO, P.R. Integrating Time-Compression Technology into existing management Infrastructure, Proceeding of the 2nd Time compression Technology conference, 29-30 September 1997, pp163 – 170, Rapid News Publications Plc.

[5] CHANTRILL, A. Rapid Prototyping Technology, Virtual Prototyping and Rapid manufacturing, PERA, Melton Mowbray, 20th January 1998.

[6] REEVES, P.E. Fused deposition modelling case study – TestConsult -, Rapid Prototyping workshop, Innovative Manufacturing Centre, Nottingham, UK, 12th – 13th November 1997, p 28

[7] GREAVES, T. HORODYSKY, M. Using Stereolithography to directly develop rapid injection mould tooling, Rapid News, Volume 5, Number 7, December 1997, published by Rapid News Publications Plc, UK

[8] SCHMITZ, T. Rapid prototyping using high speed machining, Prototyping technology international, published by UK and international press, January – March 1998

[9] DUSEL, K.H. Improvement of part accuracy – Investigation into the basics of photo-polymerisation, 5th European Conference on Rapid Prototyping & manufacturing, Dipoli Conference Centre, Helsinki, 4th – 6th July 1996, Published by: The University of Nottingham, ISBN 0 9519759 5 1

[10] JACOBS, P.J. Stereolithography error analysis, 8th European Stereolithography user Group meeting, Darmstadt, Germany, 7-8th October 1996.

[11] FLINT, B. ProtoTech Engineering applies finishing touch to Stereolithography, Unigraphics Centre line, Volume 7, Number 2, 1994

[12] CHADWICK, A.L. Surface finishing of Stereolithography models used as patterns for Rapid Tooling techniques, BEng dissertation, Department of

Manufacturing Engineering and Operations Management, University of Nottingham, June 1996

[13] DICKENS, P.M. Rapid Finishing and Tooling, Internal report, Rapid Prototyping Research Group - University of Nottingham, January 1994

[14] 3D SYSTEMS SLA-35000 sales literature, Valencia, CA, USA, P/N 70309, 31st August 1997

[15] PEACOCK, G.J. Method of making Composite Horseshoes, US Patent 746,143, December 1903

[16] BAESE, C. Photographic process for the reproduction of plastic objects, US patent, 1902

[17] HOPKINS, M.C. Photosculpture, US patent 1,382,978, June 28, 1921

[18] HOWEY, W. Pantographic Scanning, US patent 1,923,208, May 7, 1930

[19] KOJIMA, S. Method for making layer manufactured furniture, US patent 2,903,390, October 29, 1956

[20] SWAINSON, W.K. Method, Medium & Apparatus for Producing Three-dimensional figure product, US patent 4,041,476, August 9, 1971

[21] PORT, C.O. New Roles for Lasers: 'Solid Holography', Modern Plastics, Vol. 51, Number 7, July 1975, pp 64 - 66

[22] SWAINSON, W.K. Three Dimensional Pattern Making Methods, US patent 4,333,165, December 1, 1977

[23] SWAINSON, W.K. Three Dimensional Systems, US patent 4,078,229, March 7, 1978

[24] SWAINSON, W.K. Three Dimensional Systems, US patent 4,288,861, January 22, 1979

[25] DIMATTEO, P.L. Methods for generating signals defining three-dimensional object surfaces, US patent 3,866,052, February 11, 1975

[26] DIMATTEO, P.L. Method of Generating & Constructing three-dimensional Bodies, US patent 3,932,923, October 21, 1974

[27] BOGART, M. In art the end doesn't always justify the means, Smithsonian, Vol. 10, 1979, pp 104 - 110

[28] KODAMA, H. Automatic method for fabricating a three-dimensional plastic model with photo-hardening polymer, Review of scientific instruments, Vol. 52, Number 11, November 1981, pp 1770 - 1774

[29] HERBERT, A.J. Solid Object Generation, Journal of Applied Photography, Vol. 8, Number 4, August 1982, pp 185 - 188

[30] MORIHARA, T. Japanese Patent 61-114817 - 18, 1986

[31] HULL, C.W. Apparatus for production of three-dimensional object with Stereolithography, US patent 4,575,330, 1986

[32] HERBERT, A.J. A review of 3D solid object generation, Journal of Imaging Technology, Number 15, 1989, pp 186 – 190

[33] 3D SYSTEMS, The edge – competitive advantage through RP & M, Vol. 5, No. 1, 3D Systems publication, Hemel Hempstead, UK, P/N 70232/70232A4, 1995

[34] WOHLERS, T. Future Potential of Rapid Prototyping & Manufacturing around the World (Keynote Paper), 3rd European Conference on Rapid Prototyping & Manufacturing, The University of Nottingham, July 6th & 7th, 1994, pp 1 – 12, ISBN 0 9519759 2 7

[35] McQUAID, J. Zephyr experiences, 8th European Stereolithography user Group meeting, Darmstadt, Germany, 7-8th October 1996.

[36] SLA-3500 – 3D systems, Company literature PN 70309/08-31-97. January 1998, Hemel Hempstead, UK

[37] FOCKELE, M. SCHWARZE, D. Stereolithography sales literature, Fockele und Schwarze Stereolithographietechnik, Borchen-Alfen, Germany 1996.

[38] EOS, Making light work – solutions for Rapid prototyping, company sales literature, München, Germany 1997.

[39] RAPID PROTOTYPING REPORT, The newsletter of the desktop manufacturing industry, Volume 4, Number 9, published by CAD/CAM, September 1994.

[40] RAPID PROTOTYPING REPORT, The newsletter of the desktop manufacturing industry, Volume 7, Number 8, published by CAD/CAM, August 1997.

[41] WOHLERS, T. State of the Industry – Rapid Prototyping 1995 – 1996 World-wide report, published by the RP association of the SME, Dearborn, Michigan, USA, 1997

[42] CHANTRELL, A. Personal communication with director of sales for 3D Systems UK Ltd, 20th April 1998.

[43] WOHLERS, T. Rapid Prototyping State of the Industry – 1997 world wide progress report Executive summary, published by Wohlers associates Inc Colorado, USA

[44] TILLEY, K. Rapid Prototyping workshop, Innovative Manufacturing Centre, Nottingham, UK, 12th – 13th November 1997

[45] MOCTEZUMA, J.J. An integrated software package for medical Stereolithography based on computer Tomography. 3rd International workshop on RP in Medicine & Computer assisted surgery, Erlangen, Germany, October 19-21, 1995

[46] JAMIESON, R. CAD methods in Rapid Prototyping, 3rd European Conference on Rapid Prototyping & Manufacturing, The University of Nottingham, July 6th & 7th, 1994, pp 13 – 24, ISBN 0 9519759 2 7

[47] EVANS, D.G. An Investigation into the use of Rapid Prototyping by industrial designers, 6th European Conference on Rapid Prototyping & Manufacturing, The Nottingham Royal Moat House, Nottingham, UK, July 1st –3rd, 1997, ISBN 0 9519759 7 8

[48] ROCK, S.J. WOZNY, M.J. A flexible file format for solid freeform fabrication, Solid Freeform Fabrication Symposium, University of Texas at Austin, August 1991

[49] ROCK, S.J. WOZNY, M.J. Generating topological information for a "Bucket of Facets", Solid Freeform Fabrication Symposium, University of Texas at Austin, August 1992

[50] BETTANY, J.S. COBB, R.C. A rapid ceramic tooling system for prototype plastic injection moulding, 1st National conference on Rapid Prototyping and Tooling Research, Buckinghamshire College, UK, 6th – 7th November 1995, Published by Mechanical Engineering Publications London, ISBN 0 85298 982 2

[51] KIM, J.Y. LEE, K. PARK, J.C. Determining the optimum part orientation in Stereolithographic Rapid Prototyping, Internal publication, Department of Mechanical Design & Production Engineering, Seoul National University, Seoul, Korea, March 1995

[52] FRANK, D. Preferred direction of build for Rapid Prototyping, The Fifth International Conference on Rapid Prototyping, The University of Dayton, Ohio, U.S.A., June 12th –15th, 1994, pp 191 - 200

[53] LI, J. Improved Stereolithography part quality, The Third International Conference on Rapid Prototyping, The University of Dayton, Ohio, U.S.A., June 7th - 10th, pp 171 – 178, 1992

[54] KIRSCHMAN, C.F. NAMBOODRI, C. Stereolithographic support structure design for rapid prototyping, The Second International Conference on Rapid Prototyping, The University of Dayton, Ohio, U.S.A., June 1991, pp 255 – 265

[55] HAGUE, R.J.M. The use of Stereolithography models as thermally expendable patterns in investment casting, PhD thesis, Department of Manufacturing Engineering and Operations Management, University of Nottingham, May 1997.

[56] MATERIALISE. Guide to Magic's 2.2, Materialise, Heverlee, Belgium, 1993

[57] WEBB, D. GEDED, V. Computer aided support structure design for Stereolithography models, The Fifth International Conference on Rapid Prototyping, The University of Dayton, Ohio, U.S.A., June 12th -15th, 1994, pp 221 - 228

[58] JACOBS, P.F. Rapid Prototyping & Manufacturing – The fundamentals of Stereolithography, Society of Manufacturing Engineers, Dearborn, Michigan, USA, 1st Edition, 1992, ISBN 0-87263-425-6

[59] WONSILD, B. Application of support and variation in thickness of layer, Brite-Euram INSTANT-CAM report, Work area 3, Work package 9, June 1991.

[60] RUDD, N.A. Second Generation RP process combined with old fashioned sand casting, The Fourth International Conference on Rapid Prototyping, The University of Dayton, Ohio, U.S.A., June 14th -17th, 1993, pp 66 - 74

[61] SLA 190/250 User Guide 3.83, 3D systems, Valencia, USA, 1994

[62] JAYANTHI, S. HOKUF, B. LAWTON, J. Influence of post curing conditions on the mechanical properties of Stereolithographic Photo-polymer, Solid Freeform Fabrication Symposium, University of Texas at Austin, August 7th - 9th, 1995, pp 107 –117

[63] RUDD, N.A. Model turbine for hydro power machinery made as a Rapid Prototype part, 2nd European Conference on Rapid Prototyping & Manufacturing, The University of Nottingham, July 15th & 16th, 1993, pp 53 – 58, ISBN 0 9519759 1 9

[64] JAMIESON, R. New options in aerodynamic modelling; CAD, CFD, Stereolithography and shading in a workstation environment, Computer Aided Engineering Journal, Vol. 7, Number 3, June 1990, pp 75 - 79

[65] KRAMER, B. Photoelastic investigation by means of Stereolithography, 3rd European Conference on Rapid Prototyping & Manufacturing, The

University of Nottingham, July 6th & 7th, 1994, pp 275 – 285, ISBN 0 9519759 2 7

[66] STEINHAUSER, D. Automotive applications of photo-polymers – Visualisation of coolant flow and lubrication distribution in high performance transmission components, 8th European Stereolithography user Group meeting, Darmstadt, Germany, 7-8th October 1996

[67] MENGES, G. MOHREN, P. How to make injection mould tools, published by Macmillan publishing company, 2nd Edition 1986, ISBN 0 02 947570 8

[68] HORODYSKY, T.G. Case study: Using SL to produce direct developmental rapid injection mould tooling, Proceeding of the 2nd Time compression Technology conference, 29-30 September 1997, pp127 - 135, Rapid News Publications Plc.

[69] HARTLEY, M. Initial experiences using DTM's Rapidtool metal process, 6th European Conference on Rapid Prototyping & Manufacturing, The Nottingham Royal Moat House, Nottingham, UK, July 1-3 1997, ISBN 0 9519759 7 8

[70] DICKENS, P.M. Rapid Prototyping of metal parts and tooling, Proceeding of the 2nd Time Compression Technology conference, 29-30 September 1997, pp72 – 75, Rapid News Publications Plc

[71] BREITINGER, F. Rapid simultaneous product development (Part1), Rapid News, Volume 5, Number 5, Published by Rapid News Publications Ltd, September 1997

[72] PAUWELS, J. Spin casting assists automotive product designers in developing fully functional metal and plastic test parts from RP models. 8th European Stereolithography user Group meeting, Darmstadt, Germany, 7-8th October 1996

[73] WHELAN, T. GOFF, J. Moulding of thermosetting plastics, published by Van Nostrand Reinhold International Ltd, London UK, 1990, ISBN 0 442 30318 1

[74] http://3dsystems.com/ : 3D systems home page, March 98

[75] REEVES, P.E. Rapid Prototyping workshop, Innovative Manufacturing Centre, Nottingham, UK, 12th – 13th November 1997, p 28

[76] GRIFFITHS, A. CLARKE, C. Shift in focus from 'cost and quality' to 'agile' and the implications for data management strategy. Proceeding of the 2nd Time Compression Technology conference, 29-30 September 1997, pp1 - 8, Rapid News Publications Plc

[77] BAUMAN, R. World plastics outlook, http://www.modplas.com/industry/OUTLOOK.html

[78] LUCK, T. Functional plastic prototypes – Process chains and their case studies, proceeding of the 2nd Time Compression Technology conference, 29-30 September 1997, pp127 - 135, Rapid News Publications Plc.

[79] EXTRUDE-HONE, Ultrasonic flow polishing – precision surface and edge improvement, sales literature, Extrude-Hone Ltd, Milton Keynes, UK, 1997

[80] LEE, N. Plastic blow moulding handbook, published by Chapman and Hall, 1st edition, 1990, ISBN 0 442 20752 2

[81] REEVES, P.E. COBB, R.C. Surface deviation modelling of LMT processes - A comparative analysis, 5th European conference on Rapid Prototyping & Manufacturing, Dipoli conference centre, Helsinki, Finland, June 4th - 6th, 1996 pp 59 - 77, ISBN 0 9519759 5 1

[82] GIROUARD, D. Moulds for low temperature moulding processes, The Fourth International conference on Rapid Prototyping, The University of Dayton, Ohio, U.S.A., June 14th – 17th, 1993

[83] IULIANO, L. IPPOLITO, R. DE FILIPPI, A. A new user part for performance evaluation for Rapid Prototyping systems, 3rd European conference on Rapid Prototyping & Manufacturing, The University of Nottingham, 6th – 7th July 1994, p 327, ISBN 0 9519759 2 7

[84] SANDERS PROTOTYPING INC. Model Maker II – when precision counts, sales literature published by Sanders Prototyping Inc, New Hampshire, USA, 1996

[85] JACOBS, P.F. PARTANEN, J. Surface Quality, Insight, 3D systems Publication, August 1994

[86] JACOBS, P.F. RICHTER, J. Advance in Stereolithography accuracy, 2nd Solid Freeform Fabrication Symposium, University of Texas at Austin, 12th – 14th August, 1991, p 138

[87] CHUA, C.K. LEE, H.B. Integrating SLA with computer aided jewellery design and manufacture, 4th IFIP conference on computer applications in production engineering, Elsevier science publishers, Holland, 1991

[88] LEE, H.B. KO, M.S.H. GAY, R.K.L. Using computer based tools and technology to improve jewellery design and manufacture, International journal of computer applications in technology, Vol. 5, Number 1, 1992, pp 72 – 80

[89] INSTITUTO SUPERIOR TÉCNICO, INSTANT-CAM, Work Area 3 - FINAL REPORT, Brite/Euram Contract Number BREU-157, Project Number BE3527-89

[90] DANISH TECHNOLOGICAL INSTITUTE, Surface Treatment of SLA-parts, Work area 3, Work package 10 - 11, Brite/Euram Contract Number BREU-157, Project Number BE3527-89

[91] SPENCER, J.D. COBB, R.C. DICKENS, P.M. Surface finishing techniques for Rapid Prototyping, Proceeding of the SME conference - Rapid Prototyping and Manufacturing '93, Hyatt Regency Hotel, Dearborn, Michigan, May 11th - 13th 1993

[92] COBB, R.C. SPENCER, J.D. DICKENS, P.M. Vibratory Finishing of SLA parts, Solid Freeform Fabrication Symposium, University of Texas at Austin, August 9th - 11th, 1993

[93] KITTREDGE, J.B. Vibratory deburring - the dynamic science, Society of Manufacturing Engineers Technical paper, MR75 - 487, Dearborn, Michigan, USA, 1975

[94] COBB, R.C. SPENCER, J.D. DICKENS, P.M. Better Surface Finishing Techniques for RPT is a must, Proceeding of the 2nd Scandinavian Rapid Prototyping Conference, Danish Technological Institute, Aarhus, Denmark, October 4th, 5th & 6th, 1993

[95] LEE, H.B. CHUA, CK. LEONG, K.F. Case studies of jewellery prototyping using SLA, Solid Freeform Manufacturing 1st International user congress, Technical University of Dresden, October 28 - 30, 1993

[96] RHOADES, L.J. Automated finishing processes – A cost guide, The Society of Manufacturing Engineers, Dearborn, Michigan, USA, 1995, ISBN 0-87263-056-0

[97] DAVIDSON, D.A. Current applications for hardwood media in dry finishing process mass finishing, Society of Manufacturing Engineers, Deburring & Surface conditioning conference, Chicago, Illinois, USA, September 23rd - 26th, 1985

[98] DAVIDSON, D.A. Mass finishing of plastics, Product Finishing, July 1984, pp 44 - 47

[99] DAVIDSON, D.A. Current developments in dry process mass finishing, Finishers Magazine, Vol. 33, Number 7, September 1988, pp 43 - 46

[100] DAVIDSON, D.A. Developments in dry process pre-plate finishing, American electroplaters and surface finisher's society, 74th AESF conference, July 13th, 1987

[101] EMSLIE, FALLOWS LTD. Barrelling: Turning an enemy into a friend, Technical publication, Lea Manufacturing, Buxton, UK, 1994

[102] RAPID FINISHING & TOOLING, EPSRC Grant GR/J97748, final summary report, June 1997, The University of Nottingham, Dept of Manufacturing Engineering.

[103] SEGAL, J.I. COBB, R.C. Optimising arc-spray metal tooling for injection moulding, First National conference on Rapid Prototyping & Tooling Research, November 6th & 7th 1995, Mechanical Engineering Publications Ltd, London, UK, pp 189 – 199, ISBN 0 85298 982 2

[104] KOCH, M. Rapid Prototyping & Casting, 3rd European Conference on Rapid Prototyping & Manufacturing, The University of Nottingham, July 6th & 7th, 1994, pp 73 – 76, ISBN 0 9519759 2 7

[105] ARTHUR, A. DICKENS, P.M. Rapid prototyping of EDM electrodes by Stereolithography, International Symposium for Electro-machining, Ecole Polythenique federal de Lausanne, Lausanne, Switzerland, April 17th-21st, 1995, pp 691 – 700

[106] ARTHUR, A. DICKENS, P.M. Model EDM electrodes as an alternative route to complex mould and die cavities, 6th European Conference on Rapid Prototyping & Manufacturing, The Nottingham Royal Moat House, Nottingham, UK, July 1-3 1997, ISBN 0 9519759 7 8

[107] FARRELL, R.E. ROTH, D.E. Verifying finite element analysis using Stereolithography, The Fifth International Conference on Rapid Prototyping, The University of Dayton, Ohio, U.S.A., June 12th - 15th, 1994, pp 151 – 162

[108] REEVES, P.E. COBB, R.C. The finishing of Stereolithography models using resin based coatings, Solid freeform fabrication symposium, University of Texas at Austin, August 7th - 9th, 1995 pp 96 - 107

[109] REEVES, P.E. COBB, R.C. Improvements in the Surface Finish of Stereolithography Models for Manufacturing Applications, 1st National Conference in Rapid Prototyping and Tooling Research, Great Missenden, Buck's, Buckinghamshire College, 6th & 7th November 1995, ISBN 0 85298 982 2

[110] FLINT, B. ProtoTech Engineering applies finishing touch to Stereolithography, Unigraphics Centre line, Volume 7, Number 2, 1994

[111] REEVES, P.E. COBB, R.C. SL Surface Finish - The Cause, Effect & A Hands-Free solution, The Future of Model making International Conference, University of Hertfordshire, Hatfield, UK, 22nd March, 1996

[112] IKUTA, K. Ultra high resolution Stereolithography for three-dimensional micro fabrication, The Fifth International Conference on Rapid Prototyping, The University of Dayton, Ohio, U.S.A., June 12th - 15th, 1994, pp 37 - 46

[113] LOECHEL, B. MACIOSSEK, A. Galvanoplated 3D structures for micro systems, Microelectronic Engineering, Volume 23, January 1994, pp 455 - 459

[114] PEGNA, J. MAXWELL, J. HILL, E. Gas-phase Laser induced pyrolysis of tapered microstructure, Solid Freeform Fabrication Symposium, University of Texas at Austin, August 7th - 9th, 1995, pp 143 - 150

[115] CAWLEY, J.D. WEI, Z.E. LIU, W.S. NEWMAN, B.B. Al_2O_3 Ceramic made by CAM-LEM (Computer-aided manufacturing of laminated materials technology), Solid Freeform Fabrication Symposium, University of Texas at Austin, August 7th - 9th, 1995, pp 9 - 17

[116] DeJAGER, P.J. Using Slanted and ruled layers for rapid prototyping, 5th European conference on Rapid Prototyping and Manufacturing, The Dipoli Conference centre, Finland, 4 – 6th June 1996, ISBN 0 9519759 5 1

[117] MASHINSKY, L. Methods and Apparatus for producing stepless 3-dimensional object by Stereolithography, US patent 5,217,653, June 8 1993

[118] NARAHARA, H. Accuracy improvement procedures for Stereolithography parts, Journal of the Japan Society for Precision Engineering, Vol. 28, No. 4, Dec. 1994

[119] NARAHARA, H. A new method for improving performance and surface roughness in Stereolithography, Proceedings of :- The 2nd Korea-Japan Die & Mould workshop, Pusan National University, Pusan, Korea, June 28-30, 1995

[120] SMALLEY, D.R. et al. Surface resolution in three-dimensional objects by inclusion of thin fill layers, US patent 5,209,878 May 11, 1993

[121] MCALEA, K. SLS Technology advances, presented at the Rapid prototyping and manufacturing conference of the Society of Manufacturing Engineers, Dearborn, Michigan, USA, April 23rd – 25th 1996

[122] TUMER, I.Y. THOMPSON, D.C. CRAWFORD, R.H. KRISTIN, L.W. Surface characterisation of polycarbonate parts from selective laser sintering, Solid Freeform Fabrication Symposium, University of Texas at Austin, August 7th - 9th, 1995, p 181

[123] SACHS, E. BRANCAZIO, D. MILNER, J. BREDT, J. LEE, J. 3D printing surface finish improvements through on-line control, The Fifth

International Conference on Rapid Prototyping, The University of Dayton, Ohio, U.S.A., June 12th, 13th, 14th & 15th, 1994, pp 1 - 9

[124] RANK TAYLOR HOBSON, Surface Texture Parameters, Company publication 800-302/694 (English) 15MCP

[125] BOGDAN, N, Investigation of the Surface Roughness Range, CIRP Annals, 1981, Volume 30/1/1981

[126] RANK TAYLOR HOBSON, Surface analysis software for Talysurf 10, 3 or 3P, Company publication, PO BOX 36, New Star Road, Leicester, UK

[127] RANK TAYLOR HOBSON, Surftronic 3P Operating Instructions, Company publication, 221-57/685 BO 4m

[128] JOEL 4300, Scanning Electron Microscope, Operating Instructions, 1985

[129] RAHMATI, S. DICKENS, P.M. Stereolithography process improvement, 1st National Conference on Rapid Prototyping and tooling research, Buckinghamshire College 6th – 7th, November 1995, Published by MEP, ISBN 0 85298 982 2, pp 111 - 126

[130] JACOBS, P.J. Solid state laser for Stereolithography, 8th European Stereolithography user Group meeting, Darmstadt, Germany, 7-8th October 1996.

[131] JELLY, C. Rapid Prototyping simulation: past, present and future, 1st National conference on the future of design, March 1996, Published by the University of Hertfordshire, Edited by B. Holder, ISBN 1-898543-21-6

[132] CAHANA, Y. Beam shape diffractive elements for laser processing, project code 770, http://.matimop.org.il : March 1998

[133] HULL, C. Personal communication with 3D systems chief executive July 15th 1997.

[134] MATHISEN, J. http://micros.hensa.ac.uk : Shareware archive, TSR documentation, April 1997

[135] ROBINSON, J.L. Basic Fluid Mechanics, Published by McGraw-Hill Book Company, New York, 1963

[136] BUDINSKI, K.G. Surface alterations in abrasive machining, International conference on the wear of materials, Reson, Virginia, USA, Published by The society of Manufacturing Engineers, Dearborn, Michigan, USA, 1993

[137] JOHNSTON, W.S. Surface finishing with non-ferrous abrasives, Deburring and surface conditioning symposium, October 26th – 27th 1993, Published by the Society of Manufacturing Engineers, MR93-327

[138] RHOADES, L.J. Abrasive flow machining and its use, Non-traditional machining conference, Society of carbide and tool manufacturers, December 2nd – 3rd 1995, ISBN 0-87170-264-9

[139] Ultrasonic Flow Polishing – ExtrudeHone Company literature, April 1997, ExtrudeHone, Milton Keynes, UK

[140] REEVES, P.E. COBB, R.C. Reducing the surface deviation of Stereolithography using in-process techniques, Rapid Prototyping Journal, Volume 3, Number 1, 1997, ISSN 1355-2546

[141] De-JAGER, P.J. A comparison between zero and first order approximation algorithms for layered manufacturing, Rapid Prototyping Journal, Volume 3, Number 4, 1997, ISSN 1355-2546

[142] De-JAGER, P.J. Models with better surface finish using ruled and slanted slices, European Action on Rapid Prototyping EARP, No.8, May 1996

[143] ROCK, S.J. WOZNY, M.J. A flexible file format for solid freeform fabrication, Solid Freeform Fabrication Symposium, University of Texas at Austin, August 1991

[144] Rapid Manufacturing Research Group – Virginia State University, Personal E-mail communication, 14th November 1997

Published papers

Refereed journal papers

REEVES, P.E. COBB, P.E. Reducing the surface deviation of Stereolithography using in-process techniques, Rapid Prototyping Journal, MCB press, Vol3, Number 1, 1997 ISSN 1355-2546

Refereed Conference papers

REEVES, P.E. COBB, R.C. Improvements in the Surface Finish of Stereolithography Models for Manufacturing Applications, 1st national Conference in Rapid Prototyping and Tooling Research, Great Missenden, UK, 6th & 7th November 1995, ISBN 0 85298 982 2

REEVES, P.E. COBB, R.C. Surface deviation modelling of LMT processes - A comparative analysis, 5th European conference on Rapid Prototyping & Manufacturing, Dipoli conference centre, Helsinki, Finland, June 4th - 6th, 1995 pp 59 - 77, ISBN 0 9519759 5 1

REEVES, P.E. COBB, R.C. Surface deviation modelling in Rapid Prototyping, 12th National Conference on Manufacturing Research (NCMR), The University of Bath, UK, 9th - 12th September 1996

REEVES, P.E. COBB, R.C. Surface roughness investigation of Stereolithography ACES components, 2nd national Conference in Rapid Prototyping and Tooling Research, Great Missenden, UK, 18th & 19th November 1996

REEVES, P.E. DICKENS, P.M. COBB, R.C. DAVEY, N. Surface roughness of Stereolithography using an alternative build strategy. 6th European conference on Rapid Prototyping & Manufacturing, The Nottingham Royal moat house, Nottingham, UK, July 1st – 3rd 1997, ISBN 0 9519759 7 8

Symposium papers

REEVES, P.E. COBB, R.C. The finishing of Stereolithography models using resin based coatings, Solid freeform fabrication symposium, University of Texas at Austin, USA, August 7th - 9th, 1995, pp 96 - 107, ISSN 1053-2153

REEVES, P.E. COBB, R.C. SL Surface Finish - The Cause, Effect & A Hands-Free solution, The Future of Model making International Conference, University of Hertfordshire, Hatfield, UK, 22nd March, 1996, ISSN 1-898543-21-6

REEVES, P.E. COBB, R.C. DICKENS, P.M. SL surface finishing - Assessment, Prediction & Improvement-, 8th European Stereolithography user group meeting, Darmstadt, Germany, October 7 - 8th, 1996

APPENDIX A

Description of the main commercial Rapid Prototyping processes in addition to Stereolithography

Selective Laser Sintering (SLS)

Selective laser sintering is an additive manufacturing process which uses a laser to bind powder material together, either through the melting of the base material or the melting of a secondary binder. A schematic of the SLS process is shown in Figure A-1

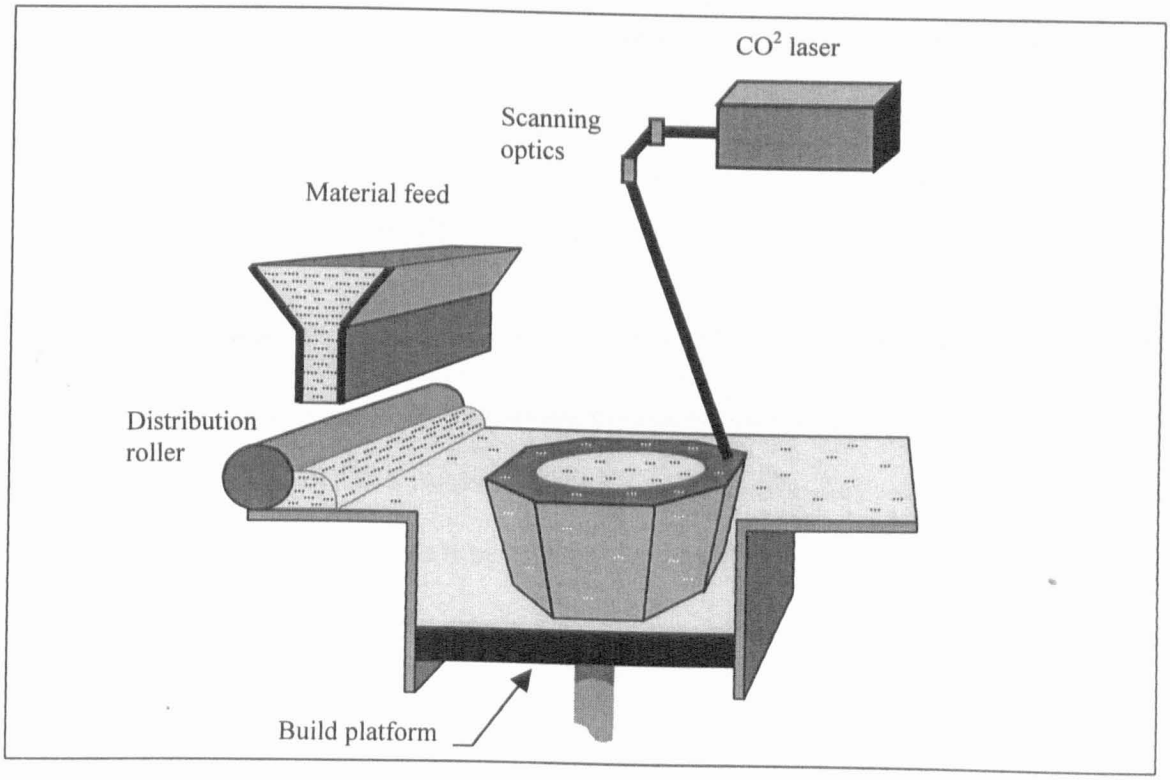

Figure A-1 The Selective laser sintering process

The process works by depositing a layer of powder onto a build platform, much in the same way as Stereolithography. The profile of the first layer is then scanned out by the laser. Unlike the photo-polymer reaction in SL, the higher power laser using in SLS causes localised heat at the focal point. If the heat exceeds the melting temperature of the powder material, adjacent particles will be bonded. This laser melting system is utilised in the German EOS laser sintering process. For materials with a higher melt temperature and those used in the American DTM system, a low melting temperature binder is coated onto the base material. It is this binder which is then sintered by the action of the laser. When the first layer is fully sintered the platform is retracted and a hopper feeder is used to deposit a fresh layer of powder material onto the previous layer, a distribution roller then ensured the new material is off a uniform thickness. The process of scanning and re-coating is repeated, until the geometry within the STL file is complete.

Unlike SLA, the SLS process does not require support structures to be added to the initial STL file, as the non-sintered material from the previous layer acts as a support medium for the next layer. At present the range of materials used in the SLS process include, polycarbonate, nylon, flexible nylon and wax. In addition a range of metallic materials are also available, however these must be fired and infiltrated with copper after sintering to reach full density and improve mechanical properties. A number of ceramic materials are also available including croning sand used for the manufacture of sand-casting cores. At present SLS is used for both prototype parts and tool cavities. With improvements in mechanical properties, accuracy and surface finish, SLS is set to become a standard manufacturing route for injection moulding tool inserts.

Fused Deposition Modelling (FDM)

Fused Deposition Model (FDM) is one of the most simplistic layer manufacturing mechanisms and is often assimilated to a robot icing a cake. The process works by depositing a semi-molten material onto a build platform, though an extrusion head moving in the X and Y-axis. A schematic of the FDM process is shown in Figure A-2

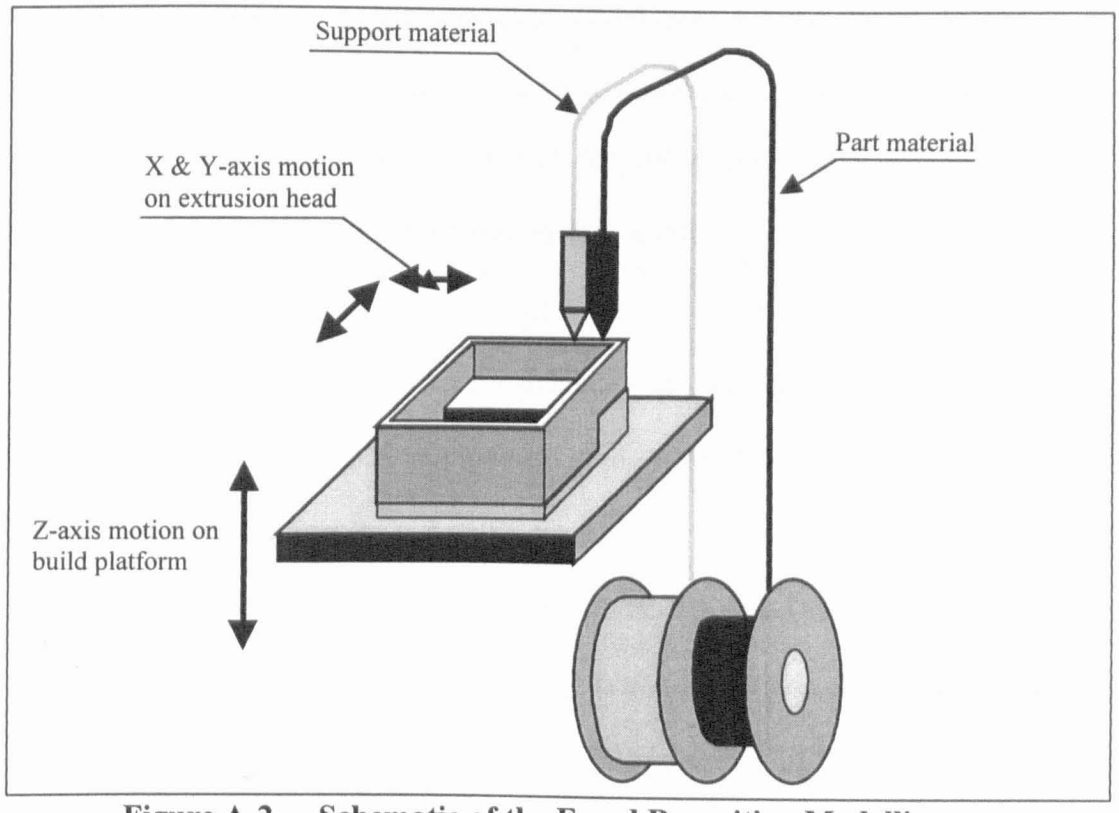

Figure A-2 Schematic of the Fused Deposition Modelling process

The FDM process works using two reels of feed material, which are heated prior to extrusion from a moving head. As the build material is taken from the feed roll, it is pushed into a heated chamber through a series of pinch rollers. The fresh material acts like a plunger, pushing molten material within the chamber out through an exit nozzle.

The position of the exit nozzle is carefully controlled above a build platform. Using slice data from the STL file the nozzle is then moved in the X and Y-axis extruding material into a series of filaments. Each filament fills an area within the layer boundary, until the layer is complete. As each new filament is extruded it is bonded to the previous layer, through localised heat. By depositing each layer of filaments at 90-degrees to the previous layer parts of 80% density can be produced with considerable strength in comparison to other layer manufacturing techniques. Unlike the SLA process, support structures are not manufactured in the same material, but are produced in a dissimilar polymer. On completion of the part the support material is separated from the build material, using either force or by dissolution in a solvent.

A number of materials are currently available for the FDM process including Nylon, investment casting wax, ABS and medical grade ABS. The main limitation of the process is build time, which can be excessive for parts of any size. One positive advantage is purchase price, which is a fraction that of similar sized SLA or SLS machines. In addition, the FDM machine can be operated in an office environment making the systems particularly suited to concept modelling within a company's CAD or design facility.

Laminated Object Manufacturing (LOM)

Laminated Object Manufacturing is the most simplistic layer manufacturing process-using laminations of cut material to produce parts. A schematic of the process is shown in Figure A-3.

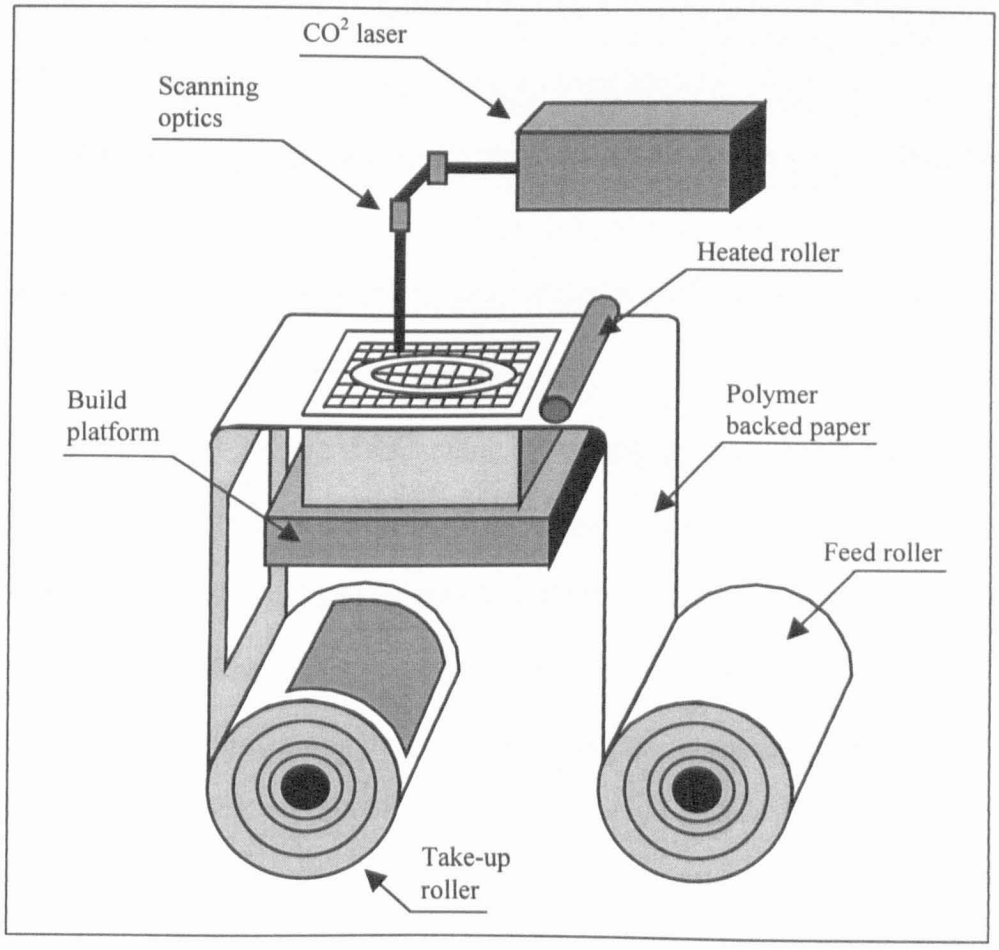

Figure A-3 Schematic of the Laminated Object Manufacturing Process

The LOM process works by fusing together layers of adhesive backed paper. The adhesive backing is a thermoplastic layer, sprayed onto the build material during manufacture. The build material is then spooled onto a 2500 feet role, in a range of widths. The roll of build material is loaded onto the machine and feed via a series of rollers over the build platform. The material is then pulled down from the build platform onto an empty take up roller. Before any scanning takes place, a heated roller is passed over the surface of the build material, causing the thermoplastic backing to melt. As the roller moves over the surface the material undergo rapid cooling and the molten polymer

solidifies. The resulting solid-liquid-solid phase change causes the material to be bonded to the build platform below. Using slice data from the STL file, the perimeter of the first layer is scanned on the surface of the sheet material using a CO_2 cutting laser. After scanning the perimeter of the part, the laser is used to cut a boarder around the part and crosshatch any material within the boarder, which is not part of the model geometry. Any waste material within the boarder can then easily be removed from the parts as a post-process operation. Following the scanning of the first layer, the build platform is retracted and the take-up roller is used to pull a fresh section of material across the build platform. The platform is then raised and the heated roller passed back over the part. After cooling the laser is used to scan the second layer perimeter and border, before cross hatching any waste material. The process is then repeated, until the geometry defined within the STL file is complete.

The main advantage of the LOM process is build time, which can be very fast for large and bulky components, in comparison to other techniques. As a rule, LOM is good for parts with a large surface area and large volume. The process is not good for parts with a large surface area and small volume as this results in the cross-hatching of much waste material.

The main limitations of LOM are waste and mechanical properties. The final part is nothing but laminated paper, producing a part good in compression but very weak in tension. Parts are also prone to moisture and have a limited life span of only 3-6 months.

In addition LOM is the only RP process which creates waste. On some parts as much as 90% of the build material can end up as non-recyclable waste.

Multi-Jet Modelling (MJM)

One of the most recent RP technologies to emerge is the Multi-Jet Modelling (MJM) or Actua process manufactured by 3D Systems. The process uses ink-jet printing technology to deposit layers of molten material onto a build platform. A schematic of the MJM process can be seen in Figure A-4.

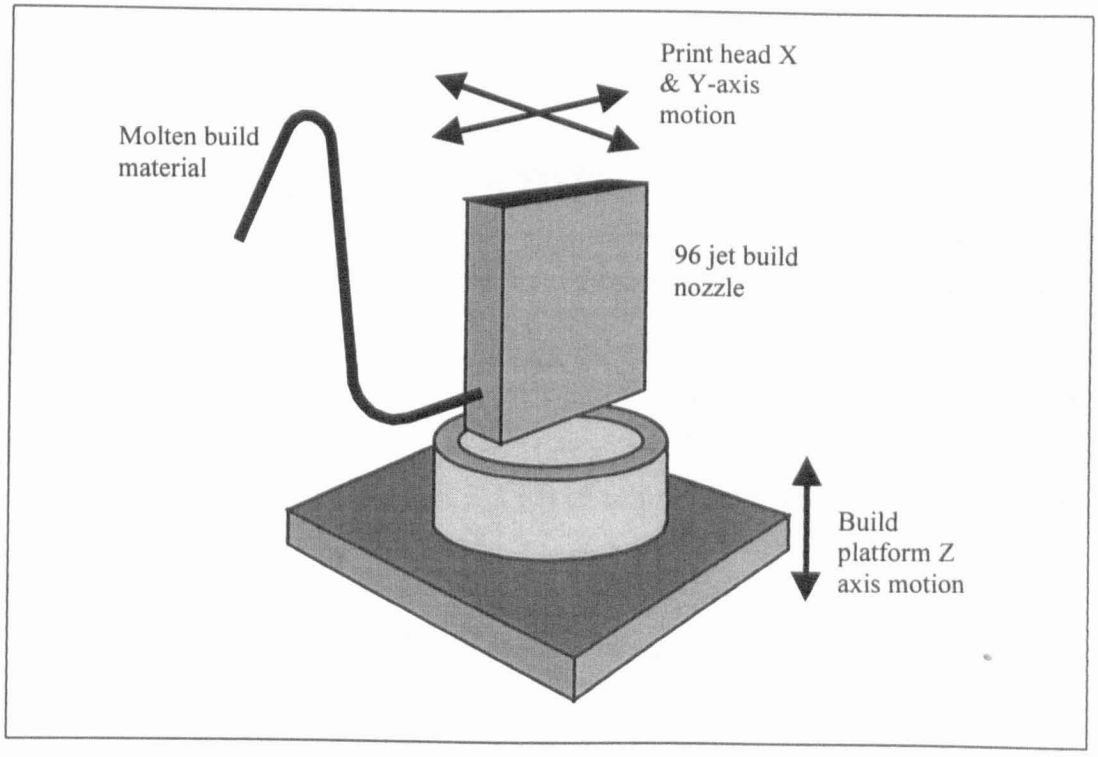

Figure A-4 Schematic of the Multi-jet Modelling Process

MJM like all other RP processes works by adding material onto a build platform, layer by layer, until the object defined by the slice data is complete. MJM is in some ways similar to the FDM process, in that molten material is deposited and bonded to the previous layer

through localised melting. Unlike FDM, the MJM process uses 96 parallel extrusion heads set at a pitch of 0.03 mm, rather than one 0.25mm extrusion nozzle on the FDM. The result is both a faster build time and more accurate parts. In addition, parts are almost 100% dense and require no post process firing or infiltration.

The main limitation of MJM is the mechanical properties of parts. At present the only build material is a paraffin based investment casting wax. Hence, parts are both brittle and susceptible to heat. The process also generates a considerable amount of support structure, which must be cleaned from the part as a post-process operation, leaving a very poor surface finish.

Drop-on-Demand inkjet (DODI)

Drop on Demand Inkjet printing or the 'Sanders' process is a combination of additive and subtractive manufacturing. A schematic of the process is shown in Figure A-5.

The process uses a combination of FDM and MJM, to produce layers by the deposition of a single bead of material though an ink jet nozzle. Following deposition, a milling cutter is moved over the part, removing a fine layer of material. By milling between each layer an accurate Z-axis datum can be maintained. Following milling the next layer is deposited onto the accurately machines substrate. Like FDM, any support structure is build in a separate material and removed from the part after manufacture using a solvent.

The DODI process is very good for high accuracy parts such as investment casting patterns for jewellery or precision engineering components. The main limitations are both build time and material properties. Like the MJM process, DODI uses a molten investment casting wax to build part. The resulting components are both brittle and prone to heat damage. Using only one deposition nozzle the DODI process is also very slow, and can take a number of days to build parts, which could be built using alternative RP techniques in a few hours. It is this build time problem which has limited the application of the DODI process to very few engineering sectors.

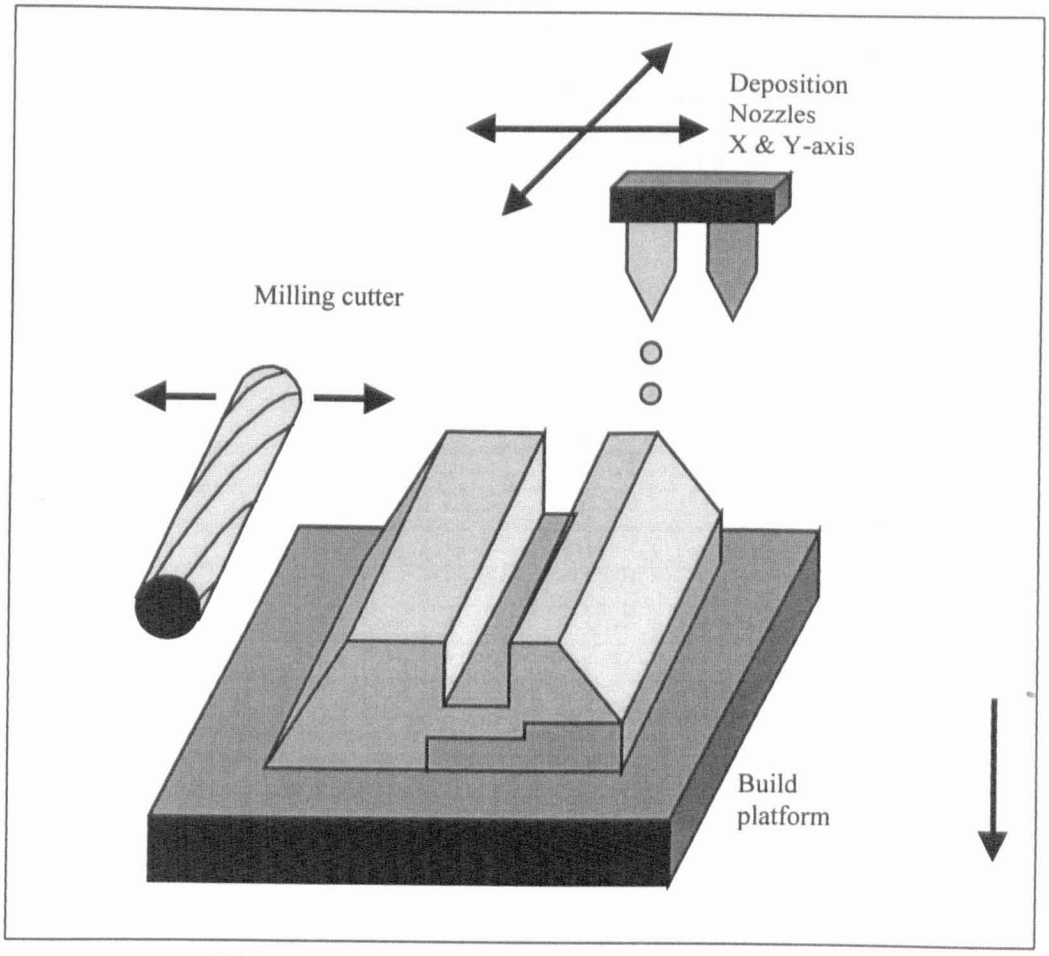

Figure A-5 Schematic of the Sanders Process

APPENDIX B

Surface roughness measurements derived for LMT benchmark samples

3D Systems, SLA Epoxy ACES, 0.15 mm layers							
Angle	Samp 1	Samp 2	Samp 3	Samp 4	Samp 5	Samp 6	Average
0	1.6	2.0	1.2	1.5	1.5	0.9	1.4
10	42.2	37.9	43.2	37.8	42.0	36.7	39.9
20	30.6	31.3	32.4	31.6	31.4	33.4	31.8
30	30.4	28.3	29.8	28.4	28.4	28.2	28.8
40	25.3	25.8	26.9	25.6	25.5	25.8	25.8
50	21.9	22.0	21.6	21.6	20.6	21.4	21.5
60	19.8	23.4	19.5	20.1	20.0	20.8	20.6
70	15.2	17.7	16.8	18.1	17.0	15.5	16.7
80	5.6	6.9	4.5	5.0	6.7	9.2	6.3
90	7.7	6.8	7.8	6.7	8.0	6.8	7.3

3D Systems, SLA Acrylic Start-Weave, 0.125 mm layers							
Angle	Samp 1	Samp 2	Samp 3	Samp 4	Samp 5	Samp 6	Average
0	4.5	5.1	5.3	4.3	4.3	4.6	4.7
10	24.0	36.6	22.5	35.2	22.3	26.3	27.8
20	24.5	24.3	23.5	25.4	19.6	23.3	23.4
30	14.9	14.6	15.9	16.9	16.1	15.4	15.6
40	19.9	11.8	11.4	15.9	9.5	13.1	13.6
50	8.4	6.8	7.9	10.8	10.8	8.5	8.9
60	7.3	5.8	5.3	7.6	5.4	5.9	6.2
70	11.4	13.3	9.8	8.5	9.9	11.1	10.7
80	7.1	6.8	6.2	6.4	7.2	6.5	6.7
90	4.3	4.9	4.4	4.0	6.7	4.8	4.8

Solider, Cubital Acrylic, 0.15 mm layers							
Angle	Samp 1	Samp 2	Samp 3	Samp 4	Samp 5	Samp 6	Average
0	3.4	2.6	3.2	3.6	3.1	2.7	3.1
10	13.8	13.5	6.8	8.2	14.0	10.2	11.1
20	11.2	12.5	4.2	7.7	12.3	12.4	10.0
30	6.9	7.9	4.1	6.0	9.5	10.1	7.4
40	18.2	10.8	9.8	13.2	14.7	14.5	13.5
50	11.7	9.2	13.4	11.7	14.3	11.6	12.0
60	14.2	11.8	13.7	13.0	9.6	12.6	12.5
70	8.3	8.0	6.0	6.8	10.0	10.8	8.3
80	10.7	11.3	11.5	8.1	9.7	14.5	11.0
90	8.7	11.6	13.8	6.7	9.7	10.7	10.2

EOS, SLS Polystyrene, 0.2 mm layers							
Angle	Samp 1	Samp 2	Samp 3	Samp 4	Samp 5	Samp 6	Average
0	23.8	20.9	27.7	26.4	20.9	30.7	25.1
10	62.9	62.1	72.0	62.3	75.8	56.4	65.2
20	30.8	37.3	49.9	49.2	52.8	59.1	46.5
30	42.4	39.3	20.9	32.7	42.3	36.1	35.6
40	32.3	39.0	36.6	29.4	39.7	48.5	37.6
50	35.7	30.0	29.3	34.0	31.0	35.5	32.6
60	37.4	29.1	28.9	26.6	27.1	23.1	27.0
70	25.7	24.0	27.6	24.9	25.1	20.8	24.7
80	24.4	21.5	19.1	22.9	22.7	20.1	21.8
90	21.9	21.5	18.3	21.9	22.2	17.9	20.6

EOS SLS Polystyrene / wax , 0.2 mm layers							
Angle	Samp 1	Samp 2	Samp 3	Samp 4	Samp 5	Samp 6	Average
0	23.6	21.0	20.8	17.1	24.9	25.2	22.1
10	33.2	39.0	39.9	47.4	45.4	55.2	43.3
20	31.1	32.2	33.7	34.5	36.3	30.0	33.0
30	24.2	28.1	18.6	35.6	24.2	33.2	27.3
40	25.6	29.6	20.4	28.0	25.3	26.1	25.8
50	23.9	23.9	28.0	19.6	24.4	29.1	24.8
60	25.2	18.9	16.7	28.8	25.6	23.2	23.1
70	22.1	17.2	10.9	13.9	20.3	16.1	16.7
80	12.0	17.4	16.0	14.5	17.4	18.7	16.0
90	21.7	11.7	16.5	16.0	15.2	15.9	16.2

DTM, SLS Fine Nylon, 0.1 mm layers							
Angle	Samp 1	Samp 2	Samp 3	Samp 4	Samp 5	Samp 6	Average
0	12.2	12.6	11.4	11.3	11.2	11.9	11.8
10	26.2	25.6	31.5	29.7	30.2	27.9	28.5
20	32.0	30.3	31.1	27.6	29.9	31.8	30.5
30	39.0	35.9	34.5	37.7	37.1	37.4	36.9
40	35.9	40.5	39.2	42.9	37.2	39.0	39.1
50	35.6	39.5	32.1	40.1	36.9	37.6	36.5
60	27.1	24.5	30.5	35.9	26.4	31.2	29.3
70	40.8	36.0	44.0	35.6	39/4	39.6	39.2
80	33.1	28.2	37.6	30.2	32.1	33.6	32.5
90	26.5	29.3	27.1	25.9	24.7	23.6	26.2

Helysis, LOM Fast paper, 0.1 mm layers							
Angle	Samp 1	Samp 2	Samp 3	Samp 4	Samp 5	Samp 6	Average
0	3.9	3.9	3.7	6.4	4.4	4.0	3.9
10	33.5	38.4	32.5	32.4	47.1	24.1	33.0
20	25.8	26.0	24.8	29.6	24.2	32.1	27.1
30	36.7	23.1	32.7	32.2	28.8	27.7	30.2
40	30.7	25.2	39.4	26.4	29.9	34.3	29.3
50	20.4	23.4	23.2	26.2	25.9	27.6	24.4
60	25.9	21.6	20.8	19.5	23.7	25.7	22.9
70	24.6	35.6	22.5	25.5	18.9	17.9	24.2
80	14.9	10.6	15.6	14.9	15.8	18.2	15.0
90	18.4	16.9	16.9	17.6	17.5	15.2	17.1

Stratasys, FDM ABS, 0.25 mm layers							
Angle	Samp 1	Samp 2	Samp 3	Samp 4	Samp 5	Samp 6	Average
0	32.7	33.3	33.4	29.0	30.2	27.3	30.9
10	58.4	55.2	55.8	55.6	56.9	57.9	56.6
20	56.9	52.5	57.7	55.6	51.5	53.3	54.5
30	38.3	38.4	38.5	38.1	39.2	38.9	38.6
40	30.9	30.9	31.9	31.0	30.7	32.1	31.2
50	26.3	27.0	26.7	25.6	26.5	26.4	26.4
60	24.5	23.6	23.5	24.7	26.0	24.2	24.4
70	22.3	21.8	23.2	22.3	23.8	22.8	22.7
80	19.0	19.5	18.6	18.9	18.8	18.7	18.9
90	18.5	18.0	17.8	17.9	17.8	17.6	17.9

3D Systems, Actua Wax, 0.09 mm layers							
Angle	Samp 1	Samp 2	Samp 3	Samp 4	Samp 5	Samp 6	Average
0	1.3	1.2	1.5	1.4	1.4	1.7	1.4
10	22.8	21.8	21.6	21.6	21.9	21.2	21.8
20	20.3	20.2	20.4	20.4	20.2	21.8	20.5
30	16.3	16.3	14.9	15.2	15.1	15.8	15.6
40	17.8	18.2	19.0	18.7	18.1	17.6	18.2
50	13.8	13.6	14.2	12.4	14.0	15.7	13.9
60	15.7	15.8	16.6	15.7	16.9	16.2	16.1
70	8.8	9.5	9.4	9.4	9.3	9.1	9.2
80	10.0	9.8	9.2	9.5	9.0	8.5	9.3
90	6.7	6.2	6.9	6.9	5.6	5.1	6.2

APPENDIX C

Surface roughness measurements derived from 3D Systems samples

All Measurements in μm Ra

3D Systems SLA 250 – Epoxy 5170, ACES									
Angle	Samp 1	Samp 2	Samp 3	Average	Angle	Samp 1	Samp 2	Samp 3	Average
0	2.1	2.1	2.42	**2.2**	92	7.1	5.9	6.2	**6.4**
2	22.5	22.8	22.2	**22.5**	94	3.1	4.7	4.2	**4.0**
4	37.8	39.2	39.0	**38.6**	96	2.9	4.8	3.9	**3.8**
6	40.6	40.5	40.7	**40.6**	98	5.5	3.9	5.1	**4.8**
8	42.3	39.3	42.4	**41.3**	100	4.6	3.5	3.6	**3.9**
10	39.1	40.0	38.8	**39.3**	102	5.1	6.5	3.2	**4.9**
12	38.8	38.4	37.5	**38.2**	104	5.0	5.2	4.9	**5.0**
14	38.2	39.1	39.4	**38.9**	106	4.9	6.5	6.0	**5.8**
16	37.6	38.0	37.3	**37.6**	108	3.9	3.9	4.0	**3.9**
18	37.0	37.0	37.7	**37.2**	110	4.0	4.2	4.4	**4.2**
20	37.7	38.2	38.0	**37.9**	112	4.7	5.2	5.0	**4.9**
22	36.0	36.0	36.0	**36.0**	114	4.8	4.8	5.6	**5.1**
24	36.0	36.1	35.0	**35.7**	116	6.9	5.5	6.1	**6.2**
26	36.9	36.5	36.2	**36.5**	118	5.3	6.3	5.5	**5.7**
28	35.7	35.8	35.8	**35.7**	120	5.3	5.1	5.2	**5.2**
30	34.0	34.4	34.8	**34.4**	122	5.4	5.2	4.9	**5.2**
32	33.8	34.4	34.8	**34.3**	124	5.3	5.8	5.8	**5.6**
34	34.4	33.9	33.8	**34.0**	126	5.9	5.7	5.8	**5.8**
36	22.9	33.3	33.2	**29.8**	128	6.0	7.4	6.4	**6.6**
38	32.0	30.9	31.3	**31.4**	130	7.6	7.4	7.8	**7.6**
40	31.3	31.0	31.1	**31.1**	132	8.7	10.8	9.3	**9.6**
42	32.7	32.6	32.7	**32.6**	134	10.1	9.6	9.2	**9.6**
44	29.1	28.2	31.4	**29.5**	136	7.1	7.3	7.6	**7.3**
46	27/0	28.1	27.3	**27.4**	138	6.4	6.7	6.0	**6.4**
48	28.4	28.5	28.4	**28.4**	140	6.4	6.9	6.9	**6.7**
50	26.1	26.6	25.9	**26.2**	142	7.8	8.0	7.7	**7.8**
52	25.6	25.6	25.6	**25.6**	144	8.9	8.7	8.7	**8.8**
54	24.7	24.9	24.8	**24.8**	146	13.2	12.8	12.9	**12.9**
56	23.0	23.1	23.2	**23.1**	148	16.7	14.9	16.2	**15.9**
58	21.4	21.4	21.2	**21.3**	150	18.8	20.6	18.4	**19.3**
60	20.2	20.2	20.4	**20.2**	152	21.9	22.2	22.1	**22.1**
62	19.6	19.2	19.4	**19.4**	154	22.6	28.9	24.7	**25.4**
64	17.5	17.2	173	**17.3**	156	31.4	32.0	33.2	**32.2**
66	15.7	15.8	15.6	**15.7**	158	31.8	32.2	32.2	**32.1**
68	14.3	14.1	14.4	**14.2**	160	33.5	33.3	31.9	**32.9**
70	12.3	12.8	11.9	**12.3**	162	34.3	37.9	36.0	**36.1**
72	11.9	11.7	11.8	**11.8**	164	41.5	44.3	41.7	**42.5**
74	10.3	10.5	10.6	**10.4**	166	46.9	47.1	44.4	**46.1**
76	10.1	10.4	10.3	**10.2**	168	50.2	48.0	46.8	**48.3**
78	9.5	9.9	9.6	**9.6**	170	52.2	45.6	52.4	**50.1**
80	8.9	9.0	9.0	**8.9**	172	57.2	59.2	61.4	**59.2**
82	7.5	7.4	7.7	**7.5**	174	52.3	47.2	53.0	**50.8**
84	6.9	6.7	6.8	**6.8**	176	51.1	49.2	50.3	**50.2**
86	6.0	6.0	6.0	**6.0**	178	41.3	40.5	43.4	**41.7**
88	6.3	6.3	6.5	**6.4**	180	9.4	10.7	11.7	**10.6**
90	6.9	6.8	6.8	**6.7**					

3D Systems SLA 250 – Acrylic 5149, Star-Weave									
Angle	Samp 1	Samp 2	Samp 3	**Average**	Angle	Samp 1	Samp 2	Samp 3	**Average**
0	1.66	1.15	1.59	**1.3**	92	5.8	5.5	5.7	**5.66**
2	24.5	23.8	24.6	**24.3**	94	5.6	4.7	3.2	**4.5**
4	32.5	31.5	31.5	**31.8**	96	4.2	3.6	3.7	**3.83**
6	22.6	23.1	22.8	**22.8**	98	3.2	3.5	3.3	**3.33**
8	23.2	22.7	22.8	**22.9**	100	3.5	3.7	3.6	**3.6**
10	25.2	26.2	25.6	**25.7**	102	3.5	3.7	4.3	**3.8**
12	27.2	27.4	26.6	**27.06**	104	3.8	3.9	4.3	**4.0**
14	23.0	23.3	24.2	**23.5**	106	4.9	4.5	5.2	**3.65**
16	21.8	22.1	22.4	**22.1**	108	6.3	5.5	4.8	**5.3**
18	24.2	23.5	23.2	**23.6**	110	6.2	6.4	5.9	**6.2**
20	22.6	22.4	22.5	**22.5**	112	6.0	5.3	5.5	**5.6**
22	17.5	17.2	17.4	**17.4**	114	6.5	5.7	6.0	**6.0**
24	16.8	17.4	16.3	**16.8**	116	6.1	5.4	6.3	**5.9**
26	14.6	14.7	14.9	**14.9**	118	6.1	6.2	6.3	**6.2**
28	14.3	14.5	14.4	**14.4**	120	10.5	11.1	10.1	**10.6**
30	13.9	13.6	13.1	**13.5**	122	6.5	8.9	6.1	**7.1**
32	11.9	12.1	11.9	**12.0**	124	6.4	6.8	6.4	**6.5**
34	11.7	11.0	10.9	**11.2**	126	5.8	7.8	11.2	**8.26**
36	11.8	11.7	11.2	**11.5**	128	12.5	10.4	14.0	**12.3**
38	13.0	15.9	11.2	**13.4**	130	7.9	8.4	8.5	**8.26**
40	12.4	11.9	10.0	**11.4**	132	7.7	11.2	10.9	**9.93**
42	10.9	10.2	11.2	**10.76**	134	12.4	11.0	8.6	**10.66**
44	13.0	12.7	13.3	**13.0**	136	8.6	8.6	9.0	**8.73**
46	8.8	9.3	9.2	**9.1**	138	9.8	9.0	8.9	**9.23**
48	6.1	6.5	6.0	**6.2**	140	8.5	8.1	9.3	**8.6**
50	5.1	5.9	5.5	**5.5**	142	7.6	7.6	7.6	**7.6**
52	4.23	4.76	4.9	**4.63**	144	6.8	7.4	6.6	**7.0**
54	5.41	5.73	5.86	**5.7**	146	7.0	7.1	6.5	**6.9**
56	5.25	4.75	5.03	**5.0**	148	6.9	6.4	6.7	**6.7**
58	4.73	4.27	4.41	**4.47**	150	7.9	8.2	8.5	**8.7**
60	4.99	4.02	4.95	**4.65**	152	11.9	13.3	12.3	**12.5**
62	3.46	3.6	4.5	**3.85**	154	13.2	13.7	13.6	**13.5**
64	3.42	3.28	3.36	**3.36**	156	11.2	15.4	16.6	**14.5**
66	3.49	3.27	3.08	**3.28**	158	16.6	15.3	17.6	**16.5**
68	2.99	3.02	3.10	**3.0**	160	17.6	17.2	18	**17.6**
70	3.39	3.06	3.21	**3.22**	162	19.9	20.1	21.2	**21.2**
72	3.83	3.69	4.55	**4.0**	164	23.5	21.7	22.6	**22.6**
74	4.11	4.13	4.57	**4.27**	166	20.6	22.1	21.8	**21.5**
76	4.89	4.64	4.33	**4.62**	168	18.2	27.0	25.0	**23.4**
78	3.67	3.72	3.89	**3.76**	170	23.1	24.7	23.9	**23.9**
80	3.42	3.88	3.6	**3.6**	172	26.9	22.1	28.1	**25.7**
82	3.44	3.44	3.5	**3.46**	174	21.1	20.9	31.5	**24.5**
84	4.02	3.96	4.0	**4.0**	176	29.5	21.9	28.1	**26.5**
86	4.3	5.36	4.47	**4.71**	178	34.4	35.4	36.6	**35.5**
88	6.8	6.8	5.13	**6.24**	180	13.9	14.0	14.3	**14.1**
90	5.1	4.5	5.2	**4.9**					

3D Systems SLA 350 – Epoxy 5190, ACES									
Angle	Samp 1	Samp 2	Samp 3	Average	Angle	Samp 1	Samp 2	Samp 3	Average
0	2.3	1.5	1.6	**1.8**	92	7.8	7.1	5.8	**6.9**
2	37.6	34.5	34.4	**35.5**	94	5.3	5.1	4.6	**5**
4	35.6	32.7	37.9	**35.4**	96	2.1	4.5	3	**3.2**
6	32.1	33.4	39.8	**35.1**	98	3.8	3.4	3.6	**3.6**
8	35.4	37.5	33.9	**35.6**	100	5.6	4.3	3.9	**4.6**
10	41.8	35.5	38.8	**38.7**	102	3.7	4.4	4.5	**4.2**
12	38.9	32.4	34	**35.1**	104	6.3	4.5	6.6	**5.8**
14	32.4	31.4	42.4	**35.4**	106	5.7	6.4	6.2	**6.1**
16	29.2	32.4	41.9	**34.5**	108	5.6	6.5	5.3	**5.8**
18	31.2	31.8	32.1	**31.7**	110	5.6	7.1	7.4	**6.7**
20	32.2	36.4	33.4	**34**	112	5.1	4.9	5.6	**5.2**
22	32.1	28.6	40.7	**33.8**	114	5.6	4.7	5.9	**5.4**
24	29.2	33.1	27.7	**30**	116	4.5	6.1	3.8	**4.8**
26	33.7	33.4	32.5	**33.2**	118	6.3	7.2	6	**6.5**
28	35.9	28.7	34.1	**32.9**	120	3.7	4.4	5.1	**4.4**
30	33.7	31.6	32.8	**32.7**	122	2.3	6.4	4.2	**4.3**
32	29.6	32.5	35.1	**32.4**	124	2.1	1.6	2.3	**2**
34	35.4	27.5	33.4	**32.1**	126	3.2	4.3	5.1	**4.2**
36	34	29.1	32.6	**31.9**	128	4.7	4.2	3.4	**4.1**
38	33.4	31.4	34.5	**33.1**	130	3.3	4.5	4.2	**4**
40	32.4	35.6	26.2	**31.4**	132	4.5	6.1	3.2	**4.6**
42	30.4	26.6	29.1	**28.7**	134	5.4	3.6	6.9	**5.3**
44	35.9	26.7	30.1	**30.9**	136	6.4	7.1	6.6	**6.7**
46	26.5	32.6	32.7	**30.6**	138	5.7	7.2	6.9	**6.6**
48	26.7	32.1	27.3	**28.7**	140	7.3	7.1	7.2	**7.2**
50	28.9	30.2	31.2	**30.1**	142	10.3	8.9	9	**9.4**
52	27.8	31.4	30.2	**29.8**	144	8.3	6.7	8.7	**7.9**
54	29.8	29.1	29.9	**29.6**	146	3.4	10.4	6.9	**6.9**
56	27.9	32.1	27.9	**29.3**	148	7.8	9.5	8.8	**8.7**
58	27.8	25.9	27.3	**27**	150	8.6	9.1	9.9	**9.2**
60	26.7	25.9	27.5	**26.7**	152	11.3	15.1	13.2	**13.2**
62	26.1	24.8	28.6	**26.5**	154	11.7	16.4	13.6	**13.9**
64	29.1	26.1	23.7	**26.3**	156	12.5	14.5	12.6	**13.2**
66	23.7	26.9	27.4	**26**	158	16.5	18.1	16.4	**17**
68	24.7	26.1	26.3	**25.7**	160	22	15.7	17.2	**18.3**
70	24.6	22.3	23.6	**23.5**	162	21.9	26.9	22	**23.6**
72	18.5	23.5	18.6	**20.2**	164	21.4	24	23.3	**22.9**
74	19.9	21.1	18.7	**19.9**	166	26.1	32.8	35.6	**31.5**
76	16.8	23.1	19.2	**19.7**	168	33.7	26.7	31.7	**30.7**
78	14.7	12.5	19	**15.4**	170	28.8	31.5	34.2	**31.5**
80	10.7	9.8	14.6	**11.7**	172	40	35.6	37.8	**37.8**
82	12.3	11.1	12.3	**11.9**	174	39.3	35.7	39.1	**38**
84	13.4	12.1	10.8	**12.1**	176	43.5	38.7	39	**40.4**
86	10.9	9.8	10.2	**10.3**	178	37.8	35.5	40.7	**38**
88	13.1	10.8	7.9	**10.6**	180	15.3	14.5	10.7	**13.5**
90	12.7	9.9	9.8	**10.8**					

3D Systems SLA 500 – Epoxy 5180, ACES									
Angle	Samp 1	Samp 2	Samp 3	**Average**	Angle	Samp 1	Samp 2	Samp 3	**Average**
0	1.6	2.1	1.5	**1.73**	92	11.4	11.7	12.5	**11.8**
2	21.8	34.2	23.7	**26.6**	94	11.0	10.8	11.7	**11.2**
4	31.1	30.7	29.9	**30.6**	96	10.5	10.0	10.3	**10.3**
6	33.9	33.6	33.9	**33.8**	98	9.5	10.2	9.4	**9.7**
8	36.6	34.9	35.4	**35.6**	100	9.9	9.7	9.8	**9.8**
10	34.7	34.9	35.1	**34.9**	102	10.1	9.6	8.1	**9.3**
12	35.5	35.2	35.0	**35.2**	104	8.6	8.2	9.0	**8.6**
14	33.9	33.8	34.8	**34.2**	106	7.4	8.4	9.5	**8.4**
16	32.9	33.9	32.9	**33.2**	108	7.9	7.4	7.5	**7.6**
18	33.7	33.4	31.6	**32.9**	110	11.4	10.6	12.0	**11.3**
20	31.4	31.6	31.1	**31.4**	112	7.6	7.0	6.9	**7.2**
22	30.1	30.5	30.3	**30.3**	114	7.1	6.9	6.9	**6.9**
24	29.7	30.1	29.6	**29.8**	116	8.2	7.7	7.3	**7.7**
26	28.4	29.2	29.4	**29.0**	118	7.6	7.7	8.6	**7.96**
28	29.0	28.9	28.4	**28.8**	120	9.5	6.8	7.5	**7.9**
30	27.8	28.5	28.4	**28.2**	122	7.9	7.3	7.7	**7.63**
32	27.9	27.9	27.9	**27.9**	124	7.3	7.4	7.5	**7.4**
34	27.9	27.0	26.4	**27.1**	126	7.1	6.2	7.4	**6.9**
36	26.6	26.1	25.8	**26.2**	128	8.3	7.1	8.2	**7.86**
38	26.8	26.8	26.9	**26.8**	130	8.6	10.2	9.6	**9.46**
40	26.7	26.1	26.2	**26.3**	132	12.3	11.5	11.6	**11.8**
42	26.1	25.8	26.1	**26.0**	134	13.3	13.4	11.1	**12.6**
44	24.8	24.0	24.6	**24.5**	136	7.2	8.0	9.9	**8.3**
46	23.9	24.4	22.8	**23.7**	138	8.9	8.1	8.0	**8.3**
48	24.2	23.7	23.7	**23.8**	140	8.4	8.5	8.0	**8.3**
50	23.3	23.1	23.3	**23.2**	142	7.5	7.9	7.9	**7.76**
52	22.3	24.0	23.2	**23.2**	144	7.7	7.8	8.2	**7.9**
54	23.6	23.2	22.9	**23.2**	146	9.5	8.2	7.9	**8.5**
56	23.0	22.8	22.9	**22.9**	148	11.3	10.3	10.5	**10.7**
58	23.1	23.0	22.3	**22.8**	150	11.1	10.7	7.6	**9.8**
60	22.5	22.3	22.2	**22.3**	152	10.8	12.3	11.4	**11.5**
62	21.4	21.7	21.5	**21.5**	154	13.1	13.5	9.2	**12.1**
64	21.5	20.4	20.2	**20.7**	156	13.2	12.1	11.9	**12.4**
66	20.2	09.9	20.4	**20.1**	158	10.3	9.8	13.5	**11.2**
68	19.7	19.7	19.4	**19.6**	160	14.2	14.4	15.5	**14.7**
70	19.6	19.2	19.6	**19.5**	162	14.5	11.6	14.1	**13.4**
72	19.3	18.8	18.9	**18.9**	164	15.3	15.4	15.5	**15.4**
74	18.2	17.9	18.3	**18.13**	166	17.4	18.5	14.2	**16.7**
76	19.6	18.2	18.6	**18.6**	168	19.1	17.3	20.9	**19.1**
78	17.9	17.4	16.9	**17.4**	170	20.7	21.1	20.9	**20.9**
80	16.2	17.2	18.3	**17.2**	172	23.1	22.5	17.7	**21.1**
82	16.3	15.8	16.3	**16.1**	174	20.5	15.5	23.4	**19.8**
84	15.0	15.0	14.7	**14.9**	176	20.8	24.1	27.7	**24.2**
86	13.9	13.9	13.5	**13.7**	178	21.2	25.4	23.6	**23.4**
88	12.9	12.6	13.4	**12.9**	180	21.4	24.7	28	**25.7**
90	12.0	11.5	11.5	**11.66**					

APPENDIX D

Surface roughness measurements derived from meniscus smoothed samples

All measurements in μm Ra

3D Systems software No smoothing							
	Sample 1 Point 1	Sample 1 Point 2	Sample 1 Point 3	Sample 1 Point 4	Sample 1 Point 5	Sample 1 Point 6	Average
10 degrees	42.1	38.7	37.8	39.1	40.2	41.5	**39.9**
20 degrees	29.7	33.2	31.7	30.6	32.4	33.2	**31.8**
30 degrees	29.1	30.6	28.1	28.2	28.3	28.5	**28.8**
40 degrees	25	26.2	25.7	25.5	26.1	26.3	**25.8**
50 degrees	20.8	21.1	22.2	23	20.6	21.3	**21.5**
60 degrees	21.1	20.9	21.3	21.4	19.5	20.4	**20.6**
70 degrees	17.2	17	16.3	16.2	16.7	16.8	**16.7**
80 degrees	6.8	6.9	7.5	7.2	7.6	7.8	**7.3**
90 degrees	6.3	6.5	7.1	5.8	5.9	6.2	**6.3**

TSR software No smoothing							
	Sample 1 Point 1	Sample 1 Point 2	Sample 1 Point 3	Sample 1 Point 4	Sample 1 Point 5	Sample 1 Point 6	Average
10 degrees	40.3	41.6	38.7	42.5	40.7	39.2	**40.5**
20 degrees	32.1	34.2	32.1	30.6	30.2	35.2	**32.4**
30 degrees	27.6	28.4	28	27.1	27.3	29	**27.9**
40 degrees	23.5	22.6	23.1	23.8	24.3	23.1	**23.4**
50 degrees	23.4	21.9	23.1	22.3	21.9	21.8	**22.4**
60 degrees	19.6	18.9	20.5	20.7	20.2	18.9	**19.8**
70 degrees	15.6	15.6	16.2	16.1	15.7	15.6	**15.8**
80 degrees	8	8.8	7.6	7.8	8.6	8.4	**8.2**
90 degrees	6.8	7.1	7.1	7.6	7.3	6.7	**7.1**

TSR software Meniscus retraction distance 0.003 (1/2 Layer thickness)										
	Samp 1 Point 1	Samp 1 Point 2	Samp 1 Point 3	Samp 2 Point 1	Samp 2 Point 2	Samp 2 Point 3	Samp 3 Point 1	Samp 3 Point 2	Samp 3 Point 3	Average
10 degrees	39.8	42.3	38.9	46.8	43.5	47.6	44.4	43.5	50.1	**44.1**
20 degrees	33.4	35.4	34.7	36.5	34.7	32.9	32.6	34.8	35.5	**34.5**
30 degrees	26.4	27.6	26.7	26.1	26.9	28	26.2	25.6	26.8	**26.7**
40 degrees	17.3	16.8	18.2	18.6	17.2	16.5	17.3	16.6	17.2	**17.3**
50 degrees	12.3	12	11.2	10.1	11.2	10.6	9.1	11.4	11.9	**11.2**
60 degrees	12.4	12.3	12.8	11.3	11.6	10.1	11.2	12.5	11.1	**11.7**
70 degrees	10.2	9.8	10.9	11.5	11.6	10.9	12.1	10.9	9.7	**10.4**
80 degrees	10.8	10.3	10.4	9.3	9.9	9.1	8.8	10.6	9	**9.8**
90 degrees	10.5	11.2	10.6	12.5	10.8	11.4	11.2	10.8	10.9	**11.1**

TSR software Meniscus retraction distance 0.006 (1 Layer thickness)										
	Samp 1 Point 1	Samp 1 Point 2	Samp 1 Point 3	Samp 2 Point 1	Samp 2 Point 2	Samp 2 Point 3	Samp 3 Point 1	Samp 3 Point 2	Samp 3 Point 3	**Average**
10 degrees	6.7	7.2	7.8	6.5	7.1	6.7	6.7	6.1	6.4	**6.8**
20 degrees	11.2	10.7	9.9	9.8	10.3	10.7	10.2	10.1	11.6	**10.5**
30 degrees	13.2	12.8	13.4	12.4	13.8	12.9	11.5	11.9	12.4	**12.7**
40 degrees	21.3	20.9	20.3	19.8	19.5	20.1	20.5	20	21.2	**20.4**
50 degrees	24.4	23.4	25.3	23.7	23	23.8	25.7	24.3	26	**24.4**
60 degrees	23.2	24.7	24.1	21.9	23.4	23.1	22.5	22.6	24	**23.5**
70 degrees	18.7	21.3	19.8	19.4	19.1	20.4	20.3	19.1	18.3	**19.6**
80 degrees	7.9	8.1	8.3	9.6	9.3	8.9	9.5	7.9	8.8	**8.7**
90 degrees	9.6	9.2	9.3	8.7	8.4	8.7	8.9	9.5	9.6	**9.1**

TSR software Meniscus retraction distance 0.012 (2 Layer thickness)										
	Samp 1 Point 1	Samp 1 Point 2	Samp 1 Point 3	Samp 2 Point 1	Samp 2 Point 2	Samp 2 Point 3	Samp 3 Point 1	Samp 3 Point 2	Samp 3 Point 3	**Average**
10 degrees	3.3	3.6	3.1	4.5	4.3	4.1	3.7	3.6	4	**3.8**
20 degrees	6.7	6.4	6.5	7.2	7.4	7.1	6.1	5.9	5.2	**6.5**
30 degrees	8.1	8.3	7.8	8.1	8.4	8.6	8.3	7.8	8.2	**8.2**
40 degrees	12.4	12.2	12.6	11.9	12.2	12.7	11.6	11.5	13.4	**12.5**
50 degrees	18.9	19.5	19.9	21.4	22.6	20.5	21.7	18.7	18.6	**20.2**
60 degrees	15.6	14.8	15.1	17.1	13.7	15.4	15.2	16.1	17.4	**15.6**
70 degrees	13.1	14.4	12.6	12.7	13.6	13.2	14.3	13.4	12.4	**13.3**
80 degrees	7.6	7.8	8.4	8.2	8.5	7.6	7.9	8.3	8.6	**8.1**
90 degrees	10.8	11.3	11.6	11.1	10.7	12.6	12.8	10.5	9.4	**11.2**